

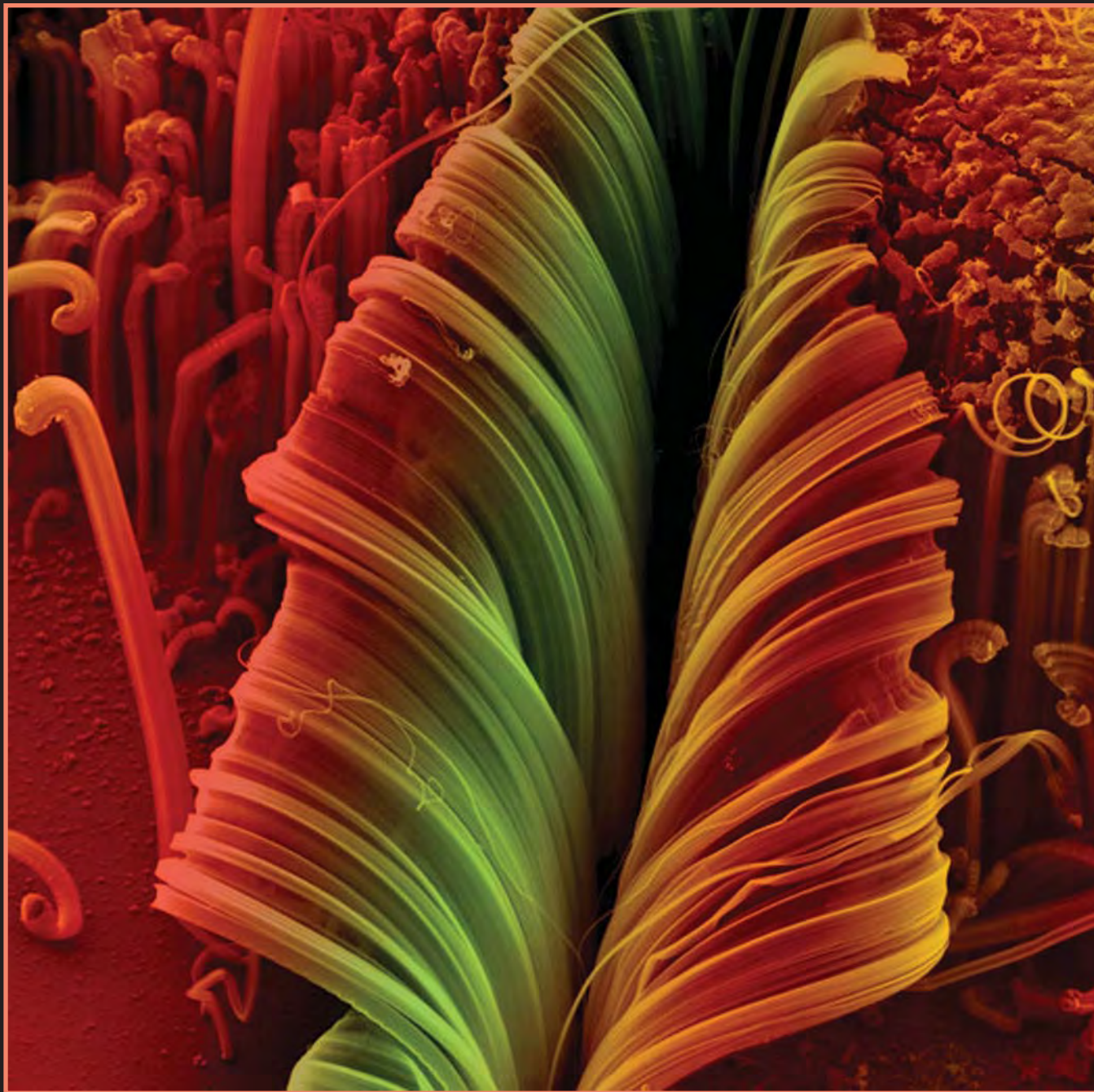
# JOM

**NEW YEAR,  
NEW BENEFITS:  
Job and  
Financial  
Security  
Resources**

A publication of The Minerals, Metals & Materials Society

JANUARY 2009

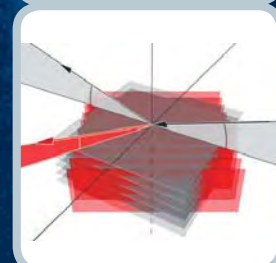
[www.tms.org/jom.html](http://www.tms.org/jom.html)



## CHARACTERIZATION AND ANALYSIS

- Phase Transformations
- Polymer-Matrix Composites
- Materials Informatics, Part II

Bruker **AXS**



# XRD Versatility Has Been Redefined

## D8 DISCOVER MR

- All Materials Science Applications on one system
- Nanomaterials to Thin Films to Chemical Structure to Geology
- 0D, 1D and **TRUE** 2D detector technology
- Full software suite for all applications

[www.bruker-axs.com](http://www.bruker-axs.com) • 1-800-234-XRAY • [info@bruker-axs.com](mailto:info@bruker-axs.com)

Please visit us at the 2009 TMS Annual Meeting booth 215.

think forward

XRD

# The Only Document as Important as Your Diploma in Advancing Your Career



Wherever you want to go in your career,  
**TMS** can help you get there.

**TMS** membership offers you opportunities every step along your career path, through a network of professionals in the minerals, metals, and materials fields and the technical exchange necessary for advancement.

Through **TMS** membership, you gain from:

Your path to  
career  
advancement  
starts with  
**TMS.**

To begin, visit  
[www.tms.org](http://www.tms.org)  
today or call,  
toll-free in the  
U.S. and  
Canada,  
**(800) 759-4TMS.**

Print and electronic subscriptions to technical journals such as *JOM*, which covers traditional, innovative, and revolutionary issues in the minerals, metals, and materials fields.

Discounted fees to international conferences and courses where your peers meet to present and discuss common challenges and the latest advances.

Discounts on technical publications and other resources to keep you current on progress in your field.

Members-only Web access to searchable technical and member databases, and much more!

Your Professional Partner for Career Advancement

**TMS**

# MEMBERSHIP APPLICATION

**PLEASE TYPE OR PRINT.**

- Mr.     Mrs.     Ms.  
 Dr.     Professor

**BIRTH DATE:**

\_\_\_\_/\_\_\_\_/\_\_\_\_

**SEND MAIL TO:**

- Business Address  
 Home Address

**TECHNICAL DIVISION SELECTION:**

- Electronic, Magnetic & Photonic Materials Division  
 Extraction & Processing Division  
 Light Metals Division  
 Materials Processing & Manufacturing Division  
 Structural Materials Division

**THROUGH WHAT MEANS WERE YOU ENCOURAGED TO JOIN TMS?**

- TMS Annual Meeting  
 TMS Fall Conference  
 Specialty Conference  
 Exhibitor  
 TMS Staffed Booth  
 JOM  
 MET TRANS, JEM, etc.  
 Publications Catalog  
 TMS Mailed Brochure  
 Non-TMS Advertisement  
 Continuing Education  
 TMS Web Site  
 Colleague  
 Other \_\_\_\_\_

Members receive a print and electronic subscription to JOM.

If you prefer to receive your copy only electronically, check here.

**NAME:** \_\_\_\_\_  
LAST FIRST MIDDLE INITIAL

**TITLE:** \_\_\_\_\_ **COMPANY OR ORGANIZATION:** \_\_\_\_\_

**BUSINESS:** \_\_\_\_\_  
STREET OR P.O. BOX CITY STATE 9 DIGIT ZIP/POSTAL CODE COUNTRY

---

PHONE FAX TOLL-FREE # E-MAIL WEB ADDRESS

**HOME:** \_\_\_\_\_  
STREET OR P.O. BOX CITY STATE 9 DIGIT ZIP/POSTAL CODE COUNTRY

---

PHONE FAX E-MAIL

**TMS KEYWORDS—CHECK ALL THAT APPLY.**

- |  |   |  |  |
|--|---|--|--|
| <input type="checkbox"/> Advanced Materials                        | <input type="checkbox"/> Electrometallurgy          | <input type="checkbox"/> Lead Zinc and Tin               | <input type="checkbox"/> Physical Properties               |
| <input type="checkbox"/> Advanced Processing                       | <input type="checkbox"/> Electronic Materials       | <input type="checkbox"/> Lightweight Materials           | <input type="checkbox"/> Polymers                          |
| <input type="checkbox"/> Aluminum                                  | <input type="checkbox"/> Energy                     | <input type="checkbox"/> Magnesium                       | <input type="checkbox"/> Powder Technology                 |
| <input type="checkbox"/> Aqueous Processing                        | <input type="checkbox"/> Environmental Effects      | <input type="checkbox"/> Manufacturing and Markets       | <input type="checkbox"/> Precious Metals                   |
| <input type="checkbox"/> Biomaterials                              | <input type="checkbox"/> Environmental Issues       | <input type="checkbox"/> Mechanical Properties           | <input type="checkbox"/> Process Mineralogy                |
| <input type="checkbox"/> Ceramics                                  | <input type="checkbox"/> Experimental Methods       | <input type="checkbox"/> Minerals                        | <input type="checkbox"/> Pyrometallurgy                    |
| <input type="checkbox"/> Characterization                          | <input type="checkbox"/> Extraction and Processing  | <input type="checkbox"/> Modeling and Simulation         | <input type="checkbox"/> Recycling and Secondary Recovery  |
| <input type="checkbox"/> Composites                                | <input type="checkbox"/> Fundamentals               | <input type="checkbox"/> Molten Metal and Solidification | <input type="checkbox"/> Shaping and Forming               |
| <input type="checkbox"/> Computer Applications and Process Control | <input type="checkbox"/> High Temperature Materials | <input type="checkbox"/> Nanotechnology                  | <input type="checkbox"/> Superconductivity                 |
| <input type="checkbox"/> Copper Nickel and Cobalt                  | <input type="checkbox"/> Intermetallics             | <input type="checkbox"/> Nontechnical Topics             | <input type="checkbox"/> Surface Modification and Coatings |
| <input type="checkbox"/> Education                                 | <input type="checkbox"/> Iron and Steel             | <input type="checkbox"/> Nuclear Materials               | <input type="checkbox"/> Synthesis and Processing          |
|  | <input type="checkbox"/> Joining                    | <input type="checkbox"/> Other Nonferrous                | <input type="checkbox"/> Titanium                          |

Check here if you would **not** like TMS to make your contact information available to other TMS members via the keyword search feature of the online TMS membership directory.

**WHICH OF THE FOLLOWING BEST DESCRIBES YOUR SECTOR OF EMPLOYMENT? (Check one.)**

- Consulting     University/Education     Industry     Government/Nonprofit  
 Retired     Unemployed     Other

**EDUCATION TO DATE:**

Name of School	Dates Attended Month/Year–Month/Year	Major/Subject Engineering Field	Degree Received or Expected Graduation Date: Month/Year
B.S. <input type="checkbox"/> _____			
M.S. <input type="checkbox"/> _____			
Ph.D. <input type="checkbox"/> _____			

REGISTERED PROFESSIONAL ENGINEER?  Yes  No    YEAR OF REGISTRATION: \_\_\_\_\_ STATE: \_\_\_\_\_

RECORD OF EXPERIENCE: Attach the most recent record of employment. If you do not possess a qualifying degree, include your last five years of experience.

**TO APPLICANT**

If you have been encouraged by a current member of TMS to submit this application, complete the following information:

Member's Name \_\_\_\_\_ Member # \_\_\_\_\_

*I agree, if elected, to accept election and to abide by the TMS bylaws.*

Signature \_\_\_\_\_ Date \_\_\_\_\_

PREPAYMENT OF \$115 IS REQUIRED. (Checks should be made payable to TMS in U.S. dollars drawn on a U.S. bank.)

- Check Enclosed     Bill my credit card: (Check one.)  
 American Express     VISA     MasterCard     Diners Club

Credit Card # \_\_\_\_\_ Expiration Date \_\_\_\_\_

Cardholder's Name \_\_\_\_\_

Signature \_\_\_\_\_

**COMPLETE APPLICATION IN ITS ENTIRETY AND MAIL WITH PAYMENT TO:** 184 Thorn Hill Road, Warrendale, PA 15086-7514  
 Phone: (800) 759-4TMS or (724) 776-9000 • Fax: (724) 776-3770

FOR OFFICE USE ONLY
ID
BIRTH
ELECTED
TYPE
CATEGORY
SECTION
APPROVED

## POLYMER-MATRIX COMPOSITES

- 16:** **Polymer-Matrix Composites: New Fibers Offer New Possibilities:**  
Sergio Neves Monteiro
- 17:** **Natural-Fiber Polymer-Matrix Composites: Cheaper, Tougher, and Environmentally Friendly:**  
Sergio Neves Monteiro, Felipe Perissé D. Lopes, Ailton Silva Ferreira, and Denise Cristina O. Nascimento
- 23:** **The Development of a Multifunctional Composite Material for Use in Human Space Exploration Beyond Low-Earth Orbit:** S. Sen, E. Schofield, J.S. O'Dell, L. Deka, and S. Pillay
- 32:** **The Mechanical Characterization of Carbon-Nanotube-Reinforced Polymer-Matrix Nanocomposites: An Unfolding Story of Interface:** Yogeeswaran Ganesan and Jun Lou
- 38:** **The Characterization of High-Density Polyethylene/Organoclay Nanocomposites:** Tathiane Cordeiro Rodrigues, Maria Inês Bruno Tavares, Igor Lopes Soares, and Ana M. Moreira
- 43:** **Characterizing the Strain Rate Sensitivity of the Tensile Mechanical Properties of a Thermoplastic Composite:** Kevin A. Brown, Richard Brooks, and Nicholas A. Warrior

## MATERIALS INFORMATICS

- 47:** **Informatics and Integrated Computational Materials Engineering: Part II:**  
Krishna Rajan
- 48:** **Informatics for Chemical Crystallography:**  
Changwon Suh and Krishna Rajan
- 54:** **Using Data to Account for Lack of Data: Linking Material Informatics with Stochastic Analysis:**  
Baskar Ganapathysubramanian
- 59:** **A Materials Database for Exploring Material Properties:** R. Hrubciak, Lyci George, Surendra K. Saxena, and Krishna Rajan

## PHASE TRANSFORMATIONS

- 63:** **Phase Stability, Phase Transformations, and Reactive Phase Formation:**  
Sinn-wen Chen
- 64:** **High-Temperature Lead-Free Solders: Properties and Possibilities:**  
Katsuaki Suganuma, Seong-Jun Kim, and Keun-Soo Kim
- 72:** **Annealing-Induced Amorphization in a Glass-Forming Thin Film:**  
J.P. Chu
- 76:** **The Growth Kinetics of Intermetallic Layers at the Interface of a Solid Metal and a Liquid Solder:**  
V.I. Dybkov

- 80:** **Measuring Secondary Phases in Duplex Stainless Steels:**  
I. Calliari, K. Brunelli, M. Dabalà, and E. Ramous
- 84:** **Controlling Stress and Diffusion for the Low-Temperature-Ordering of L1<sub>0</sub> Ordered FePt Films:**  
Yun-Chung Wu, Liang-Wei Wang, C.C. Chiang, Cheng-Han Yang, and Chih-Huang Lai

## FEATURE

- 14:** **Human Assets: The Most Precious Capital:**  
Diran Apelian

## ALSO IN THIS ISSUE

- 2:** **In the Final Analysis**
- 4:** **Letters to the Editor**
- 4:** **Book Reviews**
- 5:** **News & Update**
- 12:** **Member News**
- 42:** **Foundation News**
- 89:** **Upcoming Editorial Topics**
- 90:** **Meetings Calendar**
- 94:** **Materials Resource Center: Jobs, Consultants, Marketplace**
- 96:** **End Notes: "Beyond Flex Time: Retaining Female Scientists and Engineers"**

**About the Cover:** University of Michigan Assistant Professor A. John Hart has attracted national media attention with his artful arrangements of carbon nanotubes. Partly for his own enjoyment, and partly to encourage interest in science, he photographs the nanotubes with optical and electron microscopes and displays them on his web site. The cover shows one such image, which he calls "Parting," that resulted when nanotubes were grown on a silicon substrate. More examples of Hart's work, including one called "Nanobama" in which the nanotubes are arranged to form the image of President-elect Barack Obama, can be found on pages 6 and 7. Photo by A. John Hart.

**"It's psychotic! They keep creating new ways to celebrate mediocrity."**

—Mr. Incredible, *The Incredibles*

I'm coming clean: One of my favorite movies is a Pixar-Disney animation called *The Incredibles*. (I know; I'm a nerd. It's a well-established and widely documented fact that I'm reminded of frequently by friends, family, coworkers, and passing strangers, so there's no sense trying to conceal the fact now.) *The Incredibles* tells the story of superheroes in hiding, trying to suppress their incredibleness by pretending to be ordinary citizens. They live in tract housing, drive economy cars, hold down boring day jobs, etc., etc. A favorite theme in the movie is the idea that society strives to elevate the average as wonderful and suppress the extraordinary as something suspicious. Saying that everyone is special, a gifted child observes, "is another way of saying no one is."

While it is nice to think of everyone as special, there's nothing special about being average. I'm thinking "average" thoughts these days based on a news story that I just read in the Materials Education Community of our Materials Technology@TMS web site ([www.materialstechnology.org](http://www.materialstechnology.org)). It provides more statistical reinforcement of the generally downward spiral into average being achieved by the "educated" public within the United States.

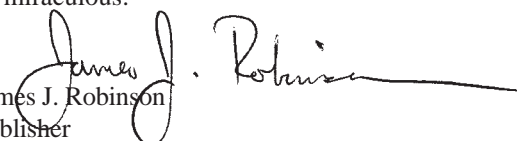
The story comes from the College Board's Commission on Access, Admissions, and Success in Higher Education. The College Board is the association that gives us the SAT and Advanced Placement programs. So, they've got some street cred to comment on such matters. (Does saying "street cred" make me sound hip? Or, did I just blow it by saying "hip"?!) The new report, *Coming to Our Senses: Education and the American Future*, shows the U.S. working hard to convert an incredible educational system to an average one. The bad news comes fast, as reflected in this excerpt from the first paragraph of the Executive Summary: "The United States, which led the world in high school completion rates throughout the 20th century, ranked just 21st out of 27 advanced economies by 2005. And our college completion rates have dropped dramatically—from number two in the world for younger workers (age 25–34) to number eleven. The United States is on the verge of losing the great global educational competitive edge it has long enjoyed." By the way, dropout rates for U.S. high school students have tripled in the last 30 years.

The College Board advocates that the United States ensure that at least 55 percent of citizens ages 25–34 hold at least a community college degree by 2025. The current mark is about 40%. Big task. Suggestions include providing voluntary preschool education that is universally available to children from low-income families, aligning the U.S. K–12 educational system with international standards and college admissions expectations, improving teacher quality while focusing on recruitment and retention, and making financial aid processes more transparent and keeping college affordable.

Good suggestions, but they require commitment, planning, effort, and money. The latter, thanks to a severe and global recession, is in short supply. With this fearful confluence, will the Gathering Storm ramp into the Perfect Storm?

What are the prospects? As I write, I see on the CNN web site that U.S. President-elect Barack Obama has named Arne Duncan, chief of the Chicago public school system, to be education secretary. I don't know much about Duncan, but I do know that in the presidential campaign Obama showed himself to be savvy to Gathering Storm issues. Let's hope that he is.

Of course, it will take a lot more than hope to reverse the downward trends articulated in report after report. Most importantly, the new president and new secretary of education can't afford to be average. They can't even be incredible. They need to be miraculous.

  
James J. Robinson  
Publisher

# JOM

184 Thorn Hill Road,  
Warrendale, PA 15086, USA

Telephone: (724) 776-9000  
Fax: (724) 776-3770

Web: [www.tms.org/jom.html](http://www.tms.org/jom.html)  
E-Mail: [jom@tms.org](mailto:jom@tms.org)

## PUBLISHER

James J. Robinson

## JANUARY ADVISORS

### Polymer-Matrix Composites:

*Materials Characterization Committee*  
Sergio Neves Monteiro, State University  
of Northern Rio de Janeiro

### Materials Informatics:

*Computational Materials Science and  
Engineering Committee*  
Krishna Rajan, Iowa State University

### Phase Transformations:

*Alloy Phases Committee*  
Sinn-wen Chen, National Tsing Hua University

## EDITORIAL STAFF

Maureen Byko, Editor

Cheryl M. Geier, Senior Graphic Designer

Francine Garrone, News Editor

Shirley A. Litzinger, Production Editor

Elizabeth Rossi, Web Developer

## PARTNER RELATIONS AND ADVERTISING STAFF

Trudi Dunlap, Director

Arlene Frances, Sales Representative

Joe Rostan, Sales Representative

Colleen Leary, Sales Representative

*JOM* (ISSN 1047-4838) is published monthly by Springer Sciences & Business Media, LLC (Springer) 233 Spring St., New York, NY 10013 in cooperation with The Minerals, Metals & Materials Society (TMS).

DISCLAIMER: The opinions and statements expressed in *JOM* are those of the authors only and are not necessarily those of TMS or the editorial staff. No confirmations or endorsements are intended or implied.

SUBSCRIPTIONS, ORDERS, AND OTHER FULFILLMENT INQUIRIES: *In the Americas*, contact Journals Customer Service, P.O. Box 2485, Secaucus, NJ 07096, USA; telephone (800) 777-4643 (in North America) or (212) 460-1500 (outside North America); e-mail [journals-ny@springer.com](mailto:journals-ny@springer.com). *Outside the Americas*, contact Journals Customer Service, Springer Distribution Center, Haberstr. 7, 69126 Heidelberg, Germany; telephone 49-6221-345-4303; e-mail [subscriptions@springer.com](mailto:subscriptions@springer.com).

TMS MEMBERS: Access this and back issues of *JOM* on-line at no charge via [members.tms.org](http://members.tms.org)

POSTMASTER: Send address changes to: *JOM*, Springer, 233 Spring Street, New York, NY 10013, USA. Periodicals postage paid at New York, NY, and additional mailing offices.

## **Now Available Through the TMS Knowledge Resource Center**

### **Complete Proceedings From all Materials Science & Technology Conferences**



- MS&T'08: October 5-9 in Pittsburgh, Pennsylvania
- MS&T'07: September 16-20 in Detroit, Michigan
- MS&T'06: October 15-19 in Cincinnati, Ohio
- MS&T'05: September 26-30 in Pittsburgh, Pennsylvania
- MS&T'04: September 26-29 in New Orleans, Louisiana
- MS&T'03: November 9-12 in Chicago, Illinois

**TMS members and students can purchase  
conference proceedings from each year on CD for \$146  
plus shipping and handling.  
(Nonmembers pay \$195.)**

*Topic-focused e-Books comprised of papers from the '06 and '07 CDs are also available:*

- Electronic, Magnetic and Photonic Materials
- Materials for Energy Applications
- Materials for Transportation Applications
- Nanotechnology

---

#### **To order these or related publications:**

Visit the TMS Knowledge Resource Center at  
<http://knowledge.tms.org> or e-mail [publications@tms.org](mailto:publications@tms.org).

---

### CAST SHOP TECHNOLOGY: HISTORY AT YOUR FINGERTIPS

Dear *JOM* Editor:

The occasion was the Cast Shop Technology session at the TMS 2008 Annual Meeting in New Orleans. A speaker who had just concluded his paper was taking audience questions. A member of the audience, after complimenting the speaker on his presentation, added the comment "I recall George Binczewski giving that same paper (movie and all) thirty five years ago." A somewhat astonishing sequence of events followed.

There were several post-session requests from attendees for a copy of that long-ago paper (were they thinking that a person would have such a 35 year old document along with him?). Immediately after the session, I casually mentioned these unusual requests to TMS Director of Partner Relations Trudi Dunlap, who was attending the TMS member service desk. She asked for the year and the paper title ("Simultaneously Casting of Alloy Composites"). Amazingly, within an hour she handed me a copy of that paper together with a CD which I could take to the commercial copy service down the hall and get all the copies I wanted. WOW! Talk about service and immediacy. Too

many of our members do not yet realize the TMS resources available to them, literally at their fingertips.

The commenter at the meeting, Dr. Neil Bryson, head of Alcan International Casting Research (retired), had a good basis for his remark. He himself had presented one of only four cast shop papers at that 1972 TMS Annual Meeting in San Francisco. This was only the second session after the meager 1971 program inaugural in New York. That was a difficult period which preceded Warren Petersen's early extended efforts to get program recognition for establishing the annual meeting Cast Shop Technology subject category. We struggled and pleaded to convince potential authors to commit to a paper presentation. Petersen's early persistence and vision is best exemplified by the historical fact that the Cast Shop sessions have evolved into the most popular at the annual meeting.

During the 25 year period, 1945–1970, under the auspices of the AIME, the precursor to the TMS, the total number of cast shop papers was less than ten. After the formal program inaugural in 1971, the next 25 year period, 1971–1995, there were a total of 610 papers presented and published. The following period, 1996–2009, yields an additional 837 cast shop paper presentations for a grand total to date of 1,447. The 53 cast

shop technology papers scheduled for the TMS 2009 Annual Meeting attest to the continuing interest in this aluminum production topic.

The TMS cast shop presentations and publications have become a tremendous resource for all phases of the industry, especially when we consider that such recorded references were comparatively non-existent prior to 1970.

More importantly, the virtual instant accessibility of these references through the TMS on-line service is somewhat overwhelming!

**George J. Binczewski**  
*Retired*

### CORRECTION

Dear Editor:

The authors of "Advances in the Manufacturing, Types, and Applications of Biosensors" [*JOM*, 59 (12) (2007), pp. 37–43] sincerely regret their oversight in not citing an extremely important reference of a review article—"Advanced Bioreporter Technologies for Targeted Sensing of Chemical and Biological Agents" by Steven Ripp and Gary S. Sayler ([www.ceb.utk.edu/bioprimer.pdf](http://www.ceb.utk.edu/bioprimer.pdf)).

The authors apologize for their oversight.

**N.M. Ravindra et al.**  
*New Jersey Institute of Technology*

### RECENTLY REVIEWED BOOKS

Available Only at *JOM* On-Line

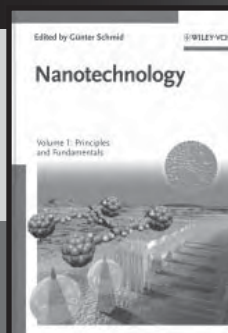
The following materials science and engineering publications have recently been reviewed by *JOM* readers. To read the reviews, or to become a *JOM* book reviewer, visit the *JOM* web site and click the Book Review link (under Complimentary On-Line Content). All book reviews are published exclusively on the *JOM* web site.

#### Macromolecules Containing Metal and Metal-Like Elements, Volume 8, Boron-Containing Particles

Alaa S. Abd-El-Aziz, Charles E. Carraher, Jr., Charles U. Pittman, Jr., and Martel Zeldin, editors  
ISBN 978-0-471-73012-5. John Wiley & Sons, Inc., Hoboken, New Jersey. 2007.  
Hardcover. 206 pages. \$150.00. Reviewed by: Pritish Kar

#### Nanotechnology—Volume 1: Principles and Fundamentals

Günter Schmid, editor  
ISBN 978-3-527-31732-5. Wiley-VCH, Weinheim, Germany. 2008.  
Hardcover. 300 pages. \$215.00. Reviewed by: Waseem Haider



Read them on-line at:  
[www.tms.org/jom.html](http://www.tms.org/jom.html)  
Click on Book Reviews



## **TMS Lends a Helping Hand in Challenging Economic Times**

As the economic crisis continues to ride heavy on the shoulders of professionals across the globe, even materials scientists and engineers might need some help advancing their careers. TMS undertook new initiatives in December 2008 to provide both practical and moral support to its members as they weather the current economic storm.

The first of the new initiatives that was implemented is the Job and Financial Security Digital Resource Center. A feature of the Members-Only web site, the resource center provides career and financial support in two sections, Employment Search and Security and Financial Planning and Management.

The Employment Search and Security section has nearly 100 resources spread over six topics. The topics are:

- **Enhancing Employability**—The topic consists of resources on developing the qualities beyond technical competence that are valued by employers
  - **Job Transition Resources**—Information gateways, portals, and sources to help get the job search started can be found under this topic
  - **Job Posting Boards**—An annotated directory of job listing and resume posting services, many geared to science and engineering careers, can be located in this topic
  - **Job Search Tool Kit**—The topic is a compendium of practical resources on resume writing, interview techniques, networking, and other job search skills
  - **Search and Legal Information**—Members can access resources on employment rights and legal protections
  - **Career Counseling, Advice, and Coaching**—People and services who can address employment-specific questions and concerns can be accessed under this topic
- The Financial Planning and Manag-

ment section marries three economic topics—long-term, short-term, and immediate financial actions. TMS members can gain access to information ranging from retirement planning to debt management, contingency planning, and saving for the future.

The four topics in this section are:

- **Planning for Life Events**—Resources are available for helping to save for retirement or college expenses.
- **Personal Finance**—The topic consists of tools and resources to maintain sound financial footing.
- **Investment Insights**—Information gateways with answers to common investment questions and concerns can be found under this topic.
- **Breaking News and Information**—Members can access financial news sources that provide up-to-date information on changes in the economy.

In addition to the Digital Resource Center, TMS has introduced “Ask the Human Resources and Benefits Expert,” where members can obtain answers to questions about human resources and benefits. This new feature enables members to e-mail questions that they might be uncomfortable asking at their workplace to the society’s human resources staff. The questions and answers will be posted on a members-only discussion board, with the identity of the member who posed the question protected. TMS has also joined a multi-society study that is being conducted by the American Society of Association Executives and The Center for Association Leadership in order to research how the economy is affecting its members. The results will allow TMS to develop targeted tactics to support its members better.

If any member has a question about the initiatives or would like to suggest possible changes, either log-in to the Discussion Board at <http://discussions.tms.org> where you can post comments and questions in the TMS Presidential and Executive Blog and Podcast Zone or contact TMS Executive Director Warren Hunt at [whunt@tms.org](mailto:whunt@tms.org).

## **TMS 2009 Annual Meeting Looks To Be Largest in History**

The TMS 2009 Annual Meeting to be held in San Francisco, California, February 15–19, is shaping up to be stronger than ever. With nearly 3,200 abstract submissions, the Annual Meeting is on track to be the largest in society history.

Despite difficult economic conditions, TMS has seen a positive response to the initiatives that were put in place to ensure a successful meeting. With over a month until the Annual Meeting commences, TMS encourages members to take advantage of these initiatives.

For the first time, a corporate rate is being offered. The discounted rate was implemented to help companies fit the cost of attending the Annual Meeting into their budgets. Employers who register five or more attendees from their company are able to receive the discounted rate of \$410 per person. Individual attendees can also receive a discounted rate if registered prior to the January 16 pre-registration deadline. After January 16, the rate will increase by \$100.

Also new this year, the Annual Meeting will offer attendees a chance to further their careers at the TMS Employer Pavilion, where they can speak face-to-face with potential employers from a variety of companies, universities, and national laboratories. A job board will also be available.

Finally, the TMS 2009 Annual Meeting web site has been redesigned to provide timely updates, detailed descriptions of symposia, networking events, and student activities, an opportunity to register, and a complete list of exhibitors.

For more information on the corporate rate, how to register, or to browse technical programs and more, visit [www.tms.org/Meetings/Annual-09/AM09home.aspx](http://www.tms.org/Meetings/Annual-09/AM09home.aspx).

## **Continuing Down the Green Path**

Materials scientists, engineers, educational professionals, and others attend-

## Metallurgraphics

### *The Creativity in Carbon Nanotubes*

From the collaboration of millions of carbon nanotubes (CNTs) standing vertically like a forest of trees extends the image of United States President-elect Barack Obama. Too small to see with the naked eye, the miniature faces were engineered from an idea that basically just “sounded cool.” That “cool” idea came to be known as the nanobama.

The image of nearly a dozen nanobamas placed in no particular pattern is just one of many images that University of Michigan Assistant Professor A. John Hart engineered, photographed with optical and electron microscopes, and displayed on the World Wide Web just prior to the United States’ November election. Hart’s idea of combining science and art has driven more than 100,000 people to his web site, [www.nanobama.com](http://www.nanobama.com), to view the images (Figure 1).

“The number one reason why we created the nanobama was because we thought people would enjoy it,” Hart said. “I would hope that demonstrations like this are useful in ways that bring concepts of new science and technology to a broader audience.”

Hart, along with Michael DeVolder, a post-doctoral fellow, and Sameh Tawfik, a doctoral candidate, both at the University of Michigan, and Will Walker, an artist, created the nanobama by converting Shepard Fairey’s image of Obama into a line drawing. The drawing was later shrunk into a smaller image

so it could be printed on a glass plate using a laser system. Using photolithography, a thin layer of photosensitive polymer on a silicon wafer was patterned. The wafer was coated with a thin layer of catalyst nanoparticle “seeds” for growth and the polymer was removed leaving the catalyst seeds in nanobama patterns. The nanobamas were grown when the wafer was placed in a high-temperature furnace and filled with a hydrocarbon gas.

Carbon nanotubes are tiny hollow cylinders that are stronger and stiffer than steel. They have a diameter that is tens of thousands of times smaller than a human hair.

Since the scientifically engineered images of Obama hit the Internet, Hart has been overwhelmed with media requests. His work has appeared in newspapers, magazines, and journals around the world. Hart sees the overwhelming interest in the miniature creations as a way to disseminate information on what small-scale science and technology can do. So far, no one from the Obama campaign has knocked on his door. But if they do, he would be happy to hear from them.

In 2003, Hart began working with CNTs as a doctoral student at Massachusetts Institute of Technology. It was during that time that he had encountered many unique images that prompted him to begin photographing his research. However, it wasn’t until three years later that Hart decided to share his collection of images with the world via [www.nanobliss.com](http://www.nanobliss.com), a Web site dedicated to his images taken through the lens of a microscope.

(Another of Hart’s works, “Parting,” is on the cover of this month’s issue.)

The Web site is broken down into categories that exhibit images that were formed through specific techniques. Figures 2, 6, and 8 were formed when carbon nanotubes were grown upward from a silicon substrate of a patterned catalyst. They can be viewed in the Nanotube Architectures section of the Web site. The Silicon Crystals section of the Web site contains images that were formed with the re-solidification of silicon wafers. The wafers were first melted by resistive heating. Those images include Figures 3, 5, 7, 9, and 10. The intricate shape of Figure 4 was developed when images were digitally stitched from several frames exceeding the normal field of view of an electron microscope.

“Most of the first nanobliss pictures happened when experiments didn’t go as planned, but the nanotube structures were more beautiful under the microscope” he said. “I began photographing them after I realized I could build a unique collection of images. Later, when I would see something visually, yet not scientifically, interesting I would still stop and take a picture of it.”

Hart hopes to continue the success of the nanobama through the visual expressions that connect nanotechnology to a broader audience.

“Plus, just having fun with things like this maintains a creative research culture,” he said. “This is no substitute for serious science but it is great to do both.”

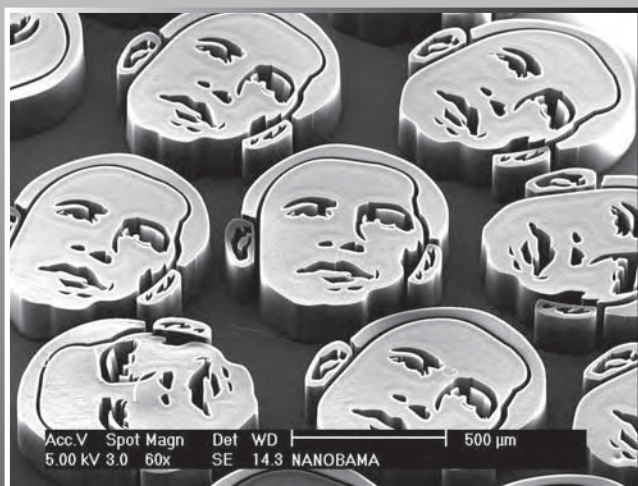


Figure 1. *Nanobama*. Nearly a dozen microscopic nanobama images were grown using a high-temperature furnace filled with hydrocarbon gas.

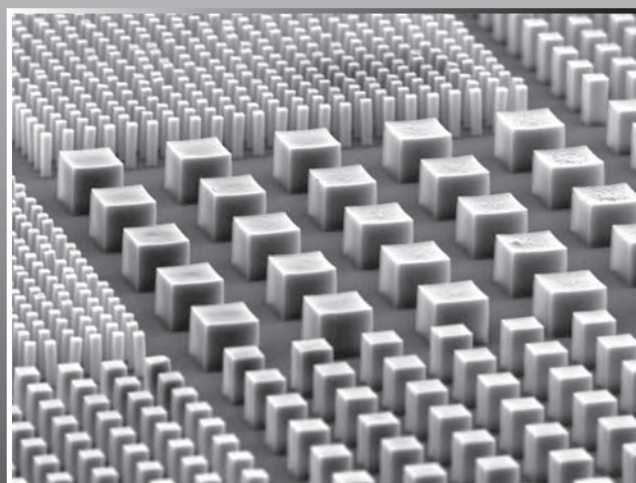


Figure 2. *Metropolis*. Carbon nanotubes were grown upward from a silicon substrate of a patterned catalyst to form this image of perfectly stacked columns resembling city blocks of buildings. The same technique was used in Figures 6 and 8.

\*All images courtesy of A. John Hart.

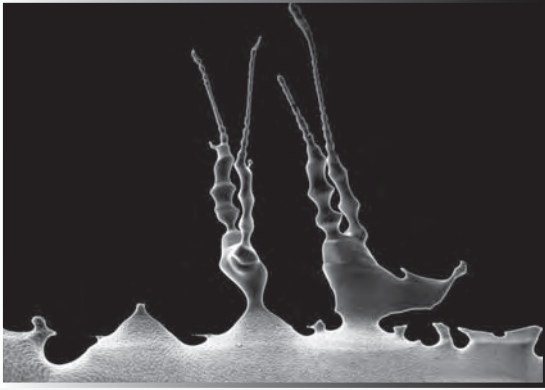


Figure 3. *Ballerina*. Figures 5, 7, 9, and 10 were formed with the re-solidification of the silicon wafers consisting of catalyst nanoparticle “seeds.” The silicon wafer was first melted by resistive heating.

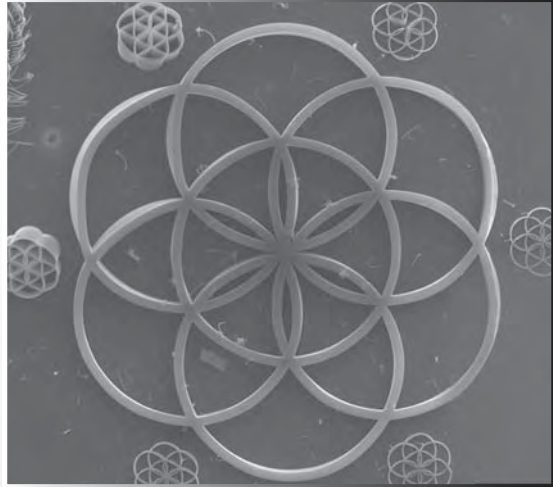


Figure 4. *Seed of Life*. The intricate shape of the image’s structure was grown by chemical vapor deposition on silicon substrate. The image was then digitally stitched from several frames exceeding the normal field of view of the scanning electron microscope. (Image by A. John Hart, Ryan Wartena, Felice Frankel, and Michael Cohen).

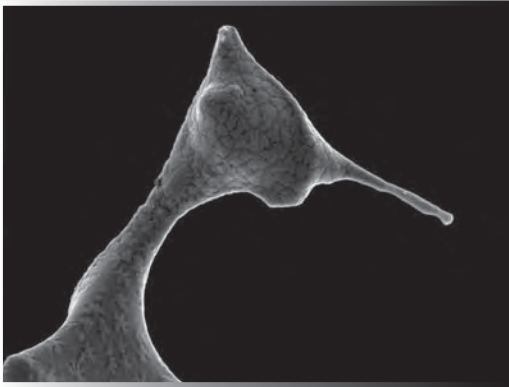


Figure 5. *Hummingbird*.

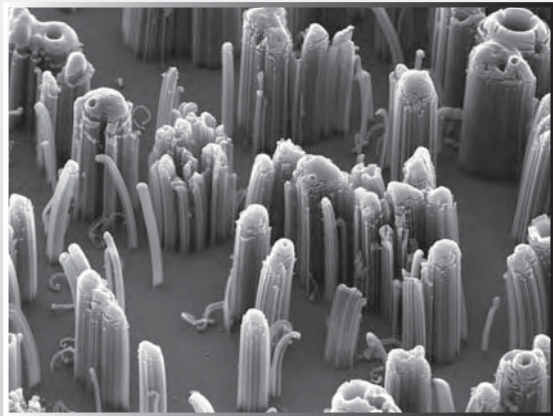


Figure 6. *Field*.



Figure 7. *Dinosaur*.

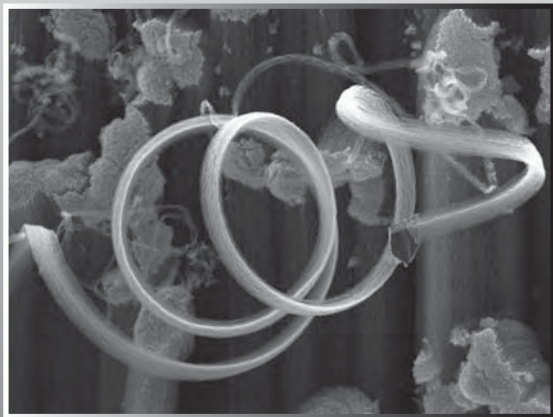


Figure 8. *Loop*.

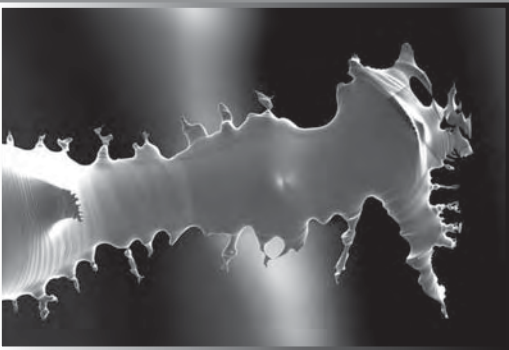


Figure 9. *Sawtooth*.

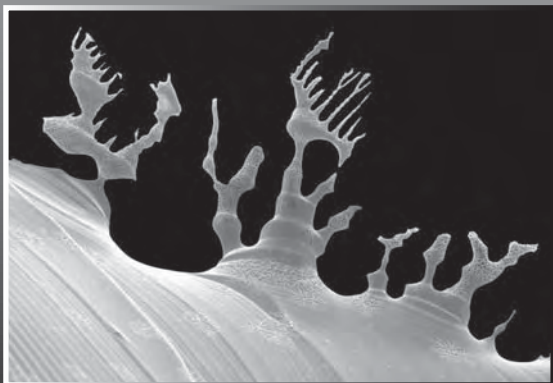


Figure 10. *Candle*. (Image by A. John Hart and Ryan Wartena).

**Aker Solutions:** Aker Solutions (Lysaker, Norway) signed a letter of intent with StatoilHydro to enter into an agreement for the delivery of drilling equipment and related operation services. The agreement will put Aker Solutions among the preferred suppliers of drilling equipment and operational services to StatoilHydro operated fields. The agreement for the delivery of Aker

ing the TMS 2009 Annual Meeting can expect to see more in the way of being green. As TMS continues to make strides to eliminate waste, recycle, and conserve energy, additional initiatives are planned to ensure the Annual Meeting continues to be green.

Those initiatives are:

- Advanced registration is now completely electronic. No printed forms were mailed to TMS members.
- The final technical program will be available to all attendees as a PDF download on the TMS 2009 Annual Meeting homepage and electronically through the TMS Personal Conference Scheduler.
- Collected proceedings will be on CD-ROM.
- TMS has replaced the plastic bags received at registration with reusable canvas bags for full-conference attendees.
- Recycling containers will be placed throughout the convention center for bottles, cans, and paper, and will be available at the close of the meeting for attendees to recycle their badge holders and final programs.
- The on-site *Today* newsletter will only be available electronically.
- Shuttles have been eliminated due to all hotels being within walking distance to the convention center.
- The Hands On Bay Area community service project on February 14 will bring volunteers together to plant an organic garden for less fortunate Bay Area families.
- The Materials and Society technical symposia addresses energy, environmental, and sustainable issues.

In addition to the efforts TMS is taking to ensure a green conference, the facilities and professional businesses that the society has chosen to work with also are implementing green initiatives. For more than a decade, the Moscone West Convention Center has recycled a variety of materials, including foam signage, vinyl banners, cardboard, and scrap metal. The TMS headquarters hotel, the San Francisco Marriott, donates more than 30,000 pounds of food leftovers annually to local nonprofit organizations. Step outside of the convention center and you can hail a hybrid taxi.

To learn more about the green initiatives that TMS and its associates plan to

Solutions drilling equipment is awarded for a three year period with an optional period and for operational services, five years.

**Alcoa Automotive Wheels:** Alcoa Automotive Wheels, a division of Alcoa Wheel and Transportation Products (Cleveland, Ohio), announced that it has been awarded platform placement of Dura-bright® technology wheels with Chrysler LLC's Street and Racing Technology (SRT) engineering organization. Two new wheels within the Chrysler SRT family, including both Dodge and Jeep platforms, will begin placement with the 2009 model year.

**Ausmelt Limited:** Ausmelt Limited (Dandenong, Australia) signed a licensing agreement with Korea Zinc Co. Ltd. for the construction of two new top submerged lance technology furnaces for lead smelting, which will be built at Korea Zinc's production facilities in Onsan, Korea. They will recover lead from up to 70,000 tonnes per annum of lead-bearing materials, including lead secondaries.

**Evonik Industries:** Evonik Industries (Essen, Germany) signed a contract for the sale of its United States and Canadian cyanide activities with Oaktree Capital Management. The cyanide business constitutes a part of the CyPlus Group owned by Evonik. The transaction is subject to approval by the regulatory authorities. It is comprised of CyPlus Group's business in the United States and Canada dedicated to the gold-mining industry.

**Outotec Oyj:** Outotec Oyj (Espoo, Finland) signed a major contract with ZAO Miheevsky GOK, a subsidiary of Russian Copper Company, for the design and delivery of a new copper concentrator plant for the Miheevsky porphyry-copper project located in Chelyabinsk, Russia. The contract exceeds 175 million Euros. Outotec's scope of delivery covers engineering for the whole concentrator plant, supply of major process equipment in six delivery packages, spare parts, and training, as well as site supervision services for installation and start-up. The equipment deliveries will take place during 2010 and 2011. The Miheevsky concentrator plant is planned to treat annually 20 million tons of copper ore and is expected to be commissioned in early 2012.

**SMS Demag:** SMS Demag (Dusseldorf, Germany), a company of the SMS group, together with Elex AG jointly founded a new company, SMS ELEX AG, on October 1, 2008. The new company will be headquartered in Schwerzenbach, Switzerland. SMS ELEX AG will produce a new generation of filter systems for cleaning flue gas in steelworks. The new company will also be focusing on the development of new flue-gas cleaning technologies for steelmaking.

**SMS Meer:** SMS Meer (Mönchengladbach, Germany), a company of the SMS group, received an order from the world's largest steel group, ArcelorMittal, for the supply of a PQF seamless tube plant. The seamless tube mill operating on the premium quality finishing (PQF®) principle has an annual capacity of 600,000 tonnes. It will be used predominantly for the production of oil country tubular goods tubes in the size range from 4½" to 16". The plant will be erected in Jubail Industrial City, north of Al Jubail on the Persian Gulf, and is scheduled to go into production in the second half of 2010.

**ThyssenKrupp Titanium:** ThyssenKrupp Titanium (Essen, Germany) started the operation of an electron beam furnace in Essen. The new unit was officially inaugurated in October. The electron beam furnace, housed in a dedicated new shop in Essen, represents the state-of-the-art in melting technology, and significantly increases ThyssenKrupp Titanium's melting capacities for titanium ingots. Due to its low weight, outstanding corrosion resistance, and high strength, titanium is in great demand. Its main uses are in the aerospace industry, including in the new Airbus A 380 and Boeing Dreamliner super jumbos. It is also used in the chemical plant construction sector, heat exchangers for power plants, seawater desalination plants, shipbuilding, offshore equipment and medical engineering.

take at the Annual Meeting, visit the Go Green! section of the TMS 2009 Annual Meeting web site at [www.tms.org/Meetings/Annual-09/gogreen.aspx](http://www.tms.org/Meetings/Annual-09/gogreen.aspx).

## Dubai Welcomes TMS

Materials scientists and engineers from across the globe came together October 19–22 to gain knowledge on the theory and practice of primary aluminum production. Nearly 60 attendees from the United Arab Emirates, Oman, Qatar, Iran, South Korea, India, England, Slovakia, Canada, and the United States participated in Industrial Aluminum Electrolysis 2008 in Dubai, United Arab Emirates (Figure 11).

The Middle East is an area that is new to TMS programming. By sponsoring the course there, TMS has opened doors to the exchange of information and ideas with a new population of professionals.

The feedback and enthusiasm from many of the attendees proved the society's exposure was overwhelmingly positive. TMS member Jim Yurko attended the course and was impressed with its outcome. "This was the first TMS course I have attended and the class exceeded my expectations," he said. "I was very impressed by TMS's ability to organize a meeting so far away." Halvor Kvande, a TMS member and the lead instructor of the course, believes it was a success for being only the second time in TMS history it was conducted outside of the United States. "It was a big step to go outside of North America and all the way to the Middle East," he said. "The attendees' evaluation scores support the impression that the course was

a success."

The course, sponsored by the TMS Light Metals Division, was designed to promote more efficient operations of aluminum smelters and to stimulate corresponding research and development. Topics that were covered included alumina quality and solubility; CO<sub>2</sub> emissions and climate change; fluoride emissions; magnetohydrodynamics; and potroom inspection items. The course will return to the United States in 2009.

## A New "Green" For Grass

Metabolix, a Cambridge, Massachusetts, biotechnology firm, has devised a way to make grass even greener. As reported in the December issue of *Popular Science*, researchers at the company have successfully developed a process for manufacturing bioplastic by growing it in the leaves of genetically engineered switchgrass. Known as polyhydroxybutyrate (PHA) and marketed under the brand Mirel, the bioplastic offers a highly biodegradable alternative to petroleum plastics, while also requiring less energy for its manufacture.

The details of Metabolix's completed greenhouse trials are described in the paper, "Production of Polyhydroxybutyrate in Switchgrass, a Value-Added Coproduct in an Important Lignocellulosic Biomass Crop," published recently in *Plant Biotechnology Journal*.

The process involves splicing bacterial genes into the DNA of the switchgrass, causing the plant to form granules of plastic within its leaves. The plastic can then be culled and turned into pellets for production, while the residual biomass

can be processed into biofuel. According to a Metabolix statement released on this new development, "This result validates the prospect for economic production of PHA polymer in switchgrass, and demonstrates for the first time an important tool for enhancing switchgrass for value-added performance as a bioenergy crop."

Switchgrass is a native prairie grass that can be grown quickly and in abundance in the United States. It has been identified by the U.S. Department of Energy as a prime feedstock for producing next generation biofuels and bio-products.

*This article first appeared in the Materials and Society section of the Materials Technology@TMS web site.*

## A 4-D Glimpse of the Nanoworld

Real-time, real-space visualizations of the fleeting changes in the structure and shape of matter on the atomic scale are now possible with a new technology developed at the California Institute of Technology (Caltech) in Pasadena. The breakthrough, dubbed four-dimensional (4-D) electron microscopy, was de-



**NETZSCH**

**Instruments & Testing Services**

**Thermal Analysis**

- Classical & High Temperature DSC, TGA & more
- Real DSC-TGA with FTIR & MS

**Conductivity & Flash Diffusivity**

- Tabletop Systems to 1100 °C

**Dilatometers**

- CTE to 2800 °C
- Sintering Optimization

**Contract Testing Services**

- Fully Equipped & Accredited

NETZSCH Instruments, Inc.  
37 North Ave.  
Burlington, MA 01803  
Call (781) 272-5353  
Fax (781) 272-5225  
e-mail: [at@nib.netzsch.us](mailto:at@nib.netzsch.us)

[www.e-Thermal.com](http://www.e-Thermal.com)



Figure 11. Nearly 60 materials scientists and engineers from ten countries came together to participate in Industrial Aluminum Electrolysis 2008 in Dubai, United Arab Emirates.



## WASHINGTON NEWS

From Betsy Houston,  
Federation of Materials Societies

### Transition "Innovation Agenda"

**Team:** On November 26, 2008, President-elect Barack Obama named members of his transition's Technology, Innovation, and Government Reform Policy Working Group to develop proposals to implement his Innovation Agenda. According to the Agenda, the new Administration will work to "create a 21st century government that is more open and effective;

leverage technology to grow the economy, create jobs, and solve our country's most pressing problems; respect the integrity of and renew our commitment to science; and catalyze active citizenship and partnerships in shared governance with civil society institutions." The Working Group is organized into four sub-teams: Innovation and Government; Innovation and National Priorities; Innovation and Science; and Innovation and Civil Society. The co-chairs are Blair Levin, a telecommunications lawyer who served as chief of staff to the chairman of the Federal Communications Commission (FCC) during the Clinton Administration; Sonal Shah, an economist who heads Google.org's global development efforts; and Julius Genachowski, a lawyer who is co-founder of Rock Creek Ventures and LaunchBox Digital, served as chief counsel to the FCC chairman during the early years of the Clinton Administration, and worked for then-Representative Charles Schumer (D-NY) in the mid-1980s. Members of the Working Group are Howard Buffet, David Burd, Dan Chenok, Aneesh Chopra, Jack Chorowsky, Cheryl Dorsey, Joshua Dubois, Judy Estrin, Tom Freeman, Jim Halpert, Mark Johnson, Michele Jolin, Tom Kalil, Kei Koizumi, Vivek Kundra, Don Lamb, John Leibovitz, Bruce McConnell, Andrew McLaughlin, Parry Norling, Beth Novacek, Spencer Overton, Lori Perine, Kartik Raghavan, Alec Ross, Paul Schmitz, Clifford Sloan, Steve Spinner, Marta Urquilla, Chris Warren, Daniel Weitzner, and Irving Wladawsky-Berger.

**Nobel Physicist Nominated as Energy Secretary:** The nomination of Dr. Steven Chu, director of Lawrence Berkeley Laboratory, as Secretary of Energy is being welcomed by the science and engineering community in Washington, D.C. Dr. Chu, who holds a Nobel Prize in physics, has testified before Congress on behalf of doubling research funding through the Department of Energy's Office of Science and in other agencies.

**Committee to Push ARPA-E in New Congress:** In response to a recently released *World Energy Outlook 2008* by the International Energy Agency, House Science, and Technology Committee Chairman Bart Gordon (D-TN) has signaled his determination to push next year for appropriations for the Advanced Research Projects Agency for Energy (ARPA-E) which has been signed into law but not funded. "The 2008 World Energy Outlook projects that worldwide, we will need more than \$26 trillion in new energy investment by 2030 just to meet demand," Gordon said. "One step we must take is to establish ARPA-E . . . a new agency at the Department of Energy that will pursue high-risk, high-reward energy technology development," he continued. "The question isn't if we can afford to do this research in the current economic climate."

**Nanotech Safety Concerns:** Two reports issued in December 2008 by the National Science Foundation (NSF) and one by the National Academies' National Research Council raise concerns about safety and public acceptance issues surrounding nanotechnology. NSF-sponsored researchers at Yale University found that "when people learn about this novel technology they become sharply divided along cultural lines." A separate study led by researchers at the University of Wisconsin-Madison and Arizona State University says nanotechnology "seems to be failing the moral litmus test of religion." The National Research Council concluded that an effective national plan for identifying and managing potential risks is essential to the acceptance of nanotechnology-enabled products. The Council committee determined that the current research plan, developed by the National Nanotechnology Initiative, does not provide a clear understanding of these risks or where the plan should be in 10 years, and federal funding to address nanotechnology-related environmental health and safety issues may be inadequate. House Science and Technology Committee Chairman Bart Gordon's (D-TN) panel developed legislation that would address many of these concerns. It would require the development of an environmental, health, and safety (EHS) plan that specifies near-term goals; identifies multi-year funding requirements for each goal; specifies responsibilities for each participating agency; and requires annual reassessments of progress.

scribed in two papers published in November 2008, along with "movies" made with the new technique of atomic changes in gold and graphite.

Scientists now can observe the static structure of objects with a resolution that is better than a billionth of a meter in length using electron microscopes, which generate a stream of individual electrons that scatter off objects to produce an image. The Caltech researchers have taken this technology to a new level by introducing the "fourth dimension" of time into high-resolution electron microscopy. They have accomplished this by precisely controlling every electron trajectory in time and space, so that the electrons arrive at the sample at specific time intervals. The resulting image produced by each electron represents a femtosecond still at that moment in time. Like the frames in a film, the sequential images generated by many millions of such images can be assembled into a digital movie of motion at the atomic scale.

"4D Imaging of Transient Structures and Morphologies in Ultrafast Electron Microscopy," published in the November 21 issue of *Science*, reported the application of 4-D electron microscopy to observe the behavior of atoms in super-thin sheets of gold and graphite. Researchers found that on a slightly longer, picosecond scale, the graphite nanosheets produce sound waves. In the images, they directly visualized the elastic movements of the sheets and determined the force holding them together, which is described by a stress-strain property known as "Young's modulus." The 4-D movies produced from the frames revealed the behavior in space and time.

In a second paper, "Nanoscale Mechanical Drumming Visualized by 4D Electron Microscopy," published in the November 2008 issue of *Nano Letters*, the Caltech researchers described their visualization of the changes in a nanometer-thick graphite membrane on a longer time scale, up to a thousandth of a second. The researchers first blasted the sample with a pulse of heat. The heated carbon atoms began to vibrate in a random, nonsynchronized fashion. Over time, however, the oscillations of the individual atoms became synchronized as different modes of the material locked in phase, emerging to become a

heartbeat-like “drumming.” Digital video, slowed down more than a billion times, illustrates this nano-drumming mechanical phenomenon, which displays a well-defined resonance that is nearly 100 times greater than can be detected by the human eardrum.

The Caltech researchers have now turned their attention to imaging the components of cells, such as proteins and ribosomes. They have already produced images of a stained rat cell and, more recently, of a protein crystal and cell in vitreous water. Their goal is to enhance the structural resolution in the images of these biomaterials by taking single-pulse snapshots before they move or deteriorate, enabling documentation of their dynamics in real time.

*This article first appeared in the Emerging Materials Technology section of the Materials Technology@TMS web site.*

### A Riveting Innovation

A new joining process suitable for polymer-metal hybrid joints has been developed by researchers at the Institute of Materials Research, GKSS Research Centre in Geesthacht, Germany. Known as friction riveting, the new technology represents an enhancement of friction stir welding of metallic alloys. Friction stir welding involves pressing a non-consumable cylindrical tool with great force into two sheets of material lying next to each other and moving the tool along the weld line. The material is heated and stirred by the friction created by the tool’s rotation, enabling the sheets to be joined.

Friction riveting produces spot connections when a rapidly rotating stud, or

rivet, is pressed onto the surface of one of the sheets, usually a thermoplastic material or lightweight alloy. In the initial phase of the process, the pin penetrates the material and a thin layer of molten plastic forms, which acts as an adhesive after the joint consolidates.

As the rivet forces its way deeper into the material, the temperature increases and the tip of the pin spreads out to a wider diameter than the original rivet. This securely fixes the pin within the material (Figure 12).

According to a November 12, 2008, statement from GKSS, the new technology is a more reliable, cost-efficient, and environmentally benign alternative to conventional processes for joining multi-material structures. Generally, these materials are adhesively bonded or mechanically fastened, which requires surface preparation generating chemical emissions and waste. Friction riveting, on the other hand, does not produce harmful emissions typically associated with fusion welding. Friction riveting also addresses the mechanical performance issue created by mechanically fastened joints which typically experience increased stress concentrations associated with the hole placed in the joint area.

The GKSS statement said the new joining process would be particularly applicable to the transportation and aircraft manufacturing industries, in which polymer-metal hybrid structures are becoming more prevalent as a means to reduce weight.

*This article first appeared in the Establishing Materials Technology section of the Materials Technology@TMS web site.*

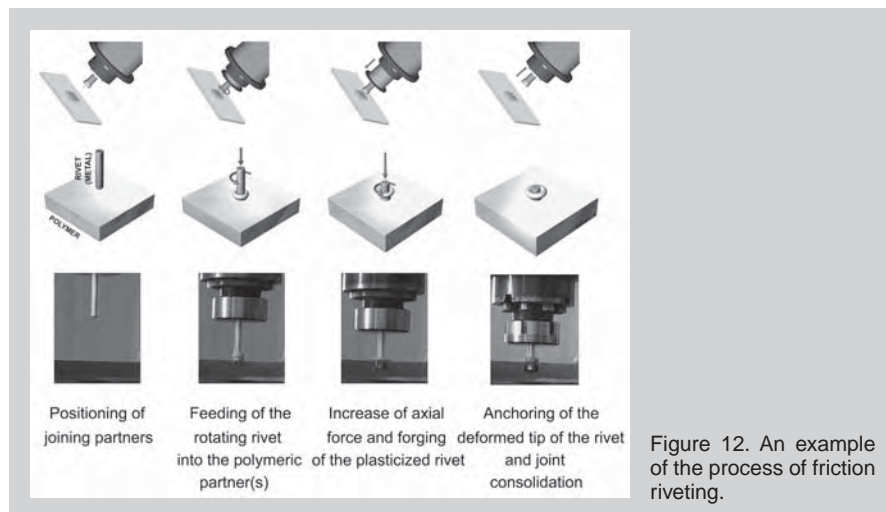


Figure 12. An example of the process of friction riveting.



### Dance Your Ph.D.



Watch as graduate and post-doctoral students, and professors interpret their Ph.D. theses in dance form in the 2009 AAAS/Science Dance Contest. <http://gonzolabs.org/dance/contestants>

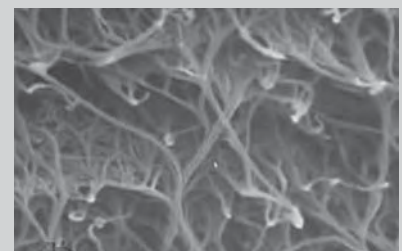
### A Rubbery Future



Richard Claus, a professor at Virginia Polytechnic Institute and State University and president of NanoSonic Inc., explains how metal rubber could shape the future of commercial aircraft.

<http://videos.howstuffworks.com/sciencentral/2938-metal-rubber-video.htm>

### Buckypaper: Silly Name, Strong Intentions



Researchers at Florida State University in Tallahassee explain how this super strong material could change the way products are engineered. Buckypaper is made from carbon nanotubes like those shown in the images on pages 6 and 7.

<http://www.mefedia.com/entry/future-planes-cars-may-be-made-of-buckypaper/11928662>



*Updates on friends and colleagues in the materials community*

## **Society Governance Changes with Member Ratification of New Bylaws**

TMS members ratified a new set of society bylaws in mid-November. The society operates under a core set of bylaws, which are voted on and approved by TMS members. The new bylaws went into effect November 17, 2008.

The TMS Board of Directors approved the bylaws on July 25, 2008, sending them on to the members for ratification. Here are a few of the key recommendations that the ad hoc Committee on Governance, in addition to the creation of new bylaws, submitted for approval:

- Have the TMS Executive Committee work with the Administrative and Technical committees to update their policies and bring

them into alignment with the new governance requirements and the bylaws.

- Create new policies that address the need for more transparent processes and re-emphasize the central role of the Board of Directors.
- Create a new Executive Committee policy that defines the construction and role of the committee and establishes it as a resource to the Board of Directors.
- Create a new Nominating Committee policy that identifies Board of Director nominees for director positions.
- Create and implement a Docu-

ment Retention and Destruction policy.

In March 2008, TMS President Diran Apelian commissioned the ad hoc Committee on Governance to review the previous TMS bylaws, administrative and policy manuals, other documents, and the practices and procedures for consistency, clarity, and to ensure accuracy of all documents. He was prompted to take action due to the Sarbanes-Oxley Act, changes in the Pennsylvania state law, and a 10-year hiatus from bylaw revisions.

To view the new TMS bylaws, visit the Society Governance section of the TMS homepage at [www.tms.org/society/bylaws.aspx](http://www.tms.org/society/bylaws.aspx).

### **TMS MEMBER RECEIVES THE NATIONAL MATERIALS ADVANCEMENT AWARD**

TMS Fellow Siegfried Hecker received the 2008 National Materials Advancement Award from the Federation of Materials Societies. He is a professor in the Department of Management Science and Engineering at Stanford University, in addition to serving as co-director of the university's Center for International Security and Cooperation and emeritus director of the Los Alamos National Laboratory.

The National Materials Advancement Award recognizes individuals who have demonstrated outstanding capabilities and contributions in advancing the multi-disciplinary field of materials science and engineering; the effective and economic use of materials in the marketplace and the application of materials developments to national problems and defense; and the development and implementation of national policy which furthers the impact of materials sciences and engineering on our society.

Hecker has been a member of TMS since 1964. He was scheduled to receive the award in Washington, D.C. in December.

## **Board Elevates Thirteen TMS Members**

On December 11, 2008, the Board of Directors voted to elevate 12 new members to Professional Member grade and another member to Junior Member grade.

Under the new bylaws, the Board of Directors is required to vote on the grade of membership a new member will be placed at.

The following new members were elevated from Non-Voting Members:

- **Bhabani Shanker Acharya:** Maputo, Mozambique; production supervisor, Mozal Sarl; Professional Member.
- **Laurent Cottignies:** Poisat, France; senior R&D engineer, Alcan CRV; Professional Member.
- **Dawn Janney:** Idaho Falls, Idaho; materials engineer, Idaho National Laboratory; Professional Member.
- **Rejin Koodakal:** Thun, Switzerland; post doctorate, EMPA; Junior Member.
- **Rick K. Lazarou:** Kentucky; chairman and chief executive officer, Lazar Anode Technologies, LLC; Professional Member.
- **Michael F. Lazorchak:** Saginaw, Michigan; sales engineer/account manager, B&P Process Equip-

ment; Professional Member.

- **Lindsay Malloy:** Ayer, Massachusetts; metallurgist, Riley Power Inc.; Professional Member.
- **Miguel Angel Neri:** Chihuahua, Mexico; researcher and professor, CIMAV, S.C. (Advanced Materials Research Center); Professional Member.
- **Irina Skripnik:** New York; regional director, i-Libra LLC; Professional Member.
- **Robert J. Smollack:** Montana; operations manager, Columbia Falls Aluminum Co.; Professional Member.
- **Marcio Douglas Soares:** Michigan; director of international business, Jervis B. Webb Co.; Professional Member.
- **Jürgen Timm:** Steisslingen, Germany; project leader, Novelis Switzerland SA; Professional Member.
- **Kristen L. Watson:** Owensboro, Kentucky; coordinator/liaison officer, Lazar Anode Technologies, LLC; Professional Member.

As new members are granted membership into TMS, the Board of Directors will vote on a monthly basis to elevate membership grades.





*TMS Member Profiles*

## Meet a Member: George “Rusty” Gray III, Beekeeper, Stained Glass Artisan

By Francine Garrone

It would be silly to think materials scientists and engineers do not use their scientific knowledge to master other tasks—even hobbies. George “Rusty” Gray III believes his stained glass work and beekeeping are just that—hobbies that benefit from his science and engineering background.

“It’s a hobby, although certainly many of my designs are geometrical and have a science theme,” he said of the intricate patterns on the stained glass lamps he designed. “And I approach all my hobbies as a scholarly project. I read all I can find on the subject and study the previous masters—like in science.”

Gray, a laboratory fellow at Los Alamos National Laboratory in Los Alamos, New Mexico, became fascinated with glass as a young boy. While in grade school, he collected antique bottles, canning jars, and old glass insulators. As he matured into an adult, Gray developed an interest in sculpture. “My dad taught art and drafting as a high school teacher,” he said. “He also did woodworking, remodeling, painting, and drawing—a spectrum of artistic media blended with engineering.”

The 2009 TMS vice-president, Gray became intrigued with stained glass after seeing beautiful lamps in a Pittsburgh, Pennsylvania, museum while working toward his Ph.D. at Carnegie Mellon University. Today, he has crafted a variety of stained glass hangings; jewelry boxes; a large window at the Kappa-Kappa-Gamma sorority house at Carnegie Mellon University; lamps; and gifts for family and friends.

Gray’s main focus, however, is stained glass lamps. Each one distinct, the lamps feature multi-flat-sided assemblages or designs built on forms such as cones. He has also designed complex three-dimensional designs on flat-sided lamps. Gray has incorporated sea shells found while camping in St. John, the United States Virgin Islands,

into his work, and obsidian slices cut from pieces he collected in the Jemez Mountains in Santa Fe, New Mexico.

Many of Gray’s lamps have 400 to 600 pieces that could take a hundred hours in total from design, cutting the glass, grinding the edges, and copper foiling (the technique popularized by “Tiffany” lamps).

Gray also developed an interest in beekeeping as a young man. It was not

his love for bees that brought him to the hobby, but his love for his wife, Altana, a third-generation beekeeper. However, Gray says there is plenty of science in beekeeping. “I read all I can about strategy to beekeeping management—I subscribe to a monthly beekeeping journal,” he said.

Gray began maintaining bee hives at his father-in-law’s home in New Jersey prior to his marriage. It was not until the mid-1990s that he obtained protective gear and bee hives to begin beekeeping at his residence. His engineering knowledge became useful when bears threatened his hives and a friend’s, which he helps maintain, in Paonia, Colorado. “The enclosure around the bee hives is powered by a deep cycle battery that is attached to a solar recharger as the bee yard is out in the orchard away from an electric source,” he said of his friend’s enclosure. “The sheet metal around the yard keeps the grass from shorting the fence and as I connected it to my grounding rod it also serves to provide a guaranteed ground right at the fence for any animal that touches it.”

Each year, Gray and his family harvest honey from the hives for cooking, to give as gifts, and to donate to their church and the United Way for auction.

“All of my hobbies are relaxing,” he said. “I am an engineer through and through—especially in my hobbies.”

To view more of Gray’s stained glass and beekeeping photos, visit the JOM Discussion Board at [iweb.tms.org/forum/default.aspx?forumid=26](http://iweb.tms.org/forum/default.aspx?forumid=26).



George “Rusty” Gray III handles a swarm while clothed in a full body beekeeper’s suit, veil, and protective gloves.



This stained glass lamp was made with sea shells found while camping with his family in St. John, United States Virgin Islands.

Each month, *JOM* will feature a TMS member and their activities outside the realm of materials science and engineering. If you have an interesting activity or know someone who does, contact Francine Garrone, *JOM* news editor, at [fgarrone@tms.org](mailto:fgarrone@tms.org).

# Human Assets: The Most Precious Capital

Diran Apelian

In the last few months we have witnessed a global economic downturn and concerns about the fiscal health of corporations. There is much talk about assets—both financial and capital. Yet, we hear very little about our most precious asset, our human assets.



The intellectual capital of the planet is the most critical asset that can address the serious issues we face. Yet, the \$700 billion Wall Street bailout was crafted in about two weeks, with Washington working around the clock to get things done. It is not only the size of the bailout that is of concern, but also the kinetics of the reaction on the Hill! The concern and the attention that we as a nation placed on our financial assets say much about our values.

Where is the urgency regarding our human asset? Why aren't we outraged about the education deficit and why do we value financial assets over human assets? To paraphrase and embellish an observation by Thomas Friedman, what we need is not just a bailout of our economy, but a buildup of our people.

One would think that education of our children would be the highest priority, in America and across the globe. Unfortunately, a close look at schools across the United States points out that we do not place a value on the most precious capital we have: our children. The resources we have channeled for educating the next generation is pitiful when we compare it to the resources we have allocated for defense, etc.

We need to invest in, nurture, and cultivate our human assets. The place to start is with our schools—primary

and secondary (K–12), as well as with higher education and research funding at our graduate schools. The 2007 National Academies Press publication *Rising Above the Gathering Storm* clearly pointed out that our economic security was in question because of the decline in investments in R&D budgets, as well as investments for the development of the intellectual capital of the nation. It is not surprising that economic security is directly coupled with human assets as well as the intellectual capital that we cherish and want.

Yet, in our major cities, and particularly the inner-city schools, we are wasting the opportunity to impact our future. Comparing K–12 teacher salaries to salaries in other sectors of society is not a good testament of our values. Imagine what would happen if starting annual salaries for mathematics, science, and English teachers were \$70,000. We need to ensure that our educational system is first rate, that we have the best facilities, the best-prepared teachers, and we need to be diligent in the outcomes we expect.

Muhammad Yunus and the Grameen Bank (a bank he founded) won the Nobel Peace Prize in 2006 for investing in people and reversing poverty in Bangladesh. It is a universal theme; investing in education is the most crucial investment we can make to fight poverty, to fight crime, and in brief to fight so many ills that have their roots in ignorance of the populace. I am reminded of a bumper sticker I saw at our university parking lot that read: "If you think education is expensive, try ignorance"

At the Metal Processing Institute, we are in touch with close to 100 corporations that are partners and consortium members. The one constant message we hear from these corporations is the

graying of the workforce and the concern as to where the next generation of knowledge workers will come from. Take the aerospace industry as an example. It is a powerful force within the U.S. economy and one of the nation's most competitive sectors in the global marketplace. It contributes over 15 percent to the gross domestic product and supports over 15 million high quality U.S. jobs. Aerospace products provide the largest trade surplus of any manufacturing sector. Yet only a handful of universities and centers in America are working on superalloys, structural materials, titanium, etc. Moreover, the funding in structural materials does not reflect the importance of the industry to the economy. Funding is needed to support these industries, and in turn to enable a generation of students to be educated in our graduate schools who will be our future knowledge workers.

Last, we need to get the message out that science and engineering education opens doors to a variety of career paths where one can make a world of difference. We need to all work in unison with one message that materials science and engineering (MSE) is an enabler to address societal challenges and that careers in MSE are exciting, wide-open opportunities, and in demand.

In closing, this is my last column in *JOM* as I finish my term as TMS president. I want to thank you for your support this past year. We have accomplished much and we will continue to do so under the leadership of Ray Peterson, who will be installed as our next president in San Francisco at our Annual Meeting (February 2009). See you all in San Francisco.

Diran Apelian is a professor in the Mechanical Engineering Department of Worcester Polytechnic Institute and the 2008 TMS President.

# JOM: Home of Award-Winning Papers

Papers published in *JOM* are automatically eligible for the following awards:

## EXTRACTION & PROCESSING DIVISION SCIENCE AWARD

**Sponsor:** Extraction & Processing Division

**Recognizes:** A paper, or series of closely related papers with at least one common author, that represents a notable contribution to the scientific understanding of extraction and processing metallurgy, with emphasis on nonferrous metals.

## EXTRACTION & PROCESSING DIVISION TECHNOLOGY AWARD

**Sponsor:** Extraction & Processing Division

**Recognizes:** A paper, or series of closely related papers with at least one common author, that represents a notable contribution to the advancement of the technology of extraction and processing metallurgy, with emphasis on nonferrous metals.

## LIGHT METALS DIVISION JOM BEST PAPER AWARD

**Sponsor:** Light Metals Division

**Recognizes:** The author(s) of a paper published in an issue of the preceding volume year of *JOM* under a light-metals related technical topic.



James W. Evans (left) receives the 2008 Light Metals Division *JOM* Best Paper Award from division chair Wolfgang A. Schneider (right) at the 2008 TMS Annual Meeting.

## STRUCTURAL MATERIALS DIVISION JOM BEST PAPER AWARD

**Sponsor:** Structural Materials Division

**Recognizes:** The author(s) of a paper published in an issue of the preceding volume year of *JOM* under a structural materials technical topic.

## ROSSITER W. RAYMOND MEMORIAL AWARD

**Sponsor:** The American Institute of Mining, Metallurgical, and Petroleum Engineers

**Recognizes:** The best single- or dual-authored, peer-approved or peer-reviewed paper published during the twelve months preceding May 1 where the lead author is a member of the American Institute of Mining, Metallurgical, and Petroleum Engineers, and under the age of 35.

## JOM READER POLL

To vote, go to [www.tms.org/jomsurvey.html](http://www.tms.org/jomsurvey.html).

### Last month's question:

The automobile industry is suffering in the current economic downturn and the U.S. government has been asked to help. What support should the United States offer to the Big 3 automakers?

### Last month's answers:

- A stopgap loan to keep them solvent 18.37%
- A grant, no strings attached 0%
- A grant conditioned on retooling for energy-efficient auto production 22.45%
- None—let the market forces prevail 53.06%
- Other 6.12%

### This month's question:

What is your favorite way to "go green"?

### This month's answers:

- Reducing my carbon footprint: I drive a hybrid or electric vehicle or use mass transportation consistently.
- Facilitating sustainability: I recycle bottles, cans, and paper even when it's not mandatory.
- Reducing waste: I only print documents when absolutely necessary.
- All of the above

# Polymer-Matrix Composites: New Fibers Offer New Possibilities

Sergio Neves Monteiro



If one class of material could represent the transition to the new millennium, it would be the polymer-matrix composite (PMC).

From missile components to golf clubs, an ever increasing number of products or specific devices are made of PMCs. Some are new developments, such as the carbon fiber composites in modern commercial aircraft. Others are beneficial to both our health and the environment. Typical examples are the aramid fiber composites replacing asbestos in automotive brakes and clutch linings, as well as recyclable coconut fiber composites substituting synthetic fibers in automobile seat cushions.

Polymer-matrix composites are normally composed of a matrix reinforced with a synthetic or natural fiber. The matrix acts as the intermediate by which an externally applied load is distributed to the stronger and stiffer fibers that structurally support the composite. It protects the fibers from outside chemical (or even atmospheric) attack and abrasion. The plasticity of the matrix serves as a barrier to crack nucleation/propagation, and as such prevents catastrophic rupture.

The real advantages in terms of flexibility and expanding potential for the PMC are the different fibers available. Glass fiber is the most popular owing to its low price, easy processing, high specific strength, and chemical inertness. Carbon fiber is the current preference for advanced structural composites. It is the stiffest and strongest of all fibers. Carbon fiber manufacturing and its composite processing are cur-

rently reaching a cost-effective level that permits even common leisure and sporting goods to be relatively inexpensive. Aramid, a kind of polymeric fiber, was a fantastic development only three decades ago. This fiber is the lightest, toughest, and the most impact-resistant among the synthetic fibers. Kevlar, a well-known brand name for aramid fiber, revolutionized the market of bullet-proof vests. Other synthetic fibers, such as silicon carbide, aluminum oxide, and boron, traditionally used in metal-matrix composites, have found commercial niches as PMCs in helicopter rotor blades, circuit boards, tennis rackets, and many other items. Natural fibers are promising options for PMCs. Their environmental advantages (biodegradable, renewable, recyclable) and the large number available as native, cultivated, or industry residuals stand over other fibers. Already used in many automobile components, natural fiber composites may in the future be appraised by their environmentally friendly qualities and seen as an ally in the fight against global warming.

The PMC articles in this issue will deepen scientific and technological understanding related to this important class of material. The article by S.N. Monteiro, F. Lopes, A. Ferreira, and D. Nascimento provides an overview on natural fiber composites. The growing interest and existing applications of these composites by the automobile industry were the main motivation for the article. The economical, technical, and environmental advantages are emphasized.

The paper by S. Sen, E. Schofield, J. Scott O'Dell, L. Deka, and S. Pillay describes the development of advanced PMCs for future space exploration. This new materials will provide

shielding from cosmic radiation and micrometeoroid impact during long interplanetary missions such as NASA's planned round trip to Mars.

The article by Y. Ganesan and J. Lou provides an overview on the mechanical behavior of polymer-matrix nanocomposites. The outstanding properties of nanostructured materials are exemplified using the case of carbon-nanotube reinforced composites. The authors emphasize the role played by the interface between nanoparticulate fillers and the polymer-matrix interface.

Characterization of fundamental properties related to the behavior of thermoplastic composites under impact condition is the focus of the article by K. Brown, R. Brooks, and N. Warrior. The strain-rate sensitivity of a glass-woven-fabric-reinforced composite, considered for vehicle impact resistant components, is providing basic information on the material mechanical response in case of a crash event.

The work by T. Rodrigues, M. Tavares, I. Soares, and A. Moreira presents a review on a modern and advanced development, hybrid nanocomposites. These are new materials with improved properties such as gas barrier, thermal stability, and flame resistance for several applications, from food packaging to fuel cells.

It is hoped these articles will update the readers and motivate them to share in the belief that PMC is the millennium material. Finally, a special token of gratitude is due to Ann Hagni, whose experience and effort enabled this issue to move forward.

**Sergio N. Monteiro is a professor of Materials Science and Engineering in the Laboratory for Advanced Materials at the State University of Northern Rio de Janeiro, and is the advisor to JOM from the Characterization of Minerals, Metals and Materials Committee.**

# Natural-Fiber Polymer-Matrix Composites: Cheaper, Tougher, and Environmentally Friendly

Sergio Neves Monteiro, Felipe Perissé D. Lopes, Ailton Silva Ferreira, and Denise Cristina O. Nascimento

Natural fibers, especially lignocellulosic fibers extracted from plants, are gaining attention as polymer-matrix composite (PMC) reinforcements due to their comparative advantages over synthetic fibers. Natural fibers are relatively low cost, renewable, and biodegradable. Their production systems are associated with low equipment wear and are energy efficient. In addition, the incorporation of lignocellulosic fibers into PMCs may significantly improve some mechanical properties. This article presents an overview of the advantages and drawbacks of applying natural fibers, some of them relatively unknown, as reinforcements of PMCs. The mechanical behavior of composites incorporated with selected fibers is discussed in terms of the effect of surface micromorphology and the fiber/matrix interaction.

## INTRODUCTION

In the past century, priority has been given to synthetic fibers fabricated using energy-intensive methods. Today, there is a strong belief that the most common energy sources such as petroleum, coal, and natural gas are highly responsible for worrisome climate changes. The possibility of replacing traditional energy-intensive materials with natural ones is, therefore, now gaining attention. In fact, natural materials are considered environmentally friendly not only for their savings in process energy but also for renewable and biodegradable characteristics that render them neutral with respect to CO<sub>2</sub> emissions. Such emissions cause the atmospheric greenhouse effect responsible for global warming.<sup>1-3</sup>

The cellulose/lignin-rich fibers extracted from cultivated plants such as jute, sisal, hemp, coconut, coir, flax,

### How would you...

#### ...describe the overall significance of this paper?

*This paper studies the advantages of using natural fibers as reinforcements in polymer matrix composites, as compared with synthetic fibers, especially glass fiber. Economical, environmental, and technical aspects are discussed. Distinct characteristics of each natural lignocellulosic fiber are emphasized. It is shown that the surface structure and the fiber/matrix interface can be responsible for outstanding impact resistance.*

#### ...describe this work to a materials science and engineering professional with no experience in your technical specialty?

*Materials scientists and engineers are familiar with synthetic fiber composites in automobile and aerospace components. A novel type of composite with natural fibers is substituting the traditional ones with synthetic fibers. In addition to economical and technical advantages, the natural fiber is biodegradable and renewable, which makes them environmentally correct materials. The characterization of these "green" composites will contribute to further extend their use in engineering applications.*

#### ...describe this work to a layperson?

*This work investigates the characteristics and properties of composite materials, which are nowadays applied in many components for airplanes and cars. The point of this work is that natural vegetable fibers are replacing synthetics like glass fiber as reinforcements of composite materials. The natural fibers are cheaper and environmentally correct due to their biodegradable and renewable characteristics. Natural fibers also consume relatively less processing energy. This represents a contribution to the control of climate changes.*

wood, pineapple, and many others are typical examples of natural materials. These lignocellulosic fibers have been extensively investigated in the last decade as possible substitutes for synthetic fibers that have been traditionally used as the reinforcement phase of polymeric composites.<sup>4-6</sup> Hundreds of scientific and technological works were dedicated to investigations on the properties and structural characteristics of polymeric composites reinforced with natural lignocellulosic fibers. Although it is beyond the scope of this article to review all publications on this subject, it is relevant for the reader to be informed that, contrary to synthetic fibers (such as glass and carbon) extensively produced in highly industrialized countries, lignocellulosic fibers are cultivated mainly in tropical regions of developing countries.<sup>7</sup> This is of social importance and represents a major source of income to sustain the economy of local populations in Africa, Latin America, and South Asia.

Moreover, some of these natural fibers are relatively unknown and their reinforcement potential in polymeric matrices only recently has begun to be investigated. For instance, fibers such as curaua,<sup>8-10</sup> piassava,<sup>11-14</sup> buriti,<sup>15,16</sup> ramie,<sup>17,18</sup> and sponge-gourd<sup>19,20</sup> from the Amazon and other regions of South America, which are traditionally used in simple domestic items, are currently being studied as composite reinforcements.

## GENERAL CHARACTERISTICS

The industrial application of natural fibers as an alternative for synthetic fibers in polymer-matrix composites (PMCs) has already occurred in marketable products. A relevant case of



Figure 1. Automobile components made of natural-fiber-reinforced composites.<sup>25</sup>

lignocellulosic fiber substitution is in vehicles. The automobile industry is successfully applying composites reinforced with a variety of this type of natural fiber to replace components such as interior panels and seat cushions originally made of glass mat PMC or polymeric foams.<sup>21–25</sup> Figure 1 illustrates the different components made of natural-fiber-reinforced PMCs in a Mercedes Benz sedan.<sup>25</sup> Important technical reasons exist for this preference. A natural-fiber PMC presents less damage to tools and molding equipment, as well as relatively better finishing. Furthermore, a high degree of flexibility, which makes a natural fiber bend rather than fracture, in association with low density and non-abrasive surface, offer practical advantages for reinforcement of PMC components in comparison to glass fibers.<sup>26</sup> Additionally, as further discussed in this article, the relatively greater toughness of a natural-fiber PMC component is able to absorb the high impact energy occurring in an automobile crash.

According to R. Zah et al.,<sup>24</sup> an even stronger argument based on legislation now exists for the use of natural-fiber PMCs in automobiles. A European Community directive<sup>26</sup> requires that by 2015 member countries re-use and recover at least 95% of the material from all end-of-life vehicles. Components containing glass fibers cannot easily be separated and, therefore, are difficult to recycle. In contrast to glass fiber, natural-fiber PMCs can be completely burnt to recover energy, which is a practice accepted by the directive. Consequently, the use of natural-fiber PMCs, as il-

lustrated in Figure 1, is rapidly increasing in the automobile industry<sup>21</sup> at annual growth rates above 20%.<sup>28</sup> Zah et al.<sup>24</sup> predicted that “the future trend of extreme lightweight car design will further enhance the application potential of natural fiber composites eventually leading to the ultimate vision of S. Hill<sup>23</sup> of cars that grow on trees.”

In addition to technical and environmental advantages, low cost is the main industrial motivation for natural rather than synthetic fibers as PMC reinforcement. The most economical of all synthetics, the glass fiber has a commercial price that varies from \$3.00 to \$3.80 per kg.<sup>29</sup> By contrast, cultivated lignocellulosic fibers usually have costs that

are about one order of magnitude lower. For example, in Brazil, the export FOB price of piassava fibers is \$0.37, curaua fiber, \$0.44, and sponge-gourd, \$0.60 per kg.<sup>7</sup> It is also worth mentioning that some lignocellulosic fibers obtained from coconut husks<sup>30–32</sup> and sugar cane bagasse,<sup>33</sup> which could be used as PMC reinforcements like coir, are by-products with much lower commercial values. These economical considerations, together with environmental and technical advantages, contribute to the current interest in choosing natural fibers in PMCs. This type of fiber, however, also presents drawbacks.

From a practical point of view, natural fibers as a biomaterial have dimensions that are limited by their anatomical restrictions. In other words, it is not possible to specify a given length or diameter for a specific natural fiber. One has to accept what Mother Nature provides. In terms of length, it has been shown<sup>34</sup> that many lignocellulosic fibers have average values that are sufficient to be considered long and continuous for PMC reinforcement. Figure 2 illustrates the statistical distribution of length and diameter of commercial lots of curaua and piassava fibers.

In this figure, two points should be noted. First, that the average length of curaua, 846 mm, and piassava, 455 mm, are more than 15 times their criti-

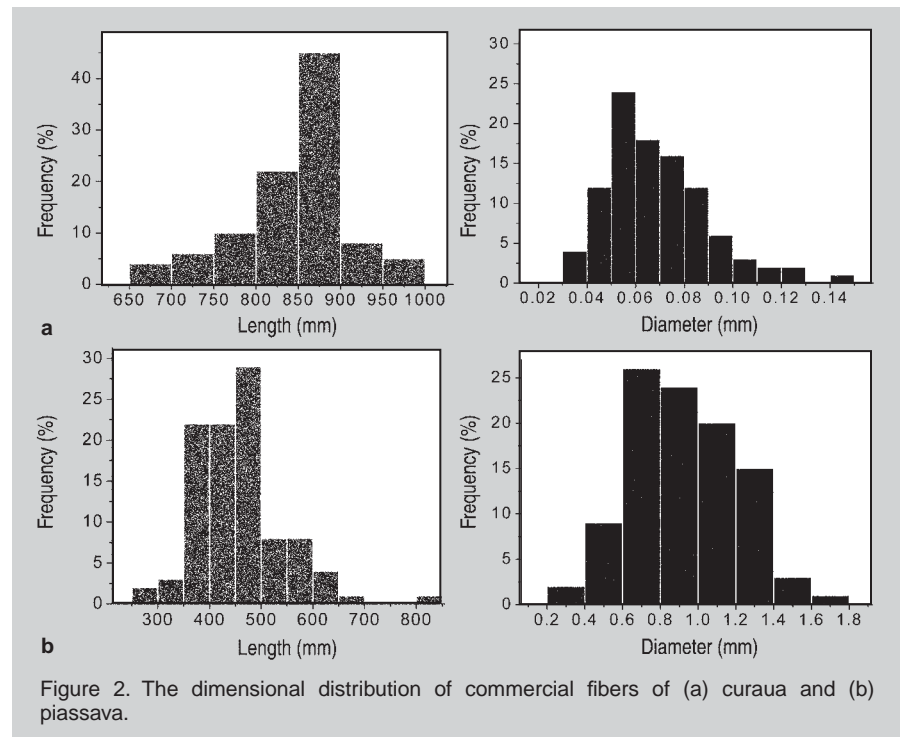


Figure 2. The dimensional distribution of commercial fibers of (a) curaua and (b) piassava.

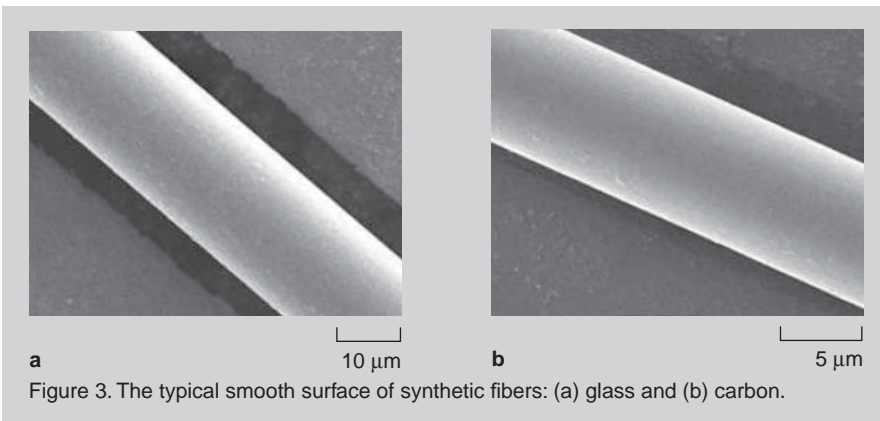


Figure 3. The typical smooth surface of synthetic fibers: (a) glass and (b) carbon.

mer (such as polyester, vinyl esters, and epoxy) normally used as composite matrix.<sup>4-6</sup> In this case, surface modification by alkali or silane treatments<sup>36,37</sup> may improve the fiber/matrix adherence and increase the PMC strength. Once again, a treatment operation results in additional cost and decreases the economical competitiveness of the natural fiber.

## SURFACE MORPHOLOGY

The surface microstructure between natural and synthetic fibers is markedly different. The conventional processing methods applied in synthetic fibers fabrication result in smooth surfaces as illustrated in Figure 3 for the most common types.

By contrast, natural fibers, especially those lignocellulosic extracted from plants, display complex surface micro-morphological details. These details vary from one kind of fiber to another and influence the adherence to the polymeric matrix in distinct ways. Consequently, they affect the mechanical behavior of the composite in correspondingly different manners. Two examples are presented to illustrate the

cal lengths, respectively, 10 mm and 15 mm.<sup>34</sup> This is considered a positive feature for optimum reinforcement of PMCs and assures effective strengthening for the composite.<sup>35</sup> Secondly, the statistical dispersion in dimensional values is quite accentuated, which, technically, is an undesirable feature. Therefore, these fibers, like all other lignocellulosics (Figure 2), can be considered non-uniform in comparison with synthetic fibers that are fabricated within precise dimensional values.

A possible solution for the limitation in length of lignocellulosic fibers is to weave (as done in cotton, flax, and ramie) the fibers into a continuous thread

that could then be wound on a spool. In this way, uniformly distributed PMCs could be automatically fabricated by pultrusion, prepreg, or filament winding processes.<sup>35</sup> However, a weave operation adds supplementary cost to the fiber and diminishes its economical advantage. Moreover, stiff fibers like piassava and coir are difficult to weave for automatic fabrication.

Another disadvantage of lignocellulosic fibers is the fact that, due to their natural wax, they are hydrophilic and adsorb water onto their surface. Consequently, a weak bonding is expected to form between the surface of a lignocellulosic fiber and a hydrophobic poly-

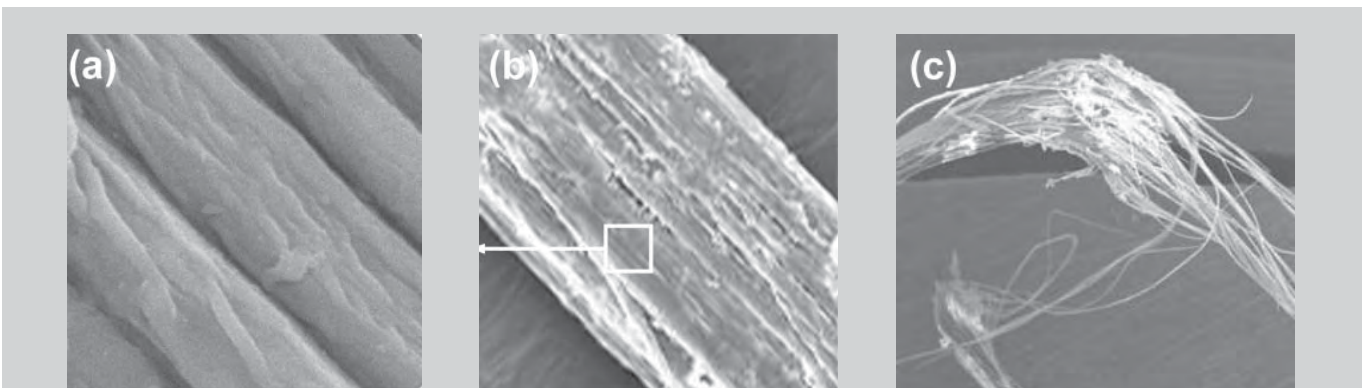


Figure 4. Curaua fiber morphology: (a) filament composition (2000 x); (b) general view of the fiber showing multiple filaments in one fiber (300 x); and (c) separation of filaments during mechanical rupture by tensile stress (80 x).

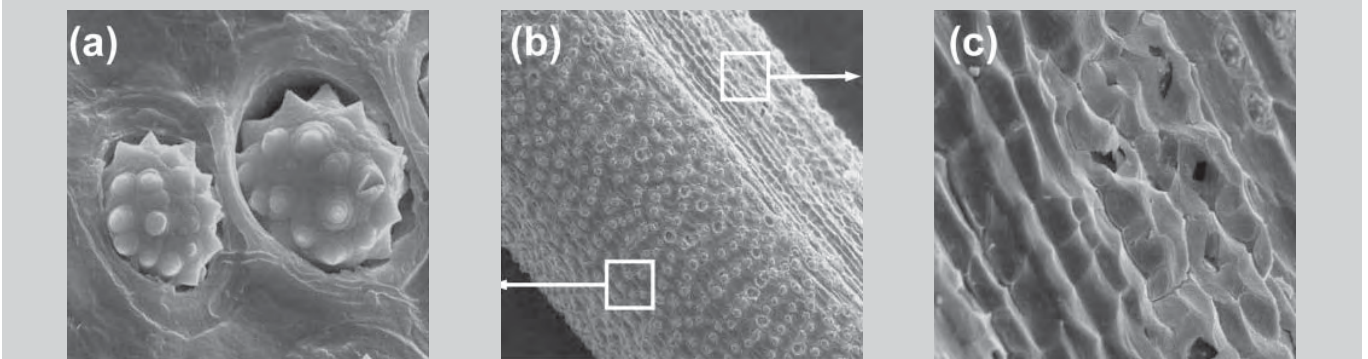


Figure 5. Surface morphology of a piassava fiber: (a) surface spiny protrusions (2000 x); (b) general view of the fiber (100 x); and (c) reentrant cells (500 x).

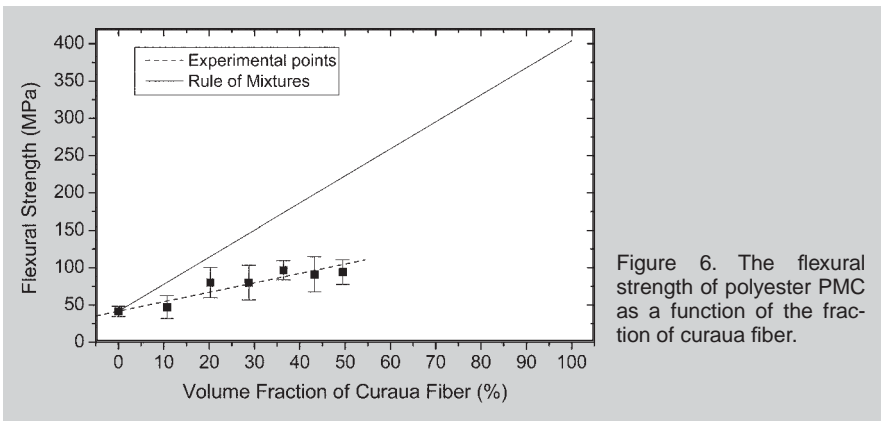


Figure 6. The flexural strength of polyester PMC as a function of the fraction of curaua fiber.

relevance of distinct lignocellulosic fiber surface structures.

Figure 4 shows the surface micro-morphology of a curaua fiber. Note the filamentary structure of the fiber. Each curaua fiber (Figure 4b) is composed of more than 50 cylindrical-shaped filaments (Figure 4a). Under an applied load, these filaments initially tend to separate from one another. Only at a relatively high tensile stress level of 1,000 MPa<sup>7</sup> would all filaments be broken, allowing the complete rupture of the fiber (Figure 4c).

The typical surface micromorphology of a piassava fiber is shown in Figure 5. Characteristic structures of the piassava can be seen in Figure 5b extending along the fiber. Most of the surface area is covered with silicon-rich spiny protrusions (Figure 5a), while the remaining area is associated with reentrant cells (Figure 5c). Both features, protrusions and reentrant cells, may interact with a polymeric matrix and affect the mechanical behavior of the composite.

The two examples presented in Figures 4 and 5 emphasize the importance of a natural fiber's surface micro-morphology. As indicated, every kind of lignocellulosic fiber has its own surface structure, similar to a fingerprint, which will affect the mechanical behavior of its reinforced PMC in a specific way. As a general rule, the complex surface structure of any natural fiber (Figures 4 and 5), in contrast to smooth synthetic fibers (Figure 3), plays a significant role in the mechanism of load transfer through the matrix interface.

## MECHANICAL BEHAVIOR

The following results were obtained in laboratory experiments described elsewhere for both curaua<sup>38,39</sup> and piassava<sup>40,41</sup> fiber-reinforced PMC.

## Curaua-Fiber-Reinforced Polyester Composites

Figure 6 shows the experimental (dashed line) polyester PMC strength,  $\sigma_c$ , as a function of the volume fraction,  $V_f$ , of curaua fibers. The solid line corresponds to the calculated composite strength,  $\sigma_c$ , obtained by the Rule of Mixtures:

$$\sigma_c = \sigma_p (1 - V_f) + \sigma_f V_f \quad (1)$$

For both phases,  $\sigma_p$  for the polyester and  $\sigma_f$  for the curaua fiber is also plotted. One should notice in Figure 6 that, within the error bars, the experimental points can be associated with a straight line up to the maximum fraction of 50% of curaua fibers that could be, in practice, incorporated into the polyester matrix.<sup>38,39</sup> This experimental line, although showing a significant increase in the composite strength with the fraction of curaua fiber, has a lower value when compared to the calculated Equation 1 by the Rule of Mixtures. The difference between the calculated  $\sigma_c$  and the experimental  $\sigma_c$  is a function of the curaua fiber fraction:

$$\sigma_c - \sigma_e = 2.4 V_f \quad (2)$$

According to this equation, the ratio  $\sigma_c/\sigma_e$  increases with the amount of fiber. For the maximum investigated  $V_f = 50\%$ , the ratio  $\sigma_c/\sigma_e$  reaches 2.2.

A model for the curaua fiber/polymer matrix interface (Figure 7) is able to explain the difference between the calculated and experimental values (Equation 2) for the PMC strength.

This model is based on the actual filamentary structure of a curaua fiber, as illustrated in Figure 4. If it is assumed that the interface in Figure 7 is formed by a polymer matrix covering half-cylinders (Figure 7c), then the stress concentration at the matrix is given by:<sup>35</sup>

$$\sigma_i = \sigma_o [1 + 2 (a/\rho)^{1/2}] \quad (3)$$

where  $a$  is the depth of the polymer penetration and  $\rho$  the fiber radius of curvature. For this interface model  $a = \rho$  and, consequently,

$$\sigma_i = 3 \sigma_o \quad (4)$$

where  $\sigma_i$  is the interfacial stress and  $\sigma_o$  an applied stress to the composite.

Equation 4 indicates a three-times reduction in the theoretically expected PMC strength due to the stress concentration generated at the curaua fiber interface with a polymeric matrix. In principle, this agrees with the experimental results shown in Figure 6, although the actual reduction was less than three times. Part of the applied stress, which is transferred to the fiber, is used to separate the filaments (Figure 4c) before total rupture.

The impact resistance of lignocellulosic-fiber-reinforced PMCs is an important property for tougher components. As mentioned earlier, automobile components are required to absorb energy during a crash. Figure 8 shows

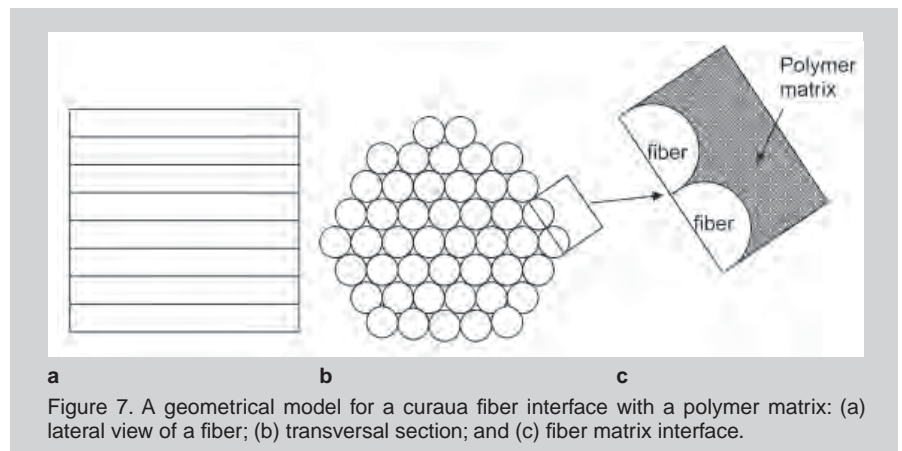


Figure 7. A geometrical model for a curaua fiber interface with a polymer matrix: (a) lateral view of a fiber; (b) transversal section; and (c) fiber matrix interface.



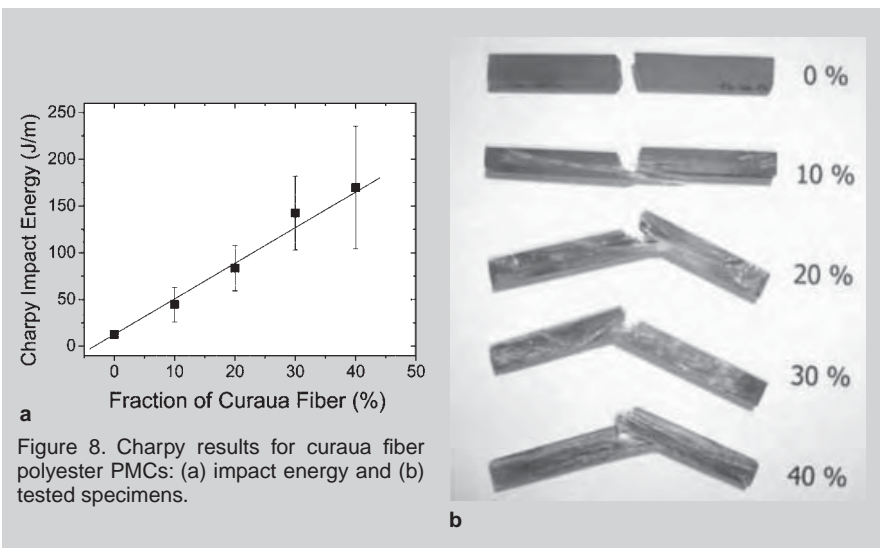


Figure 8. Charpy results for curaua fiber polyester PMCs: (a) impact energy and (b) tested specimens.

Charpy impact results for curaua-fiber-reinforced PMCs. The variation of the impact energy as a function of the fiber fraction is given in Figure 8a. Corresponding tested Charpy specimens are shown for different fractions of curaua fibers (Figure 8b). A marked increase in the impact energy (Figure 8a) indicates significant improvement in the toughness of the PMC due to curaua fibers. Dispersion in the experimental error is caused by the previously mentioned heterogeneous nature of lignocellulosic fibers.

As shown in Figure 8b, above 10% of curaua fiber results in the PMC specimen not separating into two parts (i.e., no complete rupture occurred regardless of the power of the Charpy hammer). This is a consequence of the low interfacial strength between the lignocellulosic fiber surface and the polymeric matrix. A low resistance of the interface permits the fiber to be easily separated from the matrix, which results in a much larger final area of fracture.<sup>42</sup> Specimens with more than 10% of fibers were bent enough to be projected by the Charpy hammer without complete rupture of the flexible curaua fibers (Figure 8b).

### Piassava-Fiber-Reinforced Polyester Composites

The piassava-reinforced PMC provides another interesting example of the influence of the surface micro-morphology and fiber/matrix interaction on mechanical behavior. Figure 9 shows the experimental (dashed line) polyester PMC strength,  $\sigma_c'$ , as a function of the volume fraction of the piassava

fiber. In this figure, the calculated solid straight line, corresponding to the Rule of Mixtures (Equation 1) is also displayed.

Within the error bars of the experimental dashed straight line, which goes up to 51%, the calculated line by the Rule of Mixtures fits satisfactorily. This is an indication that the experimental values conform to the predicted increase in strength for PMC reinforced with piassava fibers. Contrary to the case of curaua fibers (Equation 2), there was no difference,  $\sigma_c' - \sigma_e' = 0$ , for the case of piassava fibers (Figure 9).

Figure 10 presents a model for the surface micromorphology of the piassava fiber. In this figure, reentrant cells

(Figure 5c) increase stress and contribute to the decreasing of PMC strength in a manner similar (Equation 3) to what was proposed for the curaua-reinforced PMC. However, as shown in Figure 10, the piassava fiber also has hard silicon-rich spiny protrusions (Figure 5a) that act as anchors to make slide motion difficult with respect to the matrix. These protrusions contribute to improving the fiber adherence and add to the strength of the PMC. In the final balance, the piassava fiber provides a perfect reinforcement for a PMC as calculated by the Rule of Mixtures (Figure 9).

Charpy test results for piassava-fiber-reinforced PMCs are shown in Figure 11. The variation of the impact energy as a function of the fiber fraction is given in Figure 11a. An exponential increase in the Charpy absorbed energy was found with increasing fraction of piassava fiber.

The typical aspect of tested Charpy specimens is shown for different fractions of piassava fibers (Figure 11b). These results are similar to the ones obtained for curaua fiber PMC (Figure 8). The same debonding mechanism at a weak fiber/matrix interface creating large fracture areas applies for the piassava-fiber-reinforced PMC. In both cases, the continuous and aligned reinforcement, which is associated with these lignocellulosic fibers, substantial-

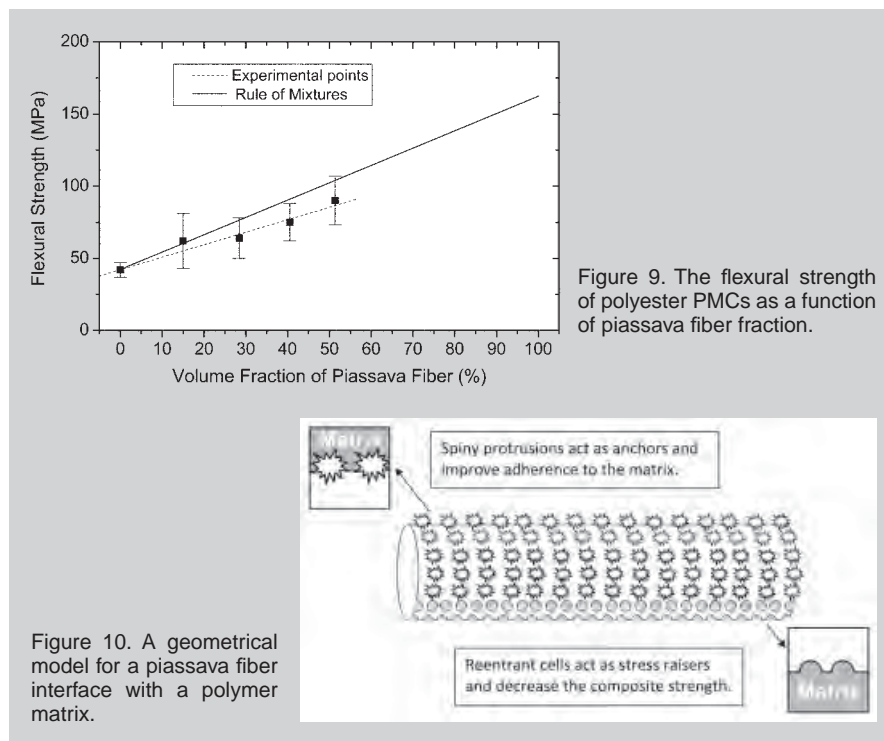


Figure 9. The flexural strength of polyester PMCs as a function of piassava fiber fraction.

Figure 10. A geometrical model for a piassava fiber interface with a polymer matrix.

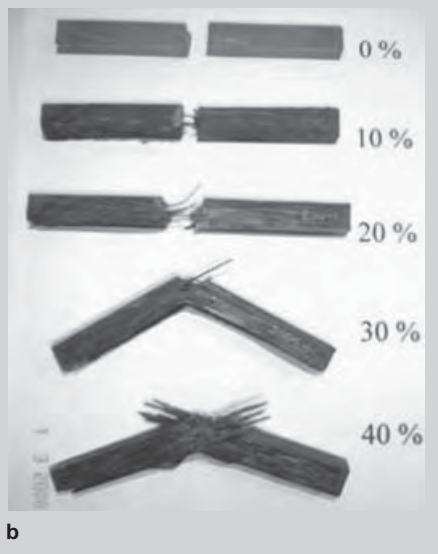
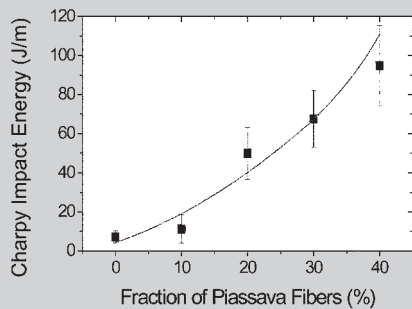


Figure 11. Charpy results for piassava fiber PMC: (a) impact energy and (b) tested specimens.

ly increases the toughness of the PMC. In comparison to synthetic fibers, this is indeed a technical advantage, which is attracting industries (such as automobile manufacturers) to the use of natural-fiber-reinforced PMCs.

## CONCLUSIONS

The next few decades should see a growing interest in the application of PMCs reinforced with natural fibers. These fibers, especially lignocellulosic extracted from cultivated plants, are abundant, biodegradable, renewable, and neutral with respect to CO<sub>2</sub> emissions that cause global warming. Natural fiber composites are less expensive and do not require as much processing energy as synthetic glass or carbon fibers. The automobile industry is increasingly using these natural fiber composites in components for economical, environmental, and technical reasons. Each lignocellulosic fiber has a specific surface micro-morphology that affects the mechanical behavior of the composites in distinct ways and can significantly improve their strength and toughness. This has been shown in many studies on well-known fibers and has been exemplified in this paper for two relatively unknown tropical fibers, curaua and piassava. The incorporation of these fibers is promising for a future of less expensive, stronger, and environmentally friendly composites.

## ACKNOWLEDGEMENTS

The authors thank the following Brazilian agencies for their support of

this research: CNPq, CAPES, FAPERJ, and TECNORTE/FENORTE. Also acknowledged is the permission to use the impact equipment by the IQ/UFRJ, as well as the scanning electron microscope by the PEMM from COPPE/UFRJ.

## References

1. S.R. Weart, *The Discovery of Global Warming* (Boston, USA: Harvard University Press, 2003).
2. J.T. Houghton, *Global Warming—The Complete Briefing*, 3rd edition (Cambridge, U.K.: Cambridge University Press, 2004).
3. A. Gore, *An Inconvenient Truth. The Planetary Emergency of Global Warming and What We Can Do About It* (Emmaus, Pennsylvania, USA: Rodale Press, 2006).
4. D. Nabi Sahed and J.P. Jog, *Advances in Polymer Technol.*, 18 (1999), pp. 221–274
5. A.K. Bledzki and J. Gassan, *Prog. Polym. Sci.*, 4 (1999), pp. 221–274.
6. A.K. Mohanty, M. Misra, and G. Hinrichsen, *Macromolecular Mat. and Engineering*, 276/277 (2000), pp. 1–24.
7. K.G. Satyanarayana, J.L. Guimarães, and F. Wypych, *Composites: Part A*, 38, (2007), pp. 1694–1709.
8. A.L. Leão, I.H. Tan, and J.C. Caraschi, *Proceedings of the International Conference on Advanced Composites* (Hurghada, Egypt, May, 1998), pp. 557–564.
9. S.N. Monteiro et al., (in Portuguese), *Rev. Mater.*, 11 (3) (2006), pp. 197–203.
10. S.N. Monteiro, A.S. Ferreira, and F.P.D. Lopes, *TMS 2008 Annual Meeting Supplemental Proceedings Volume 2: Materials Characterization, Computation and Modeling* (Warrendale, PA: TMS, March 2008), pp. 117–123.
11. R.C.M.P. Aquino, J.R.M. d'Almeida, and S.N. Monteiro, *J. Mater. Sci. Letters*, 20 (2001), pp. 1017–1019.
12. R.C.M.P. Aquino, S.N. Monteiro, and J.R.M. d'Almeida, *J. Mater. Sci. Letters*, 22 (2003), pp. 1495–1497.
13. J.F. de Deus, S.N. Monteiro, and J.R.M. D'almeida, *Polymer Testing*, 24 (2005), pp. 750–755.
14. J.R.M. d'Almeida, R.C.M.P. Aquino, and S.N. Monteiro, *Composites. Part A*, 37 (2006), pp. 1473–1479.
15. R.S. Santos, E.L.C. Silveira, and C.M.L. Souza, (in Portuguese), *Proceedings of the 30th Annual Meeting of the Brazilian Chemistry Society* (Aguas de Lindoia, Brazil: 2007), p. 1.
16. S.N. Monteiro et al., *REWAS 2008: Global Symposium on Recycling, Waste Treatment and Clean Technol-*

ogy, ed. B. Mishra, C. Ludwig, and S. Das (Warrendale, PA: TMS, 2008), pp. 517–522.

17. C.Z. Paiva, Jr. et al., *Polymer Testing*, 23 (2) (2004), pp. 131–135.

18. S.N. Monteiro et al., *REWAS 2008: Global Symposium on Recycling, Waste Treatment and Clean Technology*, ed. B. Mishra, C. Ludwig, and S. Das (Warrendale, PA: TMS, 2008), pp. 505–510.

19. J.R.M. d'Almeida, C.A. Boynard, and S.N. Monteiro, *Natural Polymers and Composites* (2000), pp. 27–31.

20. C.A. Boynard, S.N. Monteiro, and J.R.M. d'Almeida, *J. Appl. Polym. Sci.*, 87 (2003), pp. 1927–1932.

21. B.C. Suddell et al., *Proceedings of the 4th International Symposium on Natural Polymers and Composites – ISNAPol* (São Paulo, Brazil: ABPol, 2002), pp. 455–461.

22. G. Marsh, *Mater. Today*, 6 (4) (2003), pp. 36–43.

23. S. Hill, *New Scientist*, 153 (2067) (1997), pp. 36–39.

24. R. Zah et al., *J. Cleaner Production*, 15 (2007), pp. 1032–1040.

25. Mercedes-Benz web page (August, 30, 2008), [www.mercedes-benz.com.br](http://www.mercedes-benz.com.br).

26. P.J. Herrera-Franco and A. Valadez-Gonzalez, *Composite. Part A*, 35 (3) (2004), pp. 339–345.

27. European Commission, Directive 2000-53/EC of the European Parliament and of the Council of September 18, 2000 on end-of-life vehicles. *Union OJOTE* (2000), p. 9.

28. Kline & Company, *Opportunities for Natural Fibers in Plastic Composites* (Little Falls, NJ, USA: Pub. K&C, 2000), pp. 1–10.

29. Available at Aerojet web page (September, 29, 2008), [www.aerojet.com.br](http://www.aerojet.com.br).

30. C.A.S. Hill and H.P.S.A. Khalil, *J. Appl Polym. Sci.*, 77 (2000), pp. 1322–1330.

31. J. Rout et al., *Comp. Sci. Tech.*, 61 (2001), pp. 1303–1310.

32. S.N. Monteiro, F.P.D. Lopes, and J.R.M. d'Almeida, *Rev. Mater.*, 10 (4) (2005), pp. 571–576.

33. S.N. Monteiro et al., *Adv. Perform. Mater.*, 5 (3) (1998), pp. 183–191.

34. S.N. Monteiro and J.R.M. d'Almeida, (in Portuguese), *Rev. Mater.*, 11 (3) (2006), pp. 189–196.

35. W.D. Callister Jr., *Materials Science and Engineering—An Introduction*, 5 ed. (New York: John Wiley & Sons, 2000).

36. A. Valadez-Gonzalez et al., *Composites: Part B*, 30 (1999), pp. 309–320.

37. S.N. Monteiro, D.C.O. Nascimento, and L.C. Motta, *REWAS 2008: Global Symposium on Recycling, Waste Treatment and Clean Technology*, ed. B. Mishra, C. Ludwig, and S. Das (Warrendale, PA: TMS, 2008), pp. 511–516.

38. S.N. Monteiro and J.J.A. Rangel, (in Portuguese), *Proceedings of the 62nd International Congress of the Brazilian Association for Metallurgy and Materials* (São Paulo, Brazil: ABM, 2007), pp. 748–756.

39. A.S. Ferreira et al., (in Portuguese), *Proceedings of the 63rd International Congress of the Brazilian Association for Metallurgy and Materials* (São Paulo, Brazil: ABM, 2008), pp. 805–813.

40. S.N. Monteiro et al., (in Portuguese), *Rev. Mater.*, 11 (3) (2006), pp. 204–210.

41. S.N. Monteiro et al., *TMS 2008 Annual Meeting Supplemental Proceedings Volume 2: Materials Characterization, Computation and Modeling* (Warrendale, PA: TMS, 2008), pp. 55–62.

42. C.Y. Yue, H.C. Looi, and M.Y. Quek, *Int. J. of Adhesion and Adhesives*, 15 (1995), pp. 73–80.

**Sergio Neves Monteiro (professor) and Felipe Perissé D. Lopes, Ailton Silva Ferreira, and Denise Cristina O. Nascimento (graduate students) are with the State University of the Northern Rio de Janeiro, Advanced Materials Laboratory, Av. Alberto Lamego, 2000, 28013-602, Campos dos Goytacazes, Brazil. Dr. Monteiro can be reached at [sergio.neves@ig.com.br](mailto:sergio.neves@ig.com.br).**

# The Development of a Multifunctional Composite Material for Use in Human Space Exploration Beyond Low-Earth Orbit

S. Sen, E. Schofield, J. S. O'Dell, L. Deka, and S. Pillay

## Enhanced for the Web

This article appears on the JOM web site ([www.tms.org/jom.html](http://www.tms.org/jom.html)) in html format and includes links to additional on-line resources.

Long-duration human exploration beyond the low Earth orbit (LEO) mandates development of materials to minimize crew and equipment exposure to the interplanetary radiation environment. The potential for biological damage by the relatively low percentage of high-energy heavy ions in the galactic cosmic ray spectrum far outweigh that due to lighter particles because of their ionizing power and the quality of the resulting biological damage. To avoid paying a penalty due to additional weight, it would be beneficial to develop a multifunctional material as an integral part of a spacecraft structure to provide shielding effectiveness and structural integrity. This paper discusses the development of polyethylene fiber reinforced epoxy matrix structural composites that effectively satisfy both primary requirements.

## INTRODUCTION

NASA's current vision for space exploration includes long-duration human travel beyond lower Earth orbit (LEO) and sustained human presence on other planetary surfaces. For this vision to be a reality, one of the major challenges that need to be overcome is to minimize the radiation exposure to crew and equipment from the interplanetary radiation environment. Life on Earth is well protected from this radiation environment by a combination of the

## How would you...

### ...describe the overall significance of this paper?

Long-duration human exploration beyond the low Earth orbit mandates development of materials to minimize crew and equipment exposure to the interplanetary radiation environment. A polyethylene fiber-reinforced epoxy matrix composite with an open cell carbon foam and vacuum plasma deposited boron carbide coating was developed to potentially satisfy the primary requirements for radiation shielding, structural integrity, micrometeoroid impact, and atmospheric re-entry temperature resistance.

### ...describe this work to a materials science and engineering professional with no experience in your technical specialty?

Interaction of the charged particles in the interplanetary radiation environment with a shielding material takes place through several specific atomic and nuclear processes. Using a shielding material to break the heavy ions in the galactic cosmic ray flux into smaller fragments with lower ionizing power is the only realistic solution for passive radiation shielding design. The emphasis of this work was to develop a multifunctional composite architecture that will satisfy the requirements for deep space radiation shielding and also for structural integrity, micrometeoroid impact, and re-entry temperatures.

### ...describe this work to a layperson?

A challenge to NASA's vision for long-duration human space exploration is to minimize the radiation exposure to the interplanetary radiation environment. This paper discusses a multifunctional composite material that will provide shielding from cosmic radiation while also providing structural integrity, thermal management, and protection from micrometeoroid impact.

geo-magnetic field and the atmospheric overburden. In LEO, the radiation exposure of astronauts is kept below the National Council on Radiation Protection (NCRP) limits by limiting their exposure time and by taking advantage of the shielding still offered by the geo-magnetic field.<sup>1</sup> However, exposure to free space cosmic radiation during an approximately two-year round trip to Mars or during extended stays of up to a few months on the surface of the moon or Mars could result in significant biological damage. This paper discusses the development of a multifunctional composite material that will provide shielding from cosmic radiation while also providing structural integrity, thermal management, and protection from micrometeoroid impact. This emphasis on multifunctionality is to avoid paying a significant penalty in weight and cost due to addition of material solely for radiation shielding. The design for shielding solutions is dictated by the nature of interaction between the cosmic radiation environment and the proposed shielding material. It is therefore worthwhile to first describe the cosmic radiation environment and the physics of its interaction with materials.

The galactic radiation environment consists primarily of a continuous flux of galactic cosmic rays (GCRs)<sup>2,3</sup> and transient but intense fluxes of solar energetic particles (SEPs).<sup>3,4</sup> The primary constituents of the GCR spectrum are 85% protons, 14% alpha particles, and 1% heavy nuclei with energies ranging from 10 MeV/nucleon to 10 GeV/nucleon.<sup>5</sup> The intensity of these particles depends on the solar cycle as well as on the location in the inner solar system.<sup>2,5</sup> Despite their low flux, the heavy ions

in the GCR pose a serious health risk because they are highly ionizing (energy loss is proportional to the square of the atomic number for charged particles with same velocity) and because the quality of the resulting biological damage is high.<sup>6,7</sup> The SEPs, on the other hand, consist primarily of protons and alpha particles with energies ranging from a few MeV/nucleon to few hundreds of MeV/nucleon.<sup>2,4,5,7</sup>

The likelihood of occurrence for these events is highest during solar maxima and their occurrences can be predicted with some degree of confidence. Although the SEP spectrum does not contain heavy ions and their energy range is much lower than that of GCRs, they still pose serious risks to crew and equipment, particularly in the event of a severe solar storm.

Interaction of the charged particles present in the interplanetary radiation environment with a material takes place through several specific atomic and nuclear processes. Of these processes, two are of particular relevance here, namely, energy loss and fragmentation. The energy loss of charged particles per unit length of material traversed (also known as the stopping power or the linear energy transfer, LET)<sup>6,8</sup> is directly proportional to the square of their atomic number and inversely proportional to their energy. As discussed earlier, the radiation risk from GCR exposure is dominated by the small but highly ionizing flux of heavy ions. Fragmentation of the incident heavy ion projectile leads to the formation of smaller fragments moving at the same velocity as the incident particle, and are less ionizing due to their lower atomic number. Breaking up the heavy ions in the GCR flux into smaller fragments with lower ionizing power is the only realistic solution for passive radiation shielding design. It is also important in this process to minimize the production of secondaries from target fragmentation that can otherwise add to the radiation risk.<sup>9,10</sup> Therefore, any proposed radiation shielding material for use in outer space must be composed of nuclei that maximize the likelihood of projectile fragmentation while producing the minimum number of target fragments. In this respect, polyethylene (PE) has

**Table I. Density of Hydrogen Atoms in Different Materials**

Material	# Atoms/cm <sup>3</sup> × 10 <sup>22</sup>
Hydrogen	5.7
Water	6.7
Polyethylene	7.9
Polystyrene	4.7
Polyimide	2.2
Polyamide	3.0

been found to be one of the best-suited materials for radiation shielding<sup>11,12</sup> since it has a very high density of hydrogen atoms (see Table I). As hydrogen has the smallest atomic diameter, it provides a large number of interaction points or high cross section for projectile fragmentation. Moreover, the absence of elements heavier than

**Breaking up the heavy ions in the GCR flux into smaller fragments with lower ionizing power is the only realistic solution for passive radiation shielding design.**

carbon minimizes the production of target fragments, since the hydrogen nuclei consist of a single proton. It is therefore not surprising that in some quarters of the International Space Station passive radiation shielding in the form of polymeric materials is currently being used.<sup>13</sup>

As is evident from the above discussion, the superior radiation shielding effectiveness of PE has already been established. The emphasis of this paper is to develop a composite architecture based on PE that would not only be an effective radiation shield but also would have sufficient structural integrity to be considered as structural elements of a crew vehicle for long-duration exploration beyond LEO. In addition to radiation shielding and structural integrity, a truly multifunctional material for a crew vehicle should address thermal man-

agement required for mitigating the effects of temperature fluctuations in outer space, and severe re-entry temperatures, and offer ballistic protection against micrometeoroid impacts.

## **RADIATION TRANSPORT CALCULATIONS**

To determine the optimum compositions for composite fabrication, radiation transport calculations were performed. The transport code essentially solves the one-dimensional Boltzmann equation where the flux of particles of a given atomic number, energy, and spatial location are determined. Detailed discussion on the transport code is beyond the scope of this paper, and readers are directed elsewhere.<sup>14</sup> Transport calculations were performed using both the 1986–1987 solar-minimum and the 1989 solar-maximum GCR environment.<sup>15</sup> Two observables were used to evaluate the shielding effectiveness: the absorbed dose and the dose equivalent. Absorbed dose is defined as the energy absorbed by a target per unit mass from any kind of ionizing radiation. The international unit for absorbed dose is Gray (Gy) or 1 J/kg. However, it has been established that the absorbed dose required to obtain the same level of biological damage can be different for different kinds of radiation. To account for this difference in absorbed dose, the concept of dose equivalent was introduced. Dose equivalent is expressed in the units of Sievert (Sv) and defined as the product of the absorbed dose and a dimensionless quality factor, Q. This quality factor is dependent on the LET of the radiation and is prescribed by organizations such as NCRP and the International Commission of Radiological Protection. Further discussion on some of these fundamental metrics for radiation shielding can be found elsewhere.<sup>8</sup> For the present analysis, to minimize systematic uncertainties in the calculated results, dose and dose equivalent relative to PE were analyzed. Two composite architectures were evaluated for radiation shielding effectiveness.

Composite 1, an epoxy matrix reinforced with ultra-high molecular weight (UHMW) PE fabric, formed the baseline composite for structural

and radiation shielding requirements. The nominal composition of this composite was 68.0% PE and 32.0% epoxy matrix by weight. Composite 2 consisted of Composite 1 with the addition of an open cell carbon foam and plasma-deposited  $B_4C$  coating to address thermal management and ballistic protection requirements. The nominal composition for this composite was 57.2% PE, 22.0% epoxy matrix, 8.5% boron, and 12.3% carbon by weight.

Figure 1 shows transport calculation results for the two described composites. Calculation results for alu-

minum and PE are also included for comparison. Results presented in Figure 1 are based on the assumption of a solar-minimum condition when the GCR flux is at a maximum. Similar results were obtained when the 1989 solar maximum environment was used. These calculations indicate that over thicknesses ranging from 1 g/cm<sup>2</sup> to 20 g/cm<sup>2</sup> the shielding effectiveness of Composite 1 is only about 1% to 5% less than that for pure PE. The entire composite structure, including thermal and ballistic protection, is only 2% to 8% less effective than pure PE over the same thickness range. Terres-

trial and LEO requirements mandate keeping the exposure below 50 cSv/year for blood forming organs.<sup>1</sup> Using this requirement as an example, it can be seen from Figure 1 that compared to PE only a marginal increase in composite areal density (13.86 g/cm<sup>2</sup> for Composite 1 and 14.13 g/cm<sup>2</sup> for Composite 2 in comparison to 13.18 g/cm<sup>2</sup> for pure PE) will be required to achieve the same level of shielding provided by PE. However, as will be

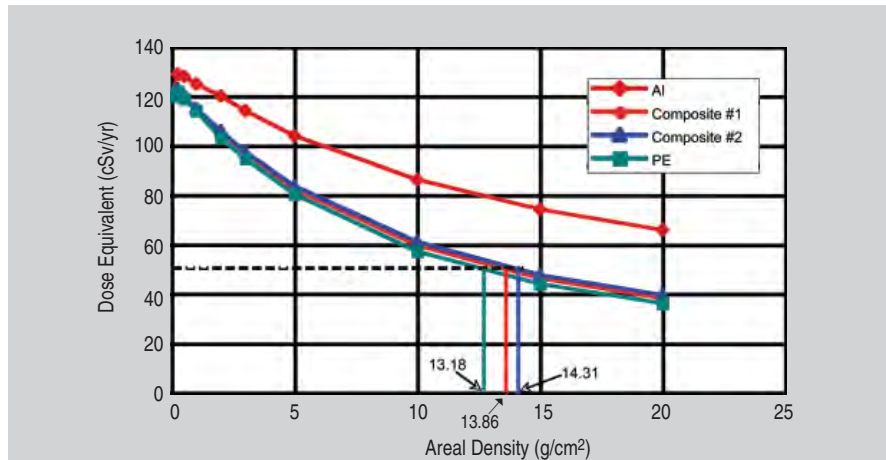


Figure 1. Dose equivalent as a function of areal density (or material thickness) for PE-fiber-reinforced epoxy matrix Composites 1 and 2; pure PE and aluminum results are from calculations using the 1986–87 solar-minimum GCR environment. Similar results were obtained when the 1989 solar maximum environment was used. Note that the material thickness can be obtained by dividing the areal density by density of the material.

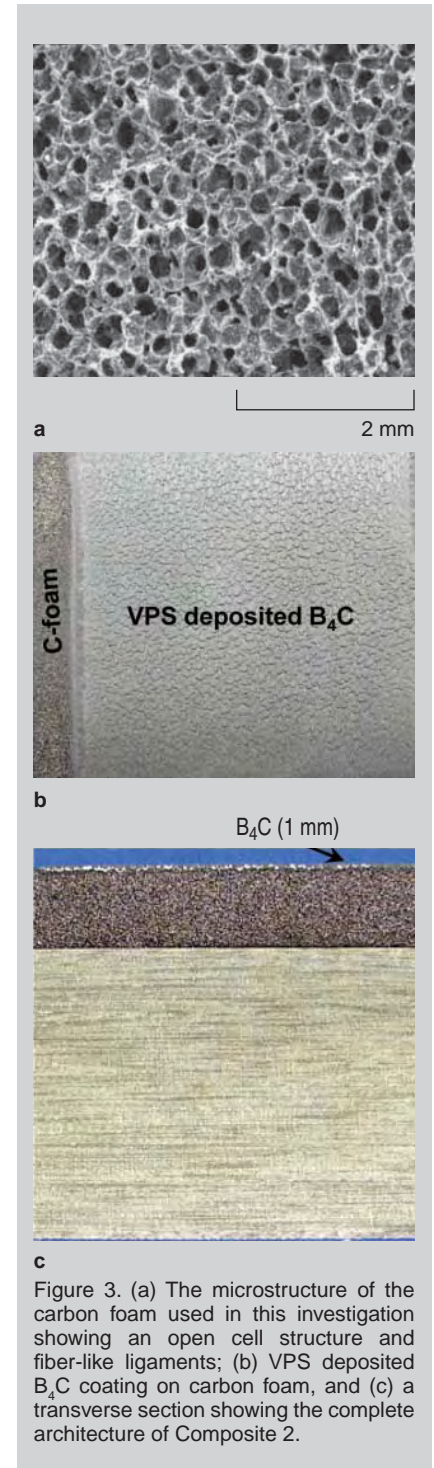


Figure 3. (a) The microstructure of the carbon foam used in this investigation showing an open cell structure and fiber-like ligaments; (b) VPS deposited  $B_4C$  coating on carbon foam, and (c) a transverse section showing the complete architecture of Composite 2.

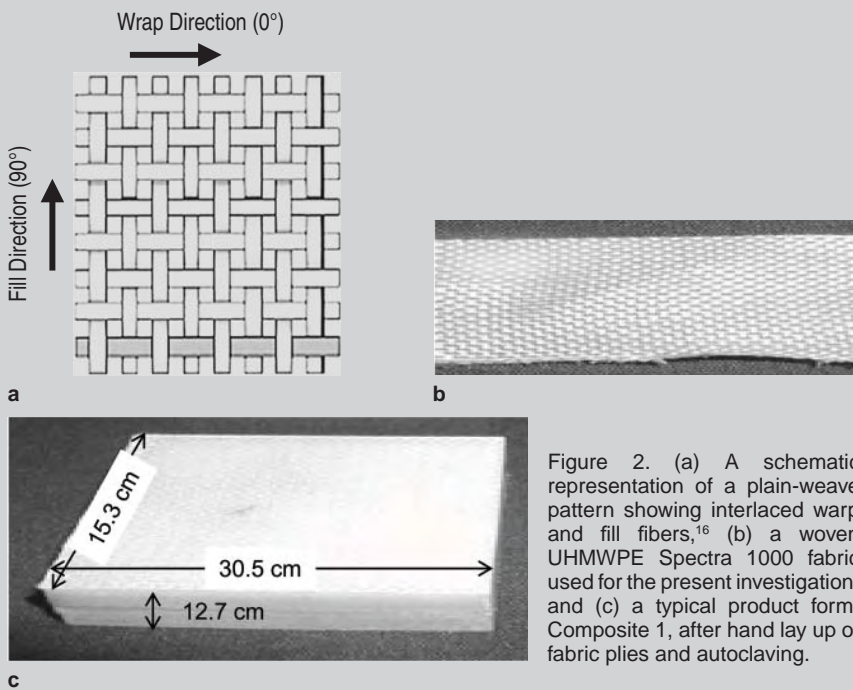


Figure 2. (a) A schematic representation of a plain-weave pattern showing interlaced warp and fill fibers,<sup>16</sup> (b) a woven UHMWPE Spectra 1000 fabric used for the present investigation, and (c) a typical product form of fabric plies and autoclaving.

**Table II. Absolute and Relative (to PE) Values of Radiation Shielding Effectiveness Metrics for the Composite Samples from the 800 MeV/u <sup>28</sup>Si Beam Exposure\***

Target	Surviving Fraction of the Primaries		Absorbed Dose (nGy)		Avg. Q After (nSv)	Dose Equivalent	
	Abs.	Rel.	Abs.	Rel.	Target	Abs.	Rel.
C #1	0.675	1.060	57.6	1.034	12.64	727.9	1.037
C #2	0.683	1.072	57.8	1.038	12.65	731.5	1.042
PE	0.637	1.000	55.7	1.000	12.61	702.0	1.000

\* All samples were approximately 4.4 gm/cm<sup>2</sup> thick.; C #1 = Composite 1, C #2 = Composite 2.

illustrated later, this increase in areal density compared to PE is offset by gains in the composites' multifunctional properties.

## DEVELOPMENT OF THE COMPOSITE ARCHITECTURE

### Composite 1: Structure and Radiation Shielding

The material product form used to fabricate the composite consisted of a high-strength fabric that was plain woven from UHMW PE Spectra 1000 fibers. Individual fibers were 30 μm in diameter with ultimate tensile strength (UTS) and modulus in the range of 3 GPa and 103 GPa, respectively.<sup>16</sup> A typical plain weave consists of fibers laid in the 0° warp and 90° fill direction as schematically shown in Figure 2a. A single-ply UHMWPE fabric is shown in Figure 2b. Several such plies were hand laid using a thermoset resin typically employed for aerospace applications. The resin system was selected based on its long pot life desirable for hand lay-up operations and its reasonably high glass transition temperature of 90°C. To enhance adhesion between the PE fabric and resin, the fabric was gas plasma treated prior to the composite lay up. For the current application, the fabric was oxidized during the plasma treatment. Gas plasma treatment promotes superior adhesion through surface roughening and increasing the surface area of the fiber, and by generating oxygen-containing functional groups on the fiber surface.<sup>17</sup> After lay up, the composite was autoclaved at 600 kPa for 24 hours during final curing. The natural exotherm produced by the resin system during curing was monitored and kept below 90°C. The finished composite was in the form of

a plate with desired dimensions for either radiation or mechanical testing. A typical 30.5 cm<sup>3</sup> × 15.2 cm<sup>3</sup> × 1.27 cm<sup>3</sup> Composite 1 plate is shown in Figure 2c. Composite 1 was used for charac-

**This composite was characterized for radiation shielding effectiveness, hypervelocity ballistic impact resistance, and thermal exposure characteristics.**

terization of mechanical and radiation shielding properties.

### Composite 2: Architecture with Thermal and Ballistic Protection Multifunctionality

A second composite sample, designated Composite 2, was fabricated to further enhance the multifunctional nature of the composite by addressing thermal management and ballistic impact resistance properties. A thermal protection system (TPS) is typically employed to withstand the space environment and extremely high heat flux encountered during re-entry. For example, the black high-temperature reusable surface insulation (HRSI) tiles typically seen on the belly of the space shuttle are exposed to approximately 1,300°C during re-entry.<sup>18</sup> It is anticipated that re-entry from a lunar mission will expose the vehicle to even higher temperatures. A combination of an open-cell carbon foam and plasma

deposited B<sub>4</sub>C coating on the exterior surface of the carbon foam was used to address these requirements (see Figure 3a). A coal-based carbon foam was selected primarily because of its low density (0.268 g/cm<sup>3</sup>), low thermal conductivity (0.25–5 W/mK depending on the cell structure), and ability to withstand temperatures up to 3,000°C in a non-oxidizing atmosphere or with suitable surface protection. Thermal conductivity of the carbon foam is comparable to that of the HRSI tiles used on the space shuttle.

B<sub>4</sub>C was deposited on the surface of the carbon foam via vacuum plasma spraying (VPS). An as-deposited B<sub>4</sub>C coating is shown in Figure 3b. The texture of the B<sub>4</sub>C coating reflects the texture of the carbon foam substrate surface. The 1 mm thick coating was deposited using a B<sub>4</sub>C powder feedstock fed through an argon plasma with H<sub>2</sub> assist gas. The VPS technique was used for this application because it provides a durable mechanical and metallurgical bond between the carbon and B<sub>4</sub>C without the use of low-temperature materials or bonding agents. Durability is essential for high-temperature applications such as re-entry vehicles. In addition, the VPS process has the ability to rapidly produce an adherent deposit on curved surfaces and for acreage applications. A 1.25 cm thick carbon foam brick with the B<sub>4</sub>C coating was bonded to the PE composite using the matrix epoxy. The complete architecture of Composite 2 is shown in Figure 3c. This composite was characterized for radiation shielding effectiveness, hypervelocity ballistic impact resistance, and thermal exposure characteristics.

## HEAVY ION EXPOSURE OF COMPOSITES

Since it is currently not feasible to test the radiation-shielding effectiveness of new materials in the free space GCR environment, the only realistic way to experimentally assess the shielding effectiveness of these materials is to expose them to heavy ion beams at an accelerator facility. Availability of beam time and appropriate beam type for such experiments can be limited since only two such facilities exist worldwide: the NASA Space Radiation Laboratory (NSRL) at the Brookhaven

National Laboratory, and the Heavy Ion Medical Accelerator (HIMAC) in Chiba, Japan. An 800 MeV/u  $^{28}\text{Si}$  (incident LET 45.96 keV/ $\mu\text{m}$ ) beam, a reasonably good GCR-proxy beam for shielding effectiveness evaluation,<sup>11,12</sup> was made available for exposure of the composite samples at HIMAC. Exposures were carried out with the assistance of personnel at NSRL. During the exposure several silicon detectors were placed upstream and downstream of the sample. Upstream detectors were used to verify the monochromatic beam source while the downstream detectors were used to determine the charges of the particles emitting from the sample material. Further details related to detector stacks, data acquisition, and shielding analysis have been presented elsewhere.<sup>11</sup>

Figure 4 shows the absolute fragment fluence per incident ion as a function of fragment charge for the composite samples as well as for PE. Fragment fluence, one of the metrics used for measuring radiation-shielding effectiveness, is defined as the number of particles with charge  $Z$  emerging from the downstream side of the sample within a 1 cm<sup>2</sup> circle centered on the beam axis. This metric is essentially a measure of the capability of a material to fragment heavy charged particles into lighter charged particles. On this basis, Figure 4 clearly illustrates that both Composites 1 and 2 are capable of fragmenting the incoming silicon beam ( $Z = 14$ ), and their performance is comparable to that of the benchmark PE material. It should be noted that fragments with  $Z < 6$  were not resolved by the detectors and as such are not shown in the figure.

It is customary for accelerator exposure measurements not to estimate the systematic uncertainties (which are typically of the order of 2% to 5%) for the sake of time and resource optimization. As a result only values that are relative to a benchmark material, PE in this case, should be evaluated. Table II lists some of these relative metrics to evaluate the shielding effectiveness of the two composites. In terms of surviving fractions (or attenuation) of the primary silicon beam, the composites are a maximum of 7.2% inferior to PE. In addition, the two composites are mar-

**Table III. Measured Mechanical Properties of Composite 1 in Comparison to Some Traditional Al Alloys used in Spacecraft Structures**

Material Type	UTS (MPa)	Density (kg/m <sup>3</sup> )	Specific UTS (N-m/kg)	Specific Modulus (N-m/kg)
Composite 1	447	980	$4.5 \times 10^5$	21.5
Al 2024/T81	481	2,768	$1.7 \times 10^5$	25.5
Al 2219/T81	455	2,851	$1.5 \times 10^5$	26.8
Al 5052/H38	290	2,680	$1.08 \times 10^5$	25.2

ginally (3.4–4.2%) inferior to PE both in terms of dose and dose-equivalent. It is equally important to note from the data that the measured shielding effectiveness of the composite samples (areal density = 4.4 g/cm<sup>2</sup>) are in agreement with the transport calculation results

**Hence, based on both experimental measurements and transport calculations it is reasonable to conclude that the developed composites will have shielding effectiveness comparable to PE and definitely much superior to currently used aluminum alloys.**

presented in Figure 1. Hence, based on both experimental measurements and transport calculations it is reasonable to conclude that the developed composites will have shielding effectiveness comparable to PE and definitely much superior to currently used aluminum alloys.

### **COMPOSITE 1: CHARACTERIZATION OF MECHANICAL PROPERTIES**

Panels of Composite 1 were machined using a waterjet to obtain dog-bone tensile testing samples according to ASTM D 638-03 specifications (see Figure 5). During testing, titanium tabs were used to reduce stress concentration and to prevent grip damage at the sample ends. Constant displacement tensile testing was performed using a

load cell of 100 kN. A total of seven Composite 1 samples were tested. A representative stress-strain curve for Composite 1 is shown in Figure 6. Unlike metallic systems, a typical yield point is not obvious for such composites. As expected, the epoxy matrix failed first, and this is indicated by the change in slope between 1.5% and 2.4% strain. Beyond this point the load was completely transferred to the PE fabric until failure occurred at about 4.4% strain. Figure 6b shows the failure of the epoxy matrix while the PE fiber bundles appear to be bound and compact. Even at final fracture of the composite (see Figure 6c) there was hardly any indication of fibrillation at the fractured surface since the presence of epoxy is clearly evident between the fiber bundles. This desirable behavior of the composite structure can be attributed to superior surface adhesion between the fabric and the epoxy matrix as a result of the fabric surface treatment using gas plasma.

The average measured UTS and elastic modulus of Composite 1 along with properties of aluminum alloys such as Al 5052, Al 2219, and Al 2024 are listed<sup>19,20</sup> in Table III. These alloys are typically used for space applications such as the International Space Station modules and space shuttle fuselage. It is evident that the PE fabric composite has UTS and specific modulus values comparable to the aluminum alloys. However, their main advantage is highlighted in the two density and UTS columns within Table III. Composite 1 is about 2.8 times lighter (lower density) than the aluminum alloys, and consequently its specific strength (strength/weight ratio) is 2.5 to 4 times greater than typical aerospace aluminum alloys. The preliminary radiation shielding and mechanical testing data presented in this paper for Composite 1 clearly illustrate that the proposed com-

posite deserves further attention as a viable multifunctional material for replacing traditional aluminum alloys.

## BALLISTIC PROPERTIES OF COMPOSITES 1 AND 2

For any composite architecture to be considered for a crew vehicle application its ballistic properties, for example, micrometeoroid impact response, have to be addressed. Terrestrially, the micrometeoroid environment can be simulated by impacting the test material

with soda lime glass bead projectiles 0.4 mm in diameter at velocities in the range of 6–7 km/s. The experimental system used for such testing is a two-stage micro-light gas gun (MLGG) as shown in Figure 7. In the first stage, an explosion at the breach end moves a piston forward, which compresses H<sub>2</sub> gas behind a diaphragm. Once the diaphragm is ruptured, the second stage initiates where the compressed gas enters the barrel and moves the projectile at hyper velocities. The projectile fi-

nally enters the target chamber where it impacts the target. The low molecular weight of H<sub>2</sub> provides the ultra-high-velocity flows needed to achieve hyper velocities.

The effectiveness of micrometeoroid impact resistance was quantified by measuring the crater diameter and the damage diameter of the samples after ballistic impact testing. The initial impact of the projectile results in a straight and narrow track, and its diameter is defined as the crater diameter. The subsequent shock wave generated within the target material is absorbed either through straining of the matrix or by creating new surfaces. The new surfaces are manifested as a damaged area and can be quantified by a corresponding damage diameter. As can be seen from Figure 8a, the projectile impact created a 3.2 mm diameter crater on the impact surface of Composite 1. In addition, the extremely high strain rate was manifested in the form of delamination and dimpling on the back surface of the composite. In comparison, the VPS-deposited B<sub>4</sub>C coating only had a comparable crater diameter with no associated damage area (Figure 8b). There was no indication of spalling or erosion on the underlying carbon foam.

To obtain a better insight into the significant improvement in ballistic resistance of Composite 2, a numerical modeling scheme was undertaken. Relevant properties, such as density, modulus of elasticity, shear modulus and Poisson's ratio, for both B<sub>4</sub>C and carbon foam were obtained from the literature.<sup>21</sup> A finite element model builder was used to mesh the B<sub>4</sub>C coating with 162,500 elements and the glass bead projectile with 2,275 elements. To match the experimental conditions, the imposed projectile impact velocity was 6 km/s. Based on the material's properties, failure strain (FS) of 0.12 and 0.01 were used for the B<sub>4</sub>C and projectile, respectively. As part of the modeling scheme, a failure strain erosion criterion was used such that the elements within the B<sub>4</sub>C coating and glass bead projectile were eroded once the plastic strain within those elements exceed 0.12 and 0.01, respectively. Figure 9a shows an example of the effect of hypervelocity ballistic impact as a function of failure strain. For FS = 0.12, the

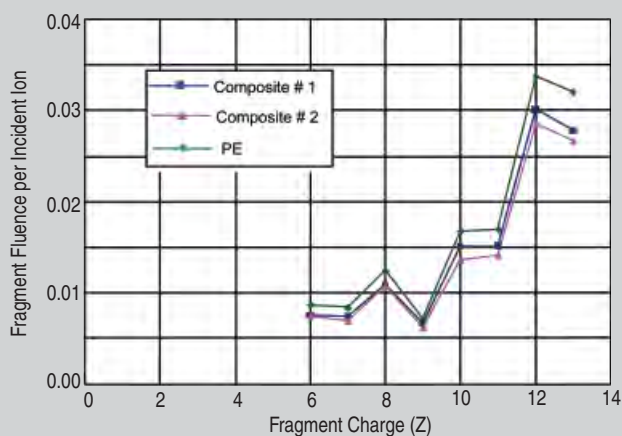


Figure 4. The absolute fragment fluence per incident ion as a function of fragment charge from 800 MeV/u <sup>28</sup>Si beam exposure. All samples had an areal density of 4.4 gm/cm<sup>2</sup>. The fragmentation efficiency of both composites was comparable to the PE benchmark material.

Figure 5. A schematic showing the dimensions (in centimeters) of the tensile test sample as per ASTM D638-03. Also shown is an actual test sample that was machined using a waterjet.

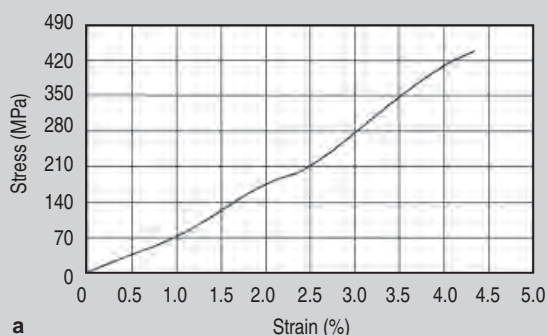
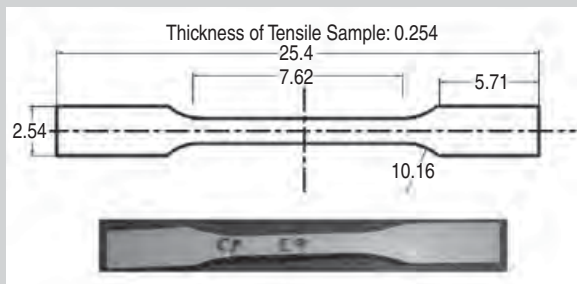
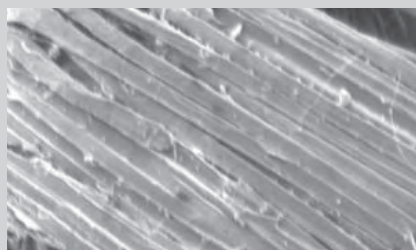


Figure 6. (a) Typical stress-strain characteristics of Composite 1. (b) A scanning electron microscope image of a typical fractured surface of Composite 1 showing the PE fiber bundles are still bound and (c) a higher-magnification view of the fiber bundles at the fractured surface showing good bonding between PE and epoxy matrix.





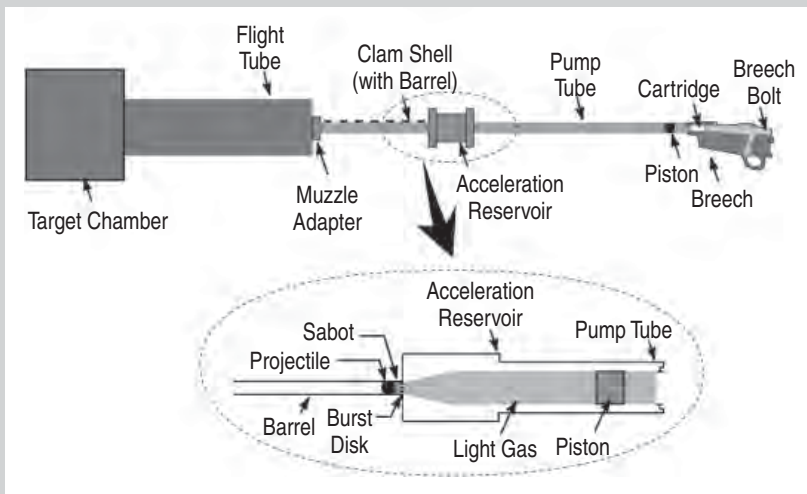


Figure 7. The operational details of a two-stage micro-light gas gun.

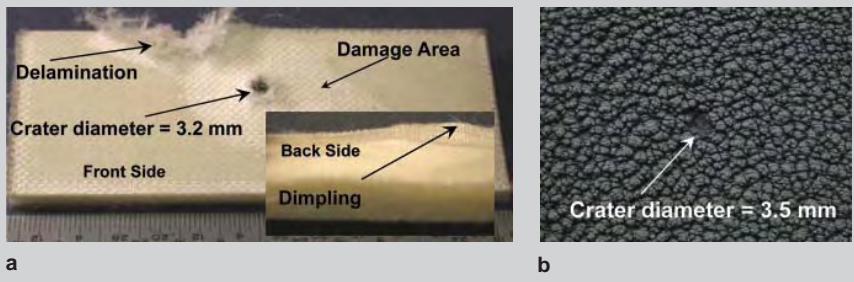


Figure 8. (a) The ballistic impact damage on Composite 1. Note the damage area, delamination, and crater diameter on the front side and dimpling on the back side (insert) of the composite in comparison to (b) impact response of VPS-deposited  $B_4C$  on Composite 2 which shows only a crater diameter with no corresponding damage area. No damage was observed in the underlying carbon foam and PE composite.

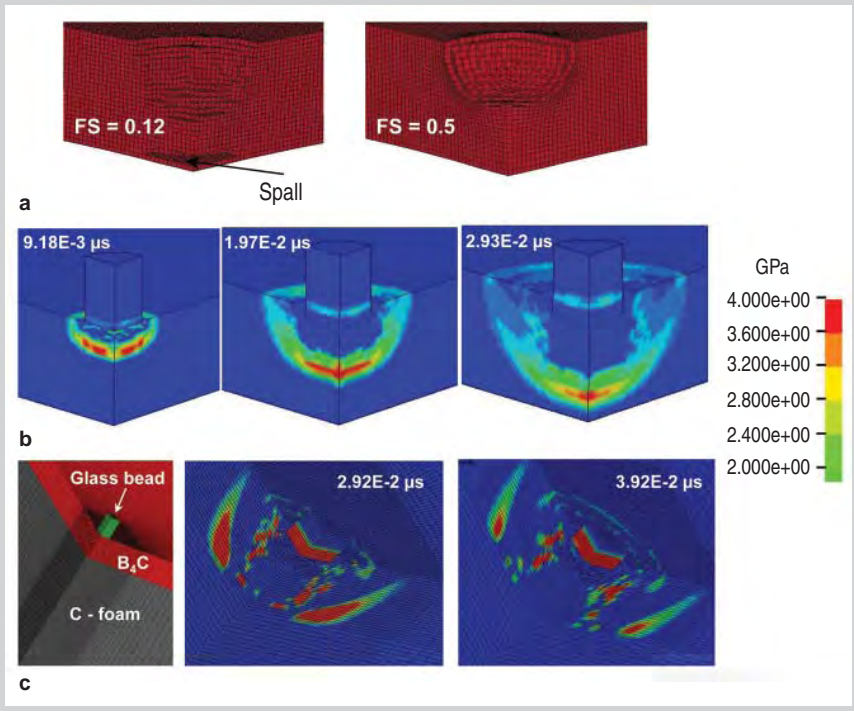


Figure 9. Finite element modeling results (a) showing the effect of hypervelocity impact as a function of material property, namely failure strain and (b) quantifying the magnitude of compressive stress propagating through the  $B_4C$  coating, (c) illustrating the reflection of compressive wave from the carbide-foam interface.

damage is more localized, and plastic strain is sufficient to cause erosion (spalling) of elements at the distal side of the  $B_4C$  coating. This is exactly what was observed for Composite 2 (Figure 8b). If, for example,  $B_4C$  was replaced by a material with  $FS = 0.5$ , no spalling would be observed at the distal side. However, the damage would no longer be localized, and would instead be manifested as bulking or volume change. The  $FS$  value for PE is much higher than 0.5, and therefore the more widespread damage observed for Composite 1 (Figure 8a) is not surprising. The projectile was completely eroded at the very early stages of impact. The model predicted that on impact a compressive stress wave of 4 GPa would be generated in the composite ahead of the projectile. Figure 9b shows the propagation of this compressive wave as a function of time. The effect of this

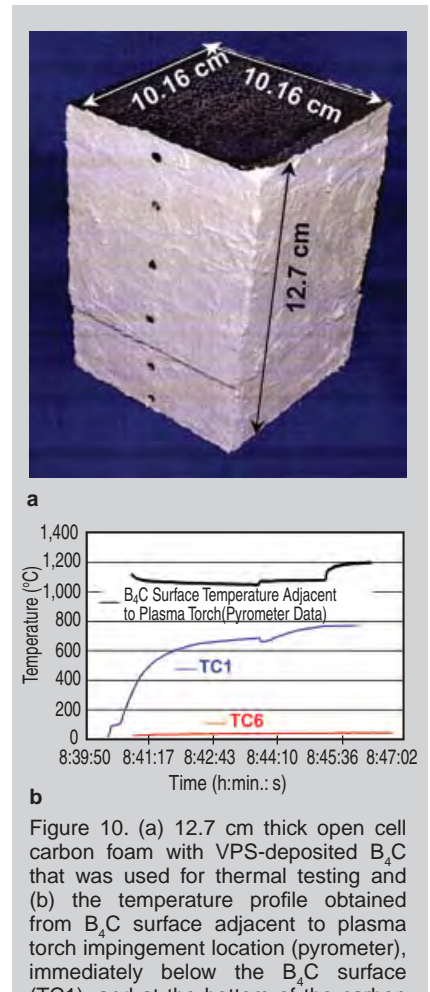


Figure 10. (a) 12.7 cm thick open cell carbon foam with VPS-deposited  $B_4C$  that was used for thermal testing and (b) the temperature profile obtained from  $B_4C$  surface adjacent to plasma torch impingement location (pyrometer), immediately below the  $B_4C$  surface (TC1), and at the bottom of the carbon foam block (TC6). Only the  $B_4C$  face was exposed to the plasma. The other sides of the carbon foam were protected with a high-temperature alumina paste.

compressive wave on the underlying carbon foam needs further analysis.

The impact response of the two-component system consisting of the B<sub>4</sub>C deposit and the underlying carbon foam was simulated to investigate whether the compressive stress wave would traverse through the carbon foam. Figure 9c shows the mesh profile at the interface of the two component system. The longitudinal and transverse wave velocity, V<sub>E</sub> and V<sub>G</sub> respectively, in a medium can be expressed as

$$V_E = \left[ \frac{\left( K_1 + \frac{4}{3}G \right)}{\rho_o} \right]^{1/2} \quad (1)$$

$$V_G = \left( \frac{G}{\rho_o} \right)^{1/2} \quad (2)$$

where K<sub>1</sub> is bulk modulus, G is the shear modulus, and ρ<sub>o</sub> is the density. Since both G and K for carbon foam are almost three orders of magnitude less than the values of B<sub>4</sub>C, V<sub>E</sub>, and V<sub>G</sub> in carbon foam are almost 18 times less than in B<sub>4</sub>C. The model predicts that the compressive wave is not transmitted through the carbon foam but is instead reflected back into the B<sub>4</sub>C top layer. This reflection is shown in Figure 9c at time steps 2.92 × 10<sup>-2</sup> μs and 3.92 × 10<sup>-2</sup> μs. This reflected wave potentially caused spalling on the distal side of the B<sub>4</sub>C layer. Previous experimental and modeling studies conducted on multilayer composites have also shown that a low modulus material such as carbon foam is preferable for prevention or minimization of longitudinal wave transmission.<sup>22</sup> The experimental and modeling results presented here demonstrate that the proposed composite architecture is capable of protecting the underlying PE structural layer from hypervelocity micrometeoroid impact.

## THERMAL CHARACTERISTICS OF COMPOSITE 2

A preliminary assessment of the thermal characteristics of Composite 2 was performed to determine the ability of B<sub>4</sub>C coating and carbon foam to protect the underlying structural PE com-

posite when subjected to the high temperatures experienced during spacecraft re-entry in Earth's atmosphere. Several pieces of carbon foam were adhered together using a high-temperature carbon-based adhesive to fabricate a 10.1 cm<sup>3</sup> × 10.1 cm<sup>3</sup> × 12.7 cm<sup>3</sup> test block (Figure 10a). The test block was dried at room temperature for 4–8 hours, then cured at 130°C for 4 hours and 260°C for 2 hours to remove adhesive volatiles. Sample thickness was 12.7 cm to closely duplicate the thickness of the HRSI space shuttle tiles. The top surface of the carbon foam was coated with a 1 mm thick B<sub>4</sub>C layer using the VPS technique as de-

**However, this preliminary testing demonstrates a path toward development of a complementary thermal protection system without significant sacrifice of the radiation shielding effectiveness.**

scribed earlier. The sides of the carbon foam were coated with an Al<sub>2</sub>O<sub>3</sub> paste to prevent excessive oxidation during the high-temperature test. Six thermocouples located along the centerline of the test block were used to monitor the temperature profile through the thickness.

During testing the B<sub>4</sub>C face of the test block was exposed to a high-temperature plasma for a duration of 7 minutes to produce the temperature profile shown in Figure 10b. A maximum surface temperature of 1,200°C was measured for the B<sub>4</sub>C coating using a two-color pyrometer. However, it should be emphasized that the pyrometer was placed at an approximate angle of 45° to the B<sub>4</sub>C face, and it was aimed a few centimeters away from the point of plasma impingement. Therefore, the temperature at the point of impingement was greater than 1,200°C. The

distance between the plasma and the test block was reduced twice to obtain higher test temperatures. Visible light glow signifying extreme heating at the point of plasma impingement was observed only when the distance was reduced to 3 cm. The test duration of 7 minutes was reasonably close to the re-entry time of 8–12 minutes recorded during the Apollo lunar missions.<sup>23</sup> Two thermocouple profiles (TC1 and TC6) are shown in Figure 10b. TC1 was placed 6.7 mm below the B<sub>4</sub>C and the carbon foam interface while TC6 was positioned 12.1 cm below the coating interface of the 12.7 cm thick test block. TC1 recorded a maximum temperature of about 800°C during the test. This indicates that the B<sub>4</sub>C coating provided significant thermal protection by dropping the temperature by more than 400°C over a thickness of 6.7 mm. More importantly, the temperature profile recorded by TC6 indicates a maximum temperature of 39°C for the duration of the test. Therefore, a structural PE composite placed below the 12.7 cm thick thermal protection system would be adequately protected. The thermal protection capability presented here is preliminary. Further refinement of the surface temperature measurement system is required to accurately estimate the high-temperature capabilities of the proposed system. However, this preliminary testing demonstrates a path toward development of a complementary thermal protection system without significant sacrifice of the radiation shielding effectiveness.

## CONCLUSION

Simulation results indicated that over thicknesses ranging from 1 g/cm<sup>2</sup> to 20 g/cm<sup>2</sup>, Composite 1 was only about 1% to 5% less effective than pure PE, while the entire composite structure, including thermal and ballistic protection, was only 2% to 8% less effective compared to pure PE. However, transport code analysis indicated that the composites were much superior to traditional aluminum aerospace alloys. These predictions were validated by subsequent sample construction and 800 MeV/μ<sup>28</sup>Si beam testing. The measured mechanical, ballistic, and thermal properties indicate that a multifunctional composite approach can

significantly compensate for the marginal increase in areal density required for the composites to be comparable to pure PE in terms of radiation shielding effectiveness. Tensile strength measurement demonstrated that the developed composites have specific strength 2.5 to 4 times greater than typical aluminum aerospace alloys. Numerical evaluation and experimental validation demonstrated that selection of an open cell carbon foam material with a VPS deposited B<sub>4</sub>C coating can be instrumental in providing protection from micrometeoroid impact and re-entry temperatures to an underlying PE structural composite.

During ballistic testing, the B<sub>4</sub>C coating was responsible for complete erosion of the projectile almost on impact. Extremely low bulk and shear modulus of the carbon foam prevented transmission of the compressive stress wave generated during impact, thereby protecting the underlying structural composite material. Also of note is the versatility of the VPS technique in depositing a well adhered B<sub>4</sub>C coating even on an irregular surface such as the open cell C foam, circumventing the problems typically associated with depositing coatings on curved and uneven surfaces for high-temperature use. Thermal testing indicated that on exposing the B<sub>4</sub>C layer to temperatures 1,200°C and above, the maximum temperature recorded at the bottom of the 12.7 cm thick carbon foam sample did not exceed 40°C. This thermal capability is comparable to that of the high-temperature ceramic tiles that are currently used on the space shuttle.

It should be noted that expected re-entry temperatures from a lunar mission will be higher, and hence much more elaborate and accurate characterization of thermal management schemes are mandated. Nevertheless, this paper has demonstrated the valid-

ity and importance of a multifunctional composite architecture that could potentially circumvent the problem of paying a penalty in additional weight to implement passive radiation shielding. Such a multifunctional composite holds the key for safe long duration missions beyond LEO. As a first step, the developed composites were selected by NASA's Materials International Space Station Experiment program for further evaluation. As part of this evaluation these samples have recently been attached to the aft side of the International Space Station and will be exposed to the LEO environment for approximately 6 months.

## ACKNOWLEDGEMENTS

*The authors are grateful to the NASA Small Business Innovative Research program for funding this effort. The experimental nuclear physics group at Brookhaven National Laboratory, New York, is acknowledged for support and expertise during exposure of the samples to heavy ion beams and data reduction. The authors are also grateful to Dr. Sheila Thibeault of NASA's Langley Research Center for technical discussions and encouragement during the course of the project. The authors wish to express their gratitude to Ms. Ernestine Cothran of BAE Systems for her patience and dedication through resolving administrative issues toward the project.*

## References

1. "Guidance on Radiation Received in Space Activities," *National Council on Radiation Protection and Measurements Report No. 98* (1989).
2. G.D. Badhwar and P. O'Neill, *Adv. Space Res.*, 17 (2) (1996), pp. 7-17.
3. J.W. Wilson, *Health Phys.*, 79 (5) (2000), p. 470.
4. M.A. Shea and D.F. Smart, *Solar Phys.*, 127 (June 1990), pp. 297-320.
5. T.A. Parnell, J.W. Watts, and T.W. Armstrong, "Radiation Effects and Protection for Moon and Mars Mission," *Proceedings of the Sixth International Conference and Exposition on Engineering, Construction, and Operations in Space, Space 98*

- (Reston, VA: American Society of Civil Engineers, 1998), pp. 232-234.
6. H. Smith, editor, *1990 Recommendations of the International Commission on Radiological Protection, Annals of the ICRP*, vol. 21/1-3 (New York: Pergamon Press, 1991).
7. "The Relative Biological Effectiveness of Radiations of Different Quality," *National Council on Radiation Protection and Measurements Report No. 104* (1990).
8. J.W. Wilson et al., *NASA Technical Paper 3682* (Hampton, VA: Langley Research Center, December 1997).
9. J.E. Turner, *Atoms, Radiation, and Radiation Protection*, 2nd edition (New York: Wiley-Interscience Publishers, 1995), pp. 160-161, 350-351.
10. F.A. Cucinotta et al., *Adv. Space Res.*, 17 (2) (1996), pp. 77-86.
11. S. Guetersloh et al., *Nucl. Instr. and Meth. in Phys. Res. B.*, 252 (2006), pp. 319-332.
12. R.K. Kaul, A.F. Barghouty, and H.M. Dache, "Radiation Transport Properties of Polyethylene-Fiber Composites," *Proceedings of the Conference on Microgravity Transport Processes in Fluid, Thermal, Biological, and Materials Sciences* (New York: Annals of the New York Academy of Sciences, 2004), pp. 138-149.
13. J. Miller et al., *Rad Res.*, 159 (2003), pp. 381-390.
14. J.W. Wilson et al., *NASA Report #1257* (Washington, D.C.: NASA, 1994).
15. P.M. O'Neil, *Adv. Space Res.*, 37 (2006), pp. 1727-1733.
16. F.C. Campbell, *Manufacturing Technology for Aerospace Structural Materials*, 1<sup>st</sup> edition (Amsterdam, The Netherlands: Elsevier Ltd., 2006).
17. D.M. Choi et al., *Polymer*, 38 (25) (1997), pp. 6243-6249.
18. *Reusable Launch Vehicle Technology Development and Test Program*, report submitted by the Committee on Reusable Launch Vehicle Technology and Test Program (Washington, D.C.: National Academy Press, 1995).
19. *ASM Materials Handbook, Volume 20* (Materials Park, OH: ASM International, 2001).
20. *Aluminum Standards and Data* (Arlington, VA: The Aluminum Association Publication, 2006), pp. 2-2-2-3.
21. G. Johnson and T. Holmquist, *J. Appl. Phys.*, 85 (12) (1999), pp. 8060-8073.
22. A. Tasdemirci and W. Hall, *J. Comp. Mat.*, 39 (11) (2005), pp. 981-1005.
23. J.E. Pavlosky and L.G. St. Leger, *NASA Technical Note # TN D-7564* (Washington, D.C.: NASA, January 1974).

**S. Sen, principal scientist for the NASA Program, is with BAE Systems, NASA Marshall Space Flight Center/EM 30, Building 4464, Room 111A, Huntsville, AL 35812, USA. E. Schofield, materials engineer, and J.S. O'Dell, project engineering manager, are with Plasma Processes Inc., Huntsville, Alabama. L. Deka, materials engineer, and S. Pillay, assistant professor, are with the Department of Material Science & Engineering, University of Alabama at Birmingham. Dr. Sen can be reached at (256) 544-8264; fax (256) 544-6660; e-mail Subhayu.Sen-1@nasa.gov.**

# The Mechanical Characterization of Carbon-Nanotube-Reinforced Polymer-Matrix Nanocomposites: An Unfolding Story of Interface

Yogeeswaran Ganesan and Jun Lou

A polymer nanocomposite is created by introducing nanoparticulates into a macroscopic polymer matrix. Polymer nanocomposites represent a new class of material alternative to conventional filled polymers and possess some extremely interesting properties. The alteration/enhancement of the properties of these materials can partially be attributed to the fact that the properties of the nanoparticulate fillers are substantially different/better than that of the micrometer-scale fillers and partially owing to the fact that when a good dispersion is obtained the filler-matrix interfacial area tends to be dramatically larger when compared to that in traditional composites. This paper presents an overview of past work done on the mechanical characterization of one such type of polymer matrix nanocomposite, the carbon-nanotube-reinforced polymer-matrix composite. The primary emphasis is on the properties of the filler/matrix interface and the methods used for interfacial characterization.

## INTRODUCTION

Ever since the discovery of carbon nanotubes (CNTs) by S. Iijima<sup>1</sup> almost two decades ago, attempts have been made to incorporate them into polymer matrices in order to exploit their superior mechanical properties. Some theoretical predictions have suggested that the stiffness of nanotubes could be as high as that of the basal plane of graphite crystals (1 TPa) or even higher.<sup>2,3</sup> Single-wall CNTs can also exhibit strength and strain-to-failure values that substantially exceed those of traditional micrometer-diameter carbon fibers.<sup>4</sup> However, the superior

### How would you...

*...describe the overall significance of this paper?*

*This paper presents an overview of past work done on the mechanical characterization of carbon-nanotube (CNT)-reinforced polymer-matrix nanocomposites with an emphasis on the filler/matrix interface. It also discusses some future directions in the field with a focus on studies using micro-electro-mechanical systems.*

*...describe this work to a materials science and engineering professional with no experience in your technical specialty?*

*The mechanical performance of a CNT-reinforced polymer-matrix composite is strongly dependent upon the filler/matrix interactions at the nanoscale. The various methodologies that have been employed to study the mechanical aspects of CNT/polymer matrix interfaces in different polymer systems have been reviewed and the main results from these investigations have been summarized in this paper.*

*...describe this work to a layperson?*

*Carbon-nanotube-reinforced polymer-matrix composites are promising materials for high stiffness, toughness, and high-strength applications. However, their mechanical properties are highly dependent upon the properties of the filler/matrix interface. Hence, much energy has been expended and numerous techniques have been explored to characterize the interfacial regions in these composites. This paper presents an overview of the interfacial characterization of such composites and explores some of the future directions in the field.*

mechanical properties of CNTs alone do not guarantee the nanocomposite's superior strength, stiffness, and fracture toughness. The effective utilization of nanotubes in composite applications depends strongly on the ability to disperse the tubes homogeneously throughout the matrix without destroying the integrity of the CNTs.<sup>5</sup> If the tubes are poorly dispersed, they tend to exhibit failure by separation from bundles or aggregates rather than failure by fracture.<sup>6</sup> It also critically depends on the effectiveness of the interfacial stress transfer which in turn depends on the nature and strength of the nanotube/matrix interface. There are three major modes of interaction between a CNT and a polymer matrix: chemical bonding, nano-mechanical interlocking, and non-bond interactions (van der Waals and electrostatic). A perfect sp<sup>2</sup> hybridized carbon structure has a limited ability to form any sort of strong covalent bonds with a surrounding polymer matrix. This is somewhat dependent on the type of matrix used since there is some evidence that a few polymers, such as polyurethane and poly(methyl methacrylate), chemically bond with pristine CNTs.<sup>7,8</sup> A nanotube's interaction with any given polymer matrix can be improved via chemical modification of the tubes with functional groups. However, a disadvantage with modifying the hollow nanotubes by sidewall functionalization is that it changes the surface structure and breaks carbon-carbon bonds along the graphite sidewall, and therefore affects the intrinsic properties of the nanotubes. Fortunately, non-disruptive chemical modifications such as wrapping of surfactants or

DNA around the nanotubes or adsorption of aromatic structures onto their sidewalls can often be adopted to improve the level of chemical interaction at the interfaces.<sup>9</sup> Nano-mechanical interlocking could be difficult in nanotube composites due to the atomically smooth surface of a carbon nanotube. There is some evidence to prove that nanotubes slide relatively easily from a surrounding polymer matrix after full debonding from the matrix.<sup>10</sup> However, this might not be the case with nanotubes with twisted, uneven surfaces or mechanically deformed nanotubes with surface steps formed by gliding of dislocations.<sup>11</sup> Some form of interlocking may exist in these systems.

There have been conflicting studies pertaining to non-bond interactions, primarily based on theoretical models or simulations, especially with regard to their impact on adhesion at the interface. As a result of the filler/matrix interactions, if there exists a strong adhesive force between the CNT and the matrix at the interface, an applied load (stress) on the composite could almost be completely transferred to the reinforcing nanotube. If the adhesion is weak, interface failure or debonding may occur at small loads, and the nanotubes could end up behaving as nanostructured flaws, introducing local stress concentrations and reducing the overall strength of the composite. While a weak interface between a nanotube and a matrix can be exploited to

produce useful functionalities such as high mechanical damping or toughness (since nanotube slippage could create significant friction and therefore a large amount of energy dissipation), it is desirable to have a composite with strong adhesion forces at the interface.

It is thus important to recognize that the mechanical performance of a CNT-reinforced polymer-matrix composite is strongly dependent upon the filler/matrix interactions at the nano-scale. The ability to design and manufacture nanocomposites with desired properties is contingent upon the ability to unveil the fundamental mechanisms governing filler/matrix interactions at relevant length scales as well as the ability to rationalize the consequences of these interactions on the macroscopic performance of the composite. There have, therefore, been a considerable number of studies devoted to this area; with continuing efforts, the story of the interface is gradually unfolding.<sup>4,12,13</sup>

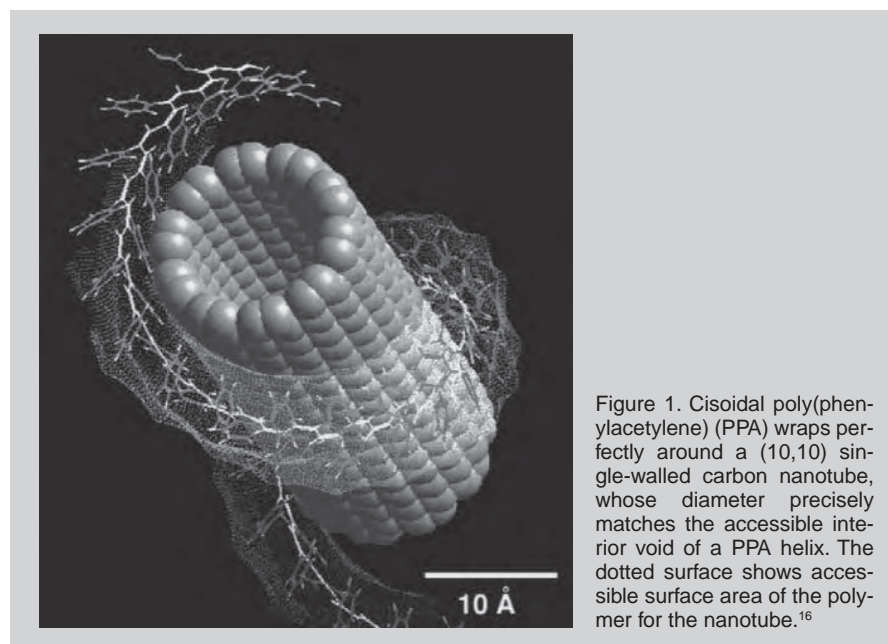


Figure 1. Cisoidal poly(phenylacetylene) (PPA) wraps perfectly around a (10,10) single-walled carbon nanotube, whose diameter precisely matches the accessible interior void of a PPA helix. The dotted surface shows accessible surface area of the polymer for the nanotube.<sup>16</sup>

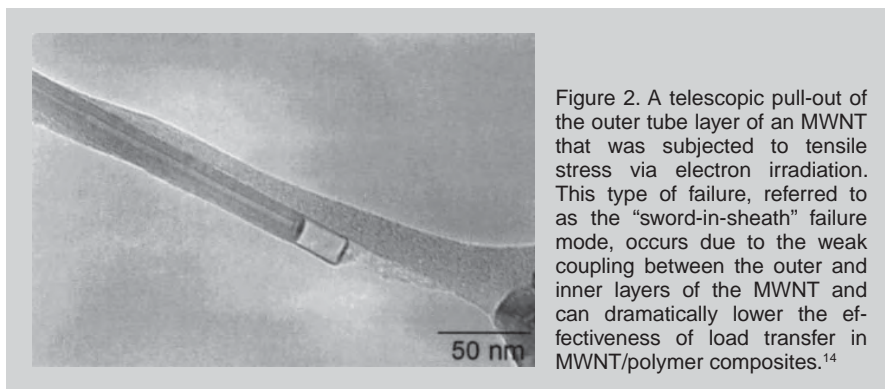


Figure 2. A telescopic pull-out of the outer tube layer of an MWNT that was subjected to tensile stress via electron irradiation. This type of failure, referred to as the “sword-in-sheath” failure mode, occurs due to the weak coupling between the outer and inner layers of the MWNT and can dramatically lower the effectiveness of load transfer in MWNT/polymer composites.<sup>14</sup>

## MODELING AND SIMULATION METHODS

The small size of the nanotube and of the nano-interfacial region presents difficulties to researchers hoping to study the interfacial properties of CNT-reinforced polymer nanocomposites. Hence, many researchers have had to rely on atomistic simulations and multi-scale modeling (combining molecular dynamics [MD] and quasi-continuum frameworks) for their studies. K. Liao and S. Li<sup>15</sup> used MD simulations to show that the interfacial strength, based on non-bond interactions, can be as high as 100 MPa for a polyethylene-MWNT system, and 160 MPa for a polystyrene-MWNT system. These strengths are one order of magnitude higher than those associated with most carbon fiber-polymer systems. The same techniques were used by V. Lordi and N. Yao<sup>16</sup> to study the binding energy (non-bond) and sliding friction stresses between CNTs and a range of polymer substrates. Interestingly, the authors concluded that the contribution of non-bond binding energy and friction forces to interfacial adhesion was only minor and that, in the absence of chemical bonding, helical conformation of polymers around CNTs could facilitate the creation of a strong interface (see Figure 1). S.J.V. Frankland et al.,<sup>17</sup> using a shear lag model to estimate the shear stress from the critical axial stress, also predicted a very low interfacial strength (2 MPa) for a CNT-polyethylene system if van der Waals forces prevailed as the weak non-bond interaction. On the other hand, the authors predicted that with the introduction of a relatively low density (<1%) of chemical bonding between the CNT and the matrix, the interfacial strength could be increased

by more than one order of magnitude. More recently, Frankland and V.M. Harik<sup>18</sup> simulated (using MD) CNT pull-out from a crystalline polymer matrix and observed linear trends in the nanotube velocity-force relation which they used to estimate an effective viscosity coefficient for interfacial sliding at the NT/polymer interface. The authors used a nanoscale analog of Newton's friction law and parameterized the pull-out force, an effective viscosity, and the strain rate in order to develop a model for CNT-polymer interfacial sliding.

Attempts have also been made to utilize the modified continuum mechanics approach to study CNT/polymer interfaces. One must note that in order for a continuum mechanics model to adequately describe such a system, a number of considerations are required to be made, since the diameter of a SWNT is generally about the same size as that of a polymer chain. H.D. Wagner<sup>19</sup> modified the classical Kelly-Tyson model to account for the tube structure of SWNTs and showed that very high interfacial strength is attainable in SWNT-reinforced composites, in agreement with the results from prior MD simulations.<sup>15,16</sup> He, however, excluded MWNT-reinforced composites from consideration, worrying about the telescopic inter-wall sliding failure that can occur in MWNTs at critical stresses as low as 0.5 MPa (see Figure 2). With the recent development of a nonlinear cohesive law for CNT/polymer interfaces directly from inter-atomic potentials,<sup>20</sup> it might in fact soon be possible for researchers to develop a continuum-based micromechanics model incorporating

appropriate cohesive laws, which can, in turn, provide a direct link between the macroscopic behavior of nanocomposites and the quantitatively measured nanoscale behavior of CNT/matrix interfaces. However, it must be noted that although these simulations and models do shed a considerable amount of light on the CNT/matrix interface, the question still remains as to how accurately they capture the physical essence of the filler/matrix interface.

### MACRO-SCALE TESTING AND MICROSCOPY METHODS

Data from standard macro-scale tests performed on CNT-reinforced composite specimens can be analyzed using equations derived from standard composite theory in order to yield valuable information on the filler/matrix interface. M.S.P. Shaffer et al.,<sup>21</sup> for example, conducted systematic tensile tests on catalytically grown MWNT-reinforced polyvinyl alcohol (PVA) thin films. The tensile elastic modulus of the composites was assessed using a dynamic mechanical thermal analyzer (DMTA) as a function of nanotube loading and temperature. The stiffnesses of the composites measured at room temperature were found to be only marginally better than that of the unreinforced polymer matrix. Based on their analysis of the test results using the Krenchel's expression for short-fiber composites,<sup>22</sup> the authors hypothesized that poor stiffness values were primarily due to imperfections in the graphitic layers of the catalytically grown nanotubes used, poor shear stress transfer between the

shells of MWNTs under tensile axial loading, and excessive bending of tubes after dispersion into the matrix.

M. Cadek et al.,<sup>23</sup> on the other hand, obtained more encouraging results with their nanoindentation experiments on arc-grown MWNT-reinforced PVA and poly(9-vinyl carbazole) (PVK) composites. The Young's modulus and hardness of the composites were both found to increase by factors as high as 1.8 and 1.6 with the addition of 1 wt.% MWNTs in PVA and 2.8 and 2.0 with the addition of 8 wt.% MWNTs in PVK. The aforementioned values were subsequently plugged into the modified Halpin-Tsai equation for randomly oriented fibers<sup>24</sup> in order to compare the interfacial strengths of the two composites. The analysis showed that strong adhesion forces existed at the interfaces in both composites with the interfacial bonding in MWNT/PVA composites being far superior to the one that existed in MWNT/PVK composites. Wagner et al.<sup>25</sup> conducted tensile tests on MWNT/polyurethane/diacrylate oligomer thin films using an Instron apparatus and observed nanotube fragmentation within the composites after failure. By plugging in the average value for fragment length within the specimens into a modified Kelly-Tyson model<sup>19,26</sup> equation, the authors were able to ascertain the stress transfer ability of the nanotube-polymer interfaces and found it to be of the order of 500 MPa and up, and thus, an order of magnitude higher than the stress transfer ability of some of the currently used advanced composites.

Both scanning and transmission electron microscopy can be used to visualize a CNT within a polymer matrix and qualitatively study factors such as nanotube dispersion, tensile fracture mechanisms, and interfacial adhesion. Qian et al.<sup>5</sup> performed in-situ transmission electron microscopy deformation studies on MWNT/polystyrene (PS) composites, prepared by a simple solution-evaporation method, in order to shed some light on the tensile fracture mechanisms in such composites. The authors adopted a technique in which the TEM electron beam was condensed onto specific regions on a thin film of the composite, thus inducing local thermal stresses which in turn initiated cracks in the composite. Cracks

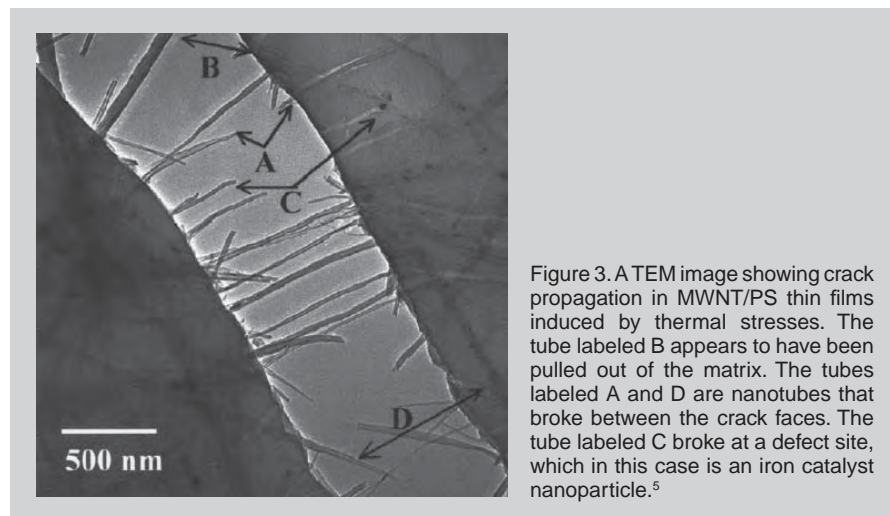


Figure 3. A TEM image showing crack propagation in MWNT/PS thin films induced by thermal stresses. The tube labeled B appears to have been pulled out of the matrix. The tubes labeled A and D are nanotubes that broke between the crack faces. The tube labeled C broke at a defect site, which in this case is an iron catalyst nanoparticle.<sup>5</sup>

were found to nucleate at low nanotube density areas and then propagate along weak nanotube–PS interfaces or relatively low nanotube density regions. The presence of nanotubes was found to be advantageous since they aligned perpendicular to the direction of crack propagation and bridged the crack faces in their wake, thus providing closure stresses across the crack faces (see Figure 3). Only when the crack opening displacement exceeded ~800 nm were the nanotubes found to break and/or pull out of the matrix. P. Watts and W. Hsu performed similar experiments on MWNT-reinforced 2-methacryloyloxyethyl phosphorylcholine (2-(diethylamino) ethyl methacrylate diblock copolymer (MPC-DEA) composites.<sup>27</sup> Their observations were similar to the ones made by Qian et al., with a notable exception being that Watts and Hsu observed no tube breakage, possibly owing to the fact that defect-free arc grown tubes were used in their experiments as opposed to catalytically grown tubes. Examination, via high-resolution microscopy, of nanotubes on fracture specimen surfaces can shed some light on the nature and strength of interfaces. Fragmentation of tubes, as observed by O. Lourie et al.<sup>28</sup> on the surface of SWNT/epoxy composite tensile fracture specimens, can provide some insight on the nature of load transfers at the interfaces. The presence of a polymer layer on a nanotube after fiber pullout can indicate a strong filler-matrix interface. It is possible, by measuring the contact angles between the nanotubes and the polymer, to estimate the actual interfacial energy for a given composite. C. Bower et al.<sup>29</sup> observed contact and adherence of polymer to most of the nanotubes examined on the surface of an MWNT/polyhydroxyaminoether composite fracture specimen. On the other hand, poor wetting and no apparent sheathing of nanotubes by epoxy was observed from SEM micrographs of fractured surfaces of an SWNT/epoxy composite by P.M. Ajayan et al.,<sup>6</sup> suggesting the existence of a weak interface.

## SPECTROSCOPY AND THERMOANALYSIS

A number of spectroscopic techniques have also been used to study the

properties of such nanocomposites at the interfacial regions. Micro-Raman spectroscopy can be used to qualitatively measure the effectiveness of load transfer in MWNT-reinforced composites because the second-order  $A_{1g}$  (disorder-induced) Raman peak position shifts with applied strain on the tubes. L.S. Schadler et al.<sup>30</sup> conducted macroscopic tensile and compression experiments on MWNT/epoxy resin composite specimens using standard testing procedures (American Society for Testing and Materials D638 and D695-91 tests) while simultaneously using Raman spectroscopy to monitor the strain on the tubes (see Figure 4). The authors found the compression modulus of the composites to be higher than the tensile modulus and that load transfer to the nanotubes was much more effective in compression. The authors attributed the ineffective load transfer to the tubes during tension to weak coupling between the outer and inner layers of the multi-wall tubes and to poor interfacial adhesion. The second-order  $A_{1g}$  mode has also been found to shift with applied strain in SWNTs. Ajayan et al.<sup>6</sup> performed tensile tests on SWNT bundle reinforced epoxy composites and observed small shifts in the second order  $A_{1g}$  band upon loading. The authors inferred that the individual nanotubes were not significantly stretched upon application of axial tension due to sliding of the nanotubes out of the bundles. Z. Jia et al.<sup>7</sup> successfully used infrared (IR) transmission spectroscopy to study the chemical bonds between nanotubes and PMMA in an MWNT/PMMA composite they synthesized by an in situ polymerization technique. The presence of a new peak in the IR spectrum of the composite at about 1,665  $\text{cm}^{-1}$  was considered as evidence for the existence of C-C bonds between the nanotubes and PMMA. Near-IR band gap fluorescence has also been used to study load transfer, strain, and interfacial adhesion limits in semiconducting SWNT-reinforced composites: Spectral shifts are proportional to strain in the tubes and marked deviations from linearity of the shifts can be interpreted as loss of nanotube-polymer adhesion and reveal slippage of individual nanotubes within the matrix. T.K. Leeuw et al.<sup>31</sup> used this technique recently to estimate

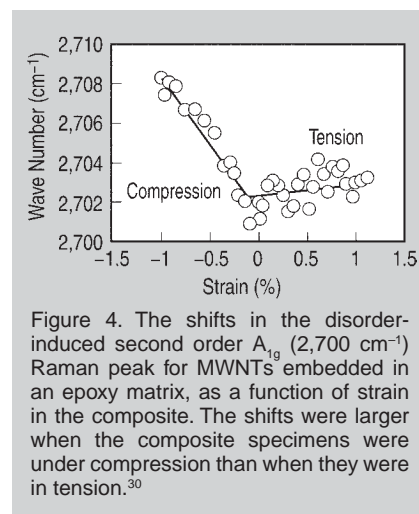


Figure 4. The shifts in the disorder-induced second order  $A_{1g}$  ( $2,700 \text{ cm}^{-1}$ ) Raman peak for MWNTs embedded in an epoxy matrix, as a function of strain in the composite. The shifts were larger when the composite specimens were under compression than when they were in tension.<sup>30</sup>

the forces required to overcome adhesion at an SWNT/PMMA interface, the values for which were found to be 1.5–6 nN.

In amorphous polymer matrices, the addition of nanotubes can either increase or decrease the mobility of polymer chains at the interface. The change in the mobility of polymer chains can be probed by measuring the glass transition temperature of the composite, typically by using techniques such as differential scanning calorimetry (DSC) or dynamic mechanical analysis (DMA).<sup>4</sup> In the case of semi-crystalline polymers such as PVA and poly(*w*-phenylenevinylene-co-2,5-dioctyloxy-*p*-phenylenevinylene) (PmPV), the addition of nanotubes can often lead to an increase in the degree of crystallinity, with the nanotubes acting as nucleation sites for crystallization of the polymer at the interface. An increase in the degree of crystallinity can improve the mechanical properties of the composite because the presence of a shell of crystalline polymer around a nanotube can strongly enhance load transfer at the interface. Also the amplified crystallinity can act as an additional component of reinforcement, thus increasing the modulus above the levels expected from nanotube addition alone. Again, thermoanalytical techniques, such as DSC and thermogravimetric analysis (TGA), can be put to use in order to quantify the crystallinity induced within these composites. Cadek et al.,<sup>23</sup> for example, used the DSC technique to study the melting behavior of a 1 wt.% MWNT/PVA composite and found that the crystallinity percentage of the

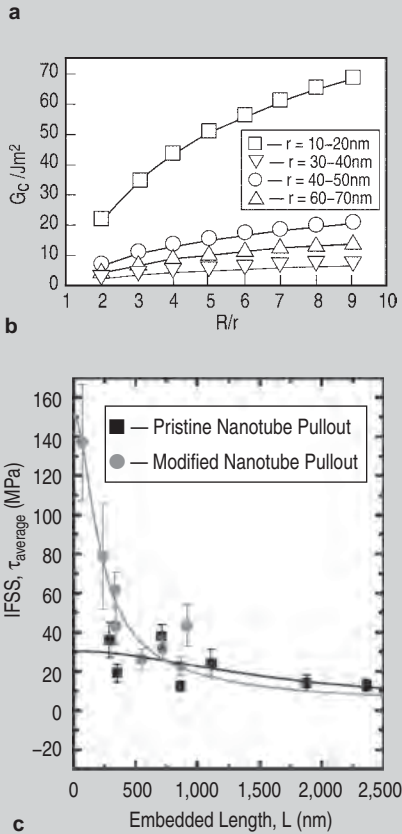
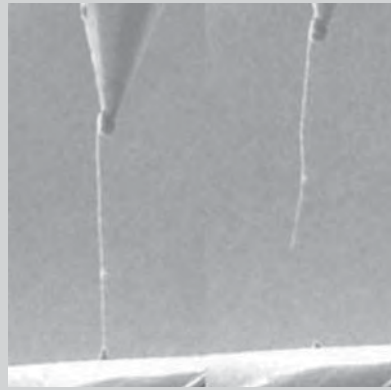


Figure 5. (a) An SEM image showing the configuration of a single nanotube pullout experiment performed by Barber et al.<sup>34</sup> The left part of the image shows a nanotube having one end attached to an AFM tip and another end embedded within a polymer matrix. The right part of the image shows the nanotube after pullout from the matrix. (b) The variation of interfacial fracture energy,  $G_c$ , for MWNT/polyethylene-butene composites as a function of the representative stress transfer parameter ( $R/r$ ) for nanotubes with different radii.<sup>33</sup> (c) The average interfacial shear strength (IFSS) plotted against the embedded length for pristine and chemically modified MWNTs pulled out from an epoxy matrix. A shear-lag model was fitted to the experimental data for pristine nanotube (black line) and chemically modified nanotube pullout (gray line) in order to ascertain the shear lag constant,  $\beta$ .

polymer increased by 13% upon nanotube addition. Similarly, J.N. Coleman et al.<sup>32</sup> used TGA oxidation data to qualitatively assess the increase in crystallinity of PmPV upon addition of 4 wt.% MWNTs.

### DIRECT LOCALIZED CHARACTERIZATION METHODS

It is worth noting that only a few of the aforementioned techniques provide any sort of quantitative information on the magnitude of the interfacial strength in such composites. Also, as all of them are indirect techniques, they are subject to numerous discrepancies. In 2002, C.A. Cooper et al.<sup>10</sup> developed a direct technique for measuring interfacial strength that involved drawing out individual MWNTs and SWNT ropes bridging across holes in the matrix using the tip of a scanning probe microscope, while recording the forces involved. The lateral force exerted by the SPM tip on the tubes was resolved into its component parallel to the relevant direction in order to ascertain the nanotube-polymer interfacial shear strength. Tests on MWNT-epoxy composites showed that the interface strength decreased with an increase in the embedded length of the nanotubes and that its values were significantly higher than those in fiber-polymer interfaces; in some cases the strength was as high as 376 MPa.

The aforementioned technique was subsequently modified by A.H. Barber et al.<sup>33</sup> to perform single fiber pullout tests to measure the interfacial strengths of MWNT/polyethylene-butene composites. Individual carbon nanotubes, attached to the end of an atomic force microscope (AFM) tip, were pushed into a molten polymer. Following solidification of the polymer, the nanotubes were pulled away, with the force required for pullout being recorded. Using an energy balance approach, the authors were able to ascertain the interfacial fracture energy,  $G_c$ , for the composites as a function of the representative stress transfer parameter ( $R/r$ , where  $R$  is the matrix radial distance from the fiber axis at which shear tends to zero and  $r$  is the nanotube radius) for nanotubes with different radii (see Figure 5b). For pristine nano-

tubes, the interfacial fracture energies were found to be between 4 J/m<sup>2</sup> and 70 J/m<sup>2</sup> and thus comparable to that of fiber pullout in other engineering composite systems such as glass-fiber-reinforced maleic anhydride modified polypropylene (6–7 J/m<sup>2</sup>), vinyl ester (13–34 J/m<sup>2</sup>), polyamide 6 (24–93 J/m<sup>2</sup>), and polyamide 6.6 (52–61 J/m<sup>2</sup>). The authors postulated that the large interfacial strength values were due to bonding of the tubes with the polymer via defects in their structure or due to the wrapping of polymer chains around the nanotubes.

The authors performed a set of similar experiments<sup>34</sup> within an SEM chamber (see Figure 5a), comparing the interfacial strengths of chemically modified (carboxyl group functionalized to induce covalent bonding with epoxide containing molecules) MWNT/epoxy composites to that of pristine MWNT/epoxy composites (see Figure 5a). The force required to pull each nanotube out of the polymer was seen to increase as the embedded length increased, with chemically modified nanotubes showing correspondingly larger pullout forces when compared with pristine ones. Also, for both types of nanotubes, at relatively large embedded lengths, the stress in the nanotubes was found to be large enough to break the nanotube instead of pulling it out from the epoxy, with the modified nanotubes requiring smaller embedded lengths for nanotube fracture. Both modified and, to a lesser extent, pristine nanotubes showed an increase in the average interfacial shear strength (IFSS), calculated by dividing the nanotube pullout force by the lateral area ( $2\pi rL$ , where  $L$  is the embedded length), with embedded length decrease, a behavior consistent with classical shear lag theory.<sup>35</sup> Using the plot of IFSS vs. nanotube embedded length (see Figure 5c), the authors determined the shear lag constant,  $\beta$ , for the composites.  $\beta$  values for pristine and modified nanotube-based composites ( $1.05 \times 10^6 \text{ m}^{-1}$  and  $7.95 \times 10^6 \text{ m}^{-1}$ , respectively) were found to be orders of magnitude greater than those calculated for larger single-fiber composites ( $1 \times 10^4$  to  $1 \times 10^5 \text{ m}^{-1}$ ),<sup>36</sup> indicating that stress transfer might be much more efficient in nanotube/polymer composites than in traditional fiber-based composites.



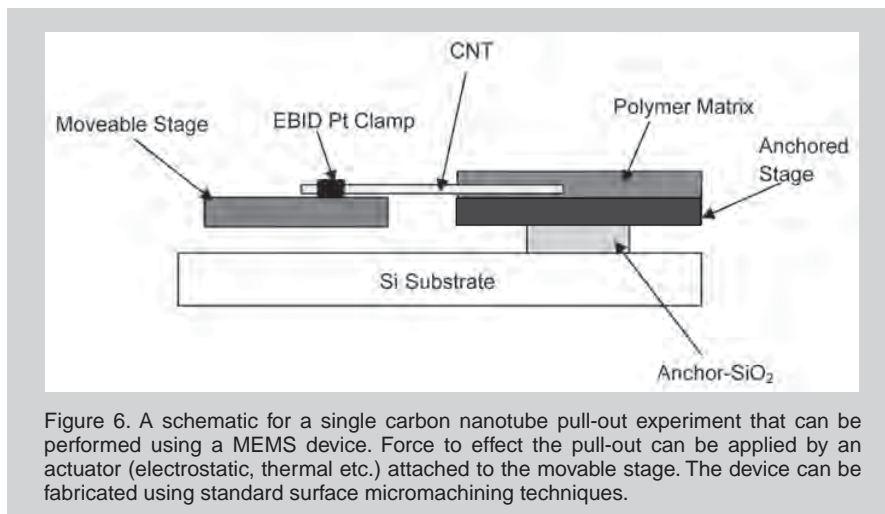


Figure 6. A schematic for a single carbon nanotube pull-out experiment that can be performed using a MEMS device. Force to effect the pull-out can be applied by an actuator (electrostatic, thermal etc.) attached to the moveable stage. The device can be fabricated using standard surface micromachining techniques.

## FUTURE DIRECTIONS

While there has been nearly one decade of research on interfacial strength and related load-transfer mechanisms in CNT reinforced polymer nanocomposites, the ability to manipulate the behavior of the CNT/polymer matrix interface to achieve desired properties still remains rather limited and largely empirical. The difficulties can be traced to two fundamental issues. First, reliable measurements of the critical interfacial parameters such as shear strength are difficult to make, given the small size of the nanotube and the lack of a robust testing platform at the nanoscale. Second, a theoretical framework connecting nanoscale interfacial features to macroscopic properties is yet to be fully developed. Any future breakthrough has to be able to address at least one of these two issues. As discussed, recent developments in the field of multi-scale modeling might help solve the second problem. The authors would like, however, to focus on the first problem by highlighting some new trends in the field of quantitative nanomechanical characterization of CNT/matrix interfaces.

Microelectromechanical-system (MEMS)-based devices possess the ability to move in a controlled fashion with measurable output signals like force and displacement and owing to their small size, can be used within an SEM or a TEM chamber, thus making them ideal candidates for a wide range of experiments at the micro- and nano-scales.<sup>37,38</sup> Using a MEMS-based testing platform to perform single fiber pullout experiments, quantitative mechanical characterization of the interfacial interaction

between individual CNTs and polymer matrices has been envisioned (see Figure 6). Although CNT manipulation and precise on-chip deposition of matrix materials can be challenging, the potential of MEMS-based techniques for localized quantitative interfacial measurements should not be underestimated.

## CONCLUSIONS

The nature and strength of the filler/matrix interface plays an important role in determining the mechanical properties of a CNT-reinforced polymer composite. Hence, much energy has been expended and numerous techniques explored to characterize the interfacial regions in these composites. While a vast majority of the aforementioned techniques are indirect and provide information that is either qualitative or based on numerous assumptions, a few direct techniques can be used to obtain quantitative data pertaining to the interface. However, further advancements, such as the development of a reliable theoretical framework based on models and simulations and a robust testing platform for localized quantitative measurements, are needed for a better understanding of the nanotube-polymer interface.

## ACKNOWLEDGEMENT

The authors would like to acknowledge the support by National Science Foundation grants NSF ECCS 0702766 and CMMI 0800896 and by Air Force Research Laboratory grant AFRL FA8650-07-2-5061.

## References

1. S. Iijima, *Nature*, 354 (1991), pp. 56–58.
2. G. Overney et al., *Z. Phys. D*, 27 (1) (1993), pp.

- 93–96.
3. B.I. Yakobson et al., *Phys. Rev. Lett.*, 76 (14) (1996), pp. 2511–2514.
4. L.S. Schadler et al., *JOM*, 59 (3) (2007), pp. 53–60.
5. D. Qian et al., *Appl. Phys. Lett.*, 76 (20) (2000), pp. 2868–2870.
6. P.M. Ajayan et al., *Adv. Mater.*, 12 (10) (2000), pp. 750–753.
7. Z. Jia et al., *Mater. Sci. Eng.*, A271 (1999), pp. 395–400.
8. K. Liao et al., *Appl. Phys. Lett.*, 79 (25) (2001), pp. 4225–4227.
9. P.M. Ajayan and J.M. Tour, *Nature*, 447 (2007), pp. 1066–1068.
10. C.A. Cooper, *Appl. Phys. Lett.*, 81 (20) (2002), pp. 3873–3875.
11. J.Y. Huang et al., *Phys. Rev. Lett.*, 100 (2008), pp. 035503-1–035503-4.
12. H.D. Wagner and R.A. Vaia, *Materials Today*, 7 (11) (2004), pp. 38–42.
13. A.V. Desai and M.A. Haque, *Thin-Walled Structures*, 43 (2005), pp. 1787–1803.
14. F.H. Gojny et al., *Chem. Phys. Lett.*, 370 (2003), pp. 820–824.
15. K. Liao, and S. Li, *Appl. Phys. Lett.*, 75 (25) (2001), pp. 4225–4227.
16. V. Lordi and N. Yao, *J. Mater. Res.*, 15 (12) (2000), pp. 2770–2779.
17. S.J.V. Frankland, *Phys. Chem. B*, 106 (12) (2002), pp. 3046–3048.
18. S.J.V. Frankland and V.M. Harik, *Surf. Sci.*, 525 (1–3) (2003), pp. L103–L108.
19. H.D. Wagner, *Chem. Phys. Lett.*, 361(1-2) (2002), pp. 57–61.
20. H. Tan et al., *Composites Science and Technology*, 67 (14) (2007), pp. 2941–2946.
21. M.S.P. Shaffer and A.H. Windle, *Adv. Matl.*, 11 (11) (1999), pp. 937–940.
22. H. Krenchel, *Fibre Reinforcement* (Copenhagen, Denmark: Akademisk Forlag, 1964).
23. M. Cadek et al., *Appl. Phys. Lett.*, 81 (27) (2002), pp. 5123–5125.
24. J.C. Halpin Affdl and J.L. Kardos, *Polym. Eng. Sci.*, 16 (5) (1976), pp. 344–352.
25. H.D. Wagner et al., *Appl. Phys. Lett.*, 72 (2) (1998), pp. 188–190.
26. A. Kelly and W.R. Tyson, *J. Mech. Phys. Solids*, 13 (1965), pp. 329–340.
27. P.C.P. Watts and W.K. Hsu, *Nanotechnology*, 14 (5) (2003), pp. L7–L10.
28. O. Lourie and H.D. Wagner, *Appl. Phys. Lett.*, 73 (24) (1998), pp. 3527–3529.
29. C. Bower et al., *Appl. Phys. Lett.*, 74 (22) (1999), pp. 3317–3319.
30. L.S. Schadler et al., *Appl. Phys. Lett.*, 73 (26) (1998), pp. 3842–3844.
31. T.K. Leeuw et al., *Nano Lett.*, 8 (3) (2008), pp. 826–831.
32. J.N. Coleman et al., *AIP Conf. Proc.*, 633 (2002), pp. 557–561.
33. A.H. Barber et al., *Composites Science and Technology*, 64 (2004), pp. 2283–2289.
34. A.H. Barber et al., *Adv. Mater.*, 18 (2006), pp. 83–87.
35. H.L. Cox, *Br. J. Appl. Phys.*, 3 (1952), pp. 72–79.
36. Z.-F. Li and D.T. Grubb, *J. Mater. Sci.*, 29 (1) (1994), pp. 189–202.
37. Y. Ganesan et al., *IEEE-NANO Conf. Proc.*, 8 (2008), pp. 783–786.
38. Y. Zhu and H.D. Espinosa, *PNAS*, 102 (41) (2005), pp. 14503–14508.

Yogeeswaran Ganesan and Jun Lou are with the Department of Mechanical Engineering and Materials Science, Rice University, 6100 Main Street, Houston, TX 77005. Dr. Lou can be reached at (713) 348-3573; fax (713) 348-5423; e-mail jlou@rice.edu.

# The Characterization of High-Density Polyethylene/Organoclay Nanocomposites

Tathiane Cordeiro Rodrigues, Maria Inês Bruno Tavares, Igor Lopes Soares, and Ana M. Moreira

*Polymeric nanocomposites, which are hybrids of polymers and modified inorganic clay with organic surfactants, are extremely attractive in both science and industry. These materials present improvements in such polymer properties as modulus, heat capacity, thermal stability, flame resistance, and so on. Research has been conducted in recent decades to obtain high-quality materials that can be used in applications like food packing, car components, and combustible cells. Polymeric nanocomposites present many advantages in relation to composites due to the quantity of filler added to the polymer and also to the improved properties. In a composite, the quantity of filler must be as high as possible (i.e., over 30%). In the polymeric nanocomposite the quantity of filler varies from 1% to 5% because of the nanosize of the particles. These nanoparticles often have a large surface area that results in improved polymer-matrix properties.*

## INTRODUCTION

Polyethylene is a commodities polymer with many uses, including food packaging which is disposed of quickly in landfills. The environmental impact is substantial as the polymer products accumulate in landfills. Research has been done to improve the polymer degradation process. Many studies were carried out to obtain blends with polysaccharides such as starch, for example,<sup>1,2</sup> but little improvement resulted. Recently the development of new polymeric nanocomposites, formed from polymers and layered silicates, have gained attention.<sup>3-5</sup> The high-density polyethylene (HDPE) lamellar silicate nanocomposite may improve the HDPE properties and may induce better degradation upon disposal.<sup>6-9</sup>

However, complete knowledge of the nanomaterial is needed to evaluate its behavior and potential applications. To obtain that knowledge, the evaluation of nanostructure ordination and molecular dynamics of these materials is necessary.

Solid-state nuclear magnetic resonance (NMR) spectroscopy was used for this work because it is an important tool for the study of both molecular structure and dynamic behavior.<sup>10,11</sup> Solid-state techniques aid in the observation of changes in structural and dynamic behavior, focusing on the polymer chains in the nanocomposite material.<sup>12-14</sup> Generally nanocomposites can be characterized by conventional techniques such as x-ray diffraction (XRD), transmission electron microscopy (TEM), thermal analysis, and mechanical properties.<sup>15-18</sup>

The main purpose of this study was to apply both conventional techniques and NMR to obtain as much information as possible on nanocomposites, especially those that are polyethylene-based. Low-field NMR was used to understand changes in the molecular mobility of the polymer matrix after organoclay is incorporated. Thus, in this work nanocomposites based on an HDPE matrix and organically modified clay were prepared by melt processing, using a twin-screw extruder, varying the shear rate parameter at 60 rpm and 90 rpm. Nanocomposites obtained were characterized through XRD, thermal analysis, impact resistance, and NMR. The XRD was employed to obtain information on crystalline ordination. Thermal analysis through differential scanning calorimetry (DSC) and thermogravimetric analysis (TGA) was carried out to evaluate changes in the glass temperature ( $T_g$ ), melting temperature ( $T_m$ ), and thermal stability. The impact resistance was measured to evaluate its variability. Solid-state NMR measurements were carried out through the relaxation time parameter ( $T_1H$ ), which is able to generate response on organoclay dispersion in the polyethylene matrix, as well as the interactions between both nanocomposite components in the nanostructured materials. The  $T_1H$  results showed that the samples present different molecular domains according to the clay dispersion; intercalation and/or exfoliation in the polymer matrix.

See the sidebar for a description of materials and methods used.

## RESULTS AND DISCUSSION

Processing parameters such as temperature, melt viscosity of the polymer,

### How would you...

...describe the overall significance of this paper?

*This paper discusses the methodology for preparation of the nanocomposite and also the use of low-field solid-state nuclear magnetic resonance as a technique to separate exfoliated and intercalated organoclay in the polymeric matrix.*

...describe this work to a materials science and engineering professional with no experience in your technical specialty?

*The authors describe an interesting work that involves a new characterization method to study polymeric nanocomposites.*

...describe this work to a layperson?

*This work presents a useful method to evaluate nanocomposites through nuclear magnetic resonance.*

## MATERIALS AND METHODS

### Samples

The polyethylene sample used in this study was supplied by Rio-Pol S/A (Rio de Janeiro, Brazil) and named EI (melt flow index: MFI = 7.0 g/min., 190°/2.16 kg). The commercial montmorillonite organoclay (OMMT) was supplied by Bentec S/A. The nature of OMMT is bentonite clay, organically modified with a quaternary alkylammonium compound (C18). Both polymers and organoclay were used as-received.

### Nanocomposite Preparation

The blending was performed using melt processing in a torque rheometer, Rheocord 9000 (formerly Haake, now Thermo Fisher Scientific, Waltham, Massachusetts), equipped with a conical counter-rotating twin screw extruder at a typical high density polyethylene (HDPE) processing temperature (190°C), operating at 60 rpm and 90 rpm, as illustrated in Figure A. The nanomaterials obtained (Figure B) from the extruder were cut into pellets and analyzed directly using low-field nuclear magnetic resonance (NMR) and thermal analysis. Films for x-ray characterization were obtained by pressing the pellets. For the impact resistance, eight measurements were done for each sample.

### Materials Characterization

The extent of clay intercalation and/or exfoliation for HDPE/organoclay nanocomposites was observed by x-ray diffraction (XRD) analysis. The films were characterized using an XRD 6000 x-ray diffractometer (Shimadzu, Kyoto, Japan) with nickel-filtered  $\text{CuK}\alpha$  ( $\lambda = 1.54 \text{ \AA}$ ) radiation operated at 40 kV and 30 mA. The data were recorded at  $2\theta$  rates of  $2^\circ$  per minute. The basal spacing of the nanocomposite was calculated using the Bragg's relation:

$$\lambda = 2 d \sin\theta.$$

The melting temperature and glass transition were determined for each sample in a differential scanning calorimetry (DSC) V4.4E (TA Instruments, New Castle, Delaware) under the following conditions: nitrogen atmosphere, 30 mL/min.; heating velocity,  $10^\circ\text{C}/\text{min.}$ , and temperature range, 10–250°C. The thermogravimetric analyses were carried out on a TGA 7 series (PerkinElmer, Waltham, Massachusetts), with temperatures ranging from 30°C to 700°C, in nitrogen atmosphere. Impact resistance was measured in an Izod impact instrument, under conditions specified by the ASTM D 618. The samples were conditioned for 40 h at  $23 \pm 2^\circ\text{C}$  with  $50 \pm 5\%$  of relative humidity.

A low-field NMR Maran Ultra 23 spectrometer (Resonance Instruments, Skokie, Illinois), operating at 23 MHz (for protons), and equipped with an 18 mm variable temperature probe, was used to determine relaxation measurements (Figure C). Proton spin-lattice relaxation times (T<sub>1H</sub>) were determined directly by the traditional inversion recovery pulse sequence ( $180^\circ - \tau - 90^\circ$ ) and the  $90^\circ$  pulse of 4.6  $\mu\text{s}$  was calibrated automatically by the instrument software. The amplitude of the FID was sampled for twenty  $\tau$  data points, ranging from 0.1 ms to 5,000 ms, with four scans for each point and 5 s of recycle delay. The relaxation values and relative intensities were obtained by fitting the exponential data with the aid of the program WINFIT (Figure D), and the domain distribution was obtained by the WINDXP software. Both WINFIT and WINDXP are commercial programs and came with the spectrometer.

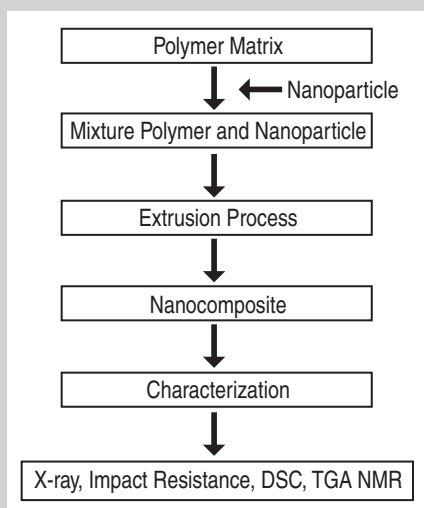


Figure A. Nanocomposite preparation and characterization. (TGA = thermogravimetric analysis).

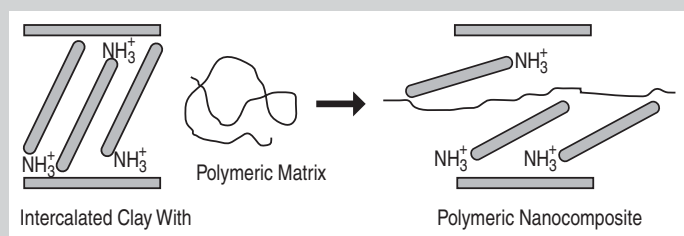


Figure B. Nanocomposite formation.



Figure C. A low-field NMR spectrometer.

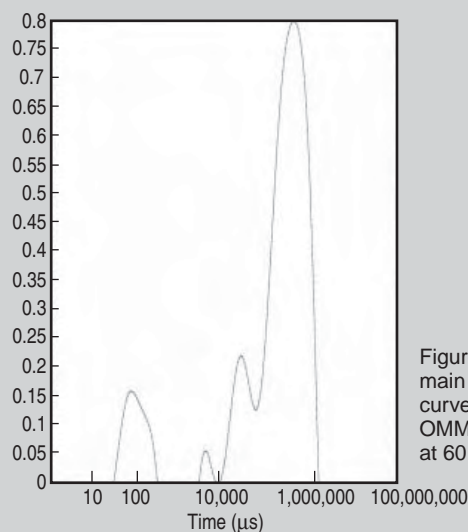


Figure D. The domain distribution curve for the EI/OMMT processed at 60 rpm.

**Table I. The Relationship of Nanocomposite Ratio, Rotation Processing, and XRD Data for OMMT and EI/OMMT Nanocomposites at the Two Shear Rates Evaluated**

Material Type (Å)	Composition (EI/OMMT)	Rotation (rpm)	XRD	
			2θ	d-spacing
OMMT	0/100	—	3.2	27.6
EI/OMMT	95/5	60	2.8	31.5
		90	3.1	28.5

mixing time, and screw speed must be evaluated to produce clay exfoliation. Also considered was that high mixing speed may lead to a higher degree of clay intercalation and/or exfoliation. During nanocomposite preparation the clay dispersion was evaluated to gain an understanding of two mechanisms: interlamellar clay spacing, which needs to be increased to facilitate polymer chains insertion, and the exfoliation process through the polymer chains intercalation.

The XRD results (Figure 1) showed that polyethylene chains were intercalated into organoclay lamellae. A slight shift in the (d001) peak was observed for all HDPE/nanoclay compounds at lower angles. Table I shows the relationship of nanocomposites ratio, rotation processing, and XRD data for montmorillonite organoclay (OMMT) and EI/OMMT nanocomposites at the two shear rates evaluated. The presence of intercalated systems was identified from the basal spacing of organoclay, as shown in Table I. Analyzing the data in the table, when the EI/OMMT was processed at 90 rpm, it did not present the same behavior as when it was processed at 60 rpm. This behavior could be explained by the diffusion characteristic of the polymer matrix. In this case the diffusion mechanism would be dominant when compared to the shear rate effect. Thus, from the XRD diffractogram, no indication of an exfoliation process was observed. It can be partially concluded that the ratio of the intercalation/exfoliation process depends on the shear rate as well as the structural diffusion of HPDE.

The thermal evaluation by DSC measurements and thermogravimetric (TG) data are listed in Table II. The DSC data showed no significant difference for both HDPE/OMMT nanocomposites when comparing the thermal parameters such as Tm and Tg with the polyethylene itself. However, a small

decrease in the TG temperature for both nanocomposites was detected and it may suggest some changes in the molecular organization of these materials due to the incorporation of the polymer in the interlamellar clay spacing. These results reveal that the thermal measurements could not give a response on the intercalation/exfoliation process because of their observation scale, which is about 100 nm.

Comparing the impact resistance of the HDPE matrix and both nanocomposites, a small decrease in the value of this parameter, from 37 J/m to 31 J/m, was observed. This can be an indication that this mechanical property was not really affected by the nanocomposite formation.

The experimentation found that the materials formed should be better eval-

**Table II. DSC and TG Results for EI and Their Nanocomposites with OMMT at Two Shear Rates (60 and 90 rpm)**

Sample	Tm <sup>a</sup>	Tc <sup>b</sup>	TG onset
			(°C)
EI	135	118	478
EI/OMMT 60	133	119	469
EI/OMMT 90	133	119	468

a = melting temperature; b = temperature of crystallization process

uated using a technique that can analyze the nanocomposite in more detail. Thus, the authors have decided to employ proton NMR relaxation time, as this measurement is not destructive. The values were achieved on sample organization, heterogeneity, and particle dispersion. The relaxation data were important to understand the changes in the molecular structural organization and molecular dynamics of the nanocomposite formed.

The hydrogen relaxation data for the samples, measured by low-field NMR, are shown in Table III. The T<sub>1</sub>H results showed that the samples presented different molecular domains. Analyzing the polyethylene resin, before and after

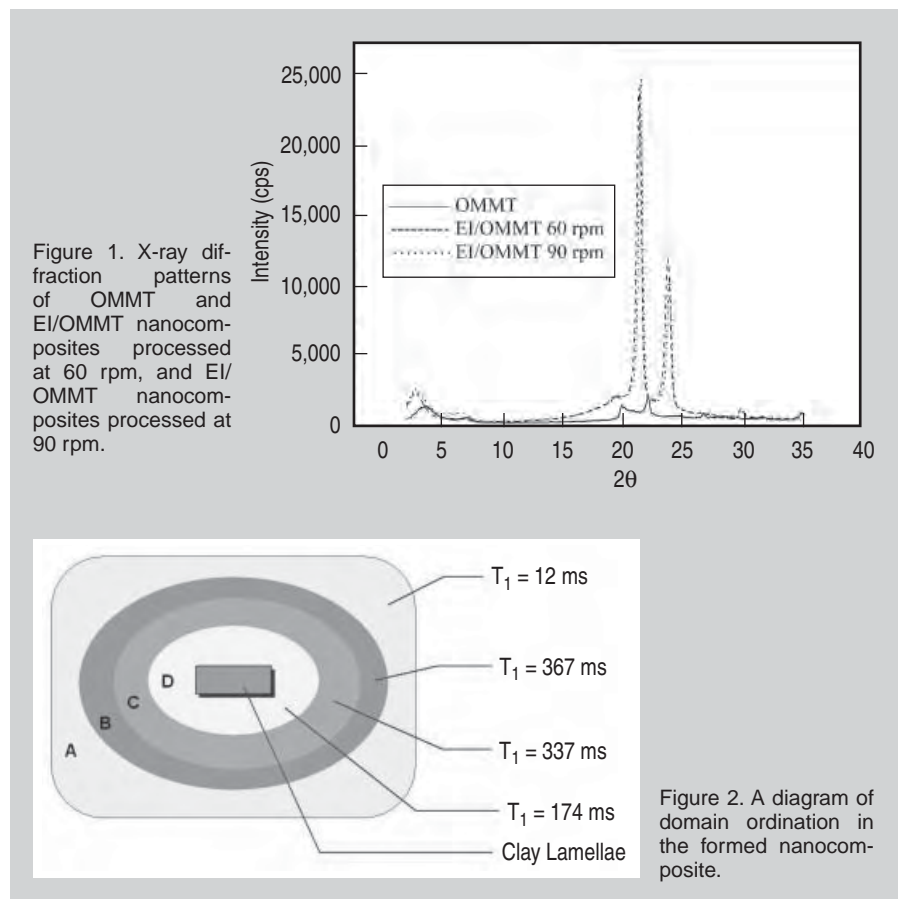


**Table III. The Low-Field NMR Relaxation Data of EI (Resin and after Processing) and EI/OMMT Nanocomposite with 5% of OMMT at 60 rpm**

Sample	T <sub>1</sub> H (ms)	Domain Intensity (%)	Assignments
EI – Resin	26	15	Mobile region
	334	85	Rigid region
Processed EI	18	18	Mobile region
	331	82	Rigid region
EI/OMMT 60 rpm	12 (a)		Mobile region
	174 (d)		Interface region
	337 (c)		Crystalline region (near to clay lamellae)
	367 (b)		Crystalline region (polymer matrix)

processing, two values for the relaxation parameter were found. One of them was attributed to the mobile region (low value), which is constituted by amorphous phase, and the other one was related to the rigid region (high value), formed by the constricted amorphous and crystalline phase, which is normally responsible for the control of the relaxation process. Considering the polyethylene/clay nanocomposite, with 5% of organoclay, four values were detected: (a) the mobile region (low value—amorphous region); (b) the interface region, which is formed by polymer chains around the clay lamellae, which is the evidence of the exfoliation because the metal present in the lamellae decreases the relaxation parameter; and (c and d) two crystalline regions. One of the crystalline phases is derived from the polymer crystallite near the clay lamellae, confirming the exfoliation processing. The higher value of relaxation data is from the polymer crystallite that is distant from the clay lamellae. The relaxation data sup-

port the first intercalation process suggested by x-ray and provide evidence of the exfoliation process. Figure 2 is a diagram that suggests the nanostructure ordination of the molecular domains formed in the HDPE/organoclay nanocomposites.

### CONCLUSIONS

From the results obtained, it can be concluded that the processing parameters affect the nanocomposite formation. The structural characteristics of polymers were able to affect significantly the clay exfoliation process. The share rates were not relevant to the nanocomposite formation for this system. The relaxation data showed different molecular domains for polyethylene and especially for the nanocomposite. The measurement of relaxation time, using low-field NMR, proved useful to evaluate changes in the molecular mobility of nanocomposites and can infer whether a sample is exfoliated and/or intercalated, since lamellar filler is used.

### ACKNOWLEDGEMENTS

The authors wish to acknowledge the contributions of CNPq and CAPES to this work.

### References

1. T.C. Rodrigues, M.I.B. Tavares, and V.J.R.R. Pita, *Macromol. Symp.*, 245 (2007), p. 166.
2. D. Bikiaris et al., *Pol. Deg. and Stab.*, 59 (1998), p. 287.
3. M.Z. Rong et al., *J. Mater. Sci. Lett.*, 19 (2000), p. 1159.
4. M.Z. Rong et al., *Polym. Commun.*, 42 (2001), p. 3301.
5. M.Z. Rong et al., *Polymer*, 42 (2001), p. 167.
6. H. Qin et al., *Polymer Degradation and Stability*, 81 (2003), p. 497.
7. J.M. Garces et al., *Advanced Mater.*, 12 (2000), p. 1835.
8. Y. Kurokawa et al., *J. Mater. Sci. Lett.*, 16 (1997), p. 1670.
9. Y. Kurokawa, H. Yasuda, and A. Oya, *J. Mater. Sci. Lett.*, 15 (1996), p. 1481.
10. F.A. Bovey and P.A. Mirau, *NMR of Polymers* (New York: Academic Press, 1996), pp. 11–19.
11. R.A. Komoroski, *High Resolution NMR Spectroscopy of Synthetic Polymers in Bulk* (Deerfield Beach, FL: VCH Publishers, 1986), pp. 118–136.
12. J.K.M. Sandres and B.K. Hunter, *Modern NMR Spectroscopy, A Guide of Chemists*, 2nd edition (Oxford, U.K.: Oxford University Press, 1996), pp. 21–23.
13. P.T. Callaghan, *Principles of Nuclear Magnetic Resonance Microscopy* (New York: Oxford University Press, Inc., 1991), pp. 135–140.
14. D.L. Vanderhart, A. Asano, and J.W. Gilman, *Chemistry of Materials*, 13 (2001), pp. 3796–3809.
15. S. Hotta and D.R. Paul, *Polymer*, 45 (2004), p. 7639.
16. M.A. Osman, J.E.R. Rupp, and U.W. Suter, *Polymer*, 46 (2005), p. 8202.
17. M. Alexandre and P. Dubois, *Materials Science and Engineering*, 28 (2000), pp. 1–63.
18. P.C. Le Baron, Z. Wang, and T.J. Pinnavaia, *Applied Clay Science*, 15 (1999), pp. 11–29.

Tathiane Cordeiro Rodrigues, Maria Inês Bruno Tavares, and Igor Lopes Soares are with Instituto de Macromoléculas Professora Eloisa Mano, Universidade Federal do Rio de Janeiro, Centro de Tecnologia, Bloco J, Ilha do Fundão, P.O. Box 68525, 21945-970, Rio de Janeiro, RJ, Brazil; Ana M. Moreira is with RioPol, Balneário Jardim Santa Clara, Duque de Ca. Dr. Tavares can be reached at [mbt@ima.ufrj.br](mailto:mbt@ima.ufrj.br).

**JOM is looking for volunteer book reviewers for its Book Review Program, which publishes reviews of recent materials science and engineering publications on the JOM web site.**

**Participants keep any book they review, provided a publication-quality review is submitted in a timely manner.**

**If you'd like to participate, here's how:**

- Go to [www.tms.org/pubs/journals/JOM-review-request.html](http://www.tms.org/pubs/journals/JOM-review-request.html)
- Read the review program guidelines and submit your request using the form provided
- If your request is approved, JOM will mail you the book
- Go to [www.tms.org/pubs/journals/JOM-review-form.html](http://www.tms.org/pubs/journals/JOM-review-form.html) to submit your review within 90 days

### Questions?

Telephone (724) 776-9000, ext. 228  
Fax (724) 776-3770 • E-mail [jom@tms.org](mailto:jom@tms.org)

**TMS**

**FOUNDATION**

# TMS Foundation News

▼ "To support the development of materials professionals within the context of our global society." ▼

## Hands On Bay Area Project Sows the Seeds to Environmental Well-Being

TMS 2009 Annual Meeting attendees will have a chance to create a lasting change in the San Francisco Bay Area prior to the start of the meeting. Like last year in New Orleans, members and guests are encouraged to roll up their sleeves and donate their time to help less fortunate families live better lives.

TMS will partner with USA Hosts/Key Events on February 14 to plant a seasonal organic garden at Alemany Farm, a section of the Alemany Public Housing Community. The garden will serve as a way to improve and expand sustainable agricultural practices in the Bay Area. With the help of local educators and farmers, the organic garden will be used as a tool to teach the community about water conservation, composting, permaculture, and other environmental topics.

"The area was chosen to help low-income youth residing in public housing in the San Francisco area," said Molly Walsh, vice president of busi-

ness development at USA Hosts/Key Events. "The program brings farmers and urban youth together—training the younger generation in sustainable agriculture and landscaping practices, organic food growing, and even marketing."

The Alemany Farm provides healthy, organic food, "green" jobs, and environmental education to the residents of the Alemany Community. The community members see the addition of the organic garden as another way to keep youth off the streets, instill pride in the community, and open a door to future opportunities, according to Walsh.

Volunteers will work together to build raised garden beds, plant seedlings, weed or turn compost bins, and lay wood chips along the paths, among other duties. The project is free and includes transportation to the project site, an on-site lunch, and an afternoon reception.

The service project is sponsored

by the TMS Foundation and provides funds to cover food and transportation expenses. The society invites all who would like to support the Hands On Bay Area project to consider making a \$25 donation through the TMS Foundation to help offset the costs. Corporate sponsorships are also available, starting at \$400. Financial contributions can be made through the TMS 2009 Annual Meeting registration form or by completing and returning the pledge form below. For more information on corporate sponsorship opportunities, contact Joe Rostan, TMS exhibit and sponsorship representative, at [jrostan@tms.org](mailto:jrostan@tms.org).

For more information on the Hands On Bay Area community service project, visit the TMS 2009 Annual Meeting web site at [www.tms.org/meetings/annual-09/HandsOnProject.aspx](http://www.tms.org/meetings/annual-09/HandsOnProject.aspx). For more information on the TMS Foundation, go to [www.tms.org/Foundation/Foundation.html](http://www.tms.org/Foundation/Foundation.html).

### Support the Bay Area Community Service Project

**Contribute to the TMS Hands On Bay Area Service Project through the TMS Foundation**

*All contributions to the TMS Foundation are tax deductible in the United States.*

Direct contributions may be mailed using this form.

Send it to **TMS Foundation, 184 Thorn Hill Road, Warrendale, PA 15086-7514** or fax: **(724) 776-3770**

Donate on-line at <https://www.tms.org/secure/forms/contribution-form.html>

#### Hands On Bay Area Contributions

- I would like to contribute \$25 to the TMS Foundation to support the Hands On Bay Area service project on February 14.
- I would like to donate the following amount to the TMS Foundation to support the Hands On Bay Area service project on February 14:  
\$ \_\_\_\_\_
- Contact me with more information about being a corporate sponsor for the TMS Hands On Bay Area service project.

Name \_\_\_\_\_ TMS Member # \_\_\_\_\_

Organization (If corporate contributor) \_\_\_\_\_

Address \_\_\_\_\_ City \_\_\_\_\_ State \_\_\_\_\_

Country \_\_\_\_\_ Zip/Postal Code \_\_\_\_\_

Telephone \_\_\_\_\_ Fax \_\_\_\_\_

#### Please check payment method (in U.S. dollars):

[ ] Check enclosed for \$ \_\_\_\_\_ Please make checks payable to TMS Foundation.

Credit Card: [ ] VISA [ ] MasterCard [ ] American Express [ ] Diner's Club

Credit Card # \_\_\_\_\_

Expiration Date \_\_\_\_\_ Cardholder Name \_\_\_\_\_

Cardholder Signature \_\_\_\_\_

# Characterizing the Strain Rate Sensitivity of the Tensile Mechanical Properties of a Thermoplastic Composite

Kevin A. Brown, Richard Brooks, and Nicholas A. Warrior

Thermoplastic composites (TPCs) are being given increased consideration for application in vehicle front-end structural crash components. However, studies on the high strain-rate behavior of TPCs have been relatively limited. In this study, the effect of strain rate on the tensile properties of a woven fabric commingled E-glass/polypropylene thermoplastic composite was investigated over a strain-rate range of  $10^{-4}$  to  $70 \text{ s}^{-1}$ . Quasi-static tests were conducted in an electromechanical universal test machine. A specially designed test rig in conjunction with a falling weight drop tower was used for high strain-rate characterization. The experimental results show that the elastic modulus, ultimate strength, and strain to failure increase with increasing strain rate.

## INTRODUCTION

The application of thermoplastic composites (TPCs) in the automotive industry has increased significantly. Thermoplastic composites are favored for their high strength-to-weight ratio, damage tolerance, and energy absorption capability as well as their corrosion resistance, good damping properties, and recyclability. Furthermore, TPCs offer the potential for low-cost rapid manufacturing with low cycle times that allow for medium to high volume production. The application of TPCs was initially restricted to semi-structural components such as front-end panels, spare wheel wells, underbody closures, and door panels.<sup>1</sup> However, there is now a desire to use continuous fiber textile thermoplastic composites for structural components such as bum-

### How would you...

...describe the overall significance of this paper?

*There is limited understanding of the effect of dynamic impact loading on the mechanical properties and failure modes of thermoplastic composites.*

*This paper shows that high-rate loading has a significant effect on the tensile stiffness, strength, and failure modes of thermoplastic composites. This is attributed to the time-dependent response of the material and its woven geometry.*

...describe this work to a materials science and engineering professional with no experience in your technical specialty?

*The material under investigation in this study is a thermoplastic composite that consists of commingled bundles (yarns) of glass and polypropylene fibers. Commingling facilitates rapid manufacturing with good material consolidation. Thermoplastic composites possess high mechanical properties and are easily shaped through thermoforming. This work highlights the changes in the tensile mechanical properties of the material observed at different loading rates.*

...describe this work to a layperson?

*This paper shows that major changes occur in the mechanical behavior of thermoplastic composites (TPCs) which result in significant energy absorption under dynamic loading. These results indicate that TPCs are potentially suitable candidate materials for vehicle crash components. Furthermore, TPCs present the opportunity to improve vehicle fuel efficiency due to their light weight, and also allow for economic high volume manufacturability and recyclability.*

pers, side impact beams, and front-end chassis frames.<sup>2,3</sup> These components are likely to sustain high strain-rate loading during a crash. Therefore, it is important to understand loading rate effects in these materials.

Experimental studies on the high strain-rate response of composites do present difficulties. Moreover, most of the high strain-rate characterization studies have focused on thermoset composites with epoxy and polyester matrices reinforced mainly with glass and carbon fibers.<sup>4-6</sup> In contrast, few attempts have been made to study the effect of strain rate on the mechanical properties of TPCs.<sup>7-11</sup>

In the study reported in this paper, the strain-rate sensitivity of a commingled woven-fabric glass-fiber-reinforced polypropylene TPC was investigated through a series of tensile tests over a strain-rate range of  $10^{-4}$  to  $70 \text{ s}^{-1}$ . The effect of strain rate on the tensile mechanical properties and the corresponding macro- and micro-scale failure modes are discussed. See the sidebar for experimental procedures.

## RESULTS AND DISCUSSION

### Stress-Strain Behavior

Figure 1 shows the typical tensile stress-strain response at different strain rates. Under quasi-static loading the stress-strain response is approximately linear elastic up to the maximum stress point followed by abrupt brittle-like failure. At a strain rate of  $36 \text{ s}^{-1}$ , the initial stress-strain response leading up to the peak stress is relatively similar to the quasi-static results. However, in contrast, the post-peak stress response

is very ductile and almost perfectly plastic with a strain to failure that is four times higher than at the quasi-static rate. Strain to failure is defined here as the strain at which the material exhibits complete cross-sectional failure. At higher strain rates, between  $50 \text{ s}^{-1}$  and  $70 \text{ s}^{-1}$ , the material stress-strain response is highly non-linear, exhibiting premature yielding followed by strain hardening and then maximum peak stress and strain softening. The strain to failure increased by a factor of 3 at strain rates greater than  $50 \text{ s}^{-1}$ .

### Strain-Rate Sensitivity

The tensile modulus and strength properties at different strain rates are presented in Table I. Figure 2 and Figure 3 illustrate the effect of strain rate on the tensile modulus and strength as a function of strain rate on a logarithmic scale, respectively. The tensile

modulus and strength are relatively insensitive to increases in strain rate up to  $36 \text{ s}^{-1}$ . However, at strain rates greater than  $36 \text{ s}^{-1}$  the tensile strength increases significantly up to 46% at the highest strain rate ( $70 \text{ s}^{-1}$ ). The tensile modulus follows a similar trend although not so pronounced, with an increase of 11%.

The increase in tensile modulus is generally explained by the viscoelastic effects of the polymeric matrix.<sup>16</sup> The effect of strain rate on the modulus and strength may also be attributed to the woven structure and geometry of the composite.<sup>17</sup> Plain-weave composites show a higher strain-rate sensitivity than satin-weave, unidirectional, and multi-directional composites because of the higher interaction between the matrix and fibers.<sup>17</sup> Furthermore, the rate sensitivity of the tensile strength can also be attributed to the rate dependence of the glass fibers.<sup>18</sup> This is supported by

**Table I. Mechanical Properties for Twintex™ at Quasi-Static and High Strain Rates**

Strain Rate ( $\text{s}^{-1}$ )	Tensile Modulus (GPa)	Tensile Strength (MPa)
$10^{-4}$	$14.46 \pm 0.92$	$269.03 \pm 10.80$
36	$13.19 \pm 0.83$	$266.75 \pm 11.32$
50	$17.51 \pm 1.22$	$382.40 \pm 23.27$
70	$16.08 \pm 3.89$	$391.88 \pm 74.64$

the fact that the tensile strength of the composite laminate is primarily governed by the fiber strength.

### Tensile Failure Modes

Under quasi-static loading, failure occurred around a localized through-thickness shear fracture plane at an angle of about  $45^\circ$  to the axis of loading as shown in Figure 4a. This may be attributed to the woven nature of the composite which tends to result in through-thickness shear failure initiation across a longitudinal fiber bundle.<sup>19</sup> The quasi-static macroscopic failure mechanisms generally included matrix cracking, localized warp fiber fracture, weft fiber pull-out, and delamination along the middle plies. At high strain rates the main failure surface is not clearly defined as damage accumulates along the entire length of the specimen gauge area (see Figure 4b). As strain rate increased, significant matrix cracking, fiber fracture, and weft fiber bundle pull-out was observed. In addition, the laminate delaminated along all ply interfaces.

Optical micrographs of the failure regions in the fractured tensile specimens at quasi-static strain rates are shown in Figure 5. Matrix cracking was observed in the weft fiber bundles as depicted in Figure 5a. These cracks propagate in an opening mode normal to the in-plane axis due to normal stresses acting in the direction of the applied load. Some of these cracks propagate toward the warp and weft fiber bundle interfaces resulting in interfacial debonding and inter-ply delamination as shown in Figure 5b. At dynamic strain rates, extensive micro-matrix cracking in the weft fiber bundles and inter-ply delamination was observed in the failure regions of the specimens (see Figure 6).

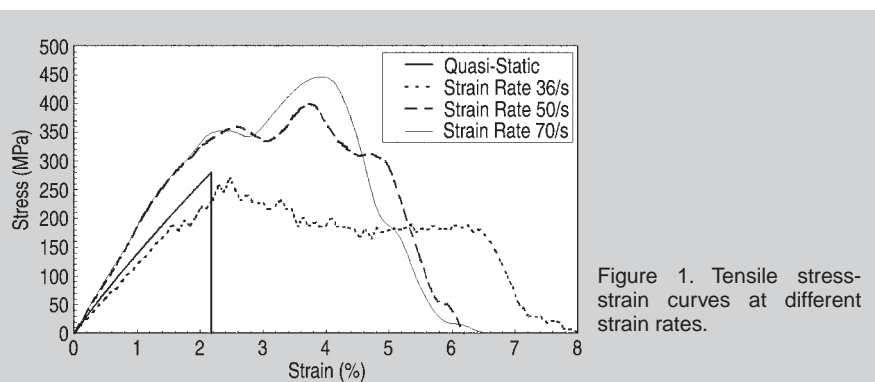


Figure 1. Tensile stress-strain curves at different strain rates.

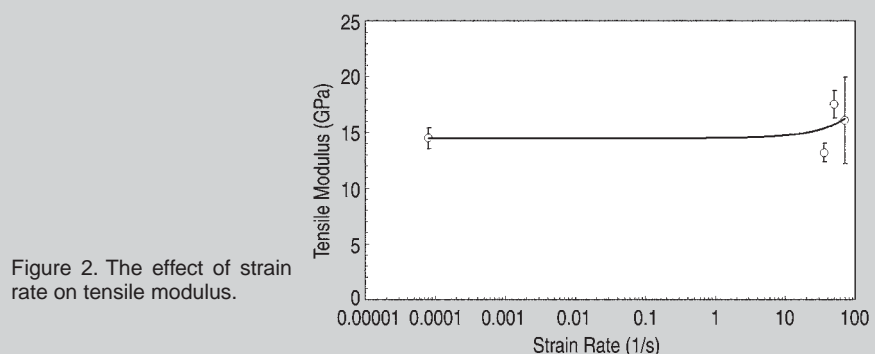


Figure 2. The effect of strain rate on tensile modulus.

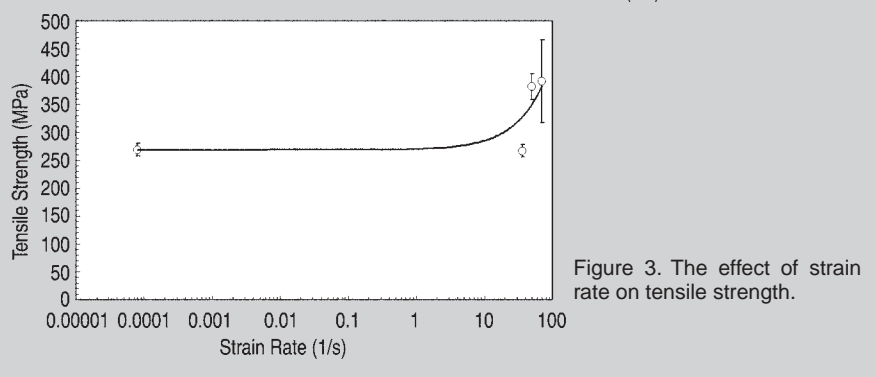


Figure 3. The effect of strain rate on tensile strength.



## EXPERIMENTAL PROCEDURE

### Material and Specimens

The material system used in this study is a commingled E-glass/polypropylene woven fabric composite, balanced 1:1 twill weave with a 60% fiber weight fraction. It is supplied by OCV Reinforcements (formerly Saint Gobain Vetrotex) under the tradename Twintex™. In this textile thermoplastic composite the yarns consist of the reinforcing glass fibers and a fibrous form of the polypropylene matrix (see Figure A). This results in a very short flow length between the fibers and matrix, which leads to good consolidation and impregnation. All tensile tests were conducted in only the warp direction due to the balanced, symmetrical nature of the Twintex woven fabric.

Test specimens were cut from flat plaque laminates (260 mm × 120 mm) with [0/90] fiber orientations. An optimized non-isothermal compression molding process was used to manufacture the flat plaques.<sup>12</sup> The manufacturing procedure involved stacking 0.5 mm thick preconsolidated sheets of Twintex in a 4.5 kW infrared oven. The stacks were heated to 200°C and then rapidly transferred to a heated tool (80°C) which was installed in an up-stroking hydraulic press. The tool was closed and a pressure of 1.6 MPa was applied for 60 s.

The quasi-static tensile specimens were straight sided, 250 mm long × 25 mm wide, with a nominal thickness of 4 mm (Figure Ba). The high strain rate specimens were also straight sided, 180 mm long × 25 mm wide, with a nominal thickness of 2.5 mm (Figure Bb). All tensile specimens had a [0/90] stacking sequence with

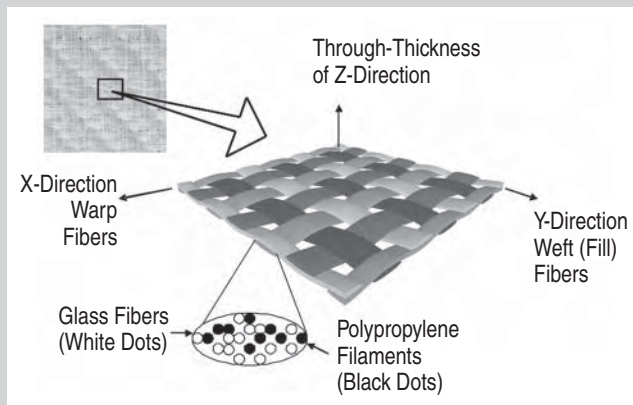


Figure A. The Twintex™ commingled E-glass/polypropylene woven fabric composite material (balanced 1:1 twill weave with a 60% fiber weight fraction).

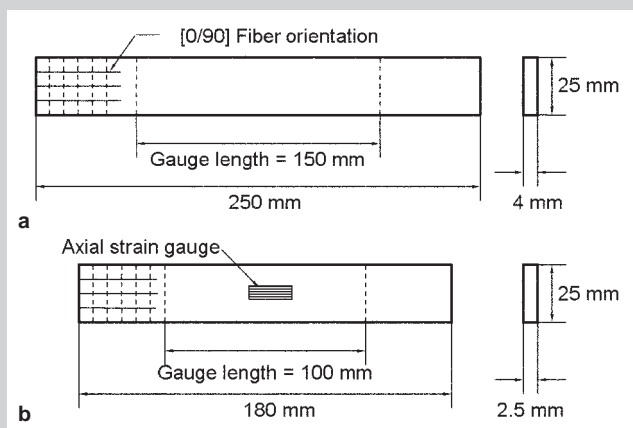


Figure B. A tensile test specimen: (a) quasi-static (b) high strain rate.

eight plies for quasi-static specimens and five plies for dynamic specimens. The reduced thickness of the dynamic specimens is necessary to ensure complete failure during testing.<sup>13</sup>

### Tensile Test Setup

Quasi-static tensile tests were conducted according to ASTM standard D3039.<sup>14</sup> The tests were conducted on an electro-mechanical universal test machine at a crosshead speed of 5 mm min<sup>-1</sup>. The specimen strain response was determined by a 50 mm gauge length extensometer with a maximum strain capability of 10%.

Dynamic tensile tests were conducted in a modified Rosand™ instrumented falling weight drop tower (see Figure C). The drop tower uses a free-falling, weighted crosshead with a striker, guided by two long steel rods, to impart an impact load. A crosshead mass of 100 kg was used in the dynamic tensile tests. The tests were conducted at speeds of 3 ms<sup>-1</sup>, 5 ms<sup>-1</sup>, and 7 ms<sup>-1</sup> which corresponded to strain rates of 36 s<sup>-1</sup>, 50 s<sup>-1</sup>, and 70 s<sup>-1</sup>, respectively. The average strain rate during the test was derived from the gradient of the strain-time history data.

A special test fixture,<sup>15</sup> in which the specimens were mounted, was fixed to the floor of the drop tower (see Figure C). The specimen is clamped at each end between steel grips. The top grip is directly bolted through the load cell to a fixed carriage. A moving carriage is supported by the lower grip and is guided by two steel rods through two linear bearings on one side and two nylon dowels on the other side. The drop tower striker imparts a load on the moving carriage which loads the specimen in tension through the lower grip as it travels downward.

In high strain rate tests, a piezoelectric load cell was used for the measurement of force data. Strain was measured with a single 120 Ohm strain gauge bonded centrally on each specimen.

### Microscopic Analysis

Optical microscopy was used to investigate the failure mechanisms in the material. Sample sections were cut from the failure region of the fractured specimens. The samples were cast in polyester resin and polished before being examined using an optical microscope with a charge-coupled device camera attachment.

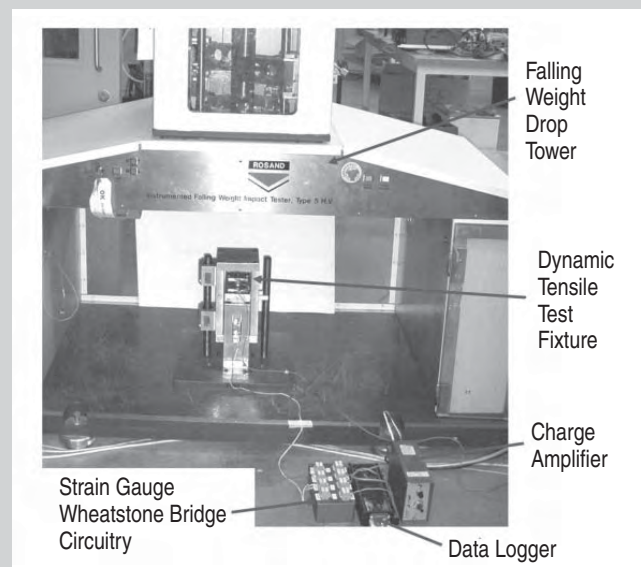


Figure C. The modified Rosand™ falling weight drop tower setup for high-strain tensile experiments. The specimen is placed in the dynamic tensile fixture.

## ACKNOWLEDGEMENTS

The authors would like to acknowledge support from the U.K. Engineering and Physical Sciences Research Council (EPSRC) through the Nottingham Innovative Manufacturing Research Centre (NIMRC). We would also like to thank OCV Reinforcements Ltd (formerly Saint-Gobain Vetrotex) for the supply of Twintex™ material.

## References

1. R. Tornqvist and B. Baser, *SAE Transactions*, Paper #2002-01-1038 (2002), pp. 603–613.
  2. “Automotive Supplement,” *Reinforced Plastics*, 47 (2) (2003).
  3. B. Griffiths, *Composite Technology* (October 2006), pp. 52–54.
  4. R.L. Sierakowski, *Applied Mechanics Reviews*, 50 (12/part 1) (1997), pp. 741–761.
  5. S. Barre et al., *Composites—Part A: Applied Science and Manufacturing*, 27 (12) (1996), pp. 1169–1181.
  6. A.M.S. Hamouda and M.S.J. Hashmi, *Journal of Materials Processing Technology*, 77 (1-3) (1998), pp. 327–336.
  7. M. Todo et al., *Composites Science and Technology*, 60 (5) (2000), pp. 763–771.
  8. N. Papadakis et al., “Strain Rate Effects Characterisation on the Tensile Properties of Thermoplastic Unidirectional Composite Laminates” (Presentation at the 10th European Conference on Composite Materials [ECCM-10], Brugge, Belgium, 2002).
  9. N. Papadakis et al., *Composites Science and Technology*, 64 (5) (2004), pp. 729–738.
  10. K. Kawata et al., “Mechanical Behaviours in High Velocity Tension of Composites” (Presentation at the 4th International Conference on Composite Materials [ICCM-4], Tokyo, Japan, 1982).
  11. B. Bonnet, “Comportement Au Choc De Matériau Composite Pour Applications Automobiles” (Ph.D. thesis, l’Ecole Nationale Supérieure des Mines de Paris, 2005).
  12. M. Wakeman, “Non-Isothermal Compression Moulding of Glass Fibre Reinforced Polypropylene” (Ph.D. thesis, University of Nottingham, 1997).
  13. K. Brown, “Finite Element Modelling of the Static and Dynamic Impact Behaviour of Thermoplastic Composite Sandwich Structures” (Ph.D. thesis, University of Nottingham, 2007).
  14. ASTM-D3039, “Standard Test Method for Tensile Properties of Polymer Matrix Composite Materials” (1995).
  15. R. Fernie, “Loading Rate Effects on the Energy Absorption of Lightweight Tubular Crash Structures” (Ph.D. thesis, University of Nottingham, 2002).
  16. S.E. Groves et al., “High Strain Rate Effects for Composite Materials” (Presentation at the 11th Symposium on Composite Materials, May 4–5 1992, Pittsburgh, PA, 1993).
  17. L.M. Welsh and J. Harding, “Effect of Strain Rate on the Tensile Failure of Woven Reinforced Polyester Resin Composites” (Presentation at the International Conference on Mechanical and Physical Behaviour of Materials under Dynamic Loading, Paris, France, 1985).
  18. O.I. Okoli, *Composite Structures*, 54 (2-3) (2001), pp. 299–303.
  19. J. Harding, *Composites*, 24 (4) (1993), pp. 323–332.
- Kevin A. Brown, Richard Brooks, and Nicholas A. Warrior are with the Department of Mechanical, Materials and Manufacturing Engineering, University of Nottingham, University Park, Nottingham, NG7 2RD, U.K. Dr. Brown can be reached at 44 (0) 115-951-3820; e-mail kevin.brown@nottingham.ac.uk.

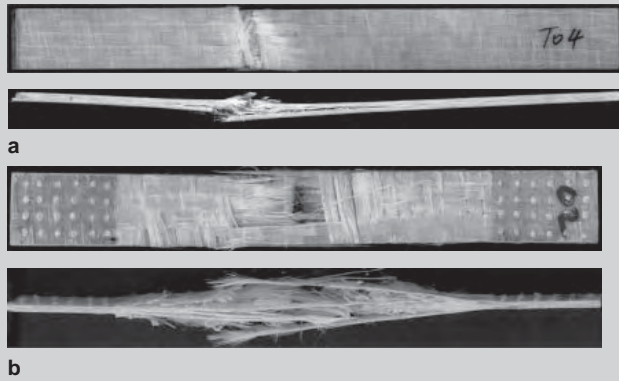


Figure 4. The typical macroscopic failure regions for the tensile specimens. (a) Quasi-static; (b) high strain rate.

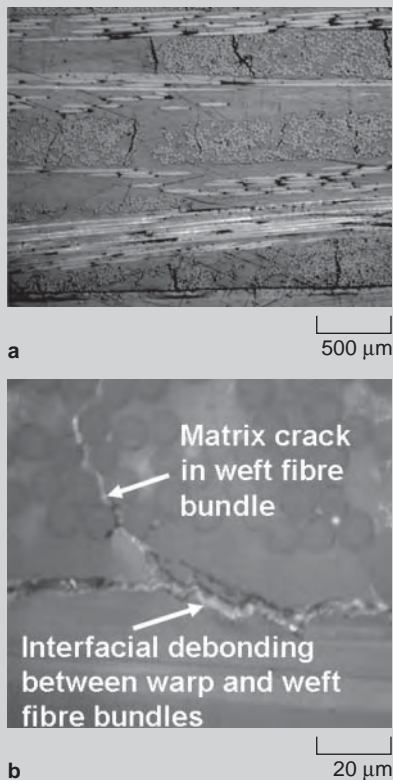


Figure 5. An optical micrograph showing the typical failure mechanisms at quasi-static strain rates. (a) Extensive cracks in the matrix of the weft fiber bundles; (b) matrix cracks propagate to the fiber bundle interface resulting in debonding of the interfaces.

## CONCLUSIONS

From this study, some key observations can be made about the effect of strain rate on the tensile mechanical properties of commingled E-glass/polypropylene thermoplastic composites over a strain-rate range of  $10^{-4}$  to  $70 \text{ s}^{-1}$ . At high strain rates (above  $36 \text{ s}^{-1}$ ), the tensile stiffness, maximum strength, and strain to failure tend to significantly increase with increase in strain rate. The failure mode of the TPC for different strain rates was char-

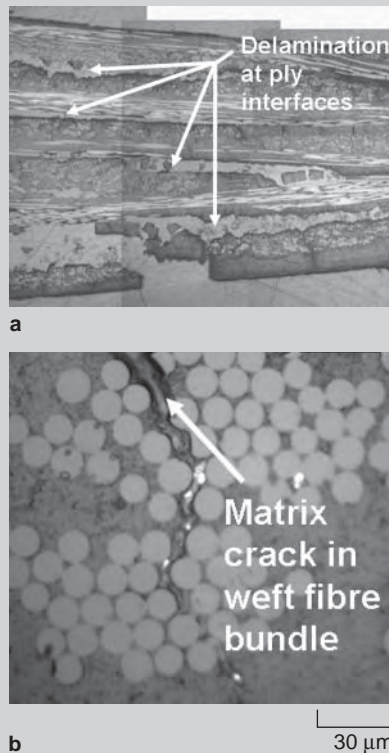


Figure 6. An optical micrograph showing the typical failure mechanisms at high strain rates. (a) Delamination at ply interfaces; (b) matrix cracks in weft fiber bundles.

acterized by matrix cracks in the weft fiber bundles that propagate normal to the loading direction along with a varying degree of intra- and inter-ply delamination. Strain-rate effects appear to be influenced primarily by the matrix viscoelasticity, the woven reinforcement architecture, and the time-dependent nature of damage accumulation. However, further detailed study is required to elucidate the relationship between failure mechanisms and the strain-rate sensitivity of the mechanical properties.

# Informatics and Integrated Computational Materials Engineering: Part II

Krishna Rajan



This issue of *JOM* presents the second in a two-part series on materials informatics. In the previous issue (March 2008), some of the basic concepts of what constitutes informatics were introduced. In this issue, we continue that theme with papers that serve to emphasize the diversity of topics that encompass the field of informatics. The timing of the publication of these *JOM* topics on materials informatics coincides with the issuing of a report of the National Materials Advisory Board on Integrated Computational Materials Engineering (ICME).<sup>1</sup> This report defines that information as including “curated data sets, structure-property models, processing-structure relationships, physical properties and thermodynamic, kinetic and structural information.” It provides a good summary of the needs, status, and challenges

the materials engineering community faces to generate this information. The report defines ICME as “the integration of materials information, captured in computational tools, with engineering product performance analysis and manufacturing-process simulation.” The report envisions an ICME system as one that integrates many different components of information that are “linked by means of a software integration tool to a designer knowledge base containing tools and models from other engineering disciplines.” At the core of this integration the report identifies what it calls “use cases” which serve as the conduit for information from databases, models, and computational tools to achieve a knowledge base that can solve materials engineering problems.

So where does informatics fit into this framework? I would suggest that the articles in this and the previous companion *JOM* issue serve to emphasize that informatics can in fact be that “hub” (Figure 1). Each paper in these issues links one or more of the compo-

nents identified in the ICME report.

In this issue, C. Suh and K. Rajan explore ways to discover knowledge and rules associated with crystal chemistry strictly by interrogating databases using data-dimensionality-reduction techniques and discover new structure-chemistry relationships. Hence materials informatics plays a key role for ICME, namely, by providing the tools to achieve that integration.

Having ways to generate information is usually viewed as an important goal but B. Ganapathysubramanian addresses a critical and very practical issue: we may not always be able to collect all the information we need. He shows how one can use stochastic modeling to deal with uncertainty caused by missing information. This then permits one to develop or enhance and refine materials-based models.

R. Hrubciak and colleagues challenge the conventional notion of databases as simple repositories of information. They provide a good example of how to organize a database so that it can be converted to a “knowledge base.” When providing the right type of web interface, they show how complex and integrated information can be made easily accessible.

## Reference

1. Committee on Integrated Computational Materials Engineering, National Research Council, *Integrated Computational Materials Engineering: A Transformational Discipline for Improved Competitiveness and National Security* (Arlington, VA: National Academy Press, 2008).

Krishna Rajan is with the Department of Materials Science and Engineering, Iowa State University, 2220 S. Hoover Hall, Ames, IA 50011; e-mail [krajan@iastate.edu](mailto:krajan@iastate.edu). He is advisor to *JOM* from the Computational Materials Science and Engineering Committee.

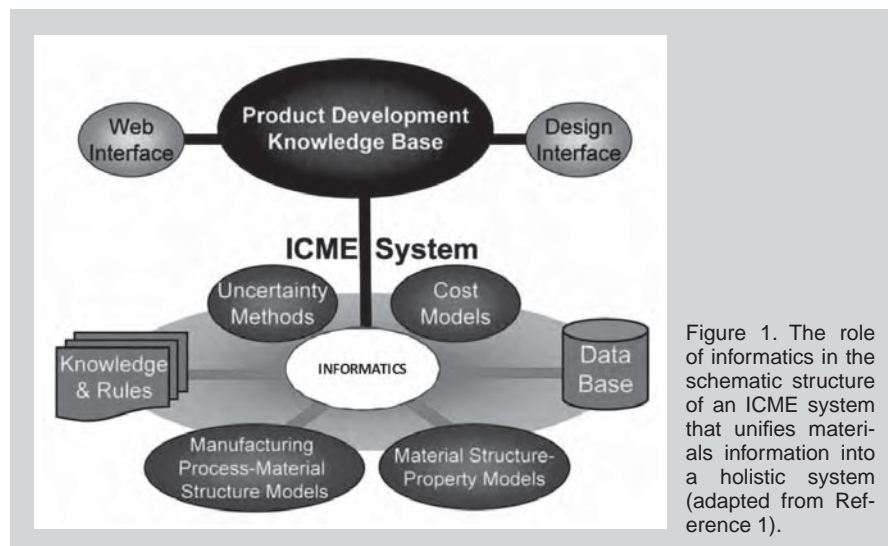


Figure 1. The role of informatics in the schematic structure of an ICME system that unifies materials information into a holistic system (adapted from Reference 1).

# Informatics for Chemical Crystallography

Changwon Suh and Krishna Rajan

*A fundamental question in inorganic crystallography is the relationship between chemical stoichiometry and crystal structure. The relationship between specific compounds and specific crystal structures is usually developed heuristically by surveying crystallographic data of known compounds. This process of structure–chemistry association has laid the historical foundation for identifying crystal structure prototypes and structural classifications. This paper demonstrates how informatics can quantitatively accelerate the discovery of structure–chemistry relationships but also be used as the foundation for developing structure–chemistry–property relationships.*

## INTRODUCTION

The search for stable compound structures based on information about the constituent elements is a classic crystal chemistry problem. When predicting new possible materials, traditionally structure maps have been used to search for stable phases. Structure mapping has played an important role as an a priori guide for finding stable phases<sup>1</sup> and serving as a visualization tool for structure–property relationships in a bivariate way. Physical factors governing stable crystal structures serve as the coordinates of structure maps. After physical factors are carefully chosen, each compound can be spatially identified by its structure type. From the viewpoint of informatics, a structure map is a classification tool whereby, through the choice of appropriate coordinates, one can map clustering of crystal-structure-related data. There is, of course, a long and distinguished tradition of such maps including Mooser–Pearson plots,<sup>2</sup> Philips and van Vechten diagrams,<sup>3,4</sup> Goldschmidt

diagrams,<sup>5</sup> and Pettifor plots,<sup>1,6</sup> just to mention a few examples. Each of these mapping schemes identifies some key parameters related to electronic or crystal structure information which are placed on orthogonal axes and the occurrence of a given crystal chemistry is then plotted accordingly. The resulting diagram maps out the relative position of structure types from which one tries to discern qualitatively if there are strong associations of certain crystal types to certain bivariate combinations of parameters. This, however, does not address the multivariate nature of the parameters associated with crystal chemistry and hence provides a strong motivation to apply data dimensionality reduction techniques.

## STRUCTURE–CHEMISTRY CLASSIFICATION

C. Suh and K. Rajan<sup>7</sup> have demonstrated a strategy for developing struc-

ture maps without any a priori assumption of which two parameters are to be selected for developing a structure map. This is treated as a multivariate analysis problem where we collectively input many of the well-known and accepted variables that can have an influence (termed “latent variables” in the jargon of informatics) on the occurrence of a given type of crystal structure. This approach can be used to identify the appropriate selection of variables for use in two-dimensional structure maps. The first step in this process is applying data dimensionality reduction techniques such as principle component analysis (PCA). The computational details are not described here but the reader is referred to numerous standard texts in the field<sup>8,9</sup> as well as papers that have used this specific multivariate data analysis method in materials science applications.<sup>10–12</sup> The generated data set includes crystallographic parameters, informatics-based prediction of bulk moduli, electronic bonding, and combined parameters and therefore it contains large amounts of factors governing crystal structure (Table I).

The PCA loading map separates structural governing factors based on their correlations and relative impacts on PCA models. Through the process of eigenvector decomposition in PCA, the original data is decomposed by two matrices: loadings and scores. The loadings are the weights for each original variable, while the scores are the projection of the sample on a rotated coordinate system. Thus, PCA loading plots map the correlation between physical parameters and score plots map the correlation between spinel nitrides. Interpretations of the loading plot are twofold:

### How would you...

...describe the overall significance of this paper?

*Informatics can provide an accelerated and robust means of discovering structure-chemistry-property relationships.*

...describe this work to a materials science and engineering professional with no experience in your technical specialty?

*This paper shows how informatics can be used as a new computational tool to aid in materials discovery and design.*

...describe this work to a layperson?

*A new computational approach is proposed for discovering what parameters govern which crystal structures are formed for different chemical compounds.*

- Degree of correlation between variables: angle between variable-origin-variable, where the origin is (0,0) position.
- Relative impact of variables on PCA model: distance from the origin to variable.

The degree of correlation between variables is determined by the angles (cosine) between them. If the angle between two variables at the origin is  $\theta$ , then  $\theta = 0^\circ$  for highly positively correlated variables,  $\theta = 180^\circ$  for highly inversely correlated variables, and  $\theta = 90^\circ$  if no correlation exists. Therefore, a PCA loading plot captures all the possible correlations within a multivariate data set in two-dimensional spaces. Since PCA reduces the dimensionality of variables with a minimal loss of information, it should be noted that correlations on a PCA map depend on the variance captured by the confined dimensions. This means they could be different from the bivariate correlation coefficient (e.g., Pearson's).

On the other hand, the relative impact of each variable can be identified by measuring the distance from the origin. Interpretation of the score plot is the same as the loading plot. The loading plot of PCA separates multiple descriptors by their characteristics, helps to detect key descriptors, and shows bond characteristics in terms of structural and electronic bonding parameters. Overall, the reason to form the shape of the shell for grouped properties is their similar impacts on the PCA model. For instance, all the parameters related with cell dimensions have similar effects on the two LV PCA models. The degree of impact on the PCA model is based on cell dimension parameters and the degree of bond strength from the radius of each shell. Thus, one may rank the relative degree of impact as: electro-negativity difference, bond length, and polyhedral volume > pseudopotential radii > bulk modulus > effective charge > bond order.

Using  $AB_2N_4$  spinel nitrides as a template, Suh and Rajan have assessed the statistical interdependency of each of the descriptors that may influence chemistry–structure–property relationships. Using PCA, they demonstrated that classical versions of structure maps

(from the early work of Hill<sup>20</sup>) based on heuristic observations for this class of crystal chemistry can in fact be reproduced via data mining. The informatics approach also provides an alternative method for visualizing structure maps

as well as interpreting structure-property relationships. Apart from being able to reproduce earlier versions of structure maps, an example is also developed for the case of a new informatics-based structure map for spinel ni-

**Table I. Governing Factors for Spinel Nitrides,  $AB_2N_4^*$**

Origin of Descriptors	Descriptors
Ab-initio derived parameters <sup>11</sup>	1. a (lattice constant) 2. u (anion parameter) 3. $BL_{A-N} = A_{8a} - N_{32e}$ 4. $BL_{B-N} = B_{16d} - N_{32e}$ 5. $Q'_A$ (effective charge) 6. $Q'_B$ 7. $Q'_N$ 8. $BO_{Cry}$ (bond order of crystal) 9. $BO_{AN}$ 10. $BO_{BN}$
Pseudopotential orbital radii related parameters <sup>12-18</sup>	11. $R_{\sigma}^A$ , 12. $R_{\sigma}^B$ , 13. $R_{\sigma}^{AN}$ , 14. $R_{\sigma}^{BN}$ , 15. $R_{\pi}^{AN}$ , 16. $R_{\pi}^{BN}$ , 17. $\overline{R}_{\sigma}$ , 18. $\overline{R}_{\pi}$ , 19. PR (weighted differences of Zunger's pseudopotential radii sums)
Crystallographic parameters (bond lengths and polyhedral volumes) from a and u	20. $A_{8a} - \square_{16c}$ or $B_{16d} - \Delta_{8b,48f}$ 21. $A_{8a} - \Delta_{48f}$ 22. $A_{8a} - \Delta_{2nd\ n.n.}^{48f}$ , $B_{16d} - B_{16d}$ , or $B_{16d} - \square_{16c}$ 23. $A_{8a} - B_{16d}$ , $B_{16d} - \Delta_{8b}$ , or $B_{16d} - \Delta_{2nd\ n.n.}^{48f}$ 24. $A_{8a} - A_{8a}$ or $A_{8a} - \Delta_{8b}$ 25. $(N_{32e} - N_{32e})_{1'}$ 26. $(N_{32e} - N_{32e})_{2'}$ 27. $(N_{32e} - N_{32e})_{3'}$ 28. $\Delta_{8b} - N_{32e}$ 29. $(\Delta_{48f} - N_{32e})_{1'}$ 30. $(\Delta_{48f} - N_{32e})_{2'}$ 31. $\square_{16c} - N_{32e}$ 32. $BL_{A-N} / BL_{B-N}$ 33. $V^{(A-8a)}_{tet}$ 34. $V^{(A-8b)}_{tet}$ 35. $V^{(A-48f)}_{tet}$ 36. $V^{(B-16d)}_{oct}$ 37. $V^{(B-16e)}_{oct}$ 38. $V^{(N-32e)}_{oct}$
Interbond angles from spinel structure	39. $\angle A-N-A$ , 40. $\angle N-B-N$ , 41. $\angle B-N-B$ , 42. $\angle A-N-B$ , * $\angle N-A-N$ (constant=109.471°)
Derived parameters (combinations of parameters or miscellaneous) <sup>19</sup>	43. $Q'_N - Q'_B$ 44. $Q'_N - Q'_A$ 45. $\Delta EN$ (from electronegativity of elements), 46. $B_0$ (from prediction of Partial Least Squares)

Note that expressions of variables for bond lengths and polyhedral volumes follows the work of Sickafus et al.,<sup>10</sup> A and B represent tetrahedral (tet) and octahedral (oct) cation sites, respectively, and  $\square$  and  $\Delta$  represent an octahedral- and tetrahedral vacancy, respectively. \* It is not used for PCA model because it is a constant.

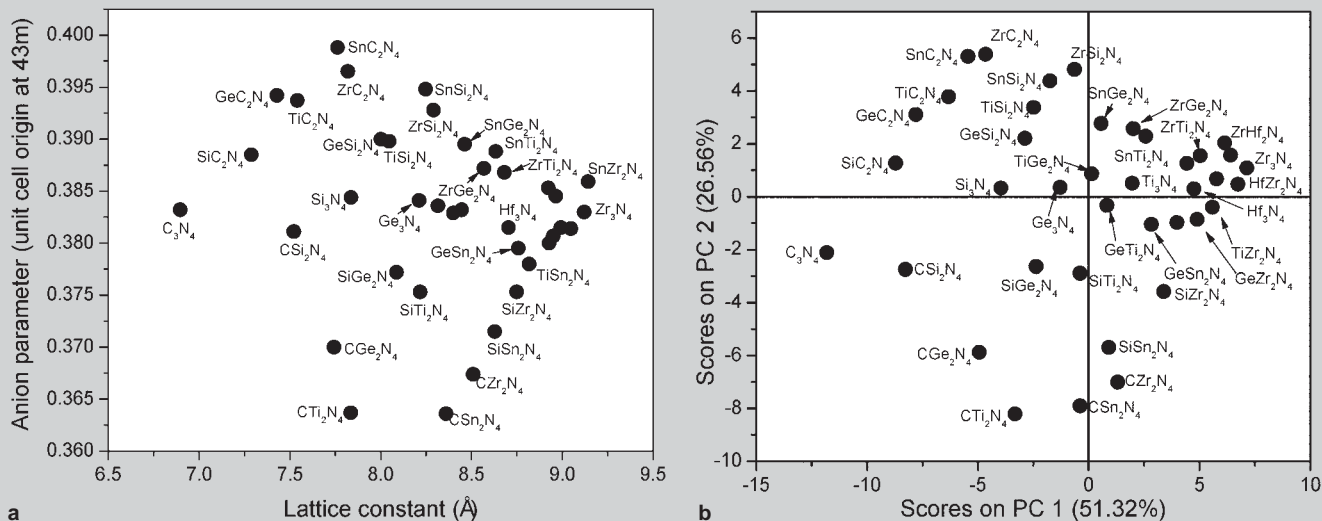


Figure 1. (a) Hill's map for spinel nitrides: Anion parameter ( $u$ ) gives the ratio of the octahedral to tetrahedral bond lengths and octahedral bond length is the same as tetrahedral bond length when  $u=0.3875$ . (b) PCA score map of site occupancy based on complex interactions between bonding and crystal chemistry (governing factors in Table I). Using PCA, it is demonstrated that Hill's map based on heuristic observations for this class of crystal chemistry in fact is reproduced via data mining techniques since the shape of this map is similar to Hill's map for spinel nitrides. For clarity, some spinel nitrides are labeled.

trides, showing data clustering associated with site occupancy.

Structure maps are essentially classification maps. They show how crystal chemistry and the associated structure can be clustered according to the pair of parameters that define the axes of the plot. As noted at the beginning of this paper, historically, there are numerous such maps that have been proposed based on different sets of parameters that reflect bonding and structure.<sup>14</sup> It is instructive to compare the multivariate PCA score plot (Figure 1) which contains all 46 variables simultaneously with the structure map proposed by Hill (Figure 1a<sup>20</sup>) which used just the anion parameter and lattice constant of the spinel oxides and sulfides. This striking similarity serves to highlight that the principal components (i.e., principal contributions) are primarily capturing lattice constants and anion parameters, which were identified as the most important parameters in PC1 and PC2, respectively, in the loading plot. While the PCA score map effectively serves as a high dimensional structure map, Hill's structure map serves as a validation of the data-mining analysis.

### QSARs FOR STRUCTURE-PROPERTY RELATIONSHIPS

While a fundamental tenet in materials science is to establish structure-property relationships, it is the life sci-

ences and organic chemistry community that has formally introduced the concept of quantitative structure activity (or also termed property) relationships (QSAR or QSPR). Unlike classical materials-science approaches, which relate structure and function

through physically based models (e.g., grain size and strength through the Hall-Petch relationship), QSARs are derived from a model independent approach; sometimes referred to as "soft modeling."

The orthogonality of the principal

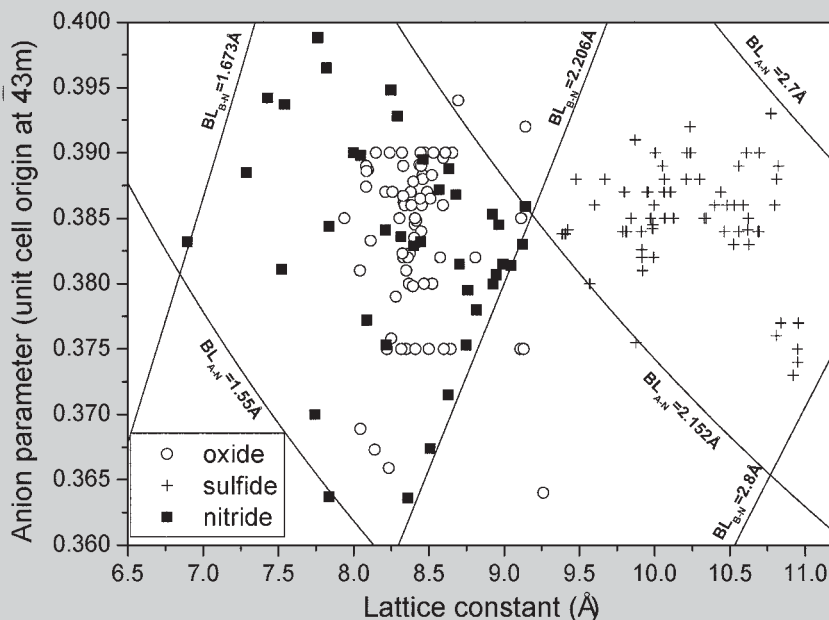


Figure 2. The original Hill map which was derived for spinel oxides and sulfides. The new data for spinel nitrides are added for comparison. The spinel nitrides and oxides are clustered approximately in the same region of the Hill structure map; however, the range of lattice constants observed for oxides for the same variability in anion parameter is narrower than it is for the nitride. Note that each equi-line of bond length is drawn for visually clear separation of oxides, sulfides, and nitrides by setting limiting values of bond length. Note that black lines of equi-bond length in the figure were calculated from geometric relations of interatomic distances as a function of  $a$  and  $u$  in a spinel structure (i.e.,  $BL_{A-N} = \sqrt{3}a(u - 1/4)$  and  $BL_{B-N} = a[2(u - 3/8)^2 + (5/8 - u)^2]^{1/2}$ ).

components eliminates the multidimensional problem, but the problem of choosing an optimum subset of predictors remains. A possible strategy is to keep only a few of the first components; however they are chosen to explain X rather than Y, and so nothing guarantees that the principal components, which “explain” X, are relevant for Y. The next step in examining the data in PCA space is to see if we can develop models based on this new data set. In other words we want to try to set up a regression model between the scores and not just the original data.

Partial least squares (PLS) regression models are based on principal components of both the independent data X and the dependent data Y. The central idea is to calculate the principal component scores of the X and the Y data matrix and to set up a regression model between the scores (and not the original data). Hence, in contrast to PCA, PLS regression finds components from X that are also relevant for Y. Specifically, PLS regression searches for a set of components (called latent vectors) that performs a simultaneous decomposition of X and Y with the constraint that these components explain as much as possible of the covariance between X and Y. This step generalizes PCA. It is followed by a regression step where the decomposition of X is used to predict Y.

As noted by R.D. Tobias,<sup>21</sup> the emphasis in PLS is on predicting the responses and not necessarily on trying to understand the underlying relationship between the variables. For example, PLS is not usually appropriate for screening out factors that have a negligible effect on the response. However, when prediction is the goal and there is no practical need to limit the number of measured factors, PLS can be a useful tool. When the number of factors gets too large (for example, greater than the number of observations), you are likely to get a model that fits the sampled data perfectly but that will fail to predict new data well. This phenomenon is called over-fitting. In such cases, although there are many manifest factors, there may be only a few underlying or latent factors that account for most of the variation in the response. The general idea of PLS is to extract these

latent factors, accounting for as much of the manifest factor variation as possible while modeling the responses well. For this reason, the acronym PLS has also been taken to mean “projection to latent structure.”

Hence PLS expresses a dependent variable (target property) in terms of linear combinations of the principal components. While the descriptors themselves may be interdependent (covariant), the PCs so generated are independent (orthogonal). The PLS equation assumes the following form for the case of ‘n’ descriptors to find the correlation factors between X and Y that have maximum variance:<sup>22</sup>

$$\text{Target property} = a_0 + a_1(\text{PC}_1) + a_2(\text{PC}_2) + a_3(\text{PC}_3) + \dots + a_n(\text{PC}_n) \quad (1)$$

The multidimensional space of X is reduced to the A-dimensional hyper plane. Since the scores are good predictors of Y, the correlation of Y is formed on this hyper plane. As in PCA, the loadings of X represent the orientation of each of the components of the plane.

The PLS method can be applied to rationalize the materials attributes relevant to materials function or property and this permits one to use PLS methods to develop explicit quantitative relationships that identify the relative contributions of different data descriptors, and the resulting relationship between all these descriptors as a linear

combination, to the final property.

For instance, Suh and Rajan explored the attributes used in electronic structure calculations and their influence on predicting bulk modulus.<sup>19</sup> Using PLS, a QSAR was developed relating bulk modulus of  $\text{AB}_2\text{N}_4$  spinels with a variety of

$$\begin{aligned} \text{Bulk modulus} = & -1.00096 \text{ EN} \\ & - 0.35682 u - 0.77228 \text{BL}_{\text{A-N}} \\ & - 0.83367 \text{BL}_{\text{B-N}} + 0.03296 \text{Q}_{\text{tet}}^* \\ & + 0.18484 \text{Q}_{\text{oct}}^* - 0.13503 \text{Q}_{\text{N}}^* \quad (2) \end{aligned}$$

where EN = weighted electronegativity difference; u = internal anion parameter;  $\text{BL}_{\text{A-N}}$  = A-N bond length;  $\text{BL}_{\text{B-N}}$  = B-N bond length;  $\text{Q}_{\text{tet}}^*$  = Mulliken effective charge for tetrahedral site ion;  $\text{Q}_{\text{oct}}^*$  = Mulliken effective charge for octahedral site ion; and  $\text{Q}_{\text{N}}^*$  = Mulliken effective charge for N ion.

By systematically exploring the number and type of variables needed, they found very strong agreement in being able to predict properties consistent with ab-initio calculations based strictly on a data-driven analysis. Based on our QSAR formulation, the role of the effective charge ( $\text{Q}^*$ ) in enhancing modulus is particularly notable. This is consistent with theoretical studies<sup>11,23</sup> that show it is the effective charge parameter which helps to define the degree of charge transfer and the level of covalency associated with the specific site occupancy of a given species. Ab-initio calculations of this effective

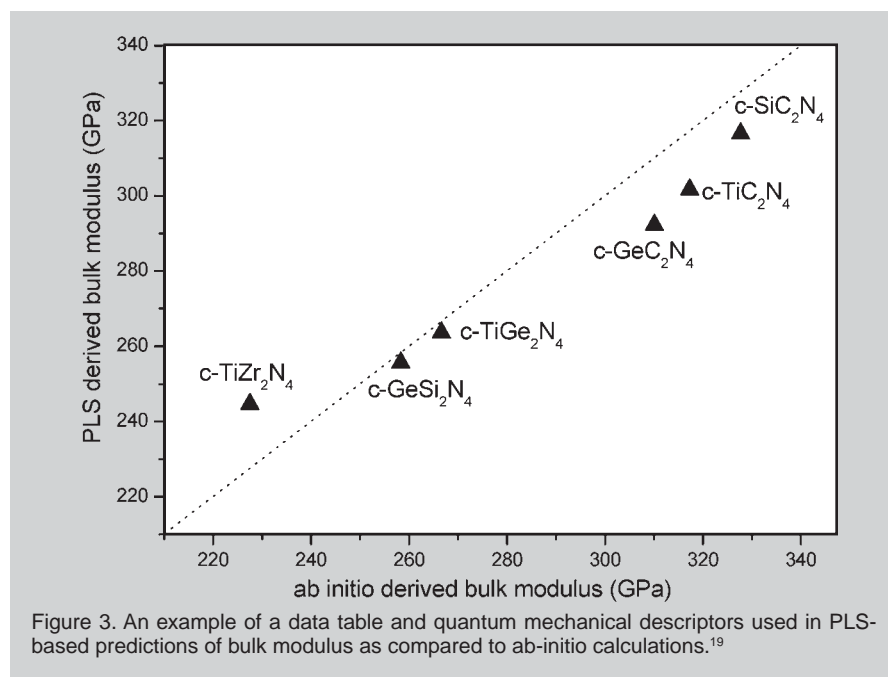


Figure 3. An example of a data table and quantum mechanical descriptors used in PLS-based predictions of bulk modulus as compared to ab-initio calculations.<sup>19</sup>

charge can then be used as a major screening parameter in identifying promising crystal chemistries for promoting the modulus. Hence, using PLS to develop a QSAR formulation combined with an interpretation of the physics governing these materials can indeed be valuable. Our predictions fit well with systems of similar electronic structure and allow us to clearly identify outliers based on these quantum mechanical calculations. Based on these predictions we can now seriously and effectively accelerate materials design by focusing on promising candidate chemistries. Those selected can then be subjected to further analysis via experimentation and computational methods to validate crystal-structure-level properties. The data generated by these selective experiments and computations also serve to refine the next generation of “training” data for another iterative round of data mining, which permits a further refinement of high-throughput predictions.

See the sidebar for details on analytical expressions for crystal chemistry.

## ACKNOWLEDGEMENT

We gratefully acknowledge support from the National Science Foundation International Materials Institute Program for Combinatorial Sciences and Materials Informatics Collaboratory (CoSMIC-IMI) – Grant no. DMR-08-33853; Air Force Office of Scientific Research Grant no. FA95500610501 and no. FA95500810316, and the Defense Advanced Research Programs Agency Center for Interfacial Engineering for MEMS (CIEMS) – Grant no. 1891874036790B.

## References

1. D.G. Pettifor, *Structure Mapping Intermetallic Compounds: Principles and Practice*, ed. J.H. Westbrook and R.L. Fleischer, Vol. 1 (Chichester, U.K.: John Wiley & Sons, 1995), pp. 419–438.
2. E. Mooser and W.B. Pearson, “On the Crystal Chemistry of Normal Valence Compounds,” *Acta Cryst.*, 12 (1959), pp. 1015–1022.
3. W. Andreoni et al., “Hard-core Pseudopotentials and Structural Maps of Solids,” *Phys. Rev. B*, 20 (12) (1979), p. 4814.
4. J.C. Phillips and J.A. Van Vechten, “Dielectric Classification of Crystal Structures, Ionization Potentials, and Band Structures,” *Phys. Rev. Lett.*, 22 (14) (1969), pp. 705–708.
5. K. Söerberg et al., “Crystal Structures and Phase Stability in Pseudobinary  $\text{CaAl}_{2-x}\text{N}_x$ ,” *J. Solid State Chem.*, 179 (8) (2006), pp. 2690–2697.

6. D. Pettifor, *Bonding and Structure of Molecules and Solids* (Oxford, U.K.: Oxford University Press, 1995).
7. C. Suh and K. Rajan, “Establishing Measurement Techniques for Mapping Structure-Property Relationships,” *Mat. Sci. Tech.* (accepted).
8. L. Eriksson et al., *Multi- and Megavariate Data Analysis—Principles and Applications* (Umeå, Sweden: Umetrics Academy, 1999).
9. R.A. Johnson and D.W. Wichern, *Applied Multivariate Statistical Analysis*, 5th Ed. (Upper Saddle River, NY: Prentice Hall, 2002).
10. K.E. Sickafus, J.M. Wills, and N.W. Grimes, “Structure of Spinel,” *J. Am. Ceram. Soc.*, 82 (12) (1999), pp. 3279–3792.
11. W.Y. Ching et al., “Theoretical Prediction of the Structure and Properties of Cubic Spinel Nitrides,” *J. Am. Ceram. Soc.*, 85 (1) (2002), pp. 75–80.

12. P. Villars, “A Three-Dimensional Structure Stability Diagram for 998 Binary AB Intermetallic Compounds,” *J. Less-Common Met.*, 92 (1983), pp. 215–238.
13. J.K. Burdett, G.D. Price, and S.L. Price, “Factors Influencing Solid-State Structure—An Analysis Using Pseudopotential Radii Structural Maps,” *Phys. Rev. B*, 24 (6) (1981), pp. 2903–2912.
14. J.K. Burdett, G.D. Price, and S.L. Price, “Role of the Crystal-Field Theory in Determining the Structures of Spinels,” *A. Am. Chem. Soc.*, 104 (1982), pp. 92–95.
15. H. Haeuseler, “Structure Field Maps for Sulfides of Composition  $\text{AB}_2\text{X}_4$ ,” *J. Solid. State. Chem.*, 86 (1990), pp. 275–278.
16. A. Zunger, “A Pseudopotential Viewpoint of the Electronic and Structural Properties of Crystals,” *Structure and Bonding in Crystals*, Vol. 1, ed. M. O’Keeffe and A. Navrotsky (New York: Academic

## ANALYTICAL EXPRESSIONS FOR CRYSTAL CHEMISTRY: LINKING GEOMETRY TO BONDING

As noted by R.M. Thompson and R.T. Down,<sup>24</sup> crystal chemistry has traditionally considered the analysis of anion-cation interactions as critical to the understanding of stability and a crystal structure’s response to temperature, pressure, and composition. A pure hard-sphere model of crystal geometry is not sufficient in addressing the link between the chemical identity of an atom and the geometry (coordination) of its environment, as described by bond lengths and bond angles. There is a need to link the geometrical distortions associated with bonding relative to an ideal hard sphere model.

Thompson and Down, for instance, have proposed formulations that account for the distortion in bond lengths and bond angles due to the ionicity of the bonding. This is quantified in terms of an “anion parameter” ( $u$ ) that quantifies the distortion of the anion

skeleton in a crystal by a measure of the average isotropic displacement of the anions from the ideal closest-packed structures. This distortion accounts for nearest-neighbor interactions and the coordination of anions associated with different chemistries. Sickafus et al.<sup>10</sup> have developed analytical expressions linking lattice parameters and anion parameters specifically for spinel structures (see Table A). For the spinel geometry, there are numerous bond lengths and bond angle distortions that need to be accounted for as anions in spinels usually are dilated away from their cubic-close-packed positions, which in turn changes bond lengths, bond angles, interstice volumes, and the symmetries of coordination polyhedra. To map all this information requires plotting the numerous relationships linking geometrical bond distortions to anion and lattice parameters. Some examples are given in Figure A. The discussion in the body of this paper takes the input variables associated with these equations tabulated in Table A and maps the high dimensional correlations between all these parameters using data dimensionality reduction techniques such as principal component analysis. From this, the authors have developed predictive models using regression tools in this high dimensional space, providing a data-driven approach to explore the multivariate nature of geometry-bonding relationships in complex structures.

**Table A. Useful Descriptors for Spinel Nitrides and Relationships between Crystallographic Descriptors and Anion Parameter. All IDs Correspond to the Descriptors in Table I (from Reference 10)**

Crystallographic Descriptors (Number Correspond to Those Cited in Table I)	Analytical Formulation Linking Lattice Parameter with Anion Parameter (Taken from Sickafus et al. <sup>10</sup> )
3	$\sqrt{3}a(u-1/4)$
4	$a[2(u-3/8)^2 + (5/8-u)^2]^{1/2}$
20	$(\sqrt{3}/8)a$
21	$(1/4)a$
22	$(\sqrt{2}/4)a$
23	$(\sqrt{11}/8)a$
24	$(\sqrt{3}/4)a$
25	$2\sqrt{2}a(u-1/4)$
26	$2\sqrt{2}a(1/2-u)$
27	$2a\{(u-3/8)^2 + 1/32\}^{1/2}$
28	$\sqrt{3}a(1/2-u)$
29	$a[2(u-1/4)^2 + (1/2-u)^2]^{1/2}$
30	$a[(u-1/4)^2 + 2(1/2-u)^2]^{1/2}$
31	$a[2(u-3/8)^2 + (u-1/8)^2]^{1/2}$
33	$(8/3)a^3(u-1/4)^3$
34	$(8/3)a^3(1/2-u)^3$
35	$(1/3)a^3(1/2-u)(u-1/4)$
36	$(16/3)a^3(1/2-u)^2(u-1/8)$
37	$(16/3)a^3(u-1/4)^2(5/8-u)$
38	$(1/192)a^3$



Press, 1981), pp. 73–135.

17. Y. Harada et al., "New Crystal Structure Maps for Intermetallic Compounds," *J. Phys.: Condens. Matter*, 9 (1997), pp. 8011–8030.

18. P. Villars and J.C. Phillips, "Quantum Structural Diagrams and High-Tc Superconductivity," *Phys. Rev. B*, 37 (4) (1988), pp. 2345–2348.

19. C. Suh and K. Rajan, "Virtual Screening and QSAR Formulations for Crystal Chemistry," *QSAR & Comb. Sci.*, 24 (1) (2005), pp. 114–119.

20. R.J. Hill, J.R. Craig, and G.V. Gibbs, "Systematics of the Spinel Structure Type," *Phys. Chem. Miner.*, 4 (1979), pp. 317–339.

21. R.D. Tobias, "An Introduction to Partial Least Squares Regression" (Cary, NC: SAS Institute Inc., 2007), <http://support.sas.com/rnd/app/papers/pls.pdf>.

22. V. Kholodovych et al., "Accurate Predictions of

Cellular Response using QSPR: A Feasibility Test of Rational Design of Polymeric Biomaterials," *Polymer*, 45 (22) (2004), pp. 7367–7379.

23. M.D. Segall et al., "Population Analysis of Plane-Wave Electronic Structure Calculations of Bulk Materials," *Phys. Rev. B*, 54 (23) (1996), pp. 16317–16320.

24. R.M. Thompson and R.T. Downs, "Quantifying Distortion from Ideal Closest-Packing in a Crystal Structure with Analysis and Application," *Acta Crystallographica Section B*, 57 (2) (2001), pp. 119–127.

**Changwon Suh and Krishna Rajan are with the Department of Materials Science and Engineering, Iowa State University, Ames, IA 50011, USA. Dr. Rajan can be reached at [krajan@iastate.edu](mailto:krajan@iastate.edu).**

24 7  
**Kn**  
KNOWLEDGE

**TMS KNOWLEDGE  
RESOURCE CENTER**

**Your Materials Books  
and More e-Store!**

<http://knowledge.tms.org>

## **2007 Nanomaterials: Fabrication, Properties & Applications**

**Editors: Wonbong Choi, Ashutosh  
Tiwari, and Seung Kang**

These papers are based on presentations prepared for the symposium 2007 Nanomaterials: Fabrication, Properties & Applications. The original symposium description is as follows: "The symposium will address the applications, fabrication and fundamental physics and chemistry of nanomaterials. Nanomaterials may be of any composition. For example, the nanomaterials may be carbon-based, silicon-based or a variety of functional materials such as semiconducting, ferroelectric and piezoelectric oxides, functional intermetallics such as ferromagnetic shape memory alloys, or complex magnetic materials for spintronics. The nanomaterials may have any morphology (i.e., wires, ropes, powders, tubes, thin films etc.) as long as their structure/property/performance/processing is dominated by phenomenon that results at the "nano" scale (1-100nm). Topics of interest related to nanomaterials include, but are not limited to:

- Controlled and directed growth
- Use in sensing of biological, chemical or other toxins
- Use in electronic, magnetic or other scientific application
- Use as building block for complex or hybrid devices and integrated systems
- Physics and chemistry or other fundamental properties
- Theoretical modeling studies

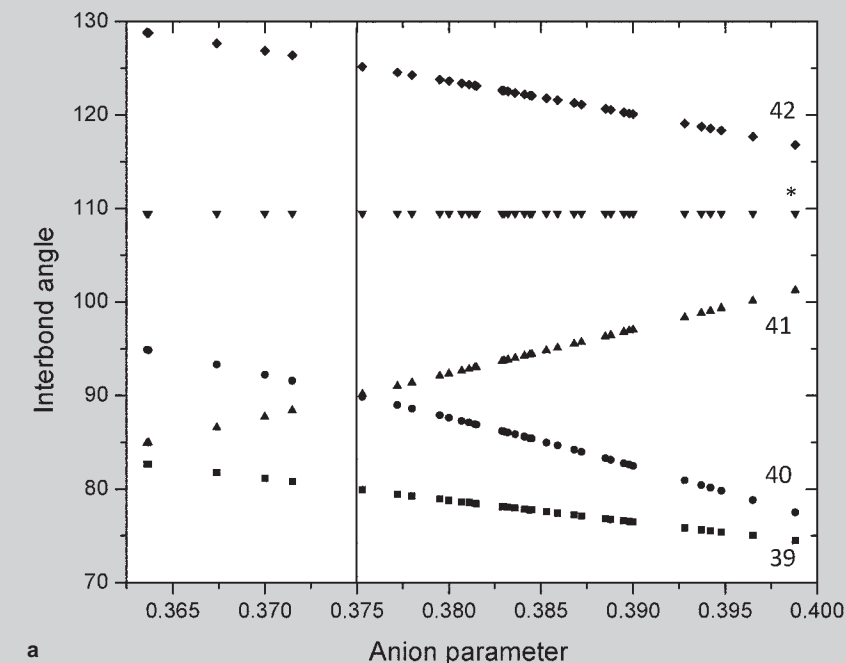
**Member price \$106**

**Student price \$106**

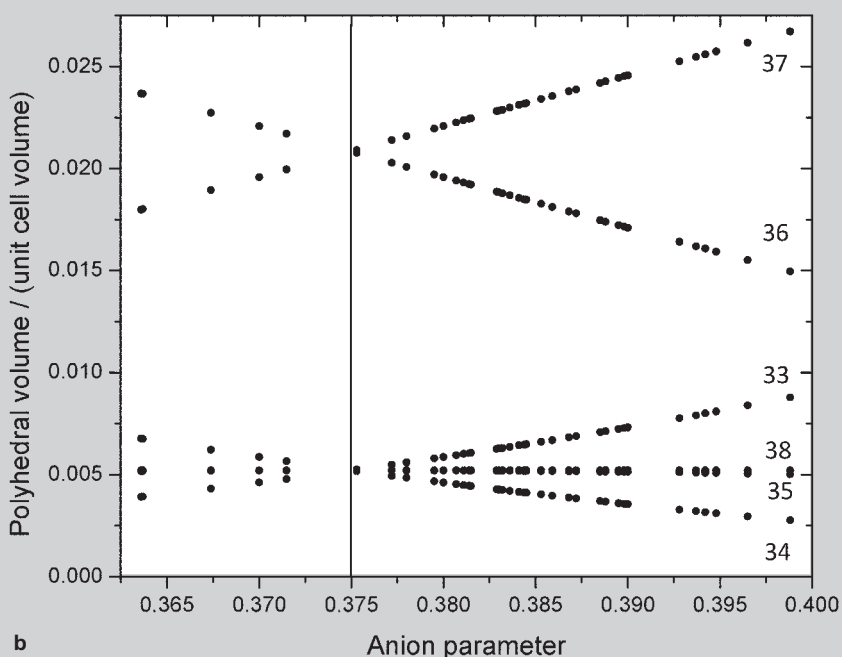
**List price \$144**

**To order these or related  
publications, contact TMS:**

E-mail [publications@tms.org](mailto:publications@tms.org)  
Phone (724) 776-9000, ext. 256  
Fax (724) 776-3770



**a**



**b**

Figure A: (a) Bond angle as a function of anion parameter, (b) polyhedral volume as a function of anion parameter.

# Using Data to Account for Lack of Data: Linking Material Informatics with Stochastic Analysis

Baskar Ganapathysubramanian

Many material systems of fundamental as well as industrial importance are significantly affected by underlying fluctuations and variations in boundary conditions, initial conditions, material property, as well as variabilities in operating and surrounding conditions. There has been increasing interest in analyzing, quantifying, and controlling the effects of such uncertain inputs on complex systems. This has resulted in the development of techniques in stochastic analysis and predictive modeling. A general application of stochastic techniques to many significant problems in engineering has been limited due to the lack of realistic, viable models of the input variability. Ideas of material informatics can be used to utilize available data about the input to construct a data-driven, computationally viable model of the input variability. This promising coupling of material informatics and stochastic analysis is investigated and some results are showcased using a simple example of analyzing diffusion in heterogeneous random media. Limited microstructural data is utilized to construct a realistic model of the thermal conductivity variability in a system. This reduced-order model then serves as the input to the stochastic partial differential equation describing thermal diffusion through random heterogeneous media.

## INTRODUCTION

With rapid advances in computational power and easier access to high-performance computing platforms, it has now become possible to computationally represent and analyze multiphysics phenomena more precisely than ever before.

As a direct consequence of this computational ability, there has been

growing awareness that such systems are affected to a significant extent by the inherent (usually unresolvable and uncontrollable) uncertainties in mate-

rial properties, fluctuations in operating conditions, and system topology. It becomes imperative to incorporate the effects of such stochastic phenomena in the computational description of the system. This paradigm shift toward a computational approach that incorporates stochastic effects and produces distributions of solutions (that mimic the error bars seen in experimental data) is called predictive modeling.

A good example of how the underlying variability affects performance is in micro-electro mechanical systems (MEMS). The material properties and the geometric parameters specifying MEMS devices play a significant part in determining the performance of the MEMS device. Commercial feasibility requires using low-cost manufacturing processes to fabricate these MEMS devices. This often results in significant uncertainties in these parameters which lead to large variations in the device performance. To accurately predict and subsequently design/tailor the performance of such systems, it becomes essential for one to include the effects of these input uncertainties into the system and understand how they propagate and alter the final solution.

Another class of problems that illustrates the necessity of incorporating the effects of uncertainty (in the lower scales) is in the design and analysis of components made of polycrystalline, functionally graded, and other heterogeneous materials. Most engineering devices involve the use of such multi-component materials which constitute a major element in structural, transport, and chemical engineering applications. They are ubiquitous, entering wherever there is a need for cheap, resilient, and strong materials. The thermal and elastic properties of such materials (par-

### How would you...

#### ...describe the overall significance of this paper?

This article highlights the applicability of ideas from material informatics for constructing viable computational models of input uncertainties (like material property distribution). This will allow realistic analysis of complex material systems while accounting for uncertainties in a data-driven framework.

#### ...describe this work to a materials science and engineering professional with no experience in your technical specialty?

Realistic modeling and design of physical systems has to account for the inherent uncertainties and noise in the system. Constructing accurate data-driven models of the input parameters (initial conditions, boundary conditions, property variations) that explicitly account for these uncertainties is critical for such analysis. This article reviews recent work on data-driven construction of input models.

#### ...describe this work to a layperson?

Experimental analysis of physical systems results in conclusions specified with error bars—implicitly accounting for the uncertainty and noise in the measurement and system. Deterministic computational analysis provides no such error bars. This article reviews recent work in augmenting computational analysis of physical systems to account for uncertainties in initial and boundary conditions as well as material property variations. Data-driven techniques that encode limited available information into viable representations of these input uncertainties are detailed.

ticularly polycrystals) are highly anisotropic and heterogeneous, depending on the local microstructure. Experimental evidence has shown that microstructural variability in polycrystalline materials can have a significant impact on the variability of macro-properties such as strength or stiffness as well as in the performance of devices made of random heterogeneous media. Nevertheless, there has been no dedicated effort in the engineering community for incorporating the effect of such microstructural uncertainty in process or device design even though it is well known that most performance-related failures of critical components are directly related with rare events (tails of the PDF) of microstructural phenomena.<sup>1-5</sup>

The above two examples clearly underscore the necessity of incorporating the effects of uncertainty in property variation and operating conditions during the analysis and design of components and devices. There are two key ingredients for constructing a framework to analyze the effects of various sources of uncertainty in a system. The first is a mathematically rigorous framework that can be used to define the stochastic differential equations representing the systems. The stochasticity (i.e., inclusion of the effects of uncertainty) in this set of differential equations enters as uncertain boundary and initial conditions, variations in properties, fluctuations, and perturbations or more generally as noise. The second ingredient is a set of techniques to construct usable, realistic models of these input uncertainties. These models should utilize available experimental information and/or expert knowledge. This is a crucial (yet understated) issue with stochastic modeling. It is necessary to provide meaningful/realistic models for the input uncertainty to draw any meaningful conclusions from the resulting solutions.

The past few years have seen progress in quantifying and modeling the effect of input uncertainties in the response of partial differential equations (PDEs) using non-statistical methods. The presence of uncertainties is incorporated by transforming the PDEs representing the system into a set of stochastic PDEs (SPDEs). The spectral

(and spectral Galerkin) representation of stochastic space<sup>6-8</sup> resulted in the development of the generalized polynomial chaos expansion (GPCE) methods.<sup>8-15</sup> An alternate strategy, particularly suited to solve large-scale problems involving high-dimensional stochastic spaces in a non-intrusive manner, resulted from recent efforts to couple the fast convergence of spectral methods with the decoupled nature of Monte-Carlo sampling.<sup>16,17</sup> One such approach has been to construct stochastic solutions using interpolating polynomials instead of spectral methods.<sup>17-19</sup> These techniques are called sparse grid collocation approaches. The sparse grid collocation strategy provides a seamless

way to scalably incorporate the effects of multiple sources of uncertainty in an embarrassingly parallel way.

Even though there has been significant progress in our computational ability to access the effects of uncertainty in complex systems, most analysis has been purely academic due to the lack of realistic stochastic models for the uncertain inputs. In such analysis, the property variability is usually assumed to be an analytically known function. Physically meaningful/useful solutions can be realized only if property statistics and data are experimentally obtained and used. The construction of viable stochastic input models based on limited data is a very interesting

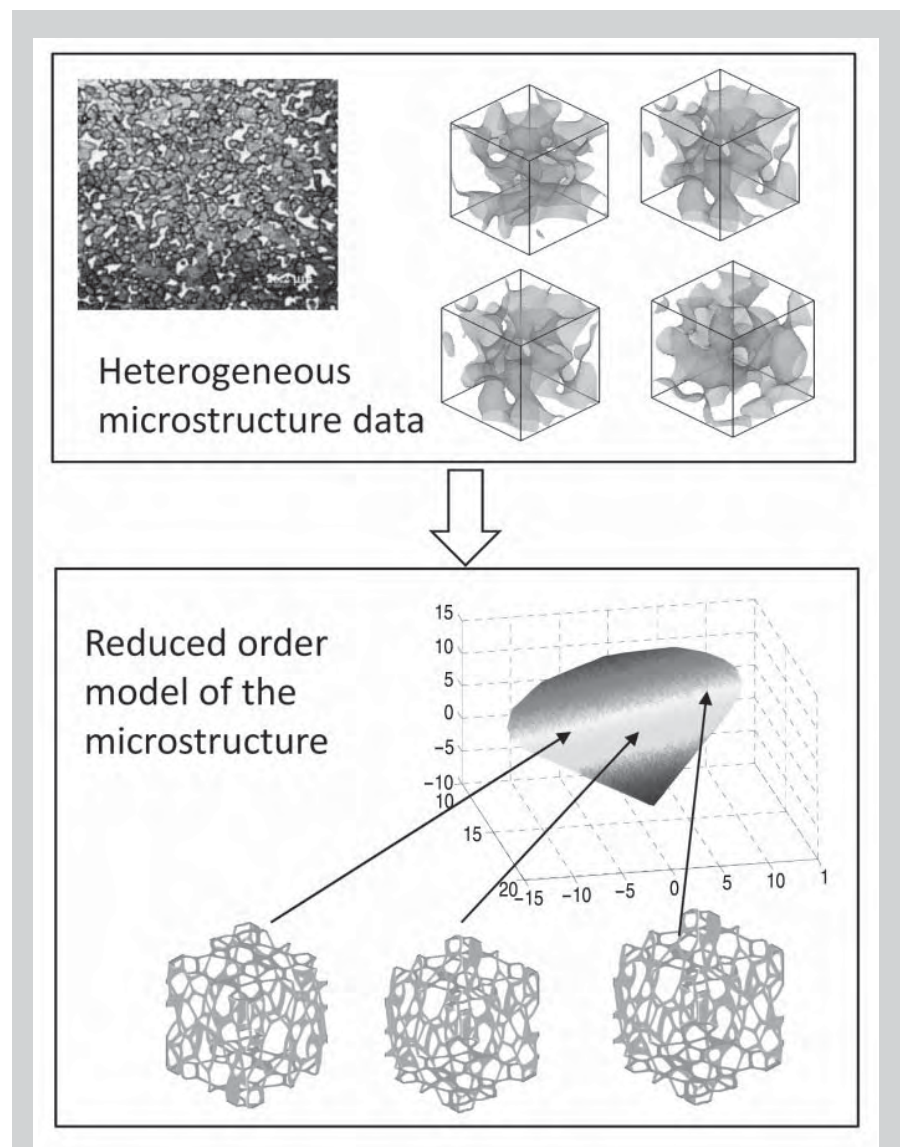


Figure 1. The basic idea of using material informatics. A large data set of heterogeneous microstructural data is available. This could be micrographs or tomographic slices or reconstructed images. Data-driven model reduction strategies are used to construct a low-dimensional representation of the possible variability in the microstructure.

and challenging mathematical problem that has only recently gained interest. Recent work has focused on developing probabilistic models of properties using maximum likelihood methods,<sup>20</sup> using domain decomposition methods,<sup>21</sup> feature extraction methods<sup>22</sup> as well as manifold learning strategies.<sup>23</sup> All of these strategies can be classified into a specific aspect of material informatics: data-driven construction of reduced order property models.

### MATERIAL INFORMATICS: DATA-DRIVEN, STOCHASTIC INPUT MODELS

With significant improvements in data collection, measurement, characterization, and reconstruction strategies, an enormous amount of material, microstructure, and property data are

available. The direct use of this enormous amount of input data would pose a significant strain on available computational resources. One has to resort to extracting key features or patterns that can then be used to succinctly represent pertinent property variations. It is therefore necessary to develop data-driven model reduction strategies to utilize experimentally available information to (dynamically) construct low-order realistic models of input uncertainties. These low-dimensional models representing the variability in the input conditions can then be utilized as the stochastic input for solving the SPDEs.

The field of material informatics offers a variety of promising avenues toward constructing such data-driven models. In References 22 and 23, we have recently developed techniques

to utilize statistical information about the variability in the property of random media and produce viable low-dimensional descriptors as inputs to the SPDE describing the evolution of the dependent variable. The basic idea involved is the topological transformation of a high dimensional space into its low-dimensional parameterization. This problem of constructing low-dimensional stochastic representations of property variation is analogous to the problem of manifold learning and parametric fitting of hyper-surfaces encountered in image processing, psychology, and cognitive sciences. The construction of the topological transformation is based on preserving some geometric characteristic of the input data. Such geometric features include distances (isometric mappings), angles (conformal mappings), and tangent bundles (local tangent mappings). Given only a finite amount of input data, the methodology constructs an accurate, low-dimensional, data-driven representation of the property variation.

This concept was applied to the analysis of the effect of limited information on simulating thermal diffusion in random heterogeneous media. The physical domain consisted of a tungsten-silver composite filling a cubical region of  $39.7 \mu\text{m} \times 39.7 \mu\text{m} \times 39.7 \mu\text{m}$ . A two-dimensional experimental image of the microstructure is provided (from S. Umekawa et al.<sup>24</sup>). This composite was produced by infiltrating a porous tungsten solid with molten silver. The steady-state temperature profile, when a constant temperature of  $0.5^\circ\text{C}$  is maintained on the left wall and a constant temperature of  $-0.5^\circ\text{C}$  is maintained on the right wall, is evaluated. All the other walls are thermally insulated.

The thermal conductivity distribution in the domain determines the thermal distribution. The thermal conductivity distribution is determined by the microstructural distribution of the two-phase composite. However, the exact microstructural distribution is unknown. The only information available is statistical functions (like volume fraction, two point correlation) that can be extracted from the experimental image. The data-driven model reduction strategy was applied to construct a re-

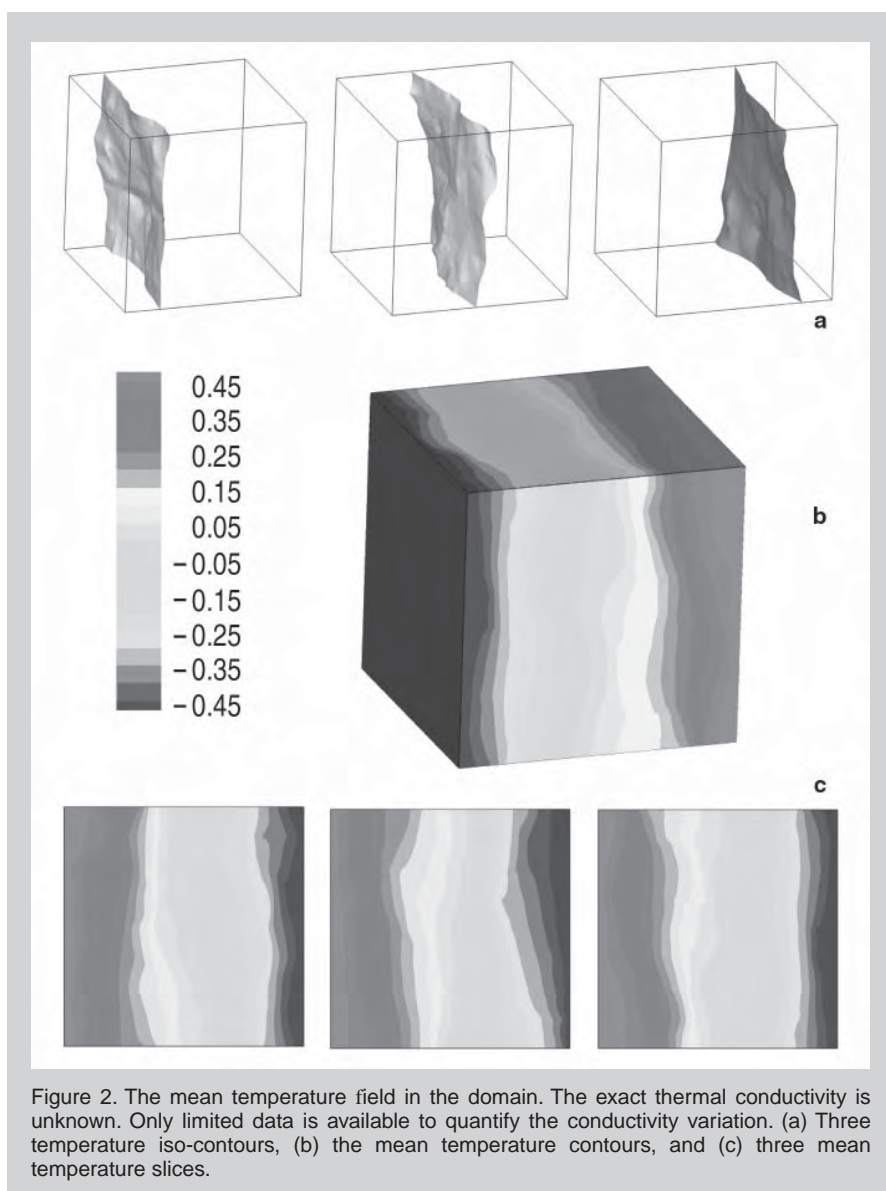


Figure 2. The mean temperature field in the domain. The exact thermal conductivity is unknown. Only limited data is available to quantify the conductivity variation. (a) Three temperature iso-contours, (b) the mean temperature contours, and (c) three mean temperature slices.

duced-order model (see Figure 1). This reduced-order model is then used as an input model to solve the stochastic differential equation modeling diffusion in random heterogeneous media. A stochastic multiscale computational strategy was utilized to solve for the stochastic temperature.<sup>23</sup> Figure 2 shows the mean temperature profile in the domain.

Utilizing limited data results in a model that shows large variability (since many distributions can satisfy limited data). This variability decreases as the amount of information being incorporated increases. In the limiting case of availability of complete information, the stochastic model collapses to a deterministic model representing a single microstructure. This sequential improvement via data assimilation is showcased in Figure 3, which depicts the temperature distribution (standard deviation and probability distribution) using input models that were constructed by incorporating different amounts of data. The first model (upper figure) was constructed by utilizing only the first-order statistics (volume fraction) while in the second case (lower figure), both first-order as well as second-order constraints (volume fraction and two-point correlation) are used. Notice the reduction in the range of variability of the temperature due to the incorporation of second-order statistics. When only first-order statistics are imposed, the range of variability of the temperature is  $[-0.5, 0.45]$  (i.e., almost 98% of the whole range of applied temperatures  $[-0.5, 0.5]$ ). When second-order statistics are also imposed, this range is reduced to about 65% of the applied temperature range. Increasing the amount of data reduces the epistemic uncertainty, thus reducing the variability in the unknown variable.

The use of ideas from material informatics (feature extraction, data mining, and model reduction) provides a seamless way of incorporating heterogeneous data into viable stochastic input models. This represents an exciting area of research and application with several open problems. These include developing mathematical, computational, and statistical insights and tools into the choice of topological transformation for constructing reduced order mod-

els; leveraging developments in pattern selection and unsupervised learning toward accelerated feature/property selection and data assimilation; mathematical analysis of the choice of the geometric characteristics on the regularity of the low-dimensional model; the use of graph-theoretic concepts in estimating geometric properties of high-dimensional manifolds; developing sequential data incorporation strategies for constructing reduced order models; and developing computation-

ally efficient (parallel and distributed) algorithms for data assimilation.

## CONCLUSIONS

Ideas from material informatics can be applied to the construction of viable reduced-order models utilized in stochastic analysis. This coupling of material informatics and stochastic analysis seems very promising, particularly because the utility of stochastic analysis in realistic applications is hindered by the lack of rigorous methodologies of

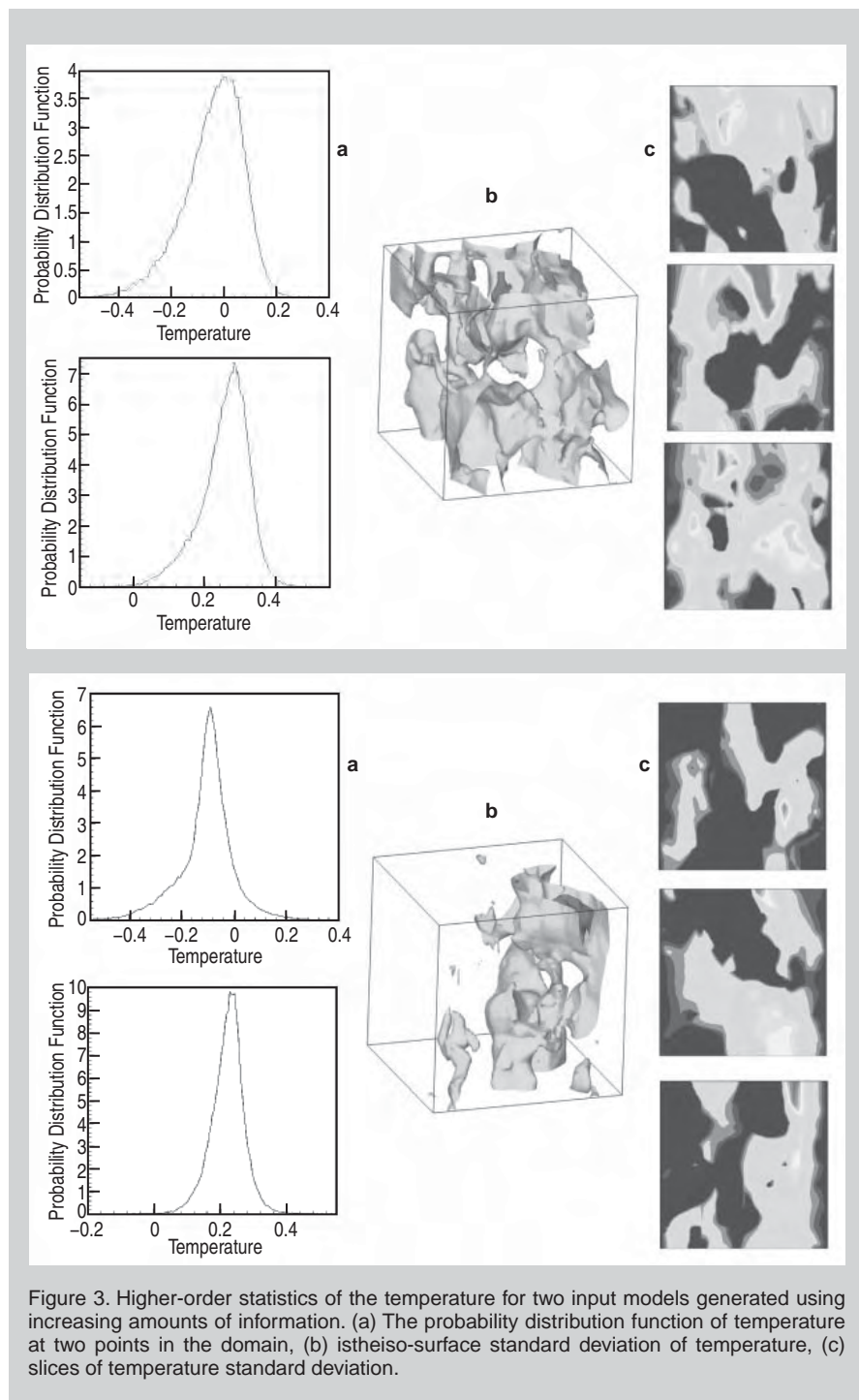


Figure 3. Higher-order statistics of the temperature for two input models generated using increasing amounts of information. (a) The probability distribution function of temperature at two points in the domain, (b) is the isosurface standard deviation of temperature, (c) slices of temperature standard deviation.

constructing realistic data-driven input models. Several open questions have been posed in the hope that this will stimulate research and development in this promising field.

## References

1. Major Aircraft Disasters, *dnausers.d-n-a.net/dnet-GOJG/Disasters.htm*.
2. Accelerated Insertion of Materials (AIM) Program (Arlington, VA: DARPA Defense Sciences Office), *www.darpa.mil/dso/thrusts/materials/novelmat/aimd3d/index.htm*.
3. Prognosis, Program (Arlington, VA: DARPA Defense Sciences Office), *www.darpa.mil/dso/thrusts/materials/novelmat/prognosis/index.htm*.
4. National Security Assessment of the U.S. Forging Industry (Washington, D.C.: Bureau of Industry and Security, U.S. Department of Commerce), *www.bis.doc.gov/defenseindustrialbaseprograms/osies/*.
5. R. Martin and D.L. Evans "Reducing Costs in Aircraft: The Metals Affordability Initiative Consortium," *JOM*, 52 (3) (200), pp. 24–28.
6. N. Wiener, "The Homogeneous Chaos," *Amer. J. Math.*, 60 (1938), pp. 897–936.
7. R.H. Cameron and W.T. Martin, "The Orthogonal Development of Non-linear Functionals in Series of Fourier-Hermite Functionals," *Ann. Math.*, 48 (1947), pp. 385–392.
8. R.G. Ghanem and P.D. Spanos, *Stochastic Finite Elements: A Spectral Approach* (Mineola, NY: Dover Publications, 1991).
9. R. Ghanem, "Probabilistic Characterization of Transport in Heterogeneous Porous Media," *Comput. Methods Appl. Mech. Engrg.*, 158 (1998), pp. 199–220.
10. D. Xiu and G.E. Karniadakis, "Modeling Uncertainty in Steady State Diffusion Problems via Generalized Polynomial Chaos," *Comput. Methods Appl. Mech. Engrg.*, 191 (2002), pp. 4927–4948.
11. B. Velamur Asokan and N. Zabarar, "Variational Multiscale Stabilized FEM Formulations for Transport Equations: Stochastic Advection-Diffusion and Incompressible Stochastic Navier–Stokes Equations," *J. Comp. Physics*, 202 (2005), pp. 94–133.
12. M.K. Deb, I.K. Babuska, and J.T. Oden, "Solution of Stochastic Partial Differential Equations using the Galerkin Finite Element Techniques," *Comput. Methods Appl. Mech. Engrg.*, 190 (2001), pp. 6359–6372.
13. I. Babuska, R. Tempone, and G.E. Zouraris, "Solving Elliptic Boundary Value Problems with Uncertain Coefficients by the Finite Element Method: The Stochastic Formulation," *Comput. Methods Appl. Mech. Engrg.*, 194 (2005), pp. 1251–1294.
14. R. Tempone, "Numerical Complexity Analysis of Weak Approximation of Stochastic Differential Equations" (Ph.D. thesis, Royal Institute of Technology, Sweden, 2002).
15. D.M. Tartakovsky and D. Xiu, "Stochastic Analysis of Transport in Tubes with Rough Walls," *J. Comput. Phys.*, 217 (2006), pp. 248–259.
16. B. Velamur Asokan and N. Zabarar, "Using Stochastic Analysis to Capture Unstable Equilibrium in Natural Convection," *J. Comp. Phys.*, 208 (2005), pp. 134–153.
17. I. Babuska, F. Nobile, and R. Tempone, *A Stochastic Collocation Method for Elliptic Partial Differential Equations with Random Input Data*, ICES Report 05-47 (Austin, TX: Institute for computational Engineering and Science, 2005).
18. D. Xiu and J.S. Hesthaven, "High-order Collocation Methods for the Differential Equation with Random Inputs," *SIAM J. Sci. Comput.*, 27 (2005), pp. 1118–1139.
19. B. Ganapathysubramanian and N. Zabarar, "Sparse Grid Collocation Schemes for Stochastic Natural Convection Problems," *J. Comp. Phys.*, 225 (2007), pp. 652–685.
20. C. Desceliers, R. Ghanem, and C. Soize, "Maximum Likelihood Estimation of Stochastic Chaos Representations from Experimental Data," *Int. J. Numer. Meth. Engrg.*, 66 (2006), pp. 978–1001.
21. L. Guadagnini, A. Guadagnini, and D.M. Tartakovsky, "Probabilistic Reconstruction of Geologic Facies," *J. Hydrol.*, 294 (2004), pp. 57–67.
22. B. Ganapathysubramanian and N. Zabarar, "Modelling Diffusion in Random Heterogeneous Media: Data-Driven Models, Stochastic Collocation and the Variational Multi-Scale Method," *J. Comput. Phys.*, 226 (2007), pp. 326–353.
23. B. Ganapathysubramanian and N. Zabarar, "A Non-linear Dimension Reduction Methodology for Generating Data-Driven Stochastic Input Models," *J. Comput. Phys.*, 227 (2008), pp. 6612–6637.
24. S. Umekawa, R. Kotfila, and O.D. Sherby, "Elastic Properties of a Tungsten-Silver Composite above and below the Melting Point of Silver," *J. Mech. Phys. Solids*, 13 (1965), pp. 229–230.

**Baskar Ganapathysubramanian is with the Department of Mechanical Engineering, Iowa State University, 2100 Black Engineering, Ames, IA 50011; e-mail baskarg@iastate.edu.**

**TMS** Your Professional Partner for Career Advancement

## New Member Benefits!

Access to Archival Journals:

*Journal of Electronic Materials*

*Metallurgical and Materials Transactions A*

*Metallurgical and Materials Transactions B*

As your professional partner, TMS has secured electronic access to the *Journal of Electronic Materials*, *Metallurgical and Materials Transaction A*, and *Metallurgical and Materials Transaction B* as part of your membership benefits.

Access these journals, plus 20 others published by Springer, at no charge by clicking on "Read Journals" from the Members-Only page at [www.tms.org](http://www.tms.org).

LEARN • NETWORK • ADVANCE

[www.tms.org](http://www.tms.org)

# A Materials Database for Exploring Material Properties

R. Hrubciak, Lyci George, Surendra K. Saxena, and Krishna Rajan

*A materials database that includes more than 2,500 solids with thermochemical and physical properties has been constructed to study the effect of chemical composition, structure, and constituent element properties on the solids. The correlation between compound entropy and the sum of constituent element entropy is clearly established and even better linear relations are possible when the solids are separated according to their crystal structure or compositional types such as carbide or oxide. A number of hydrides have been examined with this approach and many more studies involving other classes of compounds are possible.*

## INTRODUCTION

After several years of development, the Center for the Study of Matter at Extreme Conditions (CeSMEC) Database project is ready to be unveiled to the world. This report outlines and explains several stages of development, as well as goals of the project. The CeSMEC database project consists of three parts: a structured query language (SQL) database which contains all data acquired by students working at CeSMEC over several years, a newly developed web front end for data retrieval, and a Windows application for data mining and element analysis calculations.

## ELEMENT AND COMPOUND DATABASES

Element and compound data tables of experimentally measured empirical data have been compiled by students over several years through acquiring data by examining published academic literature and integrating that data with already existing databases. The element table contains all elements commonly

found in nature together with 56 different properties associated with those elements such as basic physical properties, thermodynamic properties, mechanical properties, crystal structure properties, and others.

The table also contains a list of roughly 4,000 solid inorganic compounds, compositionally classified as hydrides, carbides, oxides, etc. This compound table lists 39 different properties commonly associated with those inorganic compounds. The compound

database has complete data on thermodynamic properties of each compound such as enthalpy of formation, entropy, etc. However, other fields in the compound table are nowhere as complete as they are in the element table because no compound listed in the database can have all or even most of its properties tabulated partially because compounds have not been fully investigated.

Currently, the main focus of the database is on the properties of materials at room temperature and pressure conditions, but the inherent design of the database envisions storage of properties of materials under different temperature and pressure conditions.

The materials properties included in the database can be classified into the following categories: element properties: electron affinity, electro-negativity, ionization potential, and atomization potential; and compound properties, which can be broken down into the following:

- Electrical properties—dielectric constant, electrical resistivity, energy gap, super conduction temperature
- General properties—weight, density, boiling point, melting point, heat of sublimation, critical point temperature, triple point temperature, solubility
- Magnetic properties—magnetic susceptibility
- Mechanical properties—Brinell hardness, Poisson's ratio, rigidity modulus, velocity of sound, Vickers hardness, Young's modulus, bulk modulus, compressibility, elastic constants for crystals, hardness-micro hardness
- Optical properties—index of refraction
- Structure properties—symmetry

### How would you...

*...describe the overall significance of this paper?*

*A database of some thousand compounds with thermodynamic and physical property data has been compiled and is ready to explore mutual relationships among the properties of compounds and the properties of their constituent elements.*

*...describe this work to a materials science and engineering professional with no experience in your technical specialty?*

*Element and compound data tables of experimentally measured empirical data have been compiled. This report outlines and explains several stages of development, as well as goals of the project. Several results are presented to show the possible data mining capabilities.*

*...describe this work to a layperson?*

*Element and compound data tables of experimentally measured empirical data have been compiled by the team over several years. Data was acquired by examining published academic literature as well as integrating that data with already existing databases. These datasets are used to look for meaningful relationships between the underlying elemental properties and the compound properties.*

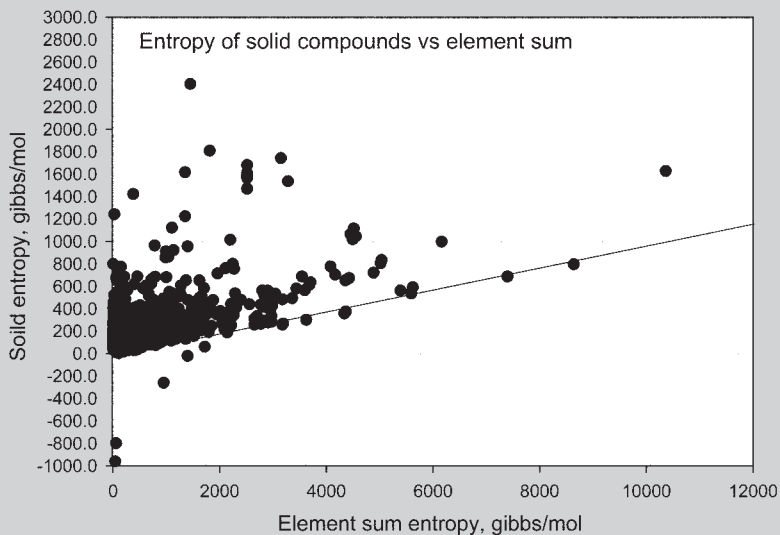


Figure 1. The relation of the sum of element entropy and that of the compound. Along the solid line the compound entropy is 10% of the sum. The solid entropy may not be less than that of the sum unless there is some peculiarity in the structure. The figure shows several solids (all solids currently in the database with entropy less than the element sum).

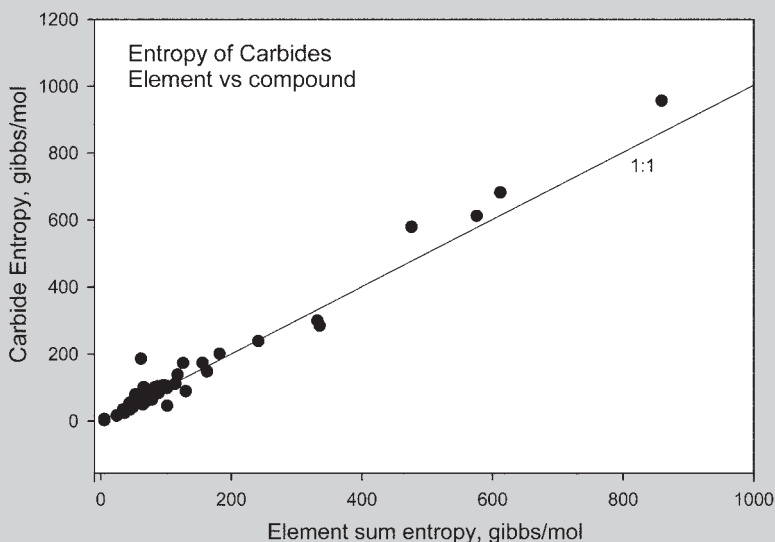


Figure 2. A plot of entropy of carbides versus element sum entropy.

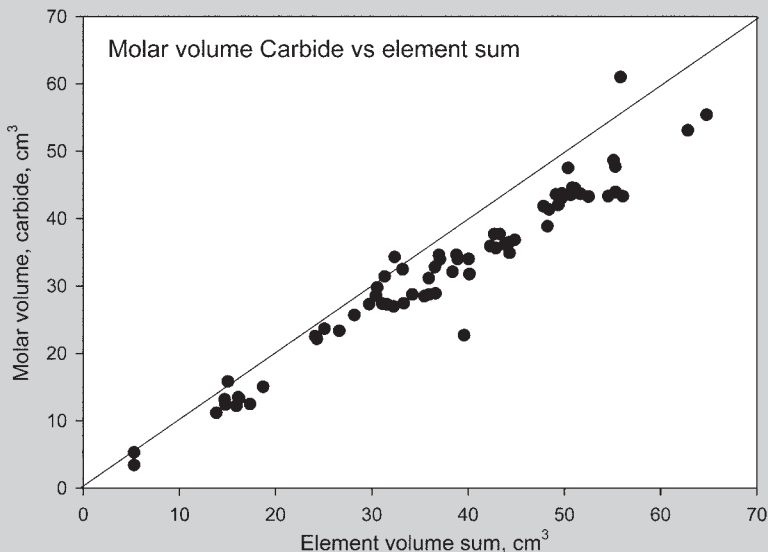


Figure 3. The relationship of the compound volume and element molar volume.

group, unit cell parameters

- Thermodynamic properties—Debye temperature, Gibbs energy, enthalpy, heat capacity, thermal conductivity, thermal expansion, lattice energies, vapor pressure

An interdisciplinary team of computer and materials scientists was employed to develop and maintain the database. The relationships between different material properties in the database are not arbitrary. The database has been built from the ground up with the fact in mind that data to be stored need to be physically consistent. For example, a strict relationship between measured empirical data about a certain thermodynamic phase of a given material needs to be consistent with the structure, among other things, related to that phase. Triggers and specialized stored procedures are being implemented to delegate these and other constraints.

The database will soon be accessed from anywhere using a web browser running on any popular operating system. A user interface has been created that allows searching the entire record, retrieving necessary data based on search criteria such as but not limited to compound formula, Chemical Abstracts Service Identification (CAS-ID), structure, composition, underlying elemental properties, and any other physical property listed in the database. The web version of the database interface is undergoing final internal testing and will be published for general viewing after the testing is completed. Several internal versions of database interface applications that allow the development team to use and insert new data were developed and used during the design process. These include standalone *Windows* applications that include all of the functionality that will be available in the online version of the user interface but also include the capability of adding new data.

## APPLICATION EXAMPLES

Having all this information available, a separate data-retrieval application was created as a side project which allowed large datasets to be retrieved from the database and element-property-based calculations to be performed. The idea is to find meaningful relationships between how the underlying el-



emental properties influence the compound properties. A large enough dataset could enable the prediction of new materials with whatever properties are needed.

How can we use a database for novel material prediction? Using even very crude analysis techniques such as simple summation of individual elemental properties, some interesting patterns can already be seen. If we have some indication that the combination of certain types of elements leads to compounds with only certain given sets of properties we can simplify the “ingredient selection” when trying to synthesize new materials. For example, Figure 1 contains a scatter plot where each dot represents a certain compound that exists in the database. The solid entropy of each compound (Gibbs/mol) has been plotted against the sum of entropies of constituting elements. The resulting figure, although not very clear, may indicate that entropy of a solid cannot be less than 10% of the total element sum. The question to now ask is what is the significance of this trend?

On the other hand if we single out only carbides a somewhat clearer picture results. Figure 2 plots all of the carbides in the database. As in the previous plot, the entropies of compounds are plotted against element sum entropies. The result is a more linear pattern. If we take a hypothetical new carbide which hasn't been created yet, and calculate or measure its entropy, will the result fit with this existing picture?

Other properties may be similarly examined. An example for volume of carbides is shown in Figure 3. Again, each dot in the scatter plot represents a certain carbide found in the database. If we plot molar volume of each carbide against the sum of its individual elements' molar volumes, very few compounds have molar volume greater than the sum of its elements' volumes. Also, it appears that there is a linear relationship between the two variables.

These findings require detailed investigation of data and as yet the data has not been classified according to various other criteria such as the crystal structure. Crystal structure considerations and other properties, once included in this approach, should yield much better understanding and predictions.

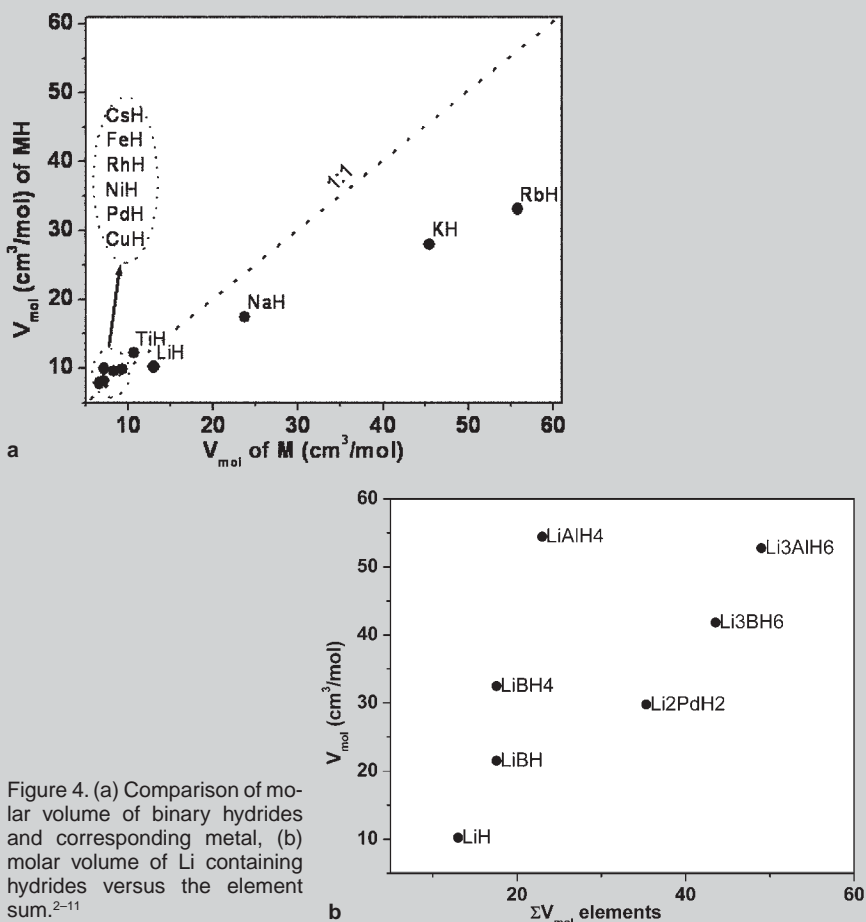


Figure 4. (a) Comparison of molar volume of binary hydrides and corresponding metal, (b) molar volume of Li containing hydrides versus the element sum.<sup>2-11</sup>

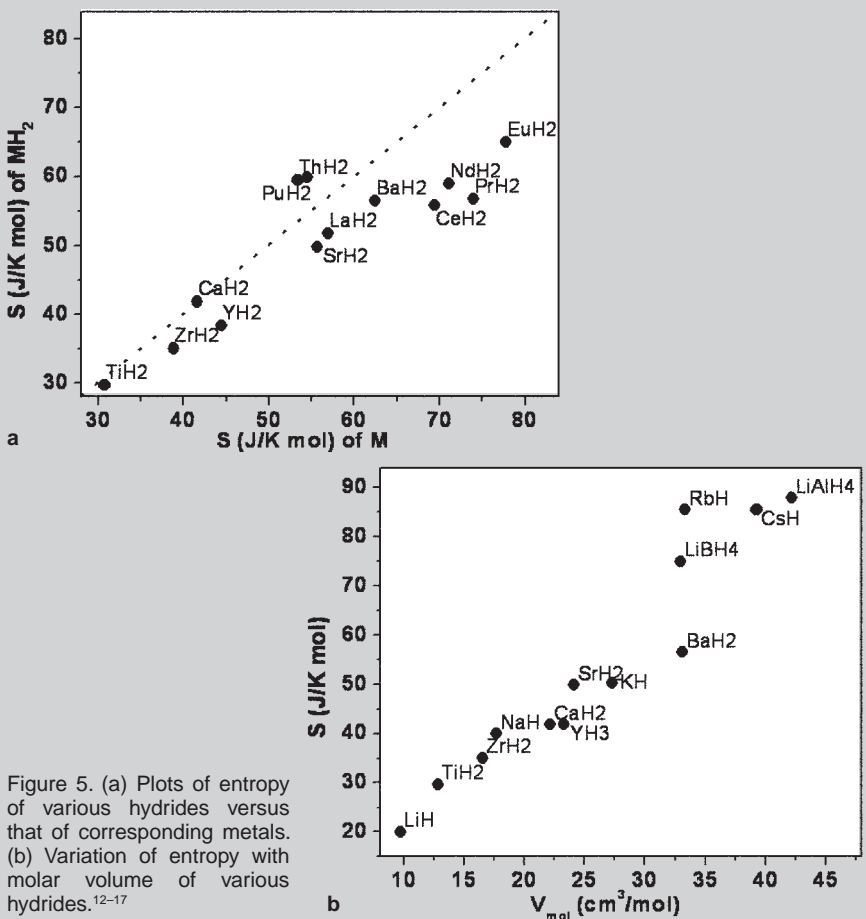


Figure 5. (a) Plots of entropy of various hydrides versus that of corresponding metals. (b) Variation of entropy with molar volume of various hydrides.<sup>12-17</sup>

The patterns presented here do not yet pave the way to determination of a phase with novel properties. We must still ask what the significance of these trends is as well as try to use other methods available for material design such as the first-principles approach as well as experiments to confirm them. But the database is beginning to offer insight into material properties which were not evident otherwise.

Hydrides are safe and efficient sources of hydrogen energy that can be tailored for onboard use. A detailed hydride research database is required for proper retrieval of information already available. The database generated at CeSMEC is an efficient tool to disseminate the material properties for hydrogen storage technology. The aim is to design new, better hydrides by combining or interpreting the database. The hydride database has enabled the study of inter-relationships of hydride material properties such as entropy, molar volume, density, unit cell volume, etc. with those of corresponding metal/metal alloys. Some such plots are

shown in Figures 4 to 6. Molar volume of a hydride can be represented as  $V_{MH} = V_M + V_H + \Delta$ , where  $V_M$  is the molar volume of metal/alloy,  $V_H$  is the molar volume of hydrogen as a metal ( $\sim 1.7 \text{ cm}^3/\text{mol}$ ), and  $\Delta$  is molar volume due to charge transfer between metal and hydrogen atoms. There may be an effect of crystal structure on the value of  $\Delta$  and hence molar volume of hydride.<sup>1</sup>

Both positive and negative deviation from linearity (1:1 metal versus hydride) can be deduced, attributable to the structural phase transition during hydrogen absorption. It appears that most of the hydrides are substitutional solid solutions with an ordered hydrogen sublattice.<sup>18</sup> There is an interrelationship between crystal chemistry and hydrogen sorption properties. Hydrides having similar symmetry may show a relation among their properties which may vary from one symmetry to another. The unavailability of proper data for most of the hydrides implies the need of further analysis of these materials so as to easily design better hydrogen storage materials.

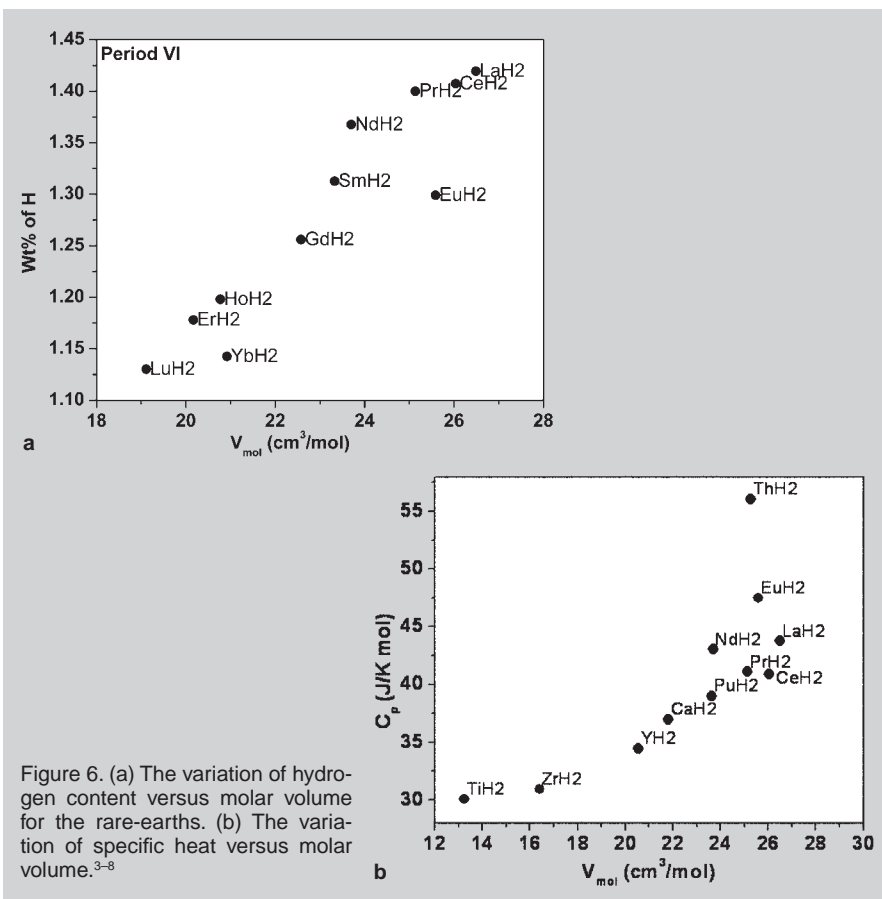
## ACKNOWLEDGEMENTS

We greatly acknowledge the financial support from National Science Foundation grant (International Materials Institute subcontract) to carry out the above research work.

## References

1. Joop van Straaten and Isaac F. Silvera, "Vibrational Mode Frequencies, Phase Diagram, and Optical Transmission of Solid Hydrogen Iodide to 25 GPa," *Phys. Rev. B*, 36 (1987), p. 9301.
2. Y. Fukai, *The Metal-Hydrogen System* (Springer Series in Material Science), 21 (1993).
3. A.V. Talyzin and B. Sundqvist, "Reversible Phase Transition in  $\text{LiAlH}_4$  under High-Pressure Conditions," *Phys. Rev. B*, 70 (2004), p. 180101(R).
4. Inorganic Crystal Structure Database (ICSD) (Karlsruhe, Germany: FIZ-Karlsruhe, 2006).
5. P. Vajeeston et al., "Huge-pressure-induced Volume Collapse in  $\text{LiAlH}_4$  and Its Implications to Hydrogen Storage," *Phys. Rev. B*, 68 (2003), p. 212101.
6. R.S. Kumar et al., "Pressure-induced Structural Phase Transition in  $\text{NaAlH}_4$ ," *Phys. Rev. B*, 75 (2007), p. 174110.
7. Geunsik Lee, Jin-Yang Lee, and Jai Sam Kim, "Ab Initio P-T Phase Diagram of  $\text{NaBH}_4$ ," *Solid State Communications*, 139 (2006), pp. 516–521.
8. J-Ph. Soulie et al., "Lithium Boro-hydride  $\text{LiBH}_4$ : I. Crystal Structure," *J. Alloys and Compounds*, 346 (2002), pp. 200–205.
9. A. Züttel et al., " $\text{LiBH}_4$  a New Hydrogen Storage Material," *J. Power Sources*, 118 (2003), pp. 1–7.
10. Ole Martin Lovvik, Ole Swang, and Susanne M. Opalka, "Modeling Alkali Alanates for Hydrogen Storage by Density-Functional Band-Structure Calculations," *J. Mater. Res.*, 20 (2005), pp. 3199–3213.
11. P. Vajeeston et al., "Theoretical Modeling of Hydrogen Storage Materials: Prediction of Structure, Chemical Bond Character, and High-Pressure Behavior," *J. Alloys and Compounds*, 404–406 (2005), pp. 377–383.
12. A. El Gridani, R. Drissi El Bouzaidi, and M. El Mouhtadi, "Elastic, Electronic and Crystal Structure of  $\text{BaH}_2$ : A Pseudopotential Study," *J. of Molecular Structure*, 577 (2002), pp. 161–175.
13. J. Tse et al., "Structural Phase Transition in  $\text{CaH}_2$  at High Pressures," *Phys. Rev. B*, 75 (2007), p. 134108.
14. B. Huang et al., "Synthesis and Structure of  $\text{Yb}_3\text{Mg}_3\text{H}_{24}$ , a New Salt-like Ternary Metal Hydride," *J. Alloys and Compounds*, 227 (1995), pp. 131–134.
15. Daisuke Kyoji et al., "A New Ternary Magnesium-Titanium Hydride  $\text{Mg}_2\text{TiH}_3$  with Hydrogen Desorption Properties Better Than Both Binary Magnesium and Titanium Hydrides," *J. Alloys and Compounds*, 372 (2004), pp. 213–217.
16. R.K. Kremer et al., "Optical Vibrations of Hydrogen in Some Rare-earth Monohalide Hydrides," *J. Phys.: Condens. Matter*, 6 (1994), pp. 4053–4066.
17. M.T. Hagstrom, J.P. Vanhanen, and P.D. Lund, " $\text{AB}_2$  Metal Hydrides for High-Pressure and Narrow Temperature Interval Applications," *J. Alloys and Compounds*, 269 (1998), pp. 288–293.
18. G.J. Thomas et al., "Microstructural Characterization of Catalyzed  $\text{NaAlH}_4$ ," *J. Alloys and Compounds*, 330–332 (2002), pp. 702–707.

R. Hrubciak, Lyci George, and Surendra K. Saxena are with the Center for the Study of Matter at Extreme Conditions, Department of Mechanical and Materials Engineering, Florida International University, Miami, FL-33199, USA. Dr. Saxena can be reached at Surendra.Saxena@fiu.edu.



# Phase Stability, Phase Transformations, and Reactive Phase Formation

Sinn-wen Chen



This special topic in *JOM*, Phase Stability, Phase Transformations, and Reactive Phase Formation, is sponsored by the Alloy Phases Committee and

presents five articles.

In the first paper, K. Suganuma and coworkers, from Osaka University, Japan, give a comprehensive overview of high-temperature lead-free solders including their properties and phase formation. High-temperature, lead-free soldering is a key technology for electronics components and assemblies, and requires a high level of process control. The interconnections must withstand temperatures beyond 250°C for a short period and offer high reliability against thermal cycling as well as good heat dissipation. Therefore, a robust design concept is needed based on materials science in order to obtain the new technology.

Y.-C. Wu et al., from National Tsing Hua University, Taiwan, study phase ordering transformation of  $L1_0$  ordered FePt film by controlling stress and diffusion. The ordering process of a disordered FePt is controlled by a kinetic process. The paper proposes several ways to accelerate phase transformation at low temperature. An extra driving force for diffusion was provided by ion irradiation or dynamic stress; the diffusion length was diminished by using atomic-scale multilayer deposition. In addition, the novel sputtering scheme, atomic-scale multilayer deposition, can effectively promote the (001) texture of  $L1_0$  FePt grown on amorphous substrates without any underlayer

J.P. Chu from National Taiwan University of Science and Technology, Taiwan, reports an interesting phase transformation phenomenon, annealing-induced amorphization in a copper-based ( $\text{Cu}_{51}\text{Zr}_{42}\text{Al}_4\text{Ti}_3$ ) glass-forming thin film. Chu found that upon annealing in the supercooled liquid region, a fully amorphous structure is developed and this leads to a softening

**These five articles clearly indicate that “phases” are important for all kinds of materials including structural materials, magnetic materials, glasses, and electronic materials.**

in hardness and an abrupt increase (~25 times) in a decreasing trend of electrical resistivity.

V.I. Dybkov, from the Institute of Problems of Materials Science, Ukraine, studies the fundamentals of the reactive phase formation in solder joints. In the course of soldering, intermetallic layers usually occur at the solid metal–liquid solder interface, while the solid simultaneously dissolves in the solder melt. The interconnection of these two processes is considered in this paper.

I. Calliari et al., from the University of Padova, Italy, investigates the phase transformation during continuous cooling and isothermal treatments of commercial duplex stainless steels. Stainless steels, especially the grade used in

this study, suffer from lower toughness caused by secondary phase precipitation especially when these steels undergo thermal treatments. In this study the influence of thermal treatment parameters on the precipitation of these secondary phases was investigated.

A phase is a homogeneous region of matter and is the building block of materials. Different spatial arrangements of molecules lead to different phases and result in different materials properties. These five articles clearly indicate that “phases” are important for all kinds of materials including structural materials, magnetic materials, glasses, and electronic materials. It can be noticed as well that the contributors are from different regions of the world. As one of the oldest committees in TMS, the Alloy Phases Committee clearly indicates the very early awareness of the importance of “phase” in material studies by the TMS members.

The Alloy Phases Committee has also sponsored a Phase Stability, Phase Transformations, and Reactive Phase Formation in Electronic Materials symposium at the TMS Annual Meeting for eight consecutive years. In the foreword of the January 2009 *Journal of Electronic Materials* special issue, it is mentioned that the internationalized “phase” (相, そう, фаза, fase, faza) is the key word. The same globalized spirit should be shared. Although it might not necessarily get hotter and more crowded, the world of materials science has undoubtedly become more flattened, and global cooperation will be the key for the future.

Sinn-wen Chen is with the Department of Chemical Engineering, National Tsing Hua University, Hsin-chu, Taiwan and is the advisor to *JOM* from the Alloy Phases Committee of the Electronic, Magnetic, & Photonic Materials Division of TMS.

# High-Temperature Lead-Free Solders: Properties and Possibilities

Katsuaki Suganuma, Seong-Jun Kim, and Keun-Soo Kim

Several candidate alloys have been proposed as alternative solders to high-temperature high-lead solders. None of them, however, can fulfill all the requirements to replace the current high-lead solders. One should understand the properties of the candidate alloys and must carefully apply these solders for high-temperature applications step by step in order to accomplish total lead-free assembly. Three major candidate alloys can be considered as high-temperature solders: Zn-Sn, Au-Sn, and bismuth-based alloys. Each has its own superior characteristics as well as some drawbacks, but all are believed to cover most of the high-temperature applications. There have been other choices appearing as high-temperature interconnections, such as materials based on conductive adhesive technology. In addition, epoxy adhesives filled with metallic solders or nanoparticles with or without silver flakes exhibit excellent stability and can maintain stable interconnection after reflow heat treatment. This paper reviews the latest work on high-temperature lead-free alternative interconnection technologies.

## INTRODUCTION

Despite numerous studies on lead-free solders in recent years,<sup>1,2</sup> there are only a limited number of reports on the research and development for high-temperature lead-free alternative solders. High lead-bearing solders are still in use and hinder the recycling of consumer electronic products even though those circuit boards are assembled with middle-temperature-range lead-free solders such as Sn-Ag-Cu. Thus, the establishment of high-temperature lead-free solders or other interconnection technologies has been an urgent priority in the electronics industry.

### How would you...

...describe the overall significance of this paper?

High-temperature lead-free solders are needed for both the electronics and automobile industries. Unfortunately, limited choices are available as high-temperature solders. Therefore, a robust design concept is needed based on materials science in order to obtain the new technology. This paper summarizes the current status on the R&D of high-temperature solders and demonstrates three possible choices.

...describe this work to a materials science and engineering professional with no experience in your technical specialty?

High-temperature solders have been widely used in various applications not only as die-attachment solders but also, for example, as materials for assembling optical components, automobile circuit boards, and circuit modules for step soldering. To comply with environmental regulations restricting lead use, new lead-free interconnection materials have been intensively investigated. The interconnections must withstand a temperature range beyond 250°C for a short period and offer high reliability against thermal cycling as well as good heat dissipation. Intensive scientific and engineering work is required to understand the potential of these alloys and the reacted interfaces with various substrates.

...describe this work to a layperson?

High-temperature lead-free soldering is a key technology for electronics components and assemblies, and requires a high level of process control. This technology can provide value-added characteristics to the products, including excellent heat conductivity and high reliability. To benefit from the new high-temperature interconnection technologies, the potential methods should be implemented in individual products at the earliest opportunity.

High-temperature solders have been widely used in various types of applications not only as die-attach solders but also for assembling optical components, automobile circuit boards, circuit modules for step soldering, etc. Table I summarizes some of the typical high-temperature solder applications with their major requirements. Since each application has its own specific requirement, a single high-lead solder cannot cover some of the applications. For instance, much of the internal joining of passive/active components such as die attachments, flip chip joints, high-lead solders, and resistors/capacitors has used 90–95 wt.% lead. For optical uses, gold-based alloys become the main solder because those devices require flux-free. For high-temperature solder, typical requirements are:

- Melting temperature in the range of 260°C to 400°C
- Softness to maintain a joint structure by relaxation of thermal stress
- Small volume expansion at reflow treatment that does not break a package
- Sufficient workability to be thin wires or sheets
- Good electric conductivity
- Good thermal conductivity
- Good mechanical properties, especially fatigue resistance
- Air tightness not to break vacuum package
- Fluxless
- No alpha ray emission

Thus the current choices have been Pb-Sn, Pb-Ag, Sn-Sb, Au-Sn, Au-Si, and some other alloy systems. Table II summarizes the current choices as high-temperature solders including some lead-free solders with their melting temperatures. Table III summarizes

**Table I. Applications of Current High-Temperature Solders and Their Requirements**

Applications	Major Solders	Major Requirements
Die-attachment of power semiconductors and ASIC	High Pb alloys Au alloys	Reflow resistance High thermal/electric conductivity Thermal fatigue resistance
Flip-chip packages	High Pb alloys Au alloys	Reflow resistance Low $\alpha$ ray emission
Internal connection of passive components	High Pb alloys	Reflow resistance
Optical packages and modules including LEDs and laser devices	Au alloys	Fluxless Reflow resistance High thermal conductivity
Quartz device	High Pb alloys	Reflow resistance Air-tightness
Heat-resistant vehicle packages	High Pb alloys	Thermal fatigue resistance Heat exposure resistance
Module packages step soldering	High Pb alloys	Reflow resistance
Heat-sink joining	Au alloys	Thermal fatigue resistance
Leading pin joining		High thermal conductivity Airtightness

typical physical and mechanical properties of selected alloys. For lead-free solders, unfortunately, a limited number of alloying systems are available. They are Sn-Sb, gold alloys, bismuth alloys, Sn-Cu alloy or composites, and zinc alloys.

Sn-Sb alloy, of which antimony content should be less than 5 wt.% to maintain good properties, has excellent mechanical properties without any intermetallic compound,<sup>3,4</sup> but the liquidus temperature is too low, around 240°C. Too much antimony makes the alloy hard and brittle by forming an intermetallic compound.<sup>3</sup> The Sn-25Ag-10Sb alloy was designed as lead-free high-temperature solder. Nevertheless, too much silver and antimony forms massive intermetallic compounds resulting in degradation of mechanical properties.<sup>5</sup> In contrast, the tin-based alloy can achieve the needed liquidus temperature, beyond 260°C, if transition metals such as copper, nickel, and cobalt are added.

For instance, Sn-4wt.%Cu binary alloy has a liquidus temperature about 300°C. This alloy forms many of the intermetallic compounds but the liquid fraction is too high at reflow temperature. Massive intermetallic formation degrades the mechanical properties of the joints. In addition, too much liquid at reflow will destroy the package by large-volume expansion. Zn-Al has long been used as a high-temperature solder for aluminum alloys

or for structural purposes.<sup>6,7</sup> The Zn-Al binary alloy has a eutectic temperature of 380°C at 6 wt.% aluminum and this alloy does not form intermetallic compounds. This alloy exhibits a fine dendrite structure which makes the alloy very hard and brittle. It is interesting to note that the alloy is somewhat brittle

while it becomes super plastic in a specific alloy microstructure with the composition. Zn-Al, Zn-Al-Cu, or Zn-Al-Mg alloys possess desirable melting temperatures.<sup>8-11</sup> By adding a third element such as copper, magnesium, or germanium, the melting temperature decreases below 350°C. The problem for these alloys is hardness and brittleness because the addition of a third element increases the formation of massive intermetallic compounds.

The authors have compared several alloy candidates (i.e., Zn-Sn, bismuth alloys, and Au-Sn eutectic alloy) by using modeling, microstructural observation, and practical die-attach joining, which is one of the typical applications suffering from harsh environments for high-temperature solders. The indispensable requirement for the high-temperature solder selection was set to be little or no intermetallic formation for the softness and ductility of the alloy. Through experiments, however, Au-Sn eutectic alloy, which contains much intermetallic compound, has been proven to be a reliable high-temperature solder.

**Table II. Typical High-Temperature Solders\***

Alloys	Composition (wt.%)	Solidus Temperature (°C)	Liquidus Temperature (°C)
High-Pb Alloy System			
Pb-Sn	Sn-65Pb	183	248
	Sn-70Pb	183	258
	Sn-80Pb	183	279
	Sn-90Pb	268	301
	Sn-95Pb	300	314
	Sn-98Pb	316	322
Pb-Ag	Pb-2.5Ag	304	304
	Pb-1.5Ag-1Sn	309	309
Sn-Sb Alloy System			
Sn-Sb	Sn-5Sb	235	240
	Sn-25Ag-10Sb (J-alloy)	228	395
Au Alloy System			
Au-Sn	Au-20Sn	280 (eutectic)	
Au-Si	Au-3.15Si	363 (eutectic)	
Au-Ge	Au-12Ge	356 (eutectic)	
Bi Alloy System			
Bi-Ag	Bi-2.5Ag	263 (eutectic)	
	Bi-11Ag	263	360
Cu Alloy System			
Cu-Sn	Sn-(1-4)Cu	227	~400
	Sn-Cu particles composites	~230	
Zn Alloy System			
Zn-Al	Zn-(4-6)Al(-Ga, Ge, Mg, Cu)	300-340	
Zn-Sn	Zn-(10-30)Sn	199	360

\*Courtesy of Senju Metals, Co., Ltd.

Table III. Comparison of Selected Properties of High-Temperature Solders

Alloys	Thermal Conductivity (W/m-K)	Thermal Expansion Coefficient (ppm)	0.2% Proof Stress (MPa)		
			23°C	100°C	150°C
Au-20Sn	57	16	275	217	165
Au-12Ge	44	13	185	177	170
Au-3Si	27	12	220	207	195
Sn-5Sb	48	23	~40	—	—
Pb-5Sn	23	30	14	10	5
Zn-(10-30)Sn	100-110	30	~43	—	—
Bi-11Ag	~9	—	~33	—	—

### DESIGN OF LIQUID FRACTION FOR REFLOW RESISTANCE

When alloyed, zinc is known to be a good choice as a high-temperature solder. Zinc itself has a melting temperature of 419.5°C. By alloying such materials as aluminum and tin, the melting temperature of zinc can be lowered to a suitable range of 300°C to 400°C. The Zn-Sn alloy has a simple binary eutectic phase diagram without any intermetallic compound in the whole range of composition and is believed to be one of the best choices. However, one of the concerns for this alloy as a high-temperature solder is the liquid formation at its eutectic temperature of 199°C, which is the reason eutectic Sn-Zn has been used as a low-temperature solder. A simple idea is to avoid the destructive expansion of the alloy due to liquid formation at reflow temperature around 250°C.<sup>12</sup> When the solid fraction is less than a certain limit even beyond solidus temperature of an alloy, the alloy solid can maintain its shape. This liquid volume limit is believed to be around 30%. One can easily calculate the volume fraction of liquid at a given temperature. Figure 1 shows the solid fraction of Zn-Sn and Zn-In alloys as a function of temperature. It is found that the volume fraction of Zn-Sn liquid can be less than 30% when tin content is less than 30%.

Differential scanning calorimetry (DSC) analysis was carried out to confirm the fundamental melting/solidification reactions of the alloys. Figure 2a and b shows the typical DSC curves of Zn-Sn and Zn-In alloys on heating and cooling, respectively. These hypereutectic alloys show two endothermic

peaks; one appears approximately at 200°C for Zn-Sn alloys and at 145°C for Zn-In alloys and the other varies from 365°C to 383°C. Each endothermic peak corresponds well to the melting properties of hypereutectic alloys. The lower and higher temperature peaks indicate the eutectic and melting temperature, respectively. None of the

Zn-Sn and Zn-In alloys shows any other significant reaction peak. The results of DSC coincide well with the binary phase diagram of alloys.

The typical microstructures of zinc-based alloys are shown in Figure 3. In the case of Zn-Sn alloys, the dark and bright color phases are the primary  $\alpha$ -Zn and eutectic  $\beta$ -Sn/ $\alpha$ -Zn phases, respectively. The primary  $\alpha$ -Zn phases were surrounded with eutectic  $\beta$ -Sn/ $\alpha$ -Zn phases, in which fine eutectic  $\alpha$ -Zn platelets disperse in a  $\beta$ -Sn matrix. A fraction of the primary  $\alpha$ -Zn phase of the Zn-Sn alloys increased while  $\beta$ -Sn/ $\alpha$ -Zn eutectic phase decreased with decreasing tin content. This is expected from the phase diagram, in which the eutectic composition is Sn-8.8wt.%Zn. After several tests, Zn-Sn solders were found to be more stable as high-temperature solder than Zn-In alloy.

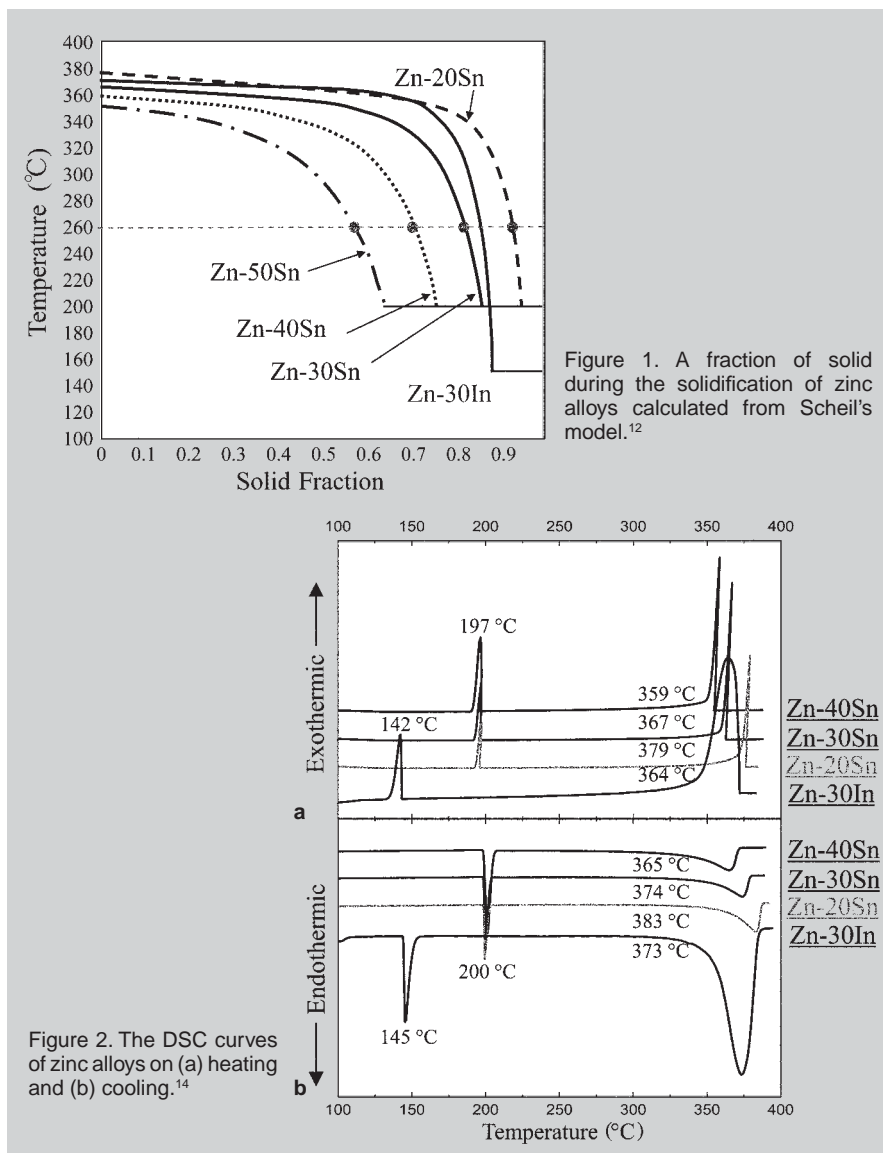


Figure 2. The DSC curves of zinc alloys on (a) heating and (b) cooling.<sup>14</sup>

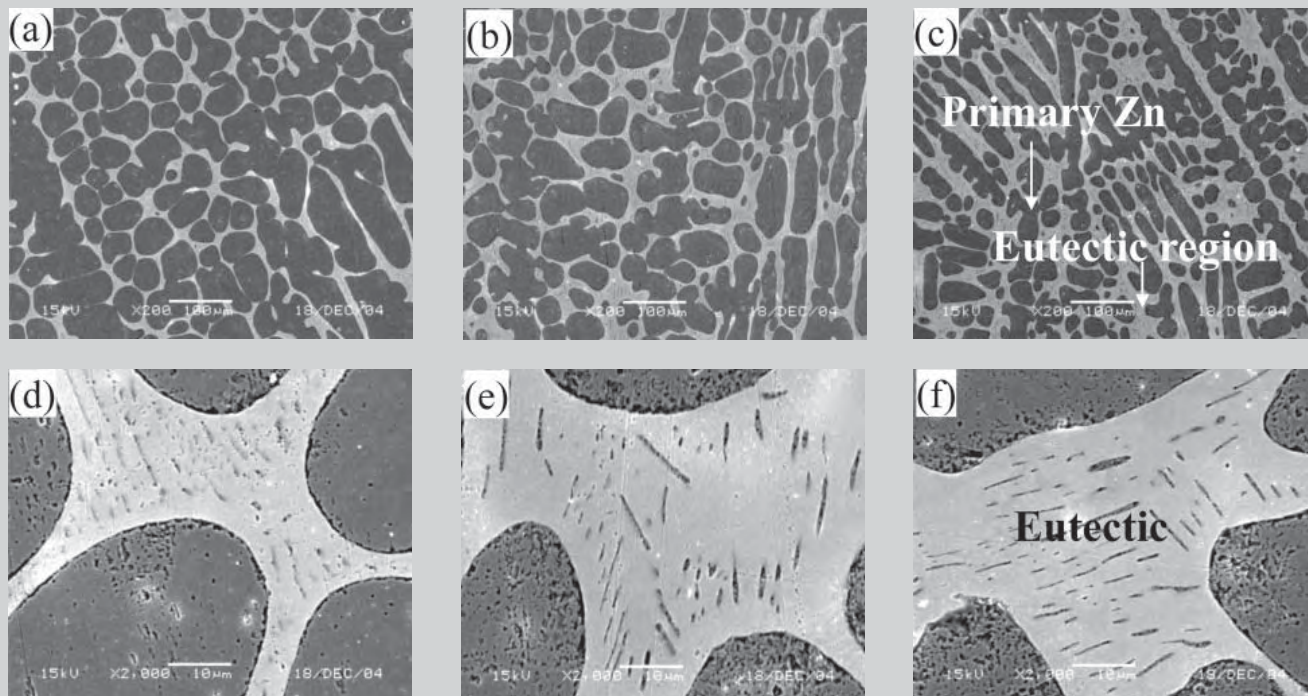


Figure 3. The microstructure of as-received alloys at a cooling rate of 3°C/min.; (a) and (d) Zn-20Sn, (b) and (e) Zn-30Sn, and (c) and (f) Zn-40Sn.<sup>14</sup>

## TENSILE PROPERTIES AND THERMAL CONDUCTIVITY OF Zn-Sn ALLOYS

Since the Zn-Sn alloy system does not form any intermetallic compound, the ductility of the alloys becomes a great advantage. Figure 4 shows the tensile properties of Zn-Sn alloys as a function of tin content. With increasing tin content, the ultimate tensile strength (UTS) and 0.2% proof stress slightly decrease while the elongation increases, which can be attributed to the increase of soft tin volume fraction. It is apparent that Zn-Sn alloys possess excellent ductility at room temperature. Figure 4 also shows the Zn-30Sn sheet formed by cold-rolling the alloy ingot.

Figure 5 compares tensile properties of the Zn-Sn alloys and Bi-Ag alloys. Bi-Ag alloys are high-temperature lead-free solder candidates. The UTS and 0.2% proof stress of the Zn-Sn alloys are relatively higher as compared with those of Bi-Ag alloys. On the other hand, the Bi-Ag alloys exhibit quite small elongation, which is one of the fatal drawbacks of the bismuth-based alloys.

The conductivity of Zn-Sn alloys was compared with the other high-temperature solders, which is shown in

Figure 6 and Table IV. The thermal conductivity of the Zn-Sn alloys exceeds 100 W/m·K, while that of Pb-5Sn and Au-20Sn is 36 W/m·K and 59 W/m·K, respectively. Bismuth-based alloys are known to have the worst thermal conductivity below 10 W/m·K. Thus, the Zn-Sn alloys have a great advantage as die-attachment solder that must possess excellent mechanical and thermal properties.<sup>13,14</sup>

## SI DIE ATTACHMENT

Figure 7 shows one of the examples of silicon die attachment on a direct bonded copper (DBC) substrate. The

face of the silicon die was coated with Au/Ag/Ni thin layers. Figure 8 shows the microstructure of the joint region of the silicon die attachment. On both sides, intermetallic compound layers are clearly observed. They were identified as  $\text{CuZn}_5$  and  $\text{Cu}_5\text{Zn}_8$  on the copper substrate side and  $\text{AgAuZn}_2$  on the silicon die side. The thickness of the intermetallic compound layers can be controlled by adjusting soldering conditions such as temperature and time. It was found that soldering temperature at 360°C to 380°C and a time of 60 s to 300 s are the best conditions for this system. Under these conditions, the

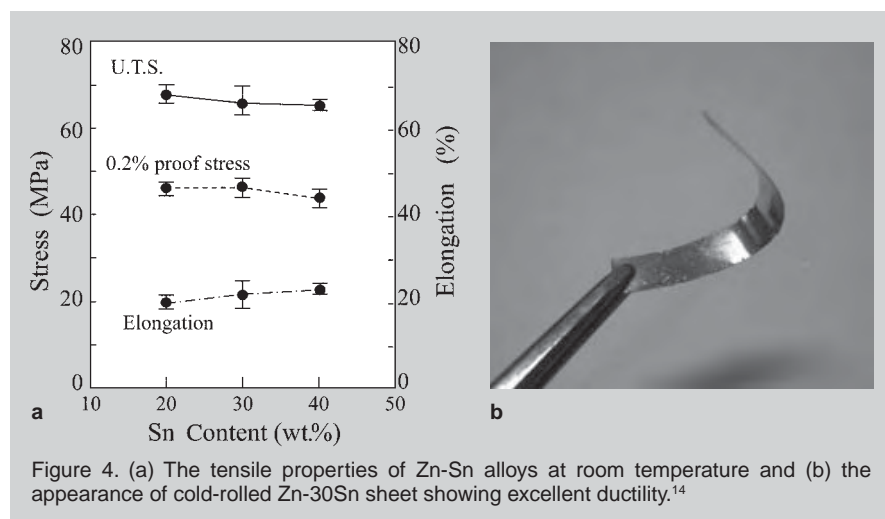


Figure 4. (a) The tensile properties of Zn-Sn alloys at room temperature and (b) the appearance of cold-rolled Zn-30Sn sheet showing excellent ductility.<sup>14</sup>

shear strength of the die exceeded that of Pb-5Sn solder.

In addition, the optimization of the metallization of both faces (i.e., a silicon die and a DBC substrate) can increase the integrity of the joint structure. In order to suppress the formation of a thick intermetallic interlayer, the authors employed a ceramic coating of TiN, which is known to be a protective barrier layer for metals.<sup>16</sup> In addition ceramics such as TiN and TiC are known to possess good bonding nature with metals and electric conductivity depending on their stoichiometry. Figure 9 shows the microstructure of the soldered Si/Zn-30Sn interface with an x-ray transmission image of the silicon die attachment. Even though several voids are found in the solder layer, these are equivalent to the conventional

high-lead solders. Excellent wetting and intimate contact can be achieved.

### STABILITY OF Zn-Sn

One of the concerns regarding the use of Zn-Sn in high-temperature solders is its stability during reflow treatment for board assembly with Sn-Ag-Cu. The temperature can reach 260°C and the die-attached components can be kept at this temperature for more than 10 min., especially for multiple reflows. To check the stability of Zn-Sn solders, the in-situ observation of the die-attached silicon on a copper substrate on multiple reflow treatment was conducted and no movement of the dies was confirmed. Figure 10 shows the shear strength of the die-attached silicon as a function of tin content with or without three reflow treatments at 260°C. The

silicon die did not move at all and no significant strength drop was found. Figure 10 also shows the transmission x-ray images comparing the silicon die and the void location and size before and after three reflows. As clearly seen from the x-ray transmission images, the silicon die is stable and no change of void size or location is confirmed.

From the Scheil's estimation shown in Figure 1, the liquid fraction at 260°C is less than 25 vol.%. No movement of liquid in the semisolid Zn-Sn alloy is expected and the solid part, 75% of the solder layer, can sustain the die-attachment structure in the multiple reflow treatment.

The second concern with the Zn-Sn alloy system is oxidation resistance in moisture. It is well known that the Sn-Zn eutectic alloy can be easily corroded in high humidity to form ZnO along grain boundaries of matrix.<sup>18</sup> Zn-Sn alloys were exposed to 85°C/85%RH for up to 1,000 h. Figure 11 shows the cross-section image of the Zn-Sn alloy near the free surface after exposure. An oxidized layer a few micrometers thick is observed from the free surface. Thus, Zn-Sn proved to be stable even in severe humidity.

Fatigue resistance in thermal cycling is one of the key factors for the die attachment structure, especially for power semiconductors. In the present work, the only silicon die attachment joints with Zn-30Sn, Au-20Sn, and Pb-5Sn solders were tested in the temperature range of -40°C to 125°C up to 2,000 cycles, which are harsh conditions for electronics equipment. Without any barrier coating, the joint with Au-20Sn maintained 90% of the initial shear strength up to 2,000 cycles. In contrast, the other two joints degraded after 500 cycles. The degradation mechanisms of the two joints are, however, quite different from each other. The joint with Pb-5Sn lost its strength due to severe cracking inside the solder layer while that with Zn-30Sn formed cracking inside the intermetallic layer on the copper substrate side. This difference indicates that the thermal cycle stability of Zn-Sn solder joints can be improved by inserting a suitable barrier layer while the Pb-5Sn solder joint cannot. Figure 12 shows the results of

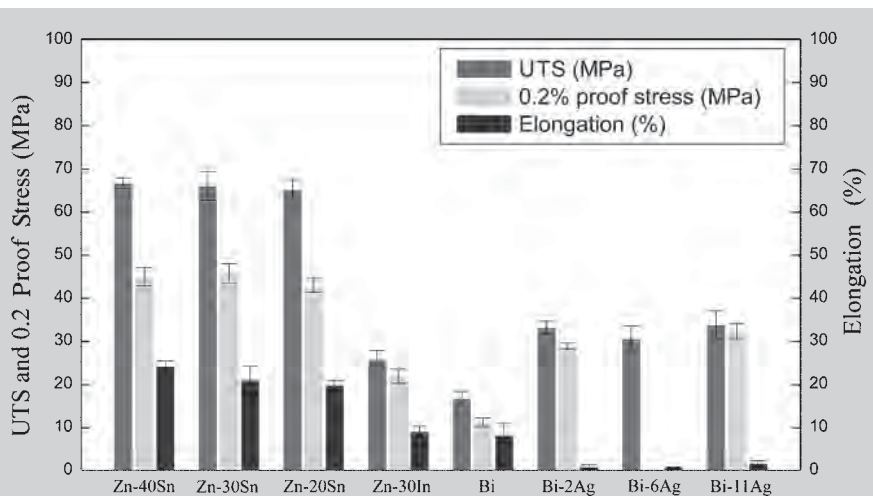


Figure 5. A comparison of tensile properties of selected high-temperature lead-free solders.<sup>14</sup>

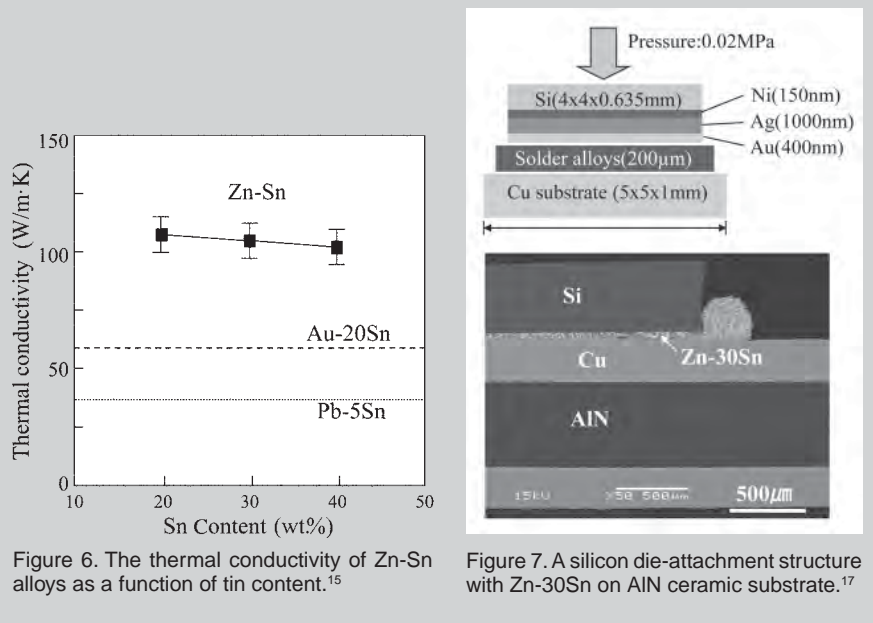


Figure 6. The thermal conductivity of Zn-Sn alloys as a function of tin content.<sup>15</sup>

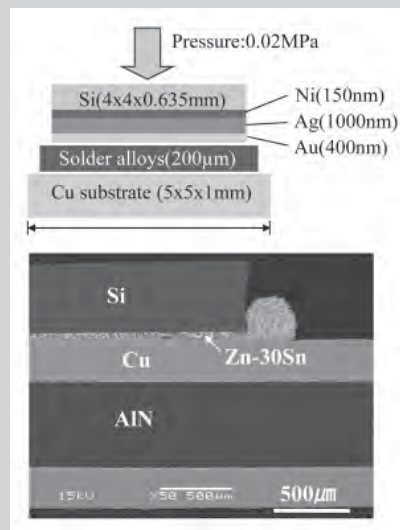


Figure 7. A silicon die-attachment structure with Zn-30Sn on AlN ceramic substrate.<sup>17</sup>



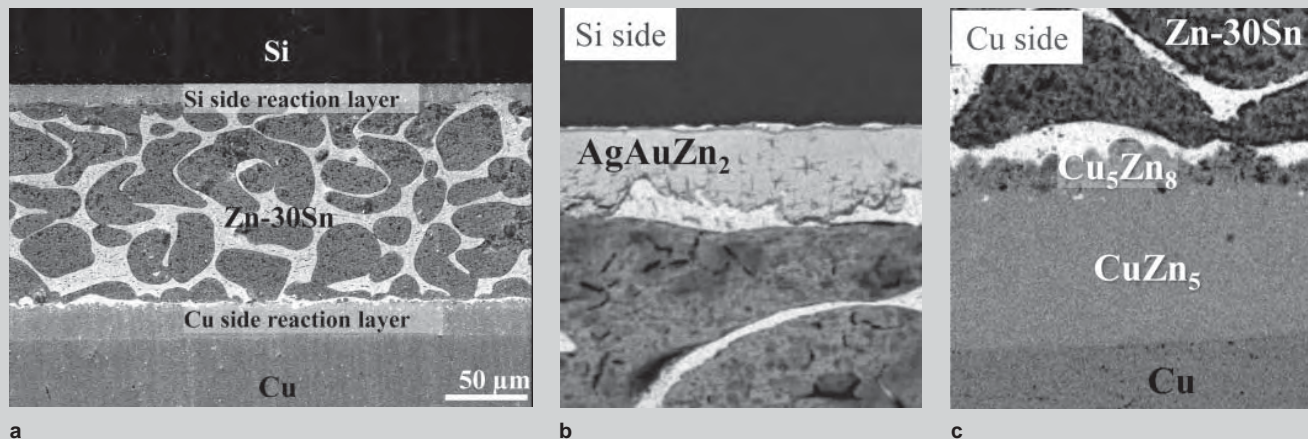


Figure 8. (a) The interface microstructure of a silicon die attachment on a copper substrate with Zn-30Sn soldered at 360°C for 60 s. (b) The silicon side and (c) the copper side.<sup>17</sup>

shear tests for the three joints with Zn-30Sn, Au-20Sn, and Pb-5Sn solders with TiN barrier layers for both sides of the solder layer. The joint strength of Pb-5Sn solder decreased as expected. No improvement was obtained with the barrier coating for this solder. In contrast, the joint with Zn-30Sn solder maintained good strength up to 2,000 cycles. Figure 13 shows the joint microstructure after 2,000 cycles. Severe cracking in the Pb-5Sn layer was found. On the other hand, the joints with Zn-30Sn and with Au-20Sn exhibit neither cracking nor void and grain growth is not apparent. Thus, Au-20Sn alloy is one of the best choices as high-temperature solder without any barrier coating on the substrate. With a suitable barrier coating such as TiN, Zn-Sn becomes the best selection because of its stability and affordability.

### IMPROVING Bi ALLOYS BY ADDING Sn AND Cu

Though bismuth alloys have some drawbacks such as low electric/thermal conductivity and brittleness, they seem to be useful because of their desirable melting temperature and low cost as high-temperature solders.<sup>3,5,20,21</sup> As shown in Figure 14, pure bismuth can exhibit some elongation at room temperature when it deforms at slow speeds. Bismuth and its alloys become brittle only at fast deformation speeds.<sup>5</sup> One of the key properties to be improved is the poor wetting of bismuth on substrates such as copper.<sup>3</sup> It has been reported that alloying tin with bismuth can improve wetting properties.<sup>19</sup>

Figure 14 shows the spreading ratio change as a function of tin content of a bismuth alloy at 290°C. With increasing tin content, up to 3 wt.%, the spreading

gradually increases and, beyond this content, saturates. This improvement of wetting can be attributed to the reaction between tin and the copper substrate.

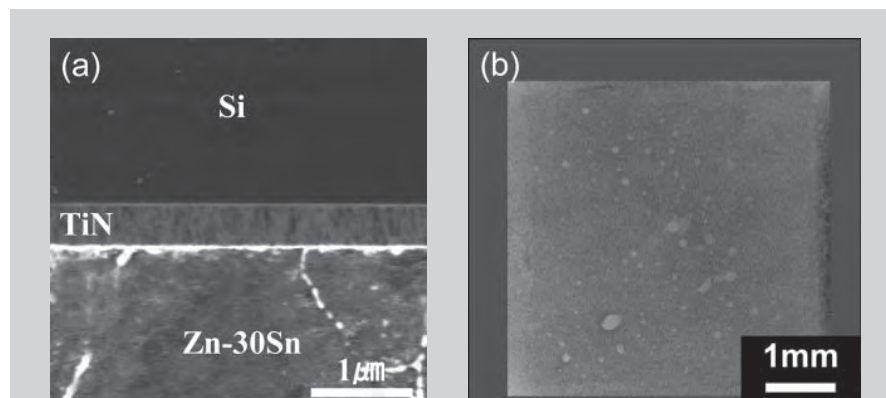


Figure 9. The interface microstructure of a silicon die attachment with TiN barrier coating on the silicon die with Zn-30Sn soldered at 390°C for 60 s.<sup>17</sup> (a) An SIM image of the interface and (b) x-ray transmission image.

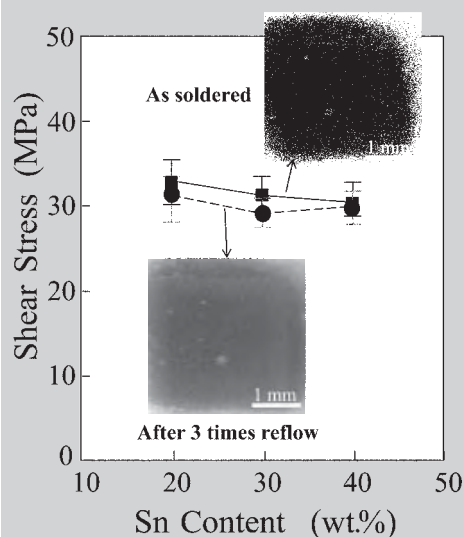


Figure 10. Shear strength as a function of tin content and x-ray transmission images of a silicon die attachment before and after three reflows at 260°C.<sup>17</sup>

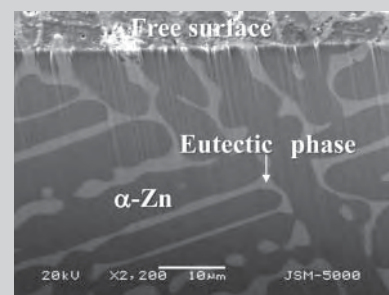


Figure 11. An SEM image of the microstructure of Zn-20Sn near the free surface after exposure at 85°C/85%RH for 1,000 h.<sup>14</sup>

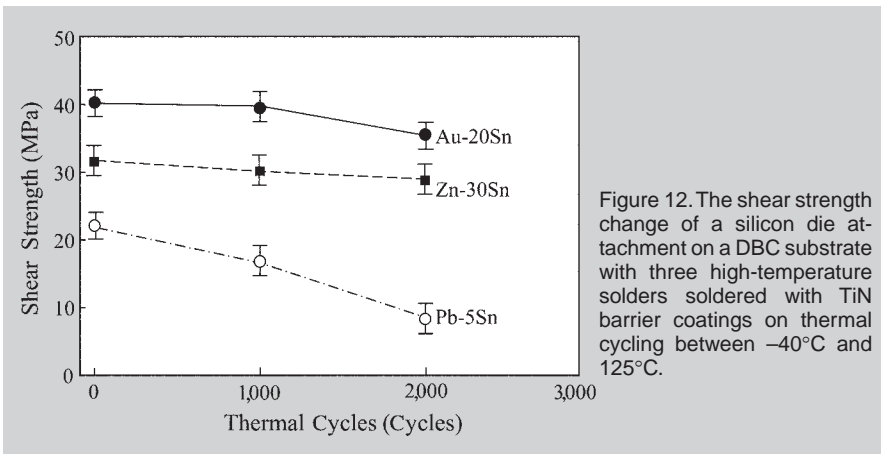


Figure 12. The shear strength change of a silicon die attachment on a DBC substrate with three high-temperature solders soldered with TiN barrier coatings on thermal cycling between  $-40^{\circ}\text{C}$  and  $125^{\circ}\text{C}$ .

Figure 15 shows the x-ray transmission image of Bi-2Sn-3Cu balls on an FR4 circuit board with metallization of Au/Ni plating. Spherical balls were obtained with good wetting on the metallization even though several voids were found inside the balls. When copper is added, tin can be trapped after heat treatment at  $290^{\circ}\text{C}$ . It was confirmed by DSC analysis that there is no liquid phase formation at around  $139^{\circ}\text{C}$ , the Bi-Sn binary eutectic temperature.

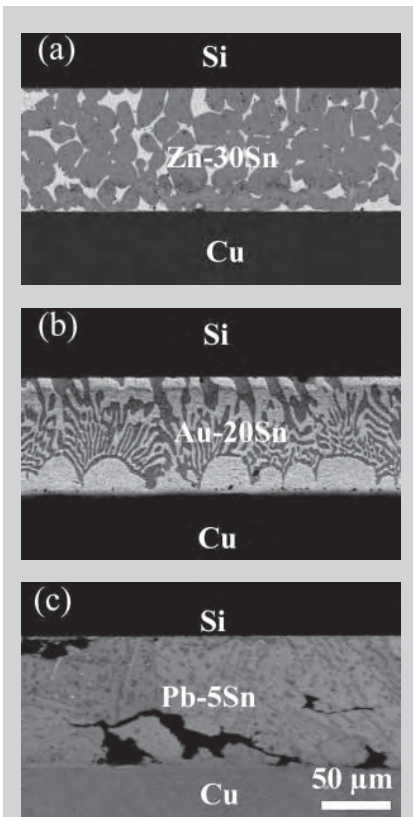


Figure 13. The microstructure of the joint layer of a silicon die attachment on a DBC substrate with three high-temperature solders soldered with TiN barrier coating after 2,000 cycles between  $-40^{\circ}\text{C}$  and  $125^{\circ}\text{C}$ .

The addition of copper to bismuth also improves the embrittlement of a copper substrate caused by grain boundary erosion.

On the other hand, bismuth reacts with a nickel substrate to form thick intermetallic compound layers of  $\text{NiBi}_3$  and  $\text{NiBi}$ .<sup>20</sup> Excess reaction induces microcracking inside the reaction layer resulting in the degradation of interface strength. Therefore, one needs to employ a suitable reaction barrier layer for this die-attaching system.

### CONDUCTIVE ADHESIVE TECHNOLOGY

Conductive adhesives such as epoxy with silver flake filling are another route to high-temperature lead-free conversion.<sup>22,23</sup> The latest R&D activity has been focused on how to secure the metallic connection among metal fillers and the interface between a substrate and fillers. The simple combination of tin-based alloy and epoxy also forms a reflow-resistant interconnection. Figure 16 shows a chip resistor mounted on an FR4 circuit board with Sn-59Bi particle-filled epoxy conductive adhesive.<sup>24</sup> Even though the melting temperature of Sn-59Bi is as low as  $139^{\circ}\text{C}$ , this joint structure can be maintained through several reflow treatments. In addition, this joint structure possesses excellent thermal cycle fatigue resistance. The initial high joint strength can be maintained during thermal cycling between  $-40^{\circ}\text{C}$  and  $125^{\circ}\text{C}$  even after 1,000 cycles.

The other approaches such as incorporating so-called transient liquid phase particles or nanoparticles into the epoxy matrix also have potential as high-temperature solder alternatives.<sup>4,25</sup>

### CONCLUSION

The selection of high-temperature lead-free solder remains a challenge. Through a phase diagram survey of all possible alloying systems, no drop-in replacement can be found. Thus, one should modify the traditional guideline for high-temperature solders and develop a new concept with scientific support. In this work, the simple design concept of a high-temperature lead-free solder alloy without any intermetallic compound was first demonstrated and, based on the designing, the potentials of Zn-xSn ( $x = 40$  wt.%, 30 wt.%, and 20 wt.%) alloys were evaluated as new high-temperature lead-free solders from various aspects as compared with other candidates. The research found that the Zn-Sn, Au-Sn, and bismuth alloys are the three best choices. Of the three, Zn-Sn alloys exhibit excellent mechanical properties such as high tensile strength and superior elongation with superior thermal conductivity and excellent stability in various environ-

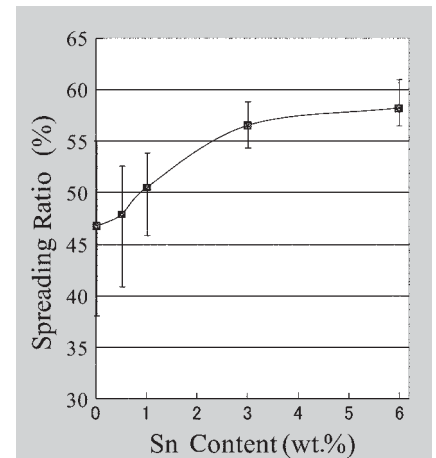


Figure 14. The change in spreading ratio of bismuth on a copper substrate at  $290^{\circ}\text{C}$  for 30 s as a function of tin content.<sup>19</sup>

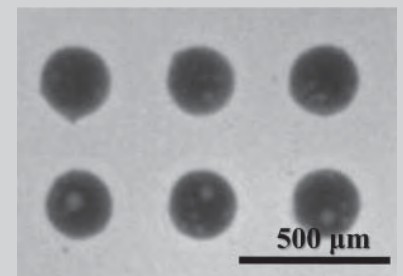


Figure 15. An x-ray transmission image of Bi-2Sn-3Cu balls on an FR4 circuit board with Au/Ni metallization reflowed at  $290^{\circ}\text{C}$  for 30 s.<sup>19</sup>

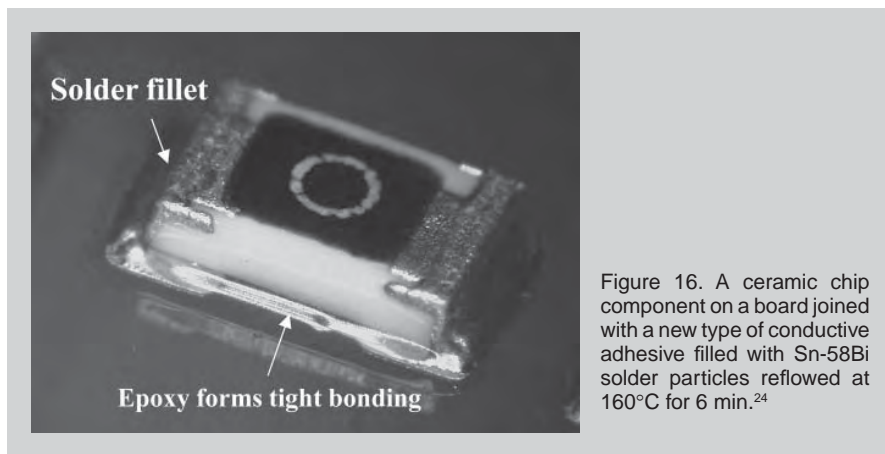


Figure 16. A ceramic chip component on a board joined with a new type of conductive adhesive filled with Sn-58Bi solder particles reflowed at 160°C for 6 min.<sup>24</sup>

ments.

It is somewhat surprising that Au-20Sn alloy exhibited superior thermal fatigue resistance even though this alloy consists of massive intermetallic compounds. Further examination is needed, such as an investigation of how large an area can be soldered with this alloy without serious degradation caused by the hardness of the solder. Intensive work has been reported on the interface microstructures of this alloy with various substrates.<sup>26-29</sup>

In addition, conductive adhesive technology has stepped into a new stage by forming metallic interconnections among metallic particle fillers inside epoxy matrix and interfaces. Further work is required to evaluate the reliability of these alloys and adhesives in the form of practical commercial products.

## ACKNOWLEDGEMENTS

*This research was supported in part by a grant from the NEDO project R&D of Alternatives to High Temperature High Lead Solder.*


## References

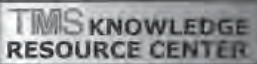
1. K. Suganuma, *Curr. Opin. Solid State Mater. Sci.*, 5 (1) (2001), pp. 55-64.
2. K.N. Tu, A.M. Gusak, and M. Li, *J. Appl. Phys.*, 93 (2003), pp. 1335-1352.
3. J.H. Kim, S.W. Jeong, and H.M. Lee, *Mater. Trans.*, 43 (2002), pp. 1873-1878.
4. S.F. Corbin, *J. Electron. Mater.*, 34 (2005), pp. 1016-1025.
5. M. Rettenmayr, P. Lambracht, and B. Kempf, *Adv. Engineer. Mater.*, 7 (2005), pp. 965-969.
6. E. Gervais, R.J. Barnhurst, and C.A. Loong, *J. Metals*, 37 (11) (1985), pp. 43-47.
7. F. Cay and C. Kurnaz, *Mater. Design*, 26 (2005), pp. 479-485.
8. M. Rettenmayr et al., *J. Electron. Mater.*, 31 (2002), pp. 278-285.
9. N. Kang et al., *J. Alloys Comp.*, (2008), doi:10.1016/j.jallcom.2007.12.048.

10. T. Shimuzu et al., *J. Electron. Mater.*, 28 (1999), pp. 1172-1175.
11. S.J. Kim et al., *Mater. Trans.*, 49 (2008), pp. 1531-1536.
12. K. Suganuma, J.-E. Lee, and K.-S. Kim, "Zn-Sn and Zn-In High Temperature Lead-Free Solders" (Presentation at the 2007 MRS Spring Meeting Symposium E: Pb-Free and RoHS-Compliant Materials and Processes for Microelectronics, San Francisco, April 11-12, 2007).
13. J.E. Lee et al., *Mater. Trans.*, 46 (2005), pp. 2413-2418.
14. J.E. Lee et al., *Mater. Trans.*, 48 (2007), pp. 584-593.
15. S.J. Kim et al., *J. Electron. Mater.* (2008), doi: 10.1007/s11664-008-0550-0.
16. S. Motojima and H. Mizutani, *J. Mater. Sci.*, 23 (1988), pp. 3435-3439.

17. S.-J. Kim et al., "Interfacial Reactions of Die Attached AlN-DBC Module Using Zn-Sn High Temperature Solders" (Presentation at the TMS 2008 Annual Meeting & Exhibition, New Orleans, March 10-14, 2008).
18. K. Suganuma et al., *J. Mater. Res.*, 13 (1998), pp. 2859-2865.
19. M. Ueshima, private communication (March 24, 2008).
20. J.M. Song, H.Y. Chuang, and Z.M. Wu, *J. Electron. Mater.*, 35 (2006), pp. 1041-1048.
21. K. Suganuma, *Polymer and Adhesives in Microelectronics and Photonics* (Piscataway, NJ: IEEE, 2007), pp. 30-35.
22. J.N. Lalena, N.F. Dean, and M.W. Weiser, *J. Electron. Mater.*, 31 (2002), pp. 1244-1249.
23. Yi Li and C.P. Wong, *Mater. Sci. Engineer. R.*, 51 (1-3) (2006), pp. 1-35.
24. T. Tashiro, private communication (March 24, 2008).
25. M. Vuorela et al, *Proc. 4th International Conference on Adhesive Joining and Coating Technology in Electronics Manufacturing 2000* (Piscataway, NJ: IEEE, 2000), pp. 147-152.
26. H.G. Song, J.W. Morris, and M.T. McCormack, *J. Electron. Mater.*, 29 (2000), pp. 1038-1046.
27. J.Y. Tsai et al., *J. Electron. Mater.*, 35 (1) (2006), pp. 65-71.
28. J.W. Yoon et al., *J. Mater. Res.*, 22 (10) (2007), pp. 2817-2824.
29. J.W. Yoon, H.S. Chun, and S.B. Jung, *J. Mater. Res.*, 22 (5) (2007), pp. 1219-1229.

Katsuki Suganuma, Seong-Jun Kim, and Keun-Soo Kim are with the Institute of Scientific and Industrial Research, Osaka University Mihogaoka 8-1, Ibaraki, Osaka 567-0047, Japan. Dr. Suganuma can be reached at [suganuma@sanken.osaka-u.ac.jp](mailto:suganuma@sanken.osaka-u.ac.jp).





Your Materials Books  
and More e-Store!  
<http://knowledge.tms.org>

**Visit the Knowledge Resource Center to reserve your copy today!**

**Aluminum Alloys:  
Fabrication, Characterization and Applications II**

**Aluminum Alloys:**  
Fabrication, Characterization  
and Applications II

Edited by:  
Wefmie Yin  
Subodh K. Das  
Zhengdong Long

This book covers all aspects of the physical and mechanical metallurgy of aluminum alloys. It addresses fundamental and applied research as well as product development, testing and implementation of aluminum foil, sheet, plate, extrusions, forgings, and composites for end applications including transportation (automotive, aerospace and marine), packaging and other key product segments. The symposium consists of invited as well as contributed papers.

**Topics include the following and related areas:**

- Products Fabrication and Applications
- Alloy Development
- Process Innovation
- Microstructure Evolution
- Mechanical Behavior
- Failure Analysis

**Member price \$69; Student price \$54; List price \$99**

**To order these or related publications, contact TMS:**  
E-mail [publications@tms.org](mailto:publications@tms.org) • Phone (724) 776-9000, ext. 256 • Fax (724) 776-3770

# Annealing-Induced Amorphization in a Glass-Forming Thin Film

J.P. Chu

Previous studies of the glass-forming zirconium- and iron-based multicomponent films reported direct experimental evidence of the annealing-induced solid-state amorphization (SSA) in the supercooled liquid region ( $\Delta T$ ). In this study, a copper-based ( $\text{Cu}_{51}\text{Zr}_{42}\text{Al}_4\text{Ti}_3$ ) film shows similar SSA and thus variations in electrical resistivity and hardness. Based on transmission electron microscopy results, the as-deposited film consists of the amorphous matrix dispersed with nanocrystallites. Upon annealing within  $\Delta T$ , extensive amorphization of the film occurs. The full amorphization in  $\Delta T$  leads to a significant increase in electrical resistivity when compared with the as-deposited condition. It is thus confirmed that annealing induces formation of various nano-scale and amorphous structures with amorphization taking place within  $\Delta T$ .

## INTRODUCTION

In the solid state, amorphization could be achieved mainly by mechanical alloying,<sup>1</sup> solid-state reaction or amorphization (SSA),<sup>2</sup> high pressure,<sup>3</sup> and shock loading<sup>4</sup> techniques. In all of these solid-state techniques except for SSA, considerable energy is generally required for ultimate amorphization. While the thermal annealing results in crystallization of the amorphous films prepared by evaporation or sputtering,<sup>5,6</sup> the formation of the amorphous phase in the SSA takes place through annealing-induced diffusive reactions in certain multilayer combinations of crystalline elemental metals, as first demonstrated by R.B. Schwarz and W.L. Johnson.<sup>2</sup> However, the extent of amorphization in this case is confined to the reacted interfacial thickness, typically a few nanometers.<sup>2,7</sup> Prior studies reported the extensive amorphization up to several or

### How would you...

...describe the overall significance of this paper?

This work presents experimental evidence that the controllable amorphization and nanocrystallization could serve as a precursor for exciting new nanomaterials. Upon annealing in the supercooled liquid region, a fully amorphous structure is developed and this leads to a softening in hardness and an abrupt increase (~25 times) in a decreasing trend of the electrical resistivity. The novel finding is that one can tailor-make film properties by modulating the annealing-induced amorphization.

...describe this work to a materials science and engineering professional with no experience in your technical specialty?

While thermal annealing results in crystallization of the amorphous films prepared by evaporation or sputtering, the glass-forming film in this study becomes fully amorphous when annealed at a certain temperature range in the supercooled liquid region. Annealing of sputtered metastable glass-forming film is found to cause the formation of various nano-scale and amorphous structures, thus resulting in changes of electrical and mechanical properties.

...describe this work to a layperson?

In the solid state, amorphization could be achieved mainly by mechanical alloying, solid-state reaction or amorphization (SSA), high pressure, and shock loading techniques. In all of these solid-state techniques except SSA, considerable energy is generally required for ultimate amorphization. In this study, the large-scale amorphization throughout the film offers advantages for easy property/microstructure characterizations.

few tens of micrometers during annealing of the sputtered glass-forming multicomponent films for the first time.<sup>8,9</sup> The large-scale amorphization throughout the film offers advantages for easy property/microstructure characterizations for potential applications. In this study, annealing of sputtered metastable glass-forming film is found to cause the formation of various nano-scale and amorphous structures, thus resulting in changes of electrical and mechanical properties. A copper-based quaternary amorphous alloy is chosen for this study because it is one of the principal materials with good glass-forming ability among a number of alloy components investigated for bulk metallic glasses (BMG).<sup>5,10,11</sup> Groups of BMG with low critical cooling rates and relatively high thermal stability have attracted attention due to their many excellent properties.<sup>5,10</sup> The recent development of BMG also makes the thin film processing and application possible because the thin film was not readily achieved in the past when metallic glasses were often available only in powder and ribbon forms. For example, the applications of thin glass-forming films as conical spring linear and micro-lens actuators in microelectromechanical systems (MEMS) have been demonstrated.<sup>12</sup> Furthermore, a sub-micrometer thick zirconium-based glass-forming coating has been found to improve the fatigue life by at least 30 times on a stainless-steel substrate.<sup>13</sup>

See the sidebar for experimental procedures.

## RESULTS

The composition (in atomic percent, at.%) of the thin film studied is determined to be  $51.3 \pm 0.1$  for Cu,  $41.5 \pm 0.2$  for Zr,  $4.3 \pm 0.1$  for Al, and  $2.9 \pm 0.3$  for Ti. The film is hereby designated as

**Table I. Thermal Analysis Results of the  $\text{Cu}_{51}\text{Zr}_{42}\text{Al}_4\text{Ti}_3$  Thin Film Prepared in this Study and  $\text{Cu}_{50}\text{Zr}_{42.5}\text{Al}_5\text{Ti}_{2.5}$  Bulk Metallic Glass<sup>9</sup>**

Alloy System	$T_g$ (K)	$T_x$ (K)	$\Delta T$ (K)	$\Delta H$ (J/g)
$\text{Cu}_{51}\text{Zr}_{42}\text{Al}_4\text{Ti}_3$ thin film	725	775	50	58
$\text{Cu}_{50}\text{Zr}_{42.5}\text{Al}_5\text{Ti}_{2.5}$ BMG <sup>9</sup>	700	764	64	55

$\text{Cu}_{51}\text{Zr}_{42}\text{Al}_4\text{Ti}_3$ . Table I shows differential scanning calorimeter (DSC) thermal analysis result of the  $\text{Cu}_{51}\text{Zr}_{42}\text{Al}_4\text{Ti}_3$  thin film, along with that of the  $\text{Cu}_{50}\text{Zr}_{42.5}\text{Al}_5\text{Ti}_{2.5}$  BMG<sup>9</sup> for comparison. The glass transition temperature ( $T_g$ ) increases from 700 K for BMG to 725 K for the thin film. In addition, the crystallization temperature ( $T_x$ ) increases from 764 K for the BMG to 775 K for the thin film. Therefore, the supercooled liquid region (SCLR,  $\Delta T$ ), defined as the difference between  $T_x$  and  $T_g$ , changes from 64 K to 50 K. Discrepancies in the thermal properties may be attributed to the differences in composition and sample preparation method. The exothermic heats during crystallization in the thin film and BMG were about the same, 55 J/g for the BMG and 58 J/g for the thin film.

To evaluate thermal behavior, the film was annealed in rapid-thermal annealing (RTA) at various temperatures up to 923 K. The annealing temperatures were selected based on DSC results. Figure 1 shows x-ray diffractometry (XRD) patterns obtained from the film in as-deposited and annealed conditions. The patterns indicate that the film in the as-deposited condition is likely of either amorphous structure or nanostructures. The nanostructures are also possible because they are beyond the detection limit of XRD. The films remain amorphous or nanocrystals with no detectable crystalline peaks up to 740 K. When annealing temperature reaches 755 K, a crystalline peak at  $\sim 42^\circ$  of  $2\theta$  is found, which is identified as orthorhombic  $\text{Cu}_{10}\text{Zr}_7$ . Yet, this peak disappears at 775 K. The disappearance of the crystalline peak at 775 K indicates the possible amorphization. Annealing at 800 K and above yields full crystallization of film. Crystalline Bragg peaks evolve at 800 K and become evident as the annealing temperature increases. Further transmission electron microscopy (TEM) confirmations are required in order to understand the structure evolution during the annealing process.

Figure 2 shows DSC thermal scan and electrical resistivity of the film in as-deposited and annealed conditions. Based on the DSC scan data in Figure 2a, the film exhibits a distinct glass transition, followed by a broad  $\Delta T$  and exothermic reaction due to crystallization. The  $T_g$ ,  $T_x$ , and  $\Delta T$  of the film are thus marked. In Figure 2b, the annealing in the  $\Delta T$  region causes dramatically different behavior. Abrupt increases in film resistivity were noted to a maximum  $\sim 4,628 \mu\Omega\text{-cm}$  at 775 K. When the annealing temperature reached 800 K, the resistivity then decreased to  $\sim 177 \mu\Omega\text{-cm}$ . Although the changes were not as extensive as in the present study, similar resistivity changes in  $\Delta T$  have also been reported in zirconium- and iron-based glass-forming films.<sup>8,9</sup> The significant increase ( $\sim 25$  times) of resistivity in this study is considered to have potential for applications such as switches and safety breakers where quick electrical resistivity change with temperature is required.

In the hardness vs. annealing temperature result in Figure 3, annealing of the film at low temperatures yields the release in the residual stress present in the as-deposited condition and thus causes decreases in hardness. When the

films are annealed at temperatures below the glass transition, the film hardness gradually increases with the annealing temperature, reaching  $\sim \text{HK}848$  at 700 K and a maximum of  $\sim \text{HK}893$  at 740 K from  $\sim \text{HK}720$  at 600 K. This beneficial strengthening effect is distinct from those of annealing-induced softening in conventional films, and is presumably attributed to the nanocrystallite/amorphous composite structure (or called nanophase composite) as proposed in zirconium- and iron-based films.<sup>8,9</sup> The film hardness increases to a maximum at 740 K, followed by a noticeable decrease to  $\sim \text{HK}725$  at 775 K for the annealing temperatures within the supercooled liquid region. Such a hardness drop is presumably to the single amorphous phase as a result of full amorphization. The higher strength in the composite structure than the monolithic amorphous phase is consistent with those reported earlier.<sup>8,9</sup> The hardness decreases at high temperatures above 850 K are caused by crystallization and extensive grain growth in the film. Both electrical resistivity and hardness properties thus show unusual changes at 775 K. This agrees with the fact that there is a distinct structure change in  $\Delta T$ .

Figures 4 and 5 show TEM bright-field images and corresponding diffraction patterns, respectively, of film in as-deposited and annealed conditions. From as-deposited to 800 K, the film shows the structure of amorphous/orthorhombic  $\text{Cu}_{10}\text{Zr}_7$  (as-deposited)  $\rightarrow$

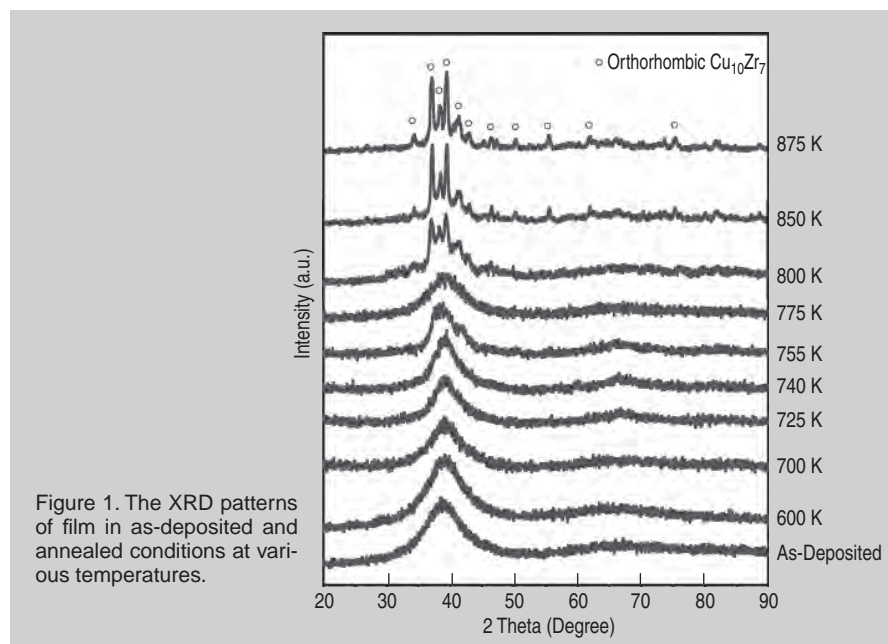


Figure 1. The XRD patterns of film in as-deposited and annealed conditions at various temperatures.

## EXPERIMENTAL PROCEDURE

The film was deposited onto glass substrates using an r.f. magnetron sputtering system with 3 mTorr working pressure. The film composition was confirmed by electron probe microanalyzer. The film was ex-situ annealed by rapid thermal annealing in a mixture gas atmosphere (95% N<sub>2</sub> + 5% H<sub>2</sub>). The annealing was performed at a heating rate of 100 K/min. with a holding time of 60 s at temperatures ranging from 600 K to 923 K. A differential scanning calorimeter was used for thermal analysis to determine temperatures in-situ for any transition and crystallization temperatures of film at the heating rate of 100 K/min. X-ray diffractometry and transmission electron microscopy were used to identify the crystal structure of the film. Electrical resistivity and ultramicrohardness were carried out using the four-point probe method and Knoop hardness tester, respectively.

composite structure of amorphous/orthorhombic Cu<sub>10</sub>Zr<sub>7</sub> (755 K) → fully amorphous (775 K) → stable crystalline of orthorhombic Cu<sub>10</sub>Zr<sub>7</sub> (800 K). The as-deposited film exhibits nanocrystallites dispersed in an amorphous matrix. According to measured d-spacings and JCPD file data, the crystalline phases in the films at as-deposited and 755 K are likely orthorhombic Cu<sub>10</sub>Zr<sub>7</sub>. After annealing at 800 K, above T<sub>x</sub>, the crystalline phase is identified to be orthorhombic Cu<sub>10</sub>Zr<sub>7</sub>. The sizes of nanocrystalline phases range from 5 nm to 15 nm. From Figure 5a, the d-spacings of as-deposited diffraction rings are measured to be 2.41, 2.10, 1.86, 1.77, 1.70, 1.49, and 1.26 Å. More crystalline spots in the diffraction pattern of Figure 5b indicate that the phase is better crystallized at 755 K. The nanocrystalline sizes are in the range of 20 nm to 35 nm. These are evidenced in the TEM image (Figure 4b) and in well-defined spotty rings in diffraction pattern (Figure 5b). Based on Figure 5b, the d-spacing of diffraction rings are 2.41, 2.10, 1.86, 1.79, 1.70, 1.49, and 1.26 Å. Annealing at 775 K in the ΔT region produces a fully amorphous structure without any observable crystalline phases, as evidenced by the TEM image of Figure 4c and by the typical broad diffused diffraction rings characteristic of a glass in Figure 5c. Neither obvious crystals nor splitting of the halo peak observed in the bright-field TEM image and diffraction pattern are in agreement with the XRD result (Figure 1). This phenomenon may be because the nanocrystalline phases dissolve in the amorphous matrix and lose their crystallinity.<sup>8,9</sup> With 25 K increase in annealing temperature to 800 K, well above the crystallization transition, the film reveals more crystalline structures with less amorphous phase. The crystalline phases are likely

to be orthorhombic Cu<sub>10</sub>Zr<sub>7</sub>. The TEM results shown in the present study are consistent with those reported in earlier studies of zirconium<sup>8</sup> and iron-based glass-forming films.<sup>9</sup>

## DISCUSSION

When considering the mechanism by which the partly amorphous as-deposited film dispersed with crystallites is transformed to the fully glassy state during annealing at 775 K, the authors ruled out the amorphization induced by impurities such as hydrogen and oxygen because of the short duration and reduced pressure of these gases during annealing.<sup>8,9</sup> Thermodynamically, the large negative heat of mixing and hence the low free energy for the amorphous phase in the glass-forming film system are used to explain the solid-state amorphization.<sup>8</sup> The as-deposited film,

consisting of the amorphous matrix dispersed with nanocrystalline phases, is metastable. Upon annealing in the ΔT, the as-deposited metastable phases transform to the relatively stable amorphous phase as an intermediate phase because the as-deposited phases have a relatively higher free energy than the amorphous phase. The intermediate amorphous phase eventually turns into the even stable crystallized phases at high temperatures above ΔT.

In addition to the thermodynamic factor, sufficient thermal energy and high interfacial energies between amorphous and nanocrystalline phases are needed for the amorphization to take place. Similarly, these are prerequisite for the SSA to occur.<sup>15</sup> The results of this study thus demonstrate, as was qualitatively hypothesized, thermal energy and interfacial energy between the nanocrystalline and glassy matrix might have strong influences on the amorphization and crystallization of film during annealing. Upon annealing at below the supercooled liquid region, the interfacial energy appears to be predominant because of the presence of nanocrystallites and the growth of nanocrystalline phases is favorable. In addition, the viscosity of the glass matrix decreases with the annealing temperature, reaching a minimum in ΔT, analo-

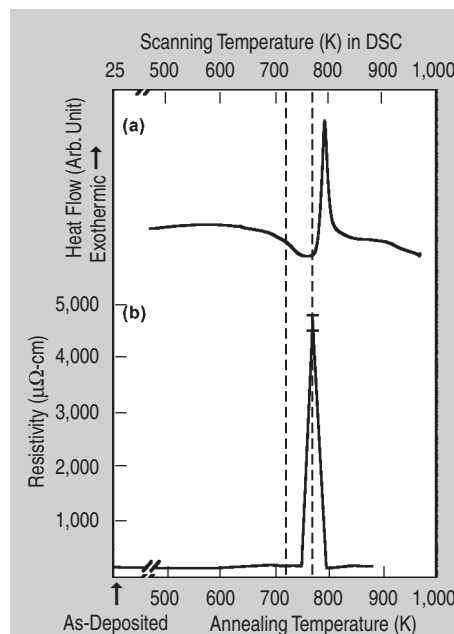


Figure 2. The (a) DSC and (b) electrical resistivity results of film in as-deposited and annealed conditions. The approximate location of SCLR is marked by dashed lines.

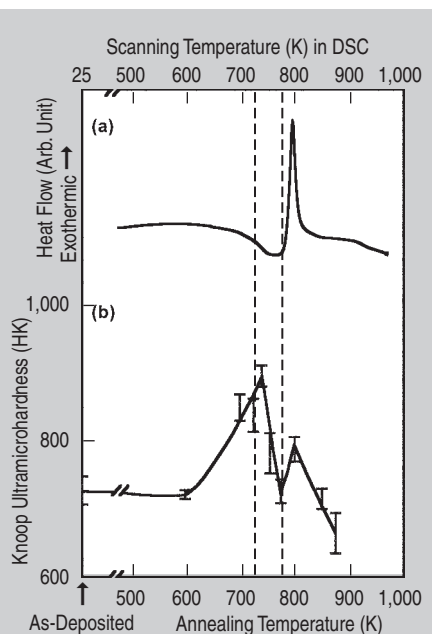


Figure 3. The (a) DSC and (b) Knoop ultramicrohardness results of film in as-deposited and annealed conditions. The approximate location of SCLR is marked by dashed lines.

gous to that required for the superplasticity<sup>16</sup> and “erasing”<sup>17</sup> properties in metallic glasses. The glassy matrix with sufficiently low viscosity in  $\Delta T$  thus allows the nanocrystalline phases to move around in the matrix. For the full amorphization at 775 K, nanocrystallites are

thermally annihilated and liquefied into the glassy matrix, on account of the combined effects of sufficient thermal energy and excessive interfacial energies. Contrary to the planar interfacial area in SSA multilayer films, the irregular and plentiful nanocrystallite/glass

interfaces that are present throughout the film are considered to yield much higher interfacial energies. Thus, large-scale amorphization could take place in the film.

## CONCLUSIONS

The glass-forming  $\text{Cu}_{51}\text{Zr}_{42}\text{Al}_4\text{Ti}_3$  film showed the phenomenon of annealing-induced nanocrystallization and amorphization. The full amorphization at 775 K is attributed to high thermal and interfacial energies between nanocrystallites and the glassy matrix. The amorphization results in the variations in the film electrical and mechanical properties within the supercooled liquid region. The most significant alteration is the increase of  $\sim 25$  times in electrical resistivity when the film becomes fully amorphous.

## ACKNOWLEDGEMENTS

The present work is supported by the National Science Council of Republic of the China in Taiwan (NSC 95-2221-E-011-224-MY3 and 96-2628-E-011-117-MY3). Mr. Chun Hui Lin is acknowledged for his contribution.

## References

1. C.C. Koch et al., *Appl. Phys. Lett.*, 43 (1983), p. 1017.
2. R.B. Schwarz and W. L. Johnson, *Phys. Rev. Lett.*, 51 (1983), p. 415.
3. S.K. Deb et al., *Nature*, 414 (2001), p. 528.
4. M.W. Chen, J.W. McCauley, and K.J. Hemker, *Science*, 299 (2003), p. 1563.
5. A.L. Greer, *Science*, 267 (1995), p. 1947.
6. J.P. Chu et al., *Mat. Sci. Eng. A*, A277 (2000), p. 11.
7. B.X. Liu, W.S. Lai, and Z.J. Zhang, *Advances in Physics*, 50 (2001), p. 367.
8. J.P. Chu et al., *Physical Review B*, 69 (2004), p. 113410.
9. J.P. Chu et al., *Appl. Phys. Lett.*, 88 (2006), p. 012510.
10. A. Inoue, *Acta Mater.*, 48 (2000), p. 279.
11. A. Inoue and W. Zhang, *Appl. Phys. Lett.*, 83 (2003), p. 2351.
12. S. Hata, K. Sato, and A. Shimokohbe, *SPIE International Symposium on Micro-Electronics and Micro-Electro-Mechanical Systems MICRO/MEMS '99*, 3892 (1999), p. 97.
13. C.L. Chiang et al., *Appl. Phys. Lett.*, 88 (2006), p. 131902.
14. A. Inoue and A. Takeuchi, *Mater. Sci. Eng., A* 375-377 (2004), p. 16.
15. Z.F. Li, W.S. Lai, and B.X. Liu, *Appl. Phys. Lett.*, 77 (2000), p. 3920.
16. J.P. Chu et al., *Appl. Phys. Lett.*, 90 (2007), p. 034101.
17. G. Kumar and J. Schroers, *Appl. Phys. Lett.*, 92 (2008), p. 031901.

J.P. Chu is with the Institute of Polymer Engineering, National Taiwan University of Science and Technology, Taipei 10607, Taiwan and can be reached at +886-2-2730-3292; fax +886-2-2737-6544; e-mail jpchu@mail.ntust.edu.tw.

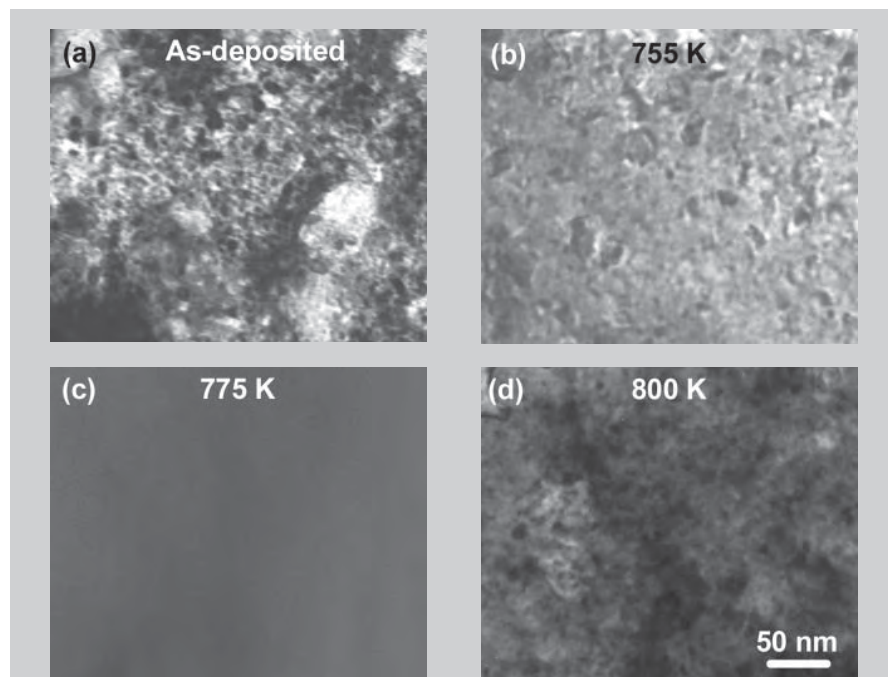


Figure 4. Transmission electron micrographs of the film in (a) as-deposited and annealed conditions at (b) 755 K, (c) 775 K, and (d) 800 K.

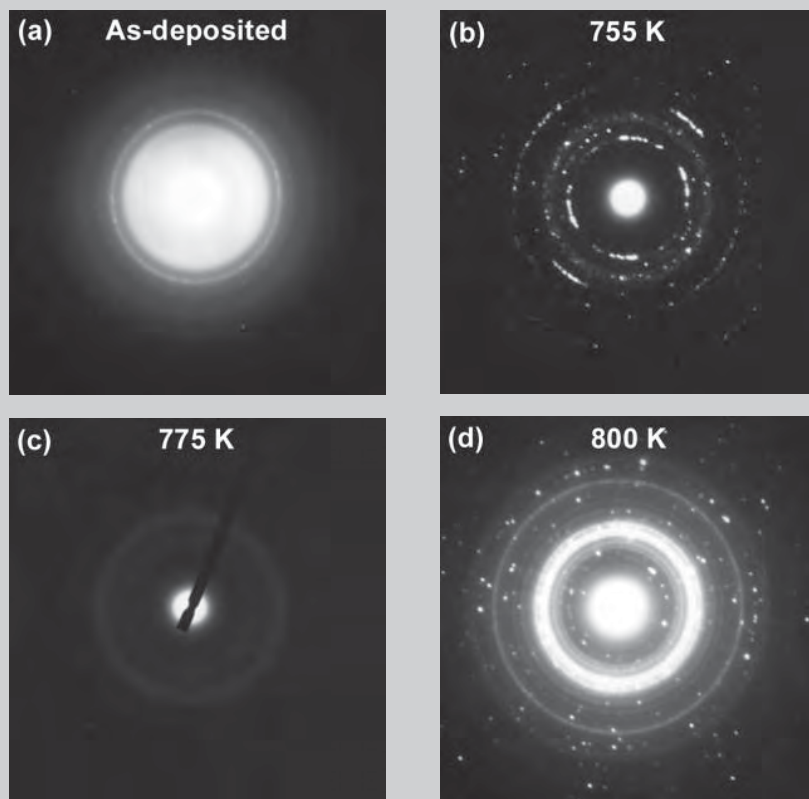


Figure 5. Transmission electron diffraction patterns of the film in (a) as-deposited and annealed conditions at (b) 755 K, (c) 775 K, and (d) 800 K.

# The Growth Kinetics of Intermetallic Layers at the Interface of a Solid Metal and a Liquid Solder

V.I. Dybkov

*During soldering, intermetallic layers can occur at the interface of a solid metal and the saturated or undersaturated solder melt. In systems with a considerable solubility in the liquid state, dissolution causes a manifold drop in layer thickness. Mathematical equations are proposed to evaluate the thickness of any intermetallic layer formed under conditions of simultaneous dissolution in the undersaturated solder melt. The main features of reactive phase formation at the solid metal-liquid solder interface are illustrated using the Co-Sn couple with the growing  $\text{CoSn}_3$  (250°C) and  $\text{CoSn}_2$  (350°C and 450°C) layers as examples.*

## INTRODUCTION

In light of worldwide legislation for the gradual reduction and subsequent removal of lead, mercury, cadmium, and other heavy metals from new equipment and products, there is an urgent need for lead-free solders and research on metal-solder joint behavior under various performance conditions. Since lead falls into the range of toxic metals, conventional Sn-Pb solders are being replaced mainly with tin-based soldering alloys containing additions of other low-melting-point metals. Therefore, it is not surprising that the interfacial interaction of lead-free solders with solid metals and alloys is receiving considerable attention in scientific and technical communities.<sup>1-18</sup>

During the soldering of solid metals with molten solders, two physicochemical processes, namely, dissolution of the solid in the liquid phase and formation of intermetallic-compound layers at their interface, take place simultaneously after wetting the solid metal surface with the solder melt. On one hand, the occurrence of inter-

metallic layers provides evidence for reliable metallurgical bonding of dissimilar materials. On the other hand, however, too-thick intermetallic layers considerably deteriorate the mechanical strength of the joint. Therefore, a reasonable compromise value of the layer thickness must be determined or evaluated in each particular case.

Conventionally, the intermetallic-layer growth kinetics are treated with the use of parabolic equations.<sup>19-21</sup>

However, if the solubility of a solid metal in a liquid soldering alloy is not zero, as is practically always the case, then the growth rate constant found experimentally proves time-dependent. As a result, the parabolic equations do not provide an adequate description of the kinetics of the intermetallic-layer growth process for most binary and multicomponent systems with a noticeable solubility in the liquid state, especially if the liquid agitation is strong.

A more general three-term mathematical equation describing the growth kinetics of any intermetallic layer under conditions of its simultaneous dissolution in a molten soldering alloy was derived in the framework of a physicochemical analysis of the reaction-diffusion process in solid-liquid systems.<sup>22</sup> Using this equation, the effect of dissolution in the undersaturated solder melt on the intermetallic layer growth rate can be readily evaluated.

If a solid metal is, for example, cobalt and the main component of a solder is tin, intermetallic layers based on the Co-Sn compounds may be expected to form at the cobalt-solder interface in the course of soldering. According to the phase diagram, four intermetallic compounds,  $\text{Co}_3\text{Sn}_2$ ,  $\text{CoSn}$ ,  $\text{CoSn}_2$ , and  $\text{CoSn}_3$ , exist in the Co-Sn binary system.<sup>23-25</sup> Also, formation of the  $\text{CoSn}_4$  layer was observed in the solid state at the corners of the Co-Sn couples.<sup>26</sup> It is yet unclear whether the  $\text{CoSn}_4$  phase is stable or metastable.

Though diffusional considerations assume the simultaneous parabolic growth for the layers of all intermetallics available on an appropriate binary phase diagram,<sup>27</sup> this does not appear to be the case. More often, layer formation is sequential, with at most two compound layers growing simultaneously

### How would you...

#### ...describe the overall significance of this paper?

*With couples of considerable solid-in-liquid solubility, the effect of dissolution on the intermetallic layer-growth kinetics during soldering must be taken into account. This paper demonstrates the magnitude of this effect using the Co-Sn couple as an example and describes it in general analytical form.*

#### ...describe this work to a materials science and engineering professional with no experience in your technical specialty?

*In the course of soldering, intermetallic layers usually occur at the solid metal-liquid solder interface, while the solid simultaneously dissolves in the solder melt. The interconnection of these two processes is considered in this paper.*

#### ...describe this work to a layperson?

*In view of the growing application of lead-free tin-based solders, research on their interfacial interaction with solid metals and alloys is badly needed. This paper analyzes physico-chemical aspects of the solid metal-liquid solder interaction and provides an analytical description of intermetallic layer-growth kinetics at the metal-solder interface.*



## Equations

$$qB_{\text{diffusing}} + pA_{\text{surface}} = A_p B_q \quad (1)$$

$$\rho A_{\text{diffusing}} + qB_{\text{surface}} = A_p B_q \quad (2)$$

$$\left(\frac{dx}{dt}\right)_{\text{growth}} = \frac{k_{0B1}}{1 + \frac{k_{0B1}x}{k_{1B1}}} + \frac{k_{0A2}}{1 + \frac{k_{0A2}x}{k_{1A2}}} \quad (3)$$

$$\left(\frac{dx}{dt}\right)_{\text{dissolution}} = b_1 = b_0 \exp(-at) \quad (4)$$

$$\frac{dx}{dt} = \frac{k_{0B1}}{1 + \frac{k_{0B1}x}{k_{1B1}}} + \frac{k_{0A2}}{1 + \frac{k_{0A2}x}{k_{1A2}}} - b_0 \exp(-at) \quad (5)$$

$$k_{0B1} + k_{0A2} < b_0 \quad (6)$$

$$k_{0B1} + k_{0A2} = b_1 \quad (7)$$

$$\frac{dx}{dt} = \frac{k_1}{x} - b_1 \quad (8)$$

$$x_{\text{max}} = \frac{k_1}{b_1} \quad (9)$$

under conditions of diffusion control.<sup>22</sup> If diffusion of one and the same component prevails in all the compounds, only one compound layer will grow.

To visualize the effect of dissolution on the process of intermetallic compound-layer formation at the interface between solid cobalt and liquid solders of composition 87.5Sn-7.5Bi-3In-1Zn-1Sb and 80Sn-15Bi-3In-1Zn-1Sb (wt.%), two sets of experiments were carried out at 250°C, 350°C, and 450°C and dipping times of 300–1,800 s. In the first set, the solder melt previously saturated with cobalt was employed. Therefore, dissolution of solid cobalt in the liquid solder did not occur. In the second, the solder melt initially contained no cobalt. Hence, when brought into contact with each other, the solid started to dissolve in the liquid phase.

See the sidebar for experimental procedures.

## RESULTS AND DISCUSSION

### Layer Phase Identity and Composition

Backscattered electron images of the cobalt-solder transition zone at 250°C

and 450°C are shown in Figure 1. With both solders, a single-phase layer of the CoSn<sub>3</sub> intermetallic compound was found to form from both saturated and undersaturated melts at 250°C and dipping times up to 1,800 s. The layer of CoSn<sub>2</sub> occurs at 350°C and 450°C. The content of other elements in both layers was rather low (0.40–1.10% Bi, 0.30–0.60% In, 0.01–0.05% Zn, and 0.03–0.50% Sb).

As seen in Figure 1, the thickness of intermetallic layers is much less in the case of the undersaturated solder melt compared to the case of the saturated melt, other conditions being identical. Thus, the effect of dissolution on the layer growth kinetics at the cobalt-solder interface is very appreciable.

### Mechanism of Intermetallic Layer Formation

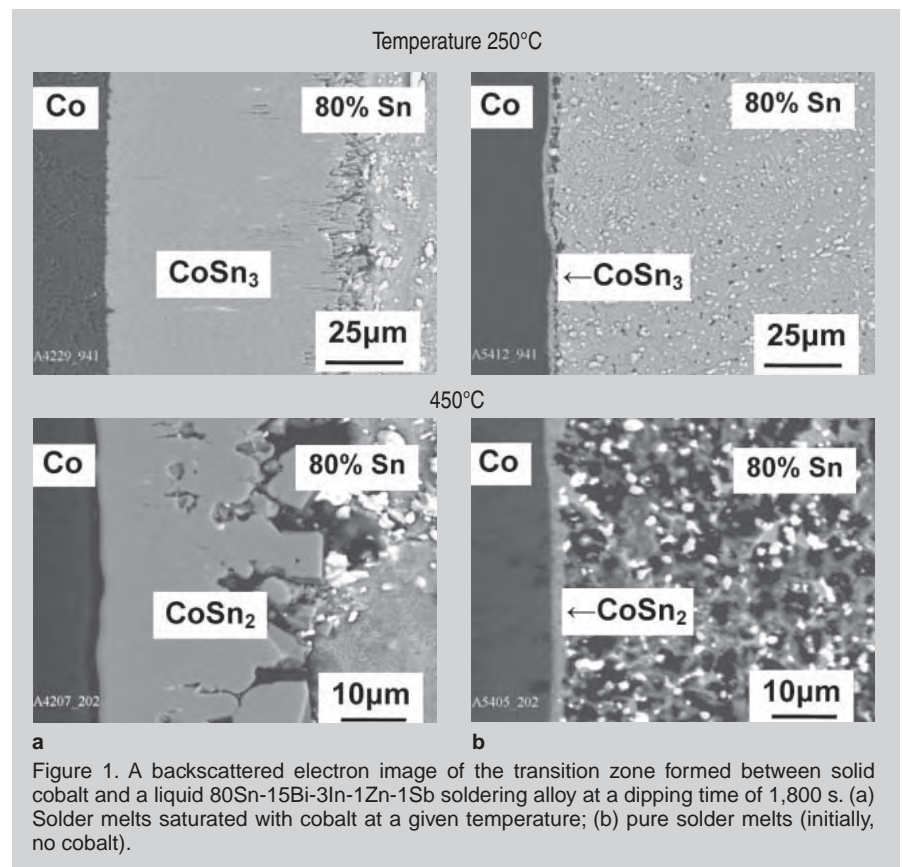
Generally, growth of any intermetallic layer A<sub>p</sub>B<sub>q</sub> at the interface between a solid metal A and a liquid solder B saturated with A at a given temperature is a result of counter-diffusion of components A and B across its bulk followed by partial chemical reactions between diffusing atoms of one component and surface atoms of another component

(see Equations 1 and 2 in the Equations table).<sup>22</sup>

These reactions yield the increases, dx<sub>B1</sub> and dx<sub>A2</sub>, in layer thickness during a small period of time, dt, as shown in Figure 2. The layer growth rate is given as Equation 3, where k<sub>0B1</sub> and k<sub>0A2</sub> are chemical constants and k<sub>1B1</sub> and k<sub>1A2</sub> are diffusional constants (reaction-diffusion coefficients). With the saturated solder melt, the layer-growth kinetics are thus initially linear (at x up to 500–600 nm) and then parabolic (x > ~1 μm).

### The Effect of Dissolution on the Layer Growth Rate

As seen in Figure 2, in the case of the undersaturated solder melt the net rate of layer formation is the difference between the sum of the rates of its growth at interfaces 1 and 2 and the rate of dissolution at interface 2. The dissolution rate is given as Equation 4, where b<sub>0</sub> = c<sub>s</sub>k/ρφ, a = ks/v, c<sub>s</sub> is the saturation concentration (solubility) of A in B at a given temperature, k is the dissolution rate constant, ρ is the density of the A<sub>p</sub>B<sub>q</sub> compound, φ is the content of A in A<sub>p</sub>B<sub>q</sub> in mass fractions, s is the surface area of the solid in con-



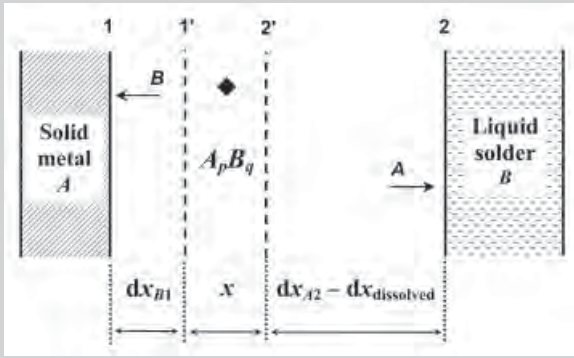


Figure 2. A schematic diagram to illustrate the process of formation of the  $A_p B_q$  intermetallic layer under conditions of its simultaneous dissolution in the solder melt. Changes in layer thickness are measured relative to an inert marker ( $\blacklozenge$ ) located in its bulk. Not to scale.

tact with the liquid, and  $v$  is the volume of the liquid.

A mathematical equation describing the  $A_p B_q$  growth kinetics at the A-B interface under conditions of dissolution in the liquid phase is shown in Equation 5. It is clear that generally the layer growth is non-parabolic. Moreover, if Equation 6 is satisfied, the  $A_p B_q$  layer must be missing from the A-B couple. It means that the sum of the rates of chemical reactions at the interfaces (and also the rate of direct reaction between A and B) is less than the initial rate of dissolution.

As seen from Equation 4, the dissolution rate decreases exponentially from  $b_0$  to  $b_t$  in the  $0 - t$  time range. Hence, in the case where Equation 7 is satisfied, the  $A_p B_q$  layer occurs at the A-B interface after some delay. At large  $t$ ,  $b_t \approx 0$ , and the layer-growth kinetics become close to parabolic.

Equation 5 cannot be solved precisely. However, its simpler forms can readily be employed in practice.

### Evaluation of Layer Thickness

If the  $A_p B_q$  layer grows under conditions of diffusion control ( $k_{OB1} \gg k_{IB1}$ )

$x, k_{0A2} \gg k_{1A2}/x$ , while the dissolution rate is constant and equal to  $b_t$ , Equation 5 reduces to Equation 8, where only one diffusional (parabolic) constant,  $k_1$ , is retained for simplicity. In such a case, the layer thickness tends with passing time to a limiting value shown in Equation 9, defined from the condition  $k_1/x - b_t = 0$ .

Equation 9 is suitable for estimating the thickness of any intermetallic layer growing under conditions of its simultaneous dissolution in the liquid phase. Calculations are carried out twice for each point,  $t$ , by putting in the denominator of Equation 9 first equal to  $(b_0 + b_t)/2$  and then  $b_t$ . Thus, two sets of the layer thickness are obtained. The first set produces the underestimated values,

$x_{\text{under}}$ . The second yields the overestimated ones,  $x_{\text{over}}$ . Clearly, experimental values,  $x_{\text{exp}}$ , should lie somewhere in between.

In the case of the saturated 80Sn-15Bi-3In-1Zn-1Sb solder melt, the experimental value of the  $\text{CoSn}_2$  layer thickness was found to be  $33.0 \times 10^{-5}$  m at  $450^\circ\text{C}$  and a dipping time of 1,800 s (see Figure 1). Hence,  $k_1 = x^2/2t = 3.0 \times 10^{-13}$   $\text{m}^2 \text{s}^{-1}$ . Other quantities necessary for calculations are  $k = 6.2 \times 10^{-5}$   $\text{m s}^{-1}$  at a disc rotational speed of 24.0  $\text{rad s}^{-1}$ ,  $c_s = 10.74$   $\text{kg m}^{-3}$  (0.15% cobalt in the soldering alloy),  $\rho_{\text{int}} = 8.91 \times 10^3$   $\text{kg m}^{-3}$ ,<sup>28</sup>  $\phi = 0.1989$  (19.89% cobalt in  $\text{CoSn}_2$ ),  $s = 1.0$   $\text{cm}^2$ ,  $v = 10.0$   $\text{cm}^3$ ,  $b_0 = 3.76 \times 10^{-7}$   $\text{m s}^{-1}$ .

Final results are presented in Table I. The agreement of calculated and experimental values appears to be quite sufficient for practical purposes to estimate the intermetallic-layer thickness at the solid metal-liquid solder interface. It is worth noting that the range in which the layer thickness varies is rather narrow, even though the time interval of 300–1,800 s is relatively wide. Since the time of soldering rarely exceeds a few minutes, the difference between  $x_{\text{under}}$  and  $x_{\text{over}}$  is seen to be within the experimental accuracy of measuring the layer thickness.

### EXPERIMENTAL PROCEDURE AND METHODS

The process of dissolution of cobalt in liquid solders and that of growth of intermetallic layers under conditions of simultaneous dissolution in the solder melt were studied by the rotating disc technique at an angular rotational speed of 24.0  $\text{rad s}^{-1}$ . Pure metals (99.91–99.999%) were used for the investigation. A flux was employed both to pre-heat the solid specimen to the experimental temperature and to protect the melt from oxidation by atmospheric air. Before the experiment, the solid cobalt specimen,  $11.28 \pm 0.02$  mm in diameter (1  $\text{cm}^2$  area) and 5–6 mm high, was pressed into a graphite tube to protect its lateral surface from the solder melt. At the end of the run the cobalt specimen was rapidly cooled down in a water bath. Its mass loss during dissolution in the melt was determined by weighing. Co-Sn-Bi-In-Zn-Sb alloys obtained after the runs were analyzed chemically to determine their cobalt content. Cobalt content was also found by electron probe microanalysis. The three values were then averaged and used in further calculations.

To investigate the growth process of intermetallic layers from saturated melts, experiments were carried out in a steel thermostat. Polished cobalt plates,  $14 \times 5 \times 3$   $\text{mm}^3$ , were mounted into graphite crucibles. The crucibles were placed in the thermostat at a required temperature. These were then filled with the flux from a moveable electric-resistance furnace and kept at the same temperature. After the temperature in the thermostat had equilibrated, the crucibles were filled with the metallic melt, previously saturated with cobalt, from another moveable electric-resistance furnace, also kept at the required temperature. Cobalt was allowed to react with the melt during a predetermined period of time in the 300–1,800 s range. Then, the graphite crucibles with their contents were withdrawn from the thermostat and rapidly cooled down in water. Bimetallic specimens obtained were cut into two parts, normal to the long side of a cobalt plate. The cobalt-solder cross sections were prepared and examined with the use of metallography, x-ray diffraction, and electron probe microanalysis.

Table I. Calculated ( $x_{\text{under}}$  and  $x_{\text{over}}$ ) and Experimental ( $x_{\text{exp}}$ ) Thicknesses of the  $\text{CoSn}_2$  Intermetallic Layer Grown from Undersaturated 80Sn-15Bi-3In-1Zn-1Sb Solder Melts\*

Time (s)	$x_{\text{under}}$ ( $\times 10^{-5}$ m)	$x_{\text{exp}}$ ( $\times 10^{-5}$ m)	$x_{\text{over}}$ ( $\times 10^{-5}$ m)
300	0.80	$0.8 \pm 0.1$	0.87
600	0.94	$1.0 \pm 0.2$	1.16
1,200	1.00	$1.5 \pm 0.2$	1.68
1,800	1.20	$1.8 \pm 0.2$	2.43

\*450°C; disc rotational speed of 24.0  $\text{rad s}^{-1}$

## ACKNOWLEDGEMENTS

This investigation was supported in part by the CRDF grant No. UKE2-2698-KV-06.

## References

1. D.R. Frear, *JOM*, 51 (3) (1999), pp. 22–27.
2. W.H. Tao et al., *Chem. Mater.*, 13 (2001), pp. 1051–1056.
3. M.Y. Chiu, S.S. Wang, and T.H. Chuang, *J. Electronic Mater.*, 31 (2002), pp. 494–499.
4. M.O. Alam, Y.C. Chan, and K.N. Tu, *J. Appl. Phys.*, 94 (2003), pp. 4108–4115.
5. Jeong-Won Yoon et al., *J. Electronic Mater.*, 33 (2004), pp. 1190–1199.
6. Hwa-Teng Lee et al., *Mater. Sci. Eng. A*, 407 (2005), pp. 36–44.
7. P.L. Liu and J.K. Shang, *Scripta Mater.*, 53 (2005), pp. 631–634.
8. M.J. Rizvi et al., *J. Alloys Comp.*, 407 (2006), pp. 208–214.
9. Chao-hong Wang and Sinn-wen Chen, *Acta Mater.*, 54 (2006), pp. 247–253.
10. Oladele A. Ogunseitan, *JOM*, 59 (7) (2007), pp. 12–17.
11. Katsuaki Sugauma et al. (Presentation at the MRS 2007 Spring Meeting, San Francisco, CA, April 9–13, 2007), E1.6.
12. Thomas Bieler et al. (Presentation at the MRS 2007 Spring Meeting, San Francisco, CA, April 9–13, 2007), E4.6.
13. Eric Chason et al. (Presentation at the MRS 2007 Spring Meeting, San Francisco, CA, April 9–13, 2007), E2.4.
14. K. Ursula, K. Moon, and C. Handwerker (Presentation at the Materials Science and Technology 2007 Conference and Exhibition, Detroit, MI, September 16–20, 2007).
15. I.E. Anderson et al. (Presentation at the Materials Science and Technology 2007 Conference and Exhibition, Detroit, MI, September 16–20, 2007).
16. K.A. Grossklaus et al. (Presentation at the Materials Science and Technology 2007 Conference and Exhibition, Detroit, MI, September 16–20, 2007).
17. K.N. Subramanian, editor, *Lead-Free Electronic Solders* (Berlin-Heidelberg: Springer, 2007).
18. K.N. Tu, *Solder Joint Technology* (Berlin-Heidelberg: Springer, 2007).
19. K. Hauffe, *Reaktionen in und an festen Stoffen* (Berlin: Springer, 1955).
20. W. Seith, *Diffusion in Metallen* (Berlin: Springer, 1955).
21. J.A. Hedvall, *Solid State Chemistry* (Amsterdam: Elsevier, 1966).
22. V.I. Dybkov, *Reaction Diffusion and Solid State Chemical Kinetics* (Kyiv: The IPMS Publications, 2002), [www.dybkov.kiev.ua](http://www.dybkov.kiev.ua).
23. A. Lang and W. Jeitschko, *Z. Metallkunde*, 87 (1996), pp. 759–764.
24. M. Jiang et al., *Calphad*, 28 (2004), pp. 213–220.
25. H. Okamoto, *J. Phase Equil. Diffusion*, 27 (2006), p. 308.
26. Chao-hong Wang and Sinn-wen Chen, *J. Mater. Res.*, 22 (2007), pp. 3404–3409.
27. K.P. Gurov, B.A. Kartashkin, and Yu. E. Ugaste, *Vzaimnaya Diffuziya v Mnogofaznikh Metallicheskih Sistemakh* (Moskva: Nauka, 1981).
28. E.E. Havinga, H. Damsma, and P. Hokkelling, *J. Less-Common Metals*, 27 (1972), pp. 169–186.

V.I. Dybkov is with the Department of Physical Chemistry of Inorganic Materials at the Institute of Problems of Materials Science, Kyiv 03180, Ukraine. He can be reached at [vdybkov@ukr.net](mailto:vdybkov@ukr.net), [vdybkov@ipms.kiev.ua](mailto:vdybkov@ipms.kiev.ua).



TMS KNOWLEDGE  
RESOURCE CENTER

Your Materials Books  
and More e-Store!  
<http://knowledge.tms.org>

Visit the Knowledge Resource Center to reserve your copy today!



### Light Metals 2009

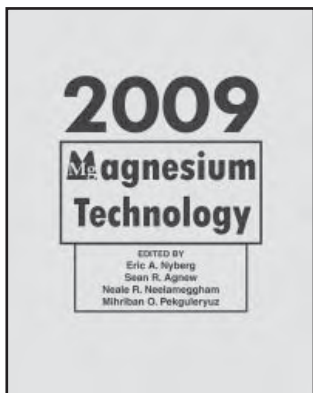
*Light Metals 2009* presents the most up-to-date information on the state of primary aluminum science and technology. It's a great mix of practical applied technology and hard science, which is of invaluable benefit to the global aluminum industry as it strives to cut costs and increase profitability.

Areas covered include:

- Alumina and Bauxite
- Aluminum Reduction Technology
- Cast Shop for Aluminum Production
- Electrode Technology for Aluminum Production
- Aluminum Hot Rolling/Aluminum Cold Rolling and Strip Process

In the light metals industry, aluminum will always have serious competition from other materials. Held at the TMS Annual Meeting & Exhibition each year, the *Light Metals* series has become the definitive annual reference source in the field of aluminum production and related light metals technologies.

**Member price \$174; Student price \$139; List price \$249**



### Magnesium Technology 2009

*Magnesium Technology 2009* presents all aspects of magnesium production, properties and application, including primary production, alloy development, performance and the global market. This all-inclusive book contains sections on wrought alloys; thermodynamics and phase transformations; casting; alloy microstructure and properties; corrosion, surface finishing and joining; creep resistant magnesium alloys; and advanced magnesium materials.

**Member price \$159; Student price \$129; List price \$229**

To order these or related publications, contact TMS:

E-mail [publications@tms.org](mailto:publications@tms.org) • Phone (724) 776-9000, ext. 256 • Fax (724) 776-3770

# Measuring Secondary Phases in Duplex Stainless Steels

I. Calliari, K. Brunelli, M. Dabalà, and E. Ramous

*The use of duplex stainless steels is limited by their susceptibility to the formation of dangerous intermetallic phases resulting in detrimental effects on impact toughness and corrosion resistance. This precipitation and the quantitative determinations of the phases have received considerable attention and different precipitation sequences ( $\sigma$  phase,  $\chi$  phase, and carbides) have been suggested. This study investigates the phase transformation during continuous cooling and isothermal treatments in commercial duplex stainless steel grades and the effects on alloy properties, and compares the most common techniques of analysis.*

## INTRODUCTION

A favorable combination of mechanical and corrosion properties characterizes duplex stainless steels (DSS), as they consist of almost equal parts of austenite and ferrite.<sup>1,2</sup> Duplex steels are more susceptible to precipitation of intermetallic phases than austenitic steels due to their high chromium and molybdenum contents and high diffusion rates in the ferrite phase. These steels are prone to form secondary phases after exposure to temperatures ranging from 450°C to 1,000°C.<sup>3</sup> The  $\sigma$  phase is a hard, brittle non-magnetic intermetallic phase, with high chromium and molybdenum contents, affecting both hot and room temperature ductility. Some authors report that  $\chi$  phase precipitates for shorter times than  $\sigma$ <sup>4</sup> and at slightly lower temperatures, but it has not been well investigated.

These precipitates cause a dramatic deterioration in toughness and corrosion resistance.<sup>5,6</sup> It has been demonstrated that over a certain amount (between 5% and 10%) of a phase like  $\sigma$  phase, the toughness of duplex steels is

reduced to values too low for practical applications, but some features of the early stages of precipitation are not yet well understood.

A very low cooling rate may determine different microstructures from surface to core, especially in large-sized bars, with a surface free of secondary phases and a core with a significant amount of them. Therefore the critical

cooling rate should be determined in order to avoid or to limit precipitation at the core. As a consequence of these characteristics, the correct procedure<sup>7,8</sup> for measuring low contents of  $\sigma$ -related phases is needed, as the requirement for manufacturing or welding DSS to be “free of intermetallic phases” may be too strict. Starting from these data, it is evident that the metallographic techniques used for secondary phase identification play a fundamental role in phase identification. Efforts have been made to determine the volume fraction of  $\sigma$  phases in austenitic<sup>9</sup> stainless steel and in duplex grades. Several electrochemical procedures<sup>10</sup> and metallographic etchants<sup>11</sup> have been tested and discussed for light microscopy,<sup>12</sup> but it is quite difficult to identify separately  $\chi$  and  $\sigma$  and to accurately quantify low amounts of such phases.

In this paper, the results concerning the formation of secondary phases in commercial DSS SAF 2205 and SAF 2507 are presented. The precipitation has been examined during continuous cooling (SAF 2205) and isothermal treatments (SAF 2205 and SAF 2507). The goal of this study was to investigate the sequence of precipitation in different thermal conditions and to compare the different techniques of precipitation analysis.

See the sidebar for experimental procedures.

## RESULTS AND DISCUSSION

### Solution-Treated Sample

The solution-treated materials have banded structure with elongated gamma islands in the longitudinal sections, while the transverse sections have ferrite and austenite grains with isotropic structure. The values of volume frac-

### How would you...

#### ...describe the overall significance of this paper?

*The paper improves the knowledge on the precipitation kinetics of dangerous intermetallic phases which have a detrimental effect on the toughness of duplex stainless steel. Furthermore, a comparison between different measuring techniques of analysis was performed.*

#### ...describe this work to a materials science and engineering professional with no experience in your technical specialty?

*This work investigated the effect of aging temperature, time of treatments, and cooling rates on the microstructure (austenite/ferrite ratio) and the amount of secondary phase precipitation on two duplex stainless steels. This work was done to find the thermal conditions to avoid toughness depletion, which can cause premature failure of these steels.*

#### ...describe this work to a layperson?

*Stainless steels, especially the grade used in this study, suffer from lower toughness caused by secondary phase precipitation especially when these steels undergo thermal treatments. In this study the influence of thermal treatment parameters on the precipitation of these secondary phases was investigated.*

tions of ferrite and austenite, measured with image analysis on an optical microscope (OM), are, respectively, austenite =  $1\pm 4\%$  and ferrite =  $49\pm 4\%$  in SAF 2205, and austenite  $45\pm 3\%$  and ferrite  $55\pm 3\%$  in SAF 2507. These are typical values for solution-annealed samples. No secondary phases were detected with scanning electron microscopy-backscattered electron microscopy (SEM-BSE).

## Heat-Treated Samples

### Murakami and Groesbeck

At first, the capabilities of Murakami and Groesbeck reagents were tested on a group of SAF 2205 samples. In Figures 1 and 2 the OM and SEM-BSE micrographs, taken at  $1,000\times$  of the sample treated at  $850^\circ\text{C}$  for 25 min., are shown. In Figure 1, the effectiveness of Groesbeck and Murakami reagents are difficult to determine. When the secondary phases are at micrometric scale the corrosion products overestimate them. On the contrary the SEM-BSE (Figure 2) micrograph shows all the phases, and the ferrite appears darker than austenite, while the secondary phases are lighter. An SEM-BSE im-

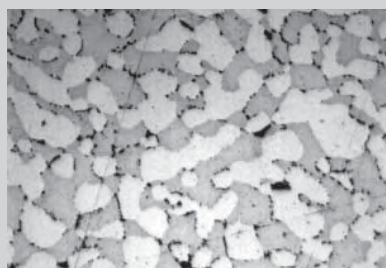


Figure 1. An OM micrograph of a sample treated at  $850^\circ\text{C}$ , 25 min., after etching with Groesbeck.

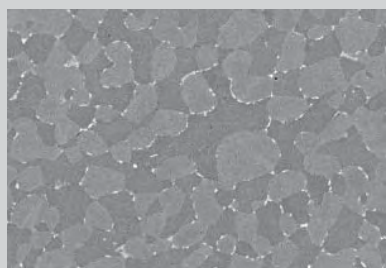


Figure 2. An SEM-BSE micrograph of a sample treated at  $850^\circ\text{C}$ , 25 min.

age at higher magnification is shown in Figure 3, in which ferrite, austenite,  $\chi$ , and  $\sigma$  are marked. The particles of  $\chi$  are brighter than  $\sigma$  as their molybdenum content is higher.

It may be concluded that the tested chemical etchants are not suitable to identify, or to accurately quantify secondary phases.

### Electrochemical Etching

The use of NaOH for 6 s, 8 s, and 10 s results in a strong etching of the grain boundaries. The presence of secondary phases is revealed with 8 s of application but the phases are not easily distinguishable from the grain boundaries, without differences between  $\chi$  and  $\sigma$ . The influence of immersion time is evident, with remarkable differences from 6 s (no secondary phases) to 8 s and 10 s. It can be concluded that NaOH is not

suitable for secondary phases measurement, as it is too affected by the immersion time. On the contrary, the immersion in modified Nital 10 results in a good detection of secondary phases, but the grain boundaries are outlined, so it is quite difficult to identify the phases with IA. Nital 10 gives a good contrast between matrix and precipitated phases: austenite is light blue, ferrite is white and all precipitated phases are dark, without any differences between  $\sigma$  and  $\chi$ . On the contrary in the SEM-BSE micrograph (Figure 2)  $\chi$  and  $\sigma$  are well identified.

The immersion in  $\text{NH}_3$  results in a strong etching of secondary phases, without any attack of grain boundaries and alloy matrix (Figure 4b). This confirms that the precipitation is mainly at grain boundaries, but no difference between  $\chi$  and  $\sigma$  was seen. On the con-

## EXPERIMENTAL PROCEDURES

The as-received materials were wrought SAF 2205 and SAF 2507 rods (30 mm) in the solution-annealed condition, with compositions reported in Table A.

Isothermal aging treatments of annealed specimens were carried out at temperatures of  $780\text{--}1,000^\circ\text{C}$  for times in the range of 5–120 min. Relatively short aging times were chosen so low amounts of secondary phases could be measured to investigate their precipitation kinetics. Continuous cooling tests were performed in a Setaram “Labsys TG” machine, in argon atmosphere. Samples (diameter 6 mm, length 8 mm) were solution treated for 5 min. at temperatures of  $1,020^\circ\text{C}$  and  $1,050^\circ\text{C}$ . The samples were then cooled in argon at various cooling rates in the range of  $0.02\text{--}0.4^\circ\text{C/s}$ . The volume fractions of ferrite and austenite in solution-treated samples were measured by image analysis on light micrographs at  $200\times$ , after etching with the Beraha reagent (room temperature [R.T.], 10 s).

Different phases were identified by scanning electron microscope (SEM) examination of unetched samples, using the backscattered electron (BSE) signal, on the basis of atomic number contrast effect: the ferrite appears slightly darker than austenite, while the secondary phases are lighter. The amounts of secondary phases were determined using image analysis software on SEM-BSE micrographs (10 fields,  $1,000\times$ ) and the contribution of each phase to total volume fractions was determined. The SEM operated at 25kV; the BSE detector was set to maximize the atomic number contrast, allowing ferrite, austenite, and secondary phases' identification. Scanning electron microscopy-electron dispersive spectroscopy determined the chemical composition of the phases on unetched samples. The secondary phases were also quantified with image analysis on optical micrographs after etching with different reagents. An investigation on the capabilities of the reagents named Murakami (aqueous solution of 10%  $\text{K}_3\text{Fe}(\text{CN})_6$  and 10% KOH) and Groesbeck (aqueous solution of 4%  $\text{KMnO}_4$ + 4% NaOH), and an electrolytic etching (Nital and concentrated solution of  $\text{NH}_3$ , 3.5 V, R.T.) was performed by etching different samples with the same reagent and the same sample with different reagents.

Instrumented Charpy-V impact specimens, after isothermal treating, were prepared in the standard form of  $10\times 10\times 55\text{ mm}^3$ . Impact testing was done at room temperature.

Table A. Chemical Composition (wt.%) of SAF 2205 and SAF 2507.

	C	Si	Mn	Cr	Ni	Mo	P	S	N	Cu	W	Fe
2205	0.03	0.56	1.46	22.75	5.04	3.19	0.025	0.002	0.160	—	—	bal
2507	0.03	0.43	0.54	24.48	6.36	4.0	0.020	0.008	0.263	0.67	0.72	bal

trary the phases are well discriminated in SEM-BSE image Figure 4a.

Thus, electrochemical etching with  $\text{NH}_3$  can be considered the best method to detect secondary phases with OM, but without any distinction between  $\chi$  and  $\sigma$ .

The capabilities of OM and SEM-

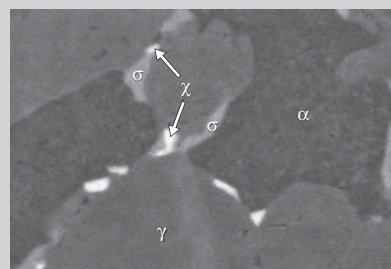
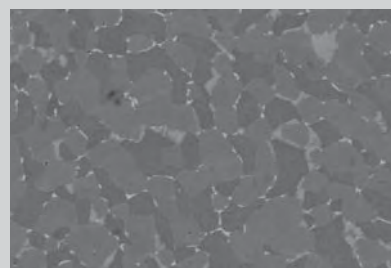


Figure 3. An SEM-BSE, high magnification image of the sample in Figure 2, with  $\chi$ ,  $\sigma$ , ferrite, and austenite.



a



b

Figure 4. (a) An SEM-BSE micrograph (900°C, 40 min.); (b) optical micrograph (900°C, 40 min.).

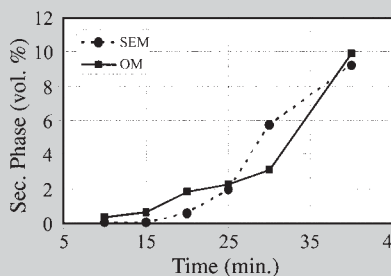


Figure 5. A match between vol. % of secondary phases measured on SEM and OM ( $\text{NH}_3$ ) micrographs (heat treatment 900°C).

BSE can be appreciated in Figure 5, where the amounts of secondary phases in the SAF 2205 as a function of holding time (temperature 900°C) is reported. In samples with a low content of secondary phases, the corrosion products enhance the boundary effect and the immersion time affects the detection of phases. The result is that at the lowest phase's contents (<1%), the OM data differ from SEM data by about 50–100%.

Pores and inclusions that may have the same gray-scale appearance as intermetallic phases may be another potential source of errors in OM images. Moreover in SEM-BSE the pores and inclusions are dark while the secondary phases are bright. They are identified as the result of the spatial distribution of elements; the uncertainty is only related to the beam resolution. The influence of secondary phases on toughness was studied through Charpy impact tests (at room temperature) (Figure 6). An attempt has been made to correlate the toughness to volume fraction of intermetallic phases since impact toughness depends on the amount and types of intermetallic phases.

In the OM data obtained on samples etched with  $\text{NH}_3$ , the discrepancy is evident, suggesting that SEM-BSE is more accurate than OM in detecting and measuring the amount of secondary phases with image analysis. The solubilized material has average impact energy of 250 J, but only 0.5% of the secondary phases, measured on SEM micrographs, reduce it to about 100 J. A further drop occurs at 1%, when the

impact energy is about 50 J, and the final severe deterioration of toughness is induced by higher values (fractions > 1.5–2%). This statement agrees with the generally accepted specification for the DSS: a phase content of less than 1% or lower to maintain the toughness value of 40–50 J.

A critical discussion of this deterioration and fracture mechanism is reported in another paper.<sup>13</sup> Starting from the discussed method capabilities and from the effects of secondary phase on toughness, the amounts of secondary phases have been measured in SAF 2205 and SAF 2507. A short summary<sup>14,15</sup> of the data is published elsewhere.

## ISOTHERMAL TREATMENT OF SAF 2205 AND SAF 2507

### Precipitation in SAF 2205

After aging at 780°C, the first precipitates were identified as  $\chi$  at high magnification (2,000–4,000x) after 1,800 s aging and become more evident after 2,400 s. The quantitative determination is not possible.

After aging at 850°C, the  $\chi$  phase appears after about 600 s, while the  $\sigma$  phase appears after about 20 min. After 30 min. the  $\chi$  phase and the  $\sigma$  phase are both present: the  $\chi$  phase is always at the ferrite/austenite and ferrite/ferrite boundaries. The  $\sigma$  phase penetrates the ferrite or grows along the ferrite/austenite boundary.

After aging at 900°C, as at 850°C, the first phase present is the  $\chi$  phase at the grain boundaries. By increasing the

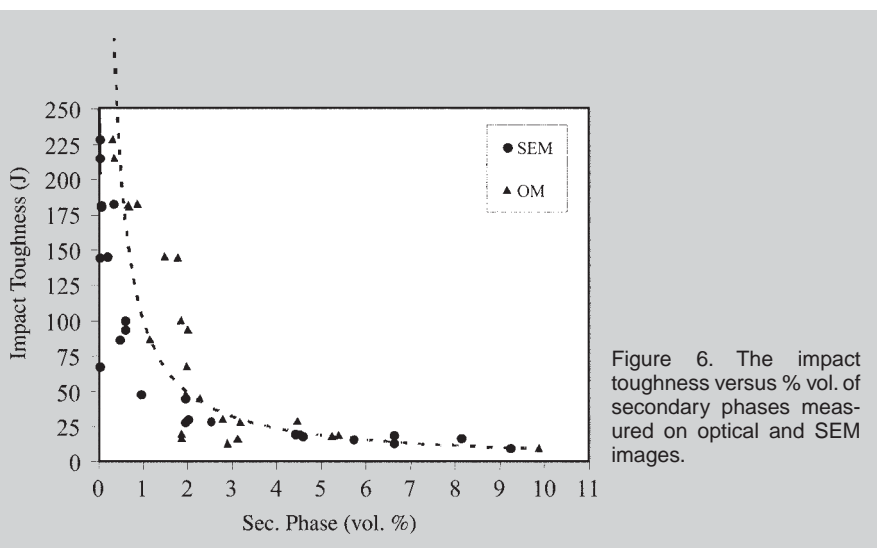


Figure 6. The impact toughness versus % vol. of secondary phases measured on optical and SEM images.

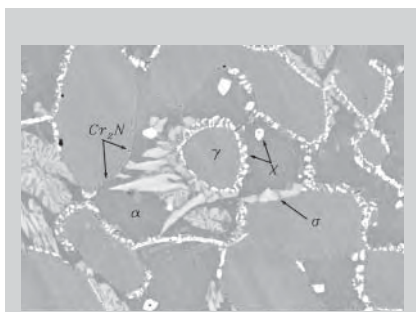


Figure 7. An SEM-BSE micrograph of the sample treated at 900°C for 2,400 s.

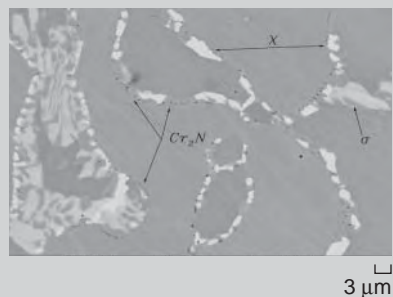


Figure 8. An SEM-BSE micrograph of the sample treated at 950°C for 4,800 s.

time, the amount of  $\chi$  phase increases and the  $\sigma$  phase also appears in the form of coarser precipitates at the  $\gamma/\alpha$  boundary, but growing into the ferrite. Although  $\sigma$  particles are, at the beginning, less numerous than the  $\chi$ -phase particles, they are coarser and grow more rapidly, quickly reaching almost the same volume fraction. By increasing the holding time, the  $\sigma$  phase grows to large particles, moving from the boundaries into the ferrite, embedding some small  $\chi$  particles. This seems to show the progressive transformation of  $\chi$  phase to  $\sigma$  phase.

### Precipitation in SAF 2507

After aging at 800°C, no precipitation was detected. When aging at 850°C, the first  $\chi$  precipitates appear after 900 s aging and become more evident after 1,200 s at boundaries and sometimes inside the ferrite grains. No  $\sigma$  phase has been detected. The small size and very low amount of the particle do not allow measurement of the volume fractions, which can be reasonably estimated to be less than 0.1%.

After aging at 900°C, the  $\chi$  phase ap-

pears after about 300 s at grain boundaries, with some isolated  $\sigma$ -phase particles. A few small dark precipitates were detected at grain boundaries, identified as  $\text{Cr}_2\text{N}$  on the basis of N peaks. After 2,400 s  $\chi$ ,  $\sigma$ , and nitrides are present:  $\chi$  phase is always at the ferrite/austenite and ferrite/ferrite boundaries (Figure 7). At this temperature the formation kinetic of  $\chi$  phase is favored.

After aging at 950°C, the first precipitates of  $\chi$  appear after 180 s, while  $\sigma$  appears after 300 s. The percentage of  $\sigma$  phase increases with time, while the percentage of  $\chi$  phase decreases after 1,800 s. Although  $\sigma$  particles are, at the beginning, less numerous than  $\chi$ -phase particles, they are coarser and grow more rapidly, quickly arriving almost to the same volume fraction. The progressive transformation of  $\chi$  to  $\sigma$ , occurring mainly after 80 min., has been noted (Figure 8). The ferrite transformation is not complete.

After aging at 1,000°C for 5 min.,  $\chi$  and  $\sigma$  have been detected mainly at grain boundaries, with a few inside the ferrite grains. The amount of each phase is about 0.5%. By increasing the time, the amount of  $\chi$  slowly decreases while the amount of  $\sigma$  increases to its maximum value after 15 minutes. Heating times longer than 20 min. can be compared to a non-complete solubilization, with a partial dissolution of the phases, and chromium, molybdenum, and tungsten in solid solution. These data confirm that the 2507 grade must be solubilized at  $T > 1,050^\circ$  if the secondary phase free structure is mandatory.

### Continuous Cooling of SAF 2205

The morphology of the phases after continuous cooling is very similar to that observed in the isothermal aging tests (the precipitation occurs at the  $\alpha/\gamma$  grain boundaries and especially at the triple points), while the formation sequence of secondary phases seems to be quite different. The total amount of secondary phases is lower for the highest solubilization temperature, in agreement with Reference 16, and strongly depends both on the cooling rates and

on the solubilization temperature. The critical cooling rate for  $\sigma$ -phase formation is 0.35°C/s, when a  $\sigma$  content of 0.2% is obtained. When the cooling rate decreases the  $\sigma$  content gradually increases and, at about 0.1–0.15°C/s, small  $\chi$ -phase particles appear. Therefore, the  $\chi$  phase forms at lower cooling rates than the  $\sigma$  phase and 0.3°C/s is the minimum cooling rate to satisfy the generally accepted toughness requirements.

## CONCLUSION

In order to study the kinetics of phase formation and their effect on fracture mechanisms the right technique to detect secondary phases in duplex stainless steels is not always the traditional one, especially when low contents of intermetallic phases are desired.

## References

1. J. Charles, *Proceedings of Duplex Stainless Steels '91* (Milano, Italy: Italian Association of Metallurgy, 1991), pp. 151–167.
2. J.O. Nilsson, *Materials Science and Technology* 8 (1992), pp. 685–700.
3. J.O. Nilsson, *Proc. 5th World Conference on Duplex Stainless Steel* (Zutphen, The Netherlands: KCI Publishing, 1997), pp. 73–82.
4. J.O. Nilsson et al., *Metallurgical and Materials Transaction A*, 27A (1996), pp. 2196–2208.
5. N. Lopez, M. Cid, and M. Piuggali, *Corrosion Science*, 41 (1991), pp. 1615–1631.
6. R.J. Johansen et al., *Proceedings of Duplex 2000* (Venezia, Italy: Italian Association of Metallurgy, 2000), pp. 405–414.
7. J. Dobranszky et al., *Spectrochimica Acta part B*, 59 (2004), pp. 1781–1788.
8. R.N. Gunn, *Proceedings of Duplex America 2000* (Zutphen, The Netherlands: KCI Publishing, 2000), pp. 299–305.
9. J. Erneman et al, *Material Science Technology*, 20 (2004), pp. 1245–1251.
10. M.A. Dominguez-Anguilar and R.C. Newman, *Corrosion Science*, 48 (2006), pp. 2560–2576.
11. J. Michalska and M. Sozanska, *Mater. Character.*, 56 (2006), pp. 355–362.
12. Y.H. Lee et al., *Material Science Technology*, 14 (1998), pp. 757–764.
13. I. Calliari, G. Straffellini, and E. Ramous, *Proceedings of international Conference on Duplex* (Grado, Italy: Italian Association of Metallurgy, 2007).
14. I. Calliari, E. Ramous, and M. Zanesco, *J. Materials Science*, 41 (2006), pp. 7643–7649.
15. I. Calliari, K. Brunelli, and E. Ramous, submitted to *Material Science and Technology*.
16. T.H. Chen and J.R. Yang, *Materials Science and Engineering*, A311 (2001), pp. 28–41.

I. Calliari, K. Brunelli, M. Dabalà, and E. Ramous are with the Department of Innovation in Mechanics and Management (DIMEG), University of Padova; via Marzolo 9, 35131 Padova, Italy. Prof. Calliari can be reached at irene.calliari@unipd.it.

# Controlling Stress and Diffusion for the Low-Temperature-Ordering of $L1_0$ Ordered FePt Films

Yun-Chung Wu, Liang-Wei Wang, C.C. Chiang, Cheng-Han Yang, and Chih-Huang Lai

*Low-temperature-ordering of  $L1_0$  ordered FePt films have been extensively studied in recent years due to its potential for future application on magnetic perpendicular media. The predominant issue of the ordering process is the diffusion of iron and platinum atoms from a disordered to an ordered phase. The diffusion can be enhanced by adjusting diffusivity, providing extra energy, or reducing energy barriers. In addition to reducing the ordering temperature of FePt, (001)-oriented granular films require perpendicular media because the magnetic easy axis of the ordered phase is [001]. Atomic-scale multilayer deposition is proposed to achieve designed film structures.*

## INTRODUCTION

$L1_0$  ordered (001) FePt has been proposed to be a promising candidate as an ultrahigh-density perpendicular recording medium due to its high magneto-crystalline anisotropy ( $K_u$ ).<sup>1</sup> However, FePt films deposited at room temperature typically require high-temperature annealing (>500°C) to obtain the  $L1_0$  phase. Although the  $L1_0$  phase of FePt is a thermodynamically stable phase at room temperature, a meta-stable disordered phase is commonly obtained while films are deposited at room temperature. This is due to the kinetic-limited process in which the energy barrier of diffusion is too high at low temperature to form the  $L1_0$  FePt phase.

In the current magnetic recording media industry, it is quite important to control the manufacture at low temperature. Namely, a reduced ordering temperature of FePt is demanded. Since diffusion is the key in the ordering process of FePt, therefore, numerous studies focus on how to accelerate the diffusion. One way to improve the dif-

fusivity of iron and platinum atoms is by adding third elements.<sup>2-5</sup> Although the ordering temperature of FePt can be effectively reduced to 300°C, the

addition of third elements leads to a reduced  $K_u$ . In previous studies, the authors tried not only to provide an extra driving force by ion irradiation<sup>6</sup> and dynamic stress<sup>7-10</sup> to accelerate the diffusion, but also to diminish the diffusion length by atomic-scale deposition to reduce the diffusion barrier.<sup>11-13</sup>

Besides an adequate manufacturing temperature, magnetic perpendicular anisotropy is required. The perpendicular anisotropy of FePt films is strongly associated with the crystalline orientation. Because the easy axis of  $L1_0$  phase is along the [001] direction, formation of the (001)-oriented  $L1_0$  phase is essential. To increase signal-to-noise ratios, a granular microstructure of FePt is preferred. The additions of amorphous  $B_2O_3$ ,  $SiO_2$ ,  $Al_2O_3$ , or MgO into FePt films are insoluble so a granular structure is formed after annealing.<sup>14-18</sup> However, the fabrication temperature of FePt granular microstructure is typically higher than 500°C.

This study demonstrates various ways, including ion irradiation, dynamic stress, PtMn underlayers, and atomic-scale multilayer deposition to reduce the ordering temperature of FePt, and reports that (001) granular  $L1_0$  FePt films can be obtained at a low ordering temperature of 350°C by inserting ultra-thin  $SiO_2$  layers in atomic-scale Fe/Pt multilayers (MLs) grown on glass or  $SiO_2/Si$  substrates.

The experimental study focused on ion irradiation, dynamic stress, PtMn underlayers, and atomic-scale multilayer deposition. The results shown here for the first three methods are for FePt with in-plane anisotropy but they can be also applied to the perpendicular FePt films as long as suitable substrates or underlayers are used. The atomic-scale multilayer deposition can achieve

### How would you...

*...describe the overall significance of this paper?*

*Ordered (001) FePt is a promising candidate as perpendicular recording medium. A high processing temperature is generally required to fabricate  $L1_0$  ordered (001) FePt, which is not feasible for manufacturing in industry. This paper proposes several ways to effectively reduce the processing temperature of FePt. It demonstrates that the  $L1_0$  ordered (001) FePt- $SiO_2$  granular films can be fabricated not only at a temperature as low as 350°C but also without an underlayer.*

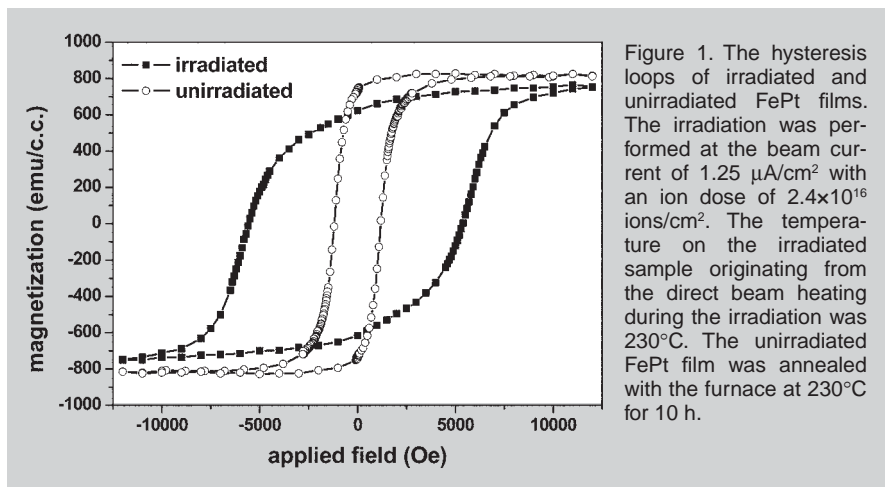
*...describe this work to a materials science and engineering professional with no experience in your technical specialty?*

*The ordering process of a disordered FePt is controlled by a kinetic process. In this paper, we propose several ways to accelerate the phase transformation at low temperature. An extra driving force for diffusion was provided by ion irradiation or dynamic stress; the diffusion length was diminished by using atomic-scale multilayer deposition. In addition, the novel sputtering scheme, atomic-scale multilayer deposition, can effectively promote the (001) texture of  $L1_0$  FePt grown on amorphous substrates without any underlayer.*

*...describe this work to a layperson?*

*To further extend the capacity of hard drives to fit future applications, a new medium material,  $L1_0$  ordered FePt, has been proposed. One of the key challenges to fabricate  $L1_0$  ordered FePt is to lower the processing temperature. This paper proposes several effective ways to reduce the processing temperature so that this material can become feasible for high-density recording media.*





(001)-oriented FePt films without underlayers.

### ION IRRADIATION

The advantages of ion irradiation are to introduce an appropriate amount of atomic species and desired energy into the films, which may create defects or lattice distortion and thus may promote phase transformation. This study found that the ordering of FePt  $L1_0$  phase can be directly induced by 2 MeV He-ion irradiation. Unlike other reports of the irradiation on magnetic films,<sup>19</sup> in which the irradiation was performed at the beam current density of the order of nA/ $\text{cm}^2$  or on the water-cooled sample stage to avoid sample heating, the beam current in this study was purposely adjusted to  $\mu\text{A}/\text{cm}^2$  scale to study the beam heating effects and the energy transfer in FePt films. FePt films of 50 nm were deposited on  $\text{SiO}_2/\text{Si}$  substrates at room temperature by using co-sputtering from elementary targets. The composition of FePt films is  $\text{Fe}_{50}\text{Pt}_{50}$ , measured by Rutherford backscattering spectrometry (RBS).

The in-plane hysteresis loop, measured by vibrating sample magnetometer (VSM), of the FePt film irradiated at the beam current of 1.25  $\mu\text{A}/\text{cm}^2$  with an ion dose of  $2.4 \times 10^{16}$  ions/ $\text{cm}^2$  is shown in Figure 1. The in-plane coercivity ( $H_{c//}$ ) of the irradiated sample is as high as 5,700 Oe. The temperature on the surface of the irradiated FePt film during irradiation was about 230°C due to direct beam heating. As shown in Figure 2, x-ray diffraction (XRD) scans reveal the evolution of the structural ordering in the irradiated FePt film. The (001) superlattice peak

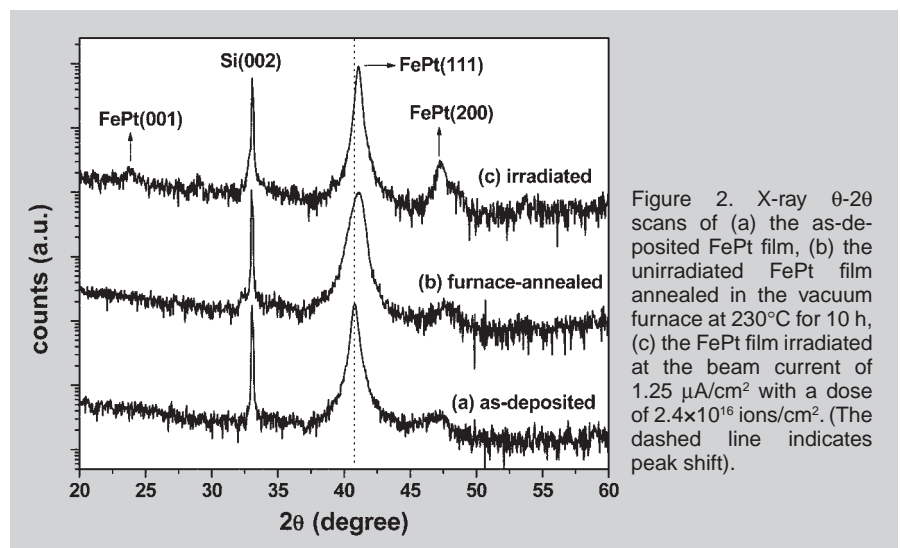
was observed after irradiation. Also, the (111) fundamental peak of the irradiated FePt film shifted toward the higher angle side, which indicates that the face-centered cubic (fcc) disordered phase has been partially transformed into the  $L1_0$  ordered phase. For comparison, an unirradiated sample was annealed using a conventional vacuum furnace at 230°C for 10 h. Ordering of FePt after conventional furnace annealing is unapparent, as shown in Figure 2, leading to a low  $H_{c//}$  of 1,200 Oe (as shown in Figure 1).

Based on the previous results, the conventional postannealing at 230°C was apparently not sufficient to provide enough energy for the ordering of FePt films. Instead, by using the ion-irradiation heating process, the energy transfer from helium ions to FePt films as well as point defects and lattice distortion induced by irradiation lead to direct ordering. The conventional annealing only provides atoms with extra ther-

mal energy to overcome the activation energy of a phase transformation. In contrast, the ion irradiation with a high beam-current density not only provides beam heating but energy transfer from incident ions. The atoms in the irradiated FePt films, therefore, have been relaxed from the original lattice points due to a succession of particle collisions and interaction. A combination of the relaxation of the ion-disturbed FePt atoms by energy transfer with the beam heating to 230°C, the mobility of the FePt atoms has been enhanced considerably. On the other hand, excess point defects such as vacancies and interstitials under the irradiation are formed with a much higher concentration than that created by conventional annealing. The excess point defects can greatly increase the diffusivity of the iron and platinum atoms. Consequently, the irradiation-enhanced diffusion promotes the ordering of irradiated FePt films.

### DYNAMIC STRESS

The previous studies strongly suggest that the tensile stress on the FePt films originating from lattice misfit between underlayers and FePt films may significantly reduce the ordering temperature of FePt. This study has shown that a low-temperature ordering of FePt can be achieved by introducing dynamic stress instead of static stress from the lattice misfit. Films with the structure of substrate/Cu (100 nm)/ $\text{Co}_{90}\text{Fe}_{10}$  (60 nm)/Pt (10 nm)/FePt (50 nm) were deposited by using a sputtering system on two kinds of substrates: Si (001)/ $\text{SiO}_2$  (200 nm) and HF-cleaned Si (001). The



latter substrate is hydrogen-terminated. The  $\text{Co}_{90}\text{Fe}_{10}$  layer was utilized to suppress the diffusion of copper into FePt due to the immiscibility of cobalt and copper at 300°C. The platinum layer was inserted to separate direct coupling between FePt and  $\text{Co}_{90}\text{Fe}_{10}$ .

The dependence of in-plane coercivity on annealing temperature for 30 min. is shown in Figure 3. The ordering temperature of FePt deposited on HF-cleaned Si (001) substrate was greatly reduced to 275°C. In addition, an  $H_{c//}$  as high as 7,000 Oe can be obtained after post-annealing at 300°C for 30 min., much greater than that of FePt deposited on Si/SiO<sub>2</sub>. This result is even much better than that obtained by the addition of copper into the FePt.<sup>2</sup> X-ray diffraction  $\theta$ -2 $\theta$  scans of annealed FePt films deposited on HF-cleaned Si (001) revealed that not only the (200) peak of copper disappeared but the extra peak of copper silicide  $\text{Cu}_3\text{Si}$  was formed after annealing.<sup>20,21</sup> On the other hand, the XRD spectra of annealed FePt samples at 300°C deposited on SiO<sub>2</sub>/Si did not show significant difference from that of the as-deposited one. Furthermore, (111) peak of the annealed FePt on HF-cleaned silicon shifted toward the high-angle side, indicating that the ordered  $\text{L1}_0$  phase of FePt was significantly enhanced on HF-cleaned Si (001) substrates. The in-plane coercivity of FePt films on HF-cleaned Si (001) substrates annealed at 275°C increased with annealing time and reached 6,200 Oe after 4 h annealing, shown in the inset of Figure 3, accompanying increased peak intensity of  $\text{Cu}_3\text{Si}$  in XRD spectra. This result is quite remarkable for the FePt

films annealed at such a low temperature.

Based on these results, the large in-plane coercivity of FePt films annealed at low temperature seems to be strongly related to the formation of the  $\text{Cu}_3\text{Si}$  phase, which may induce a favorable stress state in the FePt film to greatly reduce its ordering temperature. To investigate the effect of stress induced by the formation of  $\text{Cu}_3\text{Si}$  on the phase transformation of FePt, the in-situ stress measurement for the sample with the structure of HF-cleaned Si (001)/Cu (100 nm) was performed at a temperature ramp rate of 15°C/min. up to 300°C. As shown in Figure 4, the curvature decreased and changed to a negative value with increasing annealing temperature up to 250°C due to the development of thermal stress originating from the difference in thermal expansion coefficient between the copper film and the silicon substrate. With the annealing temperature higher than 250°C, the curvature abruptly decreases to a more negative value, that is, more convex, and the subsequent relaxation of the curvature followed. It has been reported that a metal-rich  $\text{Cu}_3\text{Si}$  phase would be the very first stage to form in the reaction of the copper film with the silicon substrate.<sup>21</sup> This reaction generally results in an increase in lattice volume which agrees with the observed negative curvature.<sup>22</sup> When the reaction starts, the sample displays a more convex curvature associated with the expanded volume due to the formation of  $\text{Cu}_3\text{Si}$ . This expanded volume induces an in-plane tensile stress and a contracted d-spacing of FePt (111) plane along

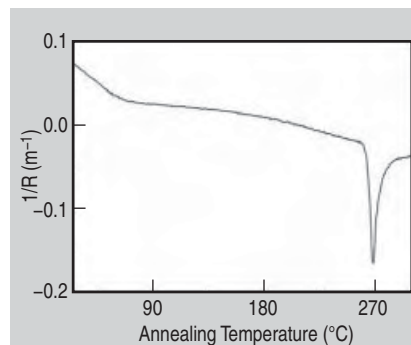


Figure 4. The in-situ stress measurement of curvature ( $1/R$ ) vs. annealing temperature for the sample with the structure of HF-cleaned Si (001)/Cu (100 nm). The measurement was performed at a temperature ramp rate of 15°C/min. up to 300°C.

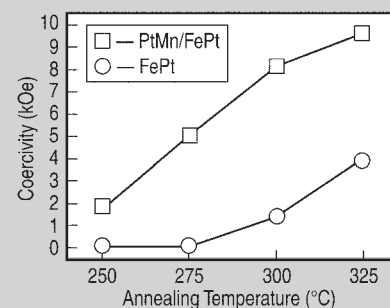


Figure 5. The in-plane coercivity dependence of annealing temperature for samples Si/SiO<sub>2</sub>/Fe 1/Pt 9/PtMn 50/FePt 50 (nm) and Si/SiO<sub>2</sub>/FePt 50 (nm).

the out-of-plane direction, accelerating the ordering process of the FePt film. The stress is significantly relaxed after the formation of  $\text{Cu}_3\text{Si}$  is completed, which might be related to the motion of copper and silicon atoms to reduce the stored strain energy. Unlike the static misfit stress originating from the lattice mismatch between FePt films and substrates (or underlayers),<sup>23-25</sup> the stress induced by the  $\text{Cu}_3\text{Si}$  phase is dynamic and varies with the evolution of  $\text{Cu}_3\text{Si}$  formation.

## PtMn UNDERLAYER EFFECT

The ordered phase of antiferromagnetic (AFM) PtMn is also  $\text{L1}_0$  phase. The typical annealing temperature to achieve the ordered phase of PtMn (250°C)<sup>26</sup> is much lower than the ordering temperature of FePt (500°C), and the  $c/a$  ratio of PtMn is 0.92 which is lower than the ratio of FePt (0.96).<sup>27</sup> The  $a$ -axis lattice constants of the ordered PtMn and FePt are 0.40 nm and 0.387 nm, respectively. The larger lattice constants and lattice deformation during phase transformation of PtMn

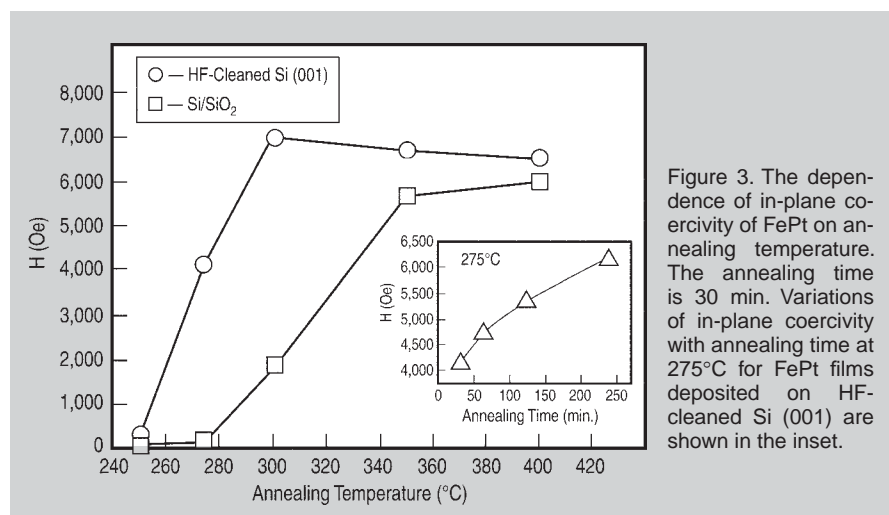


Figure 3. The dependence of in-plane coercivity of FePt on annealing temperature. The annealing time is 30 min. Variations of in-plane coercivity with annealing time at 275°C for FePt films deposited on HF-cleaned Si (001) are shown in the inset.

may promote the ordering of FePt at reduced temperature. Moreover, because of the lower  $L1_0$  ordering temperature of PtMn, PtMn is expected to be an ideal underlayer to induce ordering of the  $L1_0$  FePt phase at low temperature, as reported in the AuCu/FePt case.<sup>9</sup>

FePt films were co-sputtered from elemental targets at room temperature with a structure of Si//SiO<sub>2</sub>/Fe (1 nm)/Pt (9 nm)/PtMn (50 nm)/FePt (10–50 nm). The iron and platinum underlayers were used to enhance the PtMn and FePt (111) textures. Highly oriented (111) textures of PtMn and FePt films were obtained in the as-deposited state. The dependence of in-plane coercivity on the annealing temperature for 50 nm FePt with or without PtMn underlayers is shown in Figure 5. Field-annealed (in-plane field of 3,000 Oe) FePt films grown on PtMn underlayers show much higher in-plane coercivity than FePt films alone. Notice that  $H_{c,||}$  can reach 1,800 Oe just after 250°C annealing and be increased to 5,000 Oe after 275°C annealing. The  $H_{c,||}$  of 50 nm FePt on a PtMn underlayer annealed at 325°C is as high as 9,700 Oe. The PtMn underlayers clearly show enhanced in-plane coercivity at low-temperature annealing. Figure 6 shows the XRD results of the as-deposited and annealed FePt (50 nm) films with or without PtMn underlayers. Samples were annealed in vacuum at 300°C for two hours. For single-layer FePt, there is no major change before and after annealing, indicating a low degree of ordering. On the contrary, for the FePt films grown on PtMn underlayers, both of the (111) peaks of FePt and PtMn shift to higher angles after annealing,

indicating that phase transformation of FePt and PtMn occur during annealing. This result suggests that the ordering of PtMn at a low temperature accelerates the ordering of FePt. When the annealing temperature reaches the ordering temperature of PtMn, the a-axis of PtMn is expanded and the c-axis is compressed. These lattice changes of the PtMn layer may induce the corresponding changes of the disordered FePt lattice, which promotes the ordering of FePt at reduced temperatures.

### ATOMIC-SCALE MULTILAYER DEPOSITION

In previous sections, this paper proposed several ways to reduce the ordering temperature of FePt. However, since specific underlayers were not used to promote (001) texture, the FePt films show a large coercivity in the in-plane direction. To achieve ultra-high-density perpendicular recording media, a granular FePt film with (001)-preferred orientation is needed. This section proposes a way to reduce the ordering temperature as well as promote the (001)-preferred orientation. In the  $L1_0$  phase, the atomic arrangement of iron and platinum along [001] direction is like atomic-scale Fe/Pt multilayers (MLs). Since the perpendicular anisotropy of FePt films is strongly associated with the formation of the (001)-oriented  $L1_0$  phase, the fabrication of FePt films by annealing atomic-scale Fe/Pt MLs may not only effectively reduce the ordering temperature of FePt, but promote the perpendicular anisotropy.

Sequential planetary sputtering of atomic-scale [Fe/Pt]<sub>18</sub> (sample “A”) and [Fe/Pt/SiO<sub>2</sub>]<sub>18</sub> (sample “B”) MLs

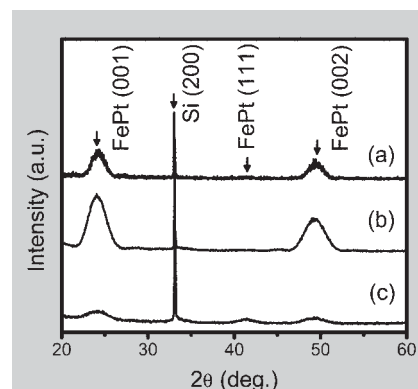


Figure 7. X-ray diffraction ( $\theta$ - $2\theta$  scans) of (a) sample A annealed at 400°C (b) sample B annealed at 350°C and (c) sample A annealed at 350°C. The annealing time is 60 s. The film structures of sample A and sample B are [Fe/Pt]<sub>18</sub> and [Fe/Pt/SiO<sub>2</sub>]<sub>18</sub>, respectively.

were performed on glass or SiO<sub>2</sub> (200 nm)/Si substrates at ambient temperature. The thickness of each iron and platinum layer in MLs was kept at 0.16 nm and 0.18 nm, similar to the thickness of a single atomic layer. The thickness of each SiO<sub>2</sub> layer was 0.56 nm. The nominal thickness of Fe<sub>55</sub>Pt<sub>45</sub> (excluding the thickness of SiO<sub>2</sub>) in each sample was fixed at 6.1 nm.

Sample “A” was annealed at 400°C for 60 s. The x-ray  $\theta$ - $2\theta$  scan, shown in Figure 7a, reveals two clear ordered peaks of  $L1_0$  FePt (001) and (002), which implies that alternate depositions of atomic-scale iron and platinum MLs can effectively induce the growth of (001)-oriented ordered FePt phase without underlayers at relatively low temperature. The sample exhibited a large out-of-plane coercivity ( $H_c$ ) of 8,400 Oe. The annealing temperature of 400°C is quite low for 6.1 nm FePt films because thinner FePt films typically require higher annealing temperatures to achieve the  $L1_0$  phase. It has been reported that a relatively high annealing temperature of 550°C is needed for [Fe/Pt]<sub>n</sub> multilayers of 6 nm.<sup>28</sup> Compared to the previous report, the thickness of each iron and platinum layer is thinner in the MLs; therefore, the diffusion length in this case can be significantly reduced, decreasing the ordering temperature.

To achieve a granular structure of FePt, samples with the structure of [Fe/Pt/SiO<sub>2</sub> (0.56 nm)]<sub>18</sub> (sample “B”) were deposited. After annealing the sample at 350°C for 60 s., the XRD spectrum,

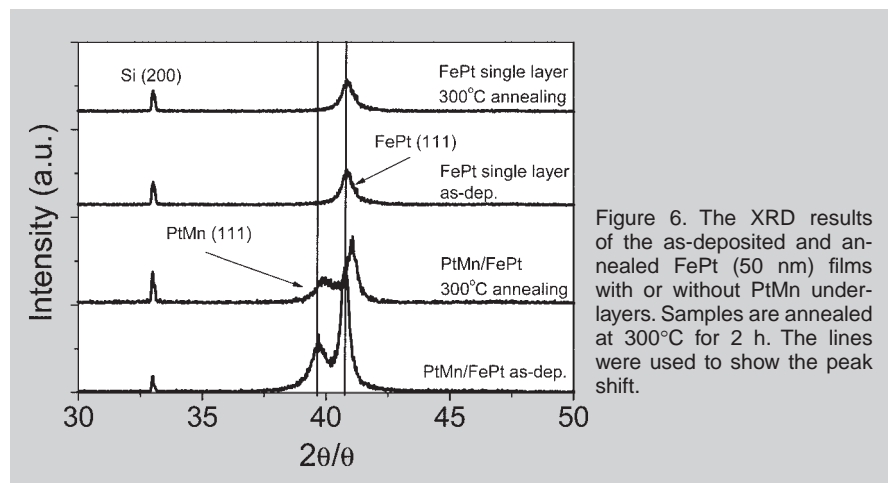


Figure 6. The XRD results of the as-deposited and annealed FePt (50 nm) films with or without PtMn underlayers. Samples are annealed at 300°C for 2 h. The lines were used to show the peak shift.

lic of China under Grant No. NSC-97-2622-E-007-002 and by the Ministry of Economic Affairs of Republic of China under Grant No. 97-EC-17-A-08-S1-006.

## References

- O.A. Ovanov, L.V. Solina, and V.A. Demshina, *Phys. Met. Metallogr.*, 35 (1973), p. 81.
- T. Maeda et al., *Appl. Phys. Lett.*, 80 (2002), p. 2147.
- Q. Yan et al., *Adv. Mater.*, 17 (2005), p. 2233.
- C.H. Lai, Y.C. Wu, and C.C. Chiang, *J. Appl. Phys.*, 97 (2005), p. 10H305.
- C.H. Lai and C.H. Ho, *J. Appl. Phys.*, 97 (2005), p. 10J314.
- C.H. Lai, C.H. Yang, and C.C. Chiang, *Appl. Phys. Lett.*, 83 (2003), p. 4550.
- C.H. Lai et al., *Appl. Phys. Lett.*, 85 (2004), p. 4430.
- C.H. Lai, C.C. Chiang, and C.H. Yang, *J. Appl. Phys.*, 97 (2005), p. 10H310.
- Y. Zhu and J.W. Cai, *Appl. Phys. Lett.*, 87 (2005), p. 032504.
- C.C. Chiang, C.H. Lai, and Y.C. Wu, *Appl. Phys. Lett.*, 88 (2006), p. 152508.
- Y.C. Wu, L.W. Wang, and C.H. Lai, *Appl. Phys. Lett.*, 91 (2007), p. 072502.
- Y.C. Wu et al., *J. Appl. Phys.*, 103 (2008), p. 07E126.
- Y.C. Wu, L.W. Wang, and C.H. Lai, *J. Appl. Phys.*, 103 (2008), p. 07E140.
- C.P. Luo et al., *Appl. Phys. Lett.*, 77 (2000), p. 2225.
- C.P. Luo and D.J. Sellmyer, *Appl. Phys. Lett.*, 75 (1999), p. 3162.
- M. Watanabe et al., *Appl. Phys. Lett.*, 76 (2000), p. 3971.
- Y. Peng, J.-G. Zhu, and D.E. Laughlin, *J. Appl. Phys.*, 99 (2006), p. 08F907.
- K. Kang et al., *Appl. Phys. Lett.*, 84 (2004), p. 404.
- D. Ravelosona et al., *Appl. Phys. Lett.*, 76 (2000), p. 236.
- C.A. Chang, *J. Appl. Phys.*, 67 (1990), p. 566.
- A. Cros, M.O. Aboelfotoh, and K.N. Tu, *J. Appl. Phys.*, 67 (1990), p. 3328.
- P.P. Buaud et al., *J. Vac. Sci. Technol. B*, 11 (1993), p. 304.
- Y.N. Hsu et al., *J. Appl. Phys.*, 89 (2001), p. 7068.
- Y. Xu, J.S. Chen, and J.P. Wang, *Appl. Phys. Lett.*, 80 (2002), p. 3325.
- Y.C. Wu et al., *IEEE Trans. Magn.*, 41 (2005), p. 3199.
- A. Maesaka, S. Ishii, and A. Okabe, *J. Appl. Phys.*, 88 (2000), p. 3982.
- Y.Q. Gao, Z.M. Wang, and S.H. Whang, *Mater. Sci. Eng. A*, 192/193 (1995), p. 53.
- H. Zeng et al., *Appl. Phys. Lett.*, 80 (2002), p. 2350.
- Y.M. Chiang, D.P. Birnie III, and W.D. Kingery, *Physics Ceramics* (New York: J. Wiley, 1997), pp. 357–358.
- J.-S. Kim, Y.-M. Koo, and B.-J. Lee, *J. Appl. Phys.*, 99 (2006), p. 053906.

Yun-Chung Wu, Liang-Wei Wang, C.C. Chiang, Cheng-Han Yang, and Chih-Huang Lai are with the Department of Materials Science and Engineering, National Tsing Hua University, Hsinchu 30013, Taiwan. Dr. Lai can be reached at [chlai@mx.nthu.edu.tw](mailto:chlai@mx.nthu.edu.tw).

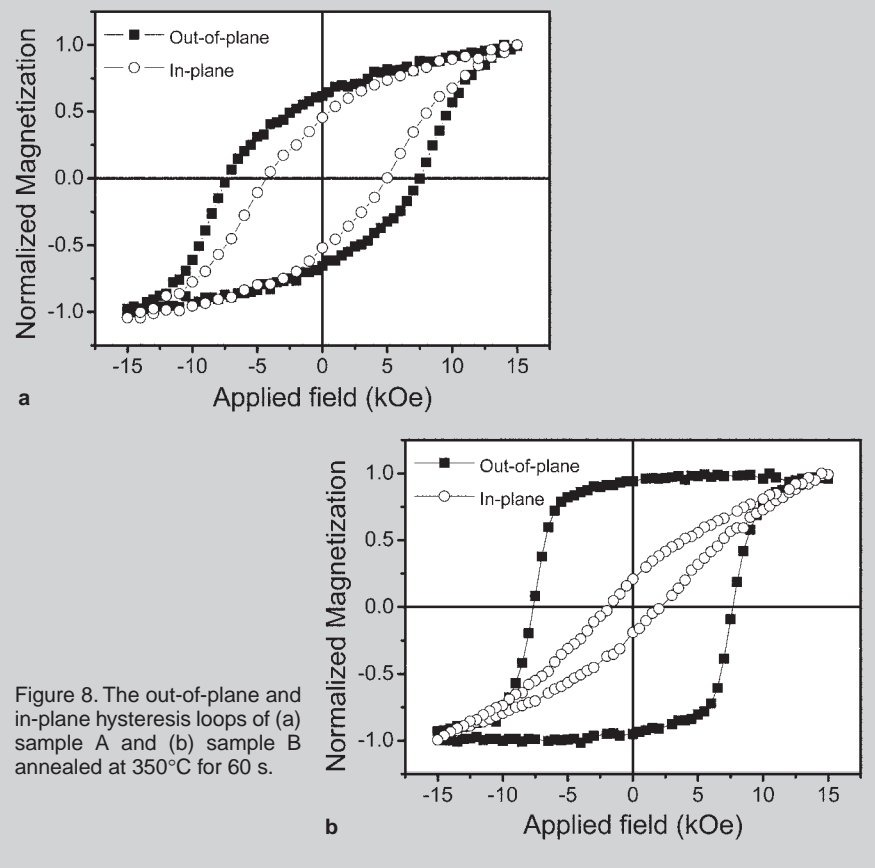


Figure 8. The out-of-plane and in-plane hysteresis loops of (a) sample A and (b) sample B annealed at 350°C for 60 s.

shown in Figure 7b, shows a distinct enhanced intensity of ordered FePt (001). For comparison, the spectrum of sample A annealed at 350°C for 60 s is also shown in Figure 7c. A substantial reduction of ordered peak was revealed. These results clearly indicate that the insertion of ultra-thin SiO<sub>2</sub> layer in atomic-scale Fe/Pt MLs can further reduce the ordering temperature. The hysteresis loop of samples A and B annealed at 350°C for 60 s were shown in Figure 8. Sample B exhibits high perpendicular anisotropy, compared to sample A, which is consistent with the results of x-ray  $\theta$ -2 $\theta$  scans, shown in Figure 7.

The plane-view bright-field TEM image of sample B demonstrates a clear granular structure. The average grain size of FePt is  $5.14 \pm 0.75$  nm. During the annealing process, the insolubility between SiO<sub>2</sub> and FePt induced SiO<sub>2</sub> segregation at grain boundaries, lead-

ing to the formation of the granular structure. Moreover, the surface energy of amorphous SiO<sub>2</sub> ( $\sim 300$  ergs/cm<sup>2</sup>)<sup>29</sup> is much smaller than that of crystalline FePt ( $\sim 2,100$  ergs/cm<sup>2</sup>).<sup>30</sup> The difference of surface energy between SiO<sub>2</sub> and FePt further provides a driving force for SiO<sub>2</sub> to diffuse into grain boundaries to reduce the interfacial energy. The results of this study reveal that not only was the granular microstructure achieved by the insertion of SiO<sub>2</sub> layers, but the ordering temperature was further reduced to 350°C. It is plausible that the diffusion of SiO<sub>2</sub> from grains to grain boundaries (or free surface) may significantly accelerate the diffusion of iron and platinum atoms; therefore, the ordering process of FePt can take place at low temperature.

## ACKNOWLEDGEMENT

This work was partially supported by the National Science Council of Repub-

## UPCOMING EDITORIAL TOPICS

### THEME: Energy

<b>April 2009</b>	Energy and Environmental Issues in Manufacturing Industries	Materials in Clean Power Systems	Global Innovations in Materials and Technologies for Energy	Manuscripts Deadline: <b>Deadline Past</b>
-------------------	---	----------------------------------	---	---

### THEME: Process Optimization and Modeling

<b>May 2009</b>	Aluminum: Bauxite-Alumina-Carbon-Reduction	Titanium: Modeling Alloys and Processes	Coupled Models of Materials Processes	Magnesium: Phase Diagrams and Solidification—Part II	Manuscripts Deadline: <b>February 2, 2009</b>
-----------------	--	---	---------------------------------------	--	--

### THEME: Electronic Materials

<b>June 2009</b>	Multi-Physics Transport Phenomena at Thin Films and Interfaces	Lead-Free Soldering and Reliability of Interconnects in Electronic Packages	Spintronic Materials and Devices	Manuscripts Deadline: <b>March 2, 2009</b>
------------------	--	---	----------------------------------	---

### THEME: High-Temperature Materials

<b>July 2009</b>	Materials Degradation and Life-Extension Issues in Light- and Boiling-Water Reactors	High-Temperature Oxidation-Resistant Alloys: Recent Developments in Science and Applications	Current Topics in Refractory Metals Research	Manuscripts Deadline: <b>April 1, 2009</b>
------------------	--	--	--	---

### THEME: Light Metals Fabrication

<b>August 2009</b>	Aluminum: Shaping and Forming	Magnesium Sheet: Strip Casting, Hot Rolling, and Formability	Manuscripts Deadline: <b>May 1, 2009</b>
--------------------	-------------------------------	--	---

### THEME: Biomaterials

<b>September 2009</b>	Biomedical Materials and Devices	Articulation of Surfaces for Bio Applications	Manuscripts Deadline: <b>June 1, 2009</b>
-----------------------	----------------------------------	---	--

## HOW TO SUBMIT A PAPER TO JOM

**JOM offers its contributors a variety of formats for articles that fall within the technical calendar topics. These formats include, but are not limited to:**

- **Overview:** 4–8 printed pages (3,200–6,400 words). A well-referenced and well-illustrated introduction to the issues affecting and recent developments occurring in a topical technology. The purpose is to thoroughly introduce the general reader to the specifics of the field.
- **Research Summary:** 3–5 printed pages (2,400–4,000 words). These papers outline recent, technically in-depth investigations in materials science and technology.
- **Applied Technology:** 2–4 printed pages (1,600–3,200 words). These articles communicate information about advancements in commercial products or processes and are typically submitted by industrial sources.
- **Design:** 2–4 printed pages (1,600–3,200 words). These articles emphasize the application of the design process in the development of a material system, process, or product.
- **Testing and Analysis:** 2–4 printed pages (1,600–3,200 words). These articles emphasize the application of analytical techniques in the study of the properties and/or performance of a material.
- **Opinion:** 1–2 printed pages (800–1,600 words). Qualified commentary by a recognized expert on a topical or controversial issue.
- **Nontechnical Feature:** 2–4 printed pages (1,600–3,200 words). These articles examine pertinent issues in education, professional affairs, and industry economics.
- **Conference Reviews:** 1–4 printed pages (800–3,200 words). These articles are synopses of technical presentations at major conferences or symposia.
- **Industrial Insight:** 2–5 printed pages (1,600–3,200 words). An experience-driven description of the economic, managerial, environmental, engineering, scientific, governmental, international, competitive, etc., factors that influence technology on an industrial scale.
- **Archaeotechnology:** 2–4 printed pages (1,600–3,200 words). These articles explore materials usage and development throughout history.

Authors should formally notify the editor of their publishing intent by submitting a 300-word abstract by completing the on-line form. An electronic abstract submission form is available at [www.tms.org/pubs/journals/JOM/abstract-author.html](http://www.tms.org/pubs/journals/JOM/abstract-author.html). Anyone wishing to publish in JOM should follow the guidelines established in the JOM Author Kit. This material, supplied on request, features detailed information on communication, manuscript preparation, and publication procedures. A slightly abridged version of the Author Kit is available on the World Wide Web at [www.tms.org/pubs/journals/jom/authorguide.html](http://www.tms.org/pubs/journals/jom/authorguide.html).

### For More Information Contact:

JOM, 184 Thorn Hill Road, Warrendale, PA 15086  
Telephone (724) 776-9000 ext. 228 • Fax (724) 776-3770 • e-mail [jom@tms.org](mailto:jom@tms.org)

**Symposia Proposals and Abstract Submissions:** For TMS-sponsored meetings, symposia proposals and abstracts must be submitted through ProgramMaster, the on-line TMS conference and proceedings management system. The system can be accessed at [www.tms.org](http://www.tms.org). Using the Meetings & Events pulldown menu, select the Upcoming TMS Meeting for which you wish to submit symposia proposal or an abstract, and follow the on-line instructions. The society especially encourages the submission of "hot-topic" symposia or special-session proposals on timely or developing subjects. To advance an idea, use the symposium creation form in ProgramMaster. Additional information can be acquired from the TMS Technical Support Services Department, 184 Thorn Hill Road, Warrendale, PA 15086; (724) 776-9000, ext. 212; fax (724) 776-3770.

#### TMS 2009 Annual Meeting

February 15–19, 2009  
San Francisco, California

The 138th TMS Annual Meeting & Exhibition will bring together more than 3,800 business leaders, engineers, scientists, and other professionals in the materials field for an outstanding exchange of technical knowledge leading to solutions in the workplace and in society. TMS 2009 will also include the International Peirce–Smith Converting Centennial Symposium. Commemorating the invention of the cylindrical converter, this symposium will address process issues in converting copper and nickel and include plenary speakers and a panel discussion. Other symposia topics include: three-dimensional materials science, aluminum technologies (primary), biomaterials, computational materials engineering, extractive metallurgy, magnesium technologies, nanomaterials, titanium technologies, and many more. **Contact:** TMS Meeting Services, 184 Thorn Hill Road, Warrendale, PA 15086; (724) 776-9000, ext. 243; e-mail: [mtgserv@tms.org](mailto:mtgserv@tms.org); [www.tms.org/Meetings/Annual-09/AnnMtg09Home.html](http://www.tms.org/Meetings/Annual-09/AnnMtg09Home.html).

#### 5th International Materials Symposium — MATERIAiS 2009

April 5–8, 2009  
Lisbon, Portugal

The conference will address all classes of materials, focusing on the latest advances in theory, modeling, simulation, characterization, processing, and industrial applications. The following topics are planned: effects only present at the nanoscale; molecularly engineered materials; crystallography, defects associated with crystal structures and their relation to physical properties; high temperature materials; materials for civil engineering applications; non-crystalline materials, including oxide, non-oxide, and

metallic glasses; integration of materials into biological systems; structural integrity: corrosion, damage, fatigue, and wear; evaluation of performance in condition simulating applications; advances in surface science and analysis methods; and others. Full-length papers received before March 1, 2009 will be published in a proceedings CD, which will be distributed to all participants. Select papers will be considered for publication in *Materials Science Forum*. **Contact:** Carlos Anjinho; Instituto Superior Tecnico; Department of Materials Engineering, av. Rovisco Pais, Lisbon 1049-001, Portugal; +351-218-418-135; e-mail: [materiais2009@ist.utl.pt](mailto:materiais2009@ist.utl.pt); [www.demat.ist.utl.pt/materiais2009](http://www.demat.ist.utl.pt/materiais2009).

#### 2009 Offshore Technology Conference—OTC.09

May 4–7, 2009  
Houston, Texas

The 2009 Offshore Technology Conference (OTC.09) is the premier offshore industry event for professionals, service industries, and suppliers to gather and discuss common issues of ocean resource development. Technological innovations and forums on economic, social, and political aspects of resource development and environmental protection have been the mainstay of this worldwide conference. This year's technical program will include such topics as: alternative energy, decommissioning, drilling technology, facilities and production operations, flow assurance, harsh environments, materials technology, ocean engineering resources, and many others. The Distinguished Achievement Awards will also be given to recognize individuals and companies that have made outstanding contributions to the offshore industry. These accomplishments represent breakthroughs, innovation, and technology enhancements, including the design, development, and construction of tools, equipment, technical services, vessels, instrumentation, and/or outstanding humani-

tarian and leadership service or contributions to environmental efforts. **Contact:** Meeting Services, Offshore Technology Conference, 222 Palisades Creek Drive, Richardson, TX 75083; (972) 952-9494; e-mail: [services@otcnet.org](mailto:services@otcnet.org); [www.otcnet.org/2009/](http://www.otcnet.org/2009/).

#### International Deep Drawing Research Group Conference —IDDRG 2009

June 1–3, 2009  
Golden, Colorado

IDDRG conferences bring together production specialists, researchers, and academics from all over the world for presentations on relevant and challenging technical topics in sheet metal forming. The conference is designed to provide ample opportunity for interactions and discussions. The special theme for the IDDRG 2009 Conference is Material Property Data for More Effective Numerical Analysis, with such topics as: test methods to determine properties for all aspects of constitutive equations; fitting experimental data to constitutive equations; new constitutive equations supported by experimental data; failure criteria supported by experimental evidence; nature of and failure of sheared edges; and testing of die materials including coatings with respect to friction and die wear. Conference topics include all aspects of sheet metal forming and related material properties normally covered at IDDRG conferences and may include: forming characteristics of new materials; innovative or improved forming processes; numerical modeling, simulation and optimum design; robust stamping processes; and rapid prototyping. Attendees will tour the ball can making plant, which demonstrates a high-speed, multi-stage, complex forming process for sheet metal forming. Copies of the proceedings in book and CD format will be available at the start of the conference. **Contact:** Chester Van Tyne; Colorado School of Mines; Department of Metallurgy

& Materials Engineering, Golden, CO 80401; (303) 273-3793; e-mail: iddrg2009@mines.edu; [iddrg2009.mines.edu/](http://iddrg2009.mines.edu/).

### **Electronic Materials Conference 2009—EMC 2009**

*June 24–26, 2009  
University Park, Pennsylvania*

Electronic materials are defined as relating to, produced, or operated by the controlled flow of electrons through a semiconductor, gas, or free space along with those relating to devices, systems, or circuits that employ components such as vacuum tubes, integrated circuits, or transistors in their design. The TMS Electronic Materials Conference is the premier annual forum on the preparation and characterization of electronic materials. Attendees include individuals actively engaged or interested in electronic materials R&D. This conference presents both invited and contributed oral presentations, an exhibition, and related activities. **Contact:** TMS Meeting Services, 184 Thorn Hill Road, Warrendale, PA 15086; (724) 776-9000, ext. 243; e-mail: [mtgserv@tms.org](mailto:mtgserv@tms.org); [www.tms.org/Meetings/Specialty/emc09/home.html](http://www.tms.org/Meetings/Specialty/emc09/home.html).

### **European Metallurgical Conference 2009**

*June 28–July 1, 2009  
Innsbruck, Austria*

The European Metallurgical Conference 2009 is a platform for the exchange of new ideas between the European and Overseas Metallurgical Communities, as well as a recognized source for mutual professional information. The conference focuses on new achievements from research, the implementation of innovative processes, and trends in production in the field of extractive non-ferrous metallurgy. This year's conference highlights concepts for energy savings and improved overall process efficiencies. The topics of this conference will be of particular interest to metal producers, engineering companies, equipment manufacturers, academic communities, and the consulting business. The following topics will be presented: resources availability, utilization, and conservation; advances in the winning and refining of non-ferrous base-, light-, precious-, and minor metals; downstream manufacturing and novel applications; energy constraints, savings, and alternative energies; consolidation in the non-ferrous

metal industry structures for improved competitiveness; sustainability considerations: economic, ecological, and political aspects; and others. One-day pre-conference field trips to recycling facilities and high-tech factories in Austria are planned along with several comprehensive post-conference tours to base- and light metals operations in Austria and Germany. **Contact:** Conference Organizer; GDMB Gesellschaft für Bergbau, Metallurgie, Rohstoff- und Umwelttechnik; P.O. Box 10 54, 38668 Clausthal-Zellerfeld, Germany; +49-5323-93790; e-mail: [emc@gdmb.de](mailto:emc@gdmb.de); [www.emc.gdmb.de/](http://www.emc.gdmb.de/).

### **Engineering Solutions for Sustainability: Materials and Resources, An International Workshop**

*July 22–24, 2009  
Lausanne, Switzerland*

With impending and burgeoning societal issues affecting both developed and emerging nations such as India and China, the global engineering community has a responsibility and an opportunity to truly make a difference and contribute. This workshop will focus on what materials and resources are integral to meeting basic societal needs in critical areas such as: energy, transportation, housing, food and water, recycling, and health. Presentations will focus on the engineering answers for cost-effective, sustainable pathways, the strategies for effective use of engineering solutions, and the role of the global engineering community. The Workshop Objectives include: share perspectives on the major engineering challenges that face our world today; identify, discuss, and prioritize engineering solution needs in each area; and establish how these fit into developing global-demand pressures for materials and human resources. **Contact:** Michele Gottwald, AIME, P.O. Box 270728, 8307 Shaffer Parkway, Littleton, CO 80127; (303) 948-4256; e-mail: [gottwald@aimehq.org](mailto:gottwald@aimehq.org); [www.spe.org/events/aime](http://www.spe.org/events/aime).

### **14th International Conference on Environmental Degradation in Nuclear Power Systems**

*August 23–27, 2009  
Virginia Beach, Virginia*

The safe and efficient operation of nuclear plants is a necessity for long-term power production without increased global carbon burden. Materials technology is a key foun-

ation upon which the nuclear technology of today prospers and the technology of tomorrow will succeed. Environmentally-induced materials degradation represents a significant fraction of materials related problems in today's nuclear power plant operation. Under extended lifetimes of 60, 80, or more years, understanding materials degradation will be even more important as these issues are of concern for both economic and safety considerations. Understanding today's materials problems is also critical for the future in advanced light water reactors as well as fusion reactors. The purpose of this conference is to foster an exchange of ideas about such problems and their remedies in nuclear power plants with water coolants of today and the future. **Contact:** Todd Allen; University of Wisconsin; 1500 Engineering Drive, Madison, WI 53706; (608) 265-4063; e-mail: [allen@engr.wisc.edu](mailto:allen@engr.wisc.edu); [www.ans.org/meetings/index.cgi?c=t#envdeg09](http://www.ans.org/meetings/index.cgi?c=t#envdeg09).

### **Conference of Metallurgists (COM 2009) Nickel-Cobalt 2009**

*August 23–26, 2009  
Sudbury, Ontario, Canada*

This conference promises to be a major international event. Key topics include hydrometallurgical processing; mineral processing; pyrometallurgical processing; economics and markets; electrowinning and electrorefining; environment, health and safety; and management and human resource issues. Also planned is an excellent selection of short courses, industrial courses, and social activities. **Contact:** Nathan Stubina; Barrick Gold Corporation, Suite 3700, 161 Bay Street, Toronto, Ontario, Canada M5J 2S1; (416) 307-7455; e-mail: [nstubina@barrick.com](mailto:nstubina@barrick.com); [www.metsoc.org/com2009](http://www.metsoc.org/com2009).

### **Thermec'2009: Sixth International Conference on Advanced Materials and Processes**

*August 25–29, 2009  
Berlin, Germany*

Thermec'2009 will cover all aspects of advanced materials processing, fabrication, structure/property relationships, and engineering applications of both ferrous and non-ferrous materials including advanced materials for biomedical applications, automotive vehicle materials, nanostructured materials, aerospace materials, and other advanced materials. Topics to be

covered include: alloys of Al, Mg, Ti, Fe-C and FeCNi; nanostructured materials; composites; intermetallics; bulk metallic amorphous materials; high-temperature/superalloys; intelligent/smart materials; and powder metallurgy/particulate materials. Special sessions will be devoted to fuel cells/hydrogen technologies, severe plastic deformation, surface engineering/coatings, modelling and simulation, texture, residual stresses, welding and joining, and thin films. **Contact:** Prof. Tara Chandra; University of Wollongong, Faculty of Engineering, Wollongong 2522, Australia; +61-242-213-008; e-mail: tara@uow.edu.au; *thermec.uow.edu.au/*.

### Defect Recognition Image Processing (DRIP) XIII

September 13–17, 2009  
Wheeling, West Virginia

For more than 20 years, DRIP conferences have focused on all aspects of defects in semiconductors including point, line, planar, and volume defects studied by a variety of techniques. This comprehensive approach has allowed for a discussion of the multifaceted effects of growth, processing, and device fabrication and their interrelationships. As the semiconductor technology has matured, so have the techniques for detection, identification, and imaging of defects. Decreasing feature size, increasing wafer size and purity level, reduction of layer thickness, and introduction of new materials have presented new challenges at every stage of semiconductor technology development. This evolution of the field continues today, and the new challenges will be the focus of DRIP XIII. **Abstracts are due March 15, 2009.** **Contact:** TMS Meeting Services, 184 Thorn Hill Road, Warrendale, PA 15086; (724) 776-9000, ext. 243; e-mail: mtgserv@tms.org; *www.tms.org/meetings/specialty/drip09/home.html*.

### 2009 International Symposium on Liquid Metal Processing and Casting

September 20–23, 2009  
Santa Fe, New Mexico

The objective of this symposium is to bring together academic and industrial researchers in the area of liquid metal processing and casting and provide an international forum for presenting and discussing the latest advances and research in these areas.

The scope of the symposium covers the following topic areas: primary and secondary melt processing including VIM, VAR, ESR, EBCHR, and PAM; physical property measurements of liquid metals; refining, evaporation, and gas/metal reactions; casting and solidification of ingots, and mechanisms for defect formations during the casting and solidification process; modeling of metallurgical processes, including heat/mass flow modeling of liquid metal and solidification; ceramic, slag, and refractory reactions with liquid metals; fundamentals of reactions involving liquid metals in production processes; and direct forming of parts from liquid metals. **Abstracts are due January 15, 2009.** **Contact:** TMS Meeting Services, 184 Thorn Hill Road, Warrendale, PA 15086; (724) 776-9000, ext. 243; e-mail: mtgserv@tms.org; *www.tms.org/Meetings/Specialty/LMPC/home.aspx*.

### 5th International Conference on Science and Technology of Ironmaking (ICSIT'09)

October 19–22, 2009  
Shanghai, China

The rapid growth of the steel industry has resulted from accelerating economic development worldwide, which is demanding the steel industry to afford more and better steel products. In the 21st century, the steel industry worldwide must aim at greater efficiency, higher productivity, better quality, and more economical utilization of natural resources, that takes into account the need for sustainable development. The task confronting us now is in supporting the development of world economy and to ensure emission control releasing the impact on global environment. The International Congress on Science and Technology of Ironmaking has been consistently providing an excellent venue to discuss and find solutions for ironmaking industry to the global problem. The Fifth Congress ICSTI'09 will cover such topics as the preparation and handling of raw materials, including recycling for dust, sludge and other residues; blast furnaces, including coke rate reduction and blast furnace performance improvement; alternative ironmaking, including innovation of direct reduction processes; and fundamentals and common issues, including modeling and simulation, process automation, and energy savings and recycling technology. **Abstracts are due January 20, 2009.** **Contact:** Liu Yongcai; The Chinese Society for Metals;

46 Dongsixida Jie, Beijing 100711, China; +86-010-6521-1206; e-mail: icsti@csm.org.cn; *www.csm.org.cn/icsti09/en/*.

### Materials Science & Technology 2009 Conference and Exhibition (MS&T'09)

October 25–29, 2009  
Pittsburgh, Pennsylvania

MS&T'09 (Materials Science & Technology 2009) is the seventh in a series of multidisciplinary annual conferences held by and for professionals in the metals and materials community. Programming and activities will be organized by TMS, the Association for Iron & Steel Technology, ASM International, and the American Ceramics Society to bring together scientists, engineers, students, suppliers, and others to discuss current research and applications, and shape the future of materials science and technology. MS&T'09 will focus on nine theme areas covering the breadth of materials science and engineering. Planned topics include: ceramic and glass materials, including microwave processing of ceramics; electronic and magnetic materials, including ferroelectrics and multiferroics; environmental and energy issues, including energy storage, fuel cells, and green engineering and environmental stewardship; fundamentals and characterization, including phase stability and recent advances in structural characterization of materials, and rigid natural composite materials; iron and steel, including steel product metallurgy and applications; materials and systems, including next generation biomaterials; nanotechnology; product manufacturing; and special topics. **Abstracts are due March 15, 2009.** **Contact:** Meetings Services Dept.; TMS; 184 Thorn Hill Road, Warrendale, PA 15086; (724) 776-9000, ext. 243; e-mail: mtgserv@tms.org; 74.55.185.84/.

### TRANSFAC '09—International Conference on Innovative Solutions for the Advancement of the Transport Industry

October 31–November 3, 2009  
Detroit, Michigan

TRANSFAC '09, co-sponsored by TMS and INASMET, will extend the themes introduced at the first meeting addressing elements of materials processing, properties, and application coupled with the real-world issues of sustainability, safety, and



productivity. A new feature of the 2009 conference will be a focus on technical cost modeling tools for materials production and selection as well as product development. An exhibition of related products and services as well as targeted workshops will complete the conference program. Technical topics to be covered include: processes, materials, structure and characterization, and applications and performance of automotive, aerospace, railway, and marine; safety and comfort in transportation; new vehicle concepts; and management and economics of transportation. Co-sponsors also include AusIMM, ASM International, Chinese Society for Metals, Japan Institute of Metals, Korean Institute of Metals and Materials, and the Metallurgical Society of CIM. **Abstracts are due January 31, 2009.** **Contact:** TMS Meetings Services, 184 Thorn Hill Road, Warrendale, PA 15086; (724) 776-9000, ext. 243; e-mail: [mtgserv@tms.org](mailto:mtgserv@tms.org); [www.tms.org/Meetings/Specialty/transfac09/home.html](http://www.tms.org/Meetings/Specialty/transfac09/home.html).

## TMS 2010 Annual Meeting

February 14–18, 2010  
Seattle, Washington

This meeting is the premier TMS event, featuring numerous sessions by all five TMS technical divisions on the latest scientific and technical developments. The meeting also features a large exhibition, short courses, tutorial lectures, award presentations, receptions and division luncheons, invited speakers, and student activities. **Contact:** TMS Meeting Services, 184 Thorn Hill Road, Warrendale, PA 15086; (724) 776-9000, ext. 243; e-mail: [mtgserv@tms.org](mailto:mtgserv@tms.org).

## Copper 2010

June 6–10, 2010  
Hamburg, Germany

The theme of the Copper 2010 Conference is Copper - Indicator of the Progress of Civilization. Copper 2010 is an important technical event for engineers, scientists,

fabricators, and users of copper. Recently copper has become an important factor in the developing economies of East Asian countries and can be seen as an indicator of the progress of civilization in each country. All relevant areas of copper production and application and their surroundings like energy savings, process optimization, health and safety issues, cost and commerce, recycling and new developments will be presented in a series of parallel sessions. The program will include such topics as mineral processing; hydrometallurgy; pyrometallurgy; electrowinning; electrometallurgy and refining; recycling; process control and optimization; sustainable development, health and safety; environmental control; downstream activities, application, and new products; and economics, as well as plenary sessions of general interest. **Contact:** Dr. Mickael Kopke; Norddeutsche Affinerie AG; Hoverstrasse 50, 20539 Hamburg, Germany; +49-10-78-83-38-01; e-mail: [cu2010@gdmb.de](mailto:cu2010@gdmb.de); [www.cu2010.gdmb.de/](http://www.cu2010.gdmb.de/).

## General Meetings

**41st Annual Canadian Mineral Processors Operators Conference:** January 20–22, 2009, Ontario, Canada; [www.min-eng.com/general/confs/9.html](http://www.min-eng.com/general/confs/9.html).

**Conference for Industry and Education Collaboration:** February 4–6, 2009, Orlando, Florida; [www.asee.org/conferences/ciec/2009/index.cfm](http://www.asee.org/conferences/ciec/2009/index.cfm).

**Asia Mining Congress 2009:** March 23–27, 2009, Singapore; [www.terrapinn.com/2009/asiamining](http://www.terrapinn.com/2009/asiamining).

**2009 IPC Printed Circuits Expo, APEX and the Designers Summit:** March 31–April 2, 2009, Las Vegas, Nevada; [www.goipcshows.org/html/main/default.htm](http://www.goipcshows.org/html/main/default.htm).

**Sustainability through Resource Conservation and Recycling 09 (SRCE 09):** April 4–5, 2009, Cape Town, South Africa; [www.goipcshows.org/html/main/default.htm](http://www.goipcshows.org/html/main/default.htm).

**Bio- and Hydrometallurgy 09 (BioHydromet 09):** April 6–7, 2009, Cape Town, South Africa; [www.min-eng.com/biohydromet09/index.html](http://www.min-eng.com/biohydromet09/index.html).

**Treatment of Mining Residues Containing Toxic Minor Metals (Toxic Metals 09):** April 8–9, 2009, Cape Town South Africa; [www.min-eng.com/toxicmetals09/index.html](http://www.min-eng.com/toxicmetals09/index.html).

**4th Global Foundry Sourcing Conference:** April 16–17, 2009, Shanghai, P.R. China; [www.fsc86.com/en](http://www.fsc86.com/en).

**Nuclear 2009: 8th International Exhibition on Nuclear Power Industry 2009:** April 19–22, 2009, Beijing, P.R. China; [www.coastal.com.hk/nuclear/](http://www.coastal.com.hk/nuclear/).

**17th International Conference on Wear of Materials:** April 19–23, 2009, Las Vegas, Nevada; [www.wom-conference.elsevier.com/index.htm](http://www.wom-conference.elsevier.com/index.htm).

**2009 China International Resources Recycling Industry Exhibition:** April 19–20, 2009, Shanghai, China; [cirr.cbichina.com/](http://cirr.cbichina.com/).

**Organic Photovoltaics 2009 Conference:** April 27–29, 2009, Philadelphia, Pennsylvania; [www.organicphotovoltaics2009.com/](http://www.organicphotovoltaics2009.com/).

**Offshore Technology Conference 2009:** May 4–7, 2009, Houston, Texas; [www.otcnet.org/2009/](http://www.otcnet.org/2009/).

**AISTech 2009: The Iron & Steel Technology Conference and Exposition:** May 4–7, 2009, St. Louis, Missouri; [www.aist.org/](http://www.aist.org/).

**29th International Exhibition–Congress on Chemical Engineering, Environmental Protections and Biotechnology (ACHEMA 2009):** May 11–15, 2009, Frankfurt, Germany; [www.achema.de/](http://www.achema.de/).

**V International Copper Hydrometallurgy Workshop—HydroCopper 2009:** May 13–15, 2009, Antofagasta, Chile; [www.hydrocopper.cl/](http://www.hydrocopper.cl/).

**Ninth International ASTM-ESIS Symposium on Fatigue and Fracture Mechanics:** May 20–22, 2009, Vancouver, BC, Canada; [www.astm.org/MEETINGS/nextsymposia.cgi?L+mystore++E08](http://www.astm.org/MEETINGS/nextsymposia.cgi?L+mystore++E08).

**Alta 2009 Nickel-Cobalt, Copper & Uranium Conference:** May 25–30, 2009, Perth, Australia; [www.altamet.com.au/Next\\_conference.htm](http://www.altamet.com.au/Next_conference.htm).

**66th Annual World Magnesium Conference:** May 31–June 2, 2009, San Francisco, California; [www.intlmg.org/news\\_30.html](http://www.intlmg.org/news_30.html).

**2nd Chaotic Modeling and Simulation International Conference (CHAOS2009):** June 1–5, 2009, Chania, Crete, Greece; [www.chaos2009.com/](http://www.chaos2009.com/).

**Physical Separation 09:** June 16–17, 2009, Falmouth, Cornwall, U.K.; [www.min-eng.com/physicalseparation09/index.html](http://www.min-eng.com/physicalseparation09/index.html).

**Materials Characterization 2009:** June 17–19, 2009, New Forest, U.K.; [www.wessex.ac.uk/conferences/2009/mc09/index.html](http://www.wessex.ac.uk/conferences/2009/mc09/index.html).

**Hot Forming of Steels & Product Properties:** June 21–24, 2009, Grado, Italy; [www.aimnet.it/hfs2009.htm](http://www.aimnet.it/hfs2009.htm).



## TRACE ELEMENT ANALYSIS

**5 Day Turnaround**

- High Purity Metals & Alloys
- Ceramics
- Glasses
- Semiconductors
- Thick Films
- Carbon, Graphite
- High Temperature Alloys

### Utilizing State of the Art Techniques

Slow Discharge Mass Spectrometry (GDMS)  
Inductively Coupled Plasma Mass Spectrometry (ICPMS)  
Spark Source Mass Spectrometry (SSMS)  
Combustion and Inert Gas Fusion Methods (LECO)

### Northern Analytical Laboratory

13 Delta Drive Unit #4  
Londonderry, NH 03053

Tel: 603-434-8400 • Fax: 603-434-8500  
E-Mail: NALABS@AOL.COM  
Website: www.northernanalytical.com

**View the latest  
position available ads  
online free of charge at  
<http://www.tms.org/classifieds.html>**

James E. Hoffmann and Associates Co.  
P.O. Box 420545  
Houston, Texas USA 77242-0545  
**JAMES E. HOFFMANN, FIMM. P.E.**  
CONSULTING EXTRACTIVE METALLURGICAL ENGINEER  
NON FERROUS, RARE, AND PRECIOUS METALS  
BUS (281) 493-9441 E-MAIL jehentp@aol.com  
FAX (713) 780-0761

**Read by thousands of the  
field's leading professionals  
and decision-makers,  
JOM can deliver an  
impressive international  
audience, both  
in print and online.**

**The new TMS Media Kit  
is now available.**

**To request your copy,  
contact Arlene Frances,  
Ad Sales Representative,  
at (724) 776-9000 ext. 280  
or by e-mail at  
[afrances@tms.org](mailto:afrances@tms.org)**

**Check out the TMS media kit at  
<http://www.tms.org/pubs/journals/JOM/ads.html>**

ISO-9001 and ISO-17025 Certified

*Analytical Services & Reference Standards*  
SEM/X-ray, Electron Microprobe, Surface  
Analysis (Auger) Metallography, Particle  
Size Counting & Surface Roughness

Quantitative analysis of small amounts of material in concentrations to 10 ppm, surface oxides, stains & cleanliness, corrosion, diffusion, reverse engineering, elemental mapping, diffusion gradients (carbon, nitrogen, etc.) Get your data by e-mail. Digital micrographs and elemental maps. We manufacture traceable standards for magnification (SEM, OM, etc.) and over 240 pure elements, alloys, glasses and compounds for micro-analysis.

*Put our years of experience to work on your specimens!*



**GELLER  
MICROANALYTICAL  
LABORATORY**

426e Boston St. (Rt. 1), Topsfield, MA 01983-1216  
978 887-7000 fax: 887-6671 www.gellermicro.com

## micron inc.

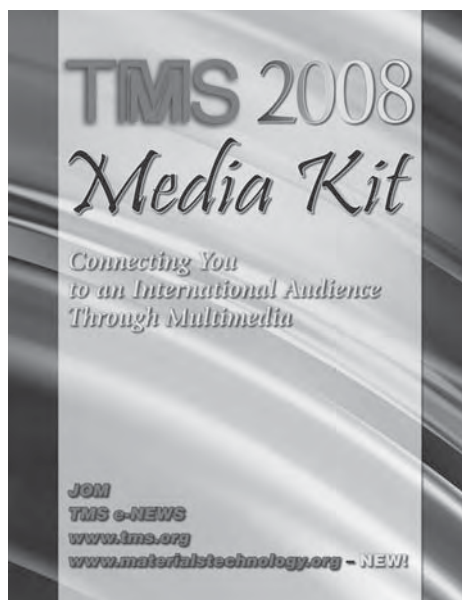
**ANALYTICAL SERVICES**

3815 LANCASTER PIKE  
WILMINGTON, DE 19805  
302-998-1184, FAX 302-998-1836

[micronanalytical@compuserve.com](mailto:micronanalytical@compuserve.com)  
[WWW.MICRONANALYTICAL.COM](http://WWW.MICRONANALYTICAL.COM)

# TMS

**Your Professional Partner  
for Career Advancement  
[www.tms.org](http://www.tms.org)**



## Thermophysical Properties Instruments & Testing Services

- Thermal Expansion
- Thermal Conductivity
- Thermal Diffusivity
- Specific Heat Capacity
- -180°C to 2800°C Range

Anter Corporation 1700 Universal Road Pittsburgh, Pa 15235-3998  
Tel: 412.795.6410 Fax: 412.795.8225 E-mail: [sales@anter.com](mailto:sales@anter.com)

ISO9001: 2000 Certified  
[www.anter.com/jom](http://www.anter.com/jom)

**anter  
corporation**



*Worldwide experience in  
technology development*

### FLOGEN Technologies

• Non-Ferrous and Ferrous Metallurgy, Inorganic and Organic Chemistry, Environment and InfoTechnology etc  
• Thermodynamic and kinetic quantification of slags, mattes, metals, etc., smelting, converting and refining process development and optimization, modeling and simulation, Atomic Absorption Spectrometry, minor and trace element analysis, electroanalytical techniques (biosensors), heavy metal pollution analysis, analytical quality assurance, mercury speciation, etc.

[www.flogen.com](http://www.flogen.com)

5757 Decelles Ave., Suite 511 Tel: (514) 344-8786  
Montreal, Quebec Fax: (514) 344-0361  
Canada H3S 2C3 Email: [secretary@FLOGEN.COM](mailto:secretary@FLOGEN.COM)

# MATERIALS SCIENCE

**Materials & Metallurgical  
Testing, Analysis & Consulting**

TEM, SEM, EDX, XRD, WDXRF, AES,  
NIR, m-FTIR, PLM/PCM, AA, ICP, GC/MS

- Materials Characterization
- Metallurgical Analysis
- XRD Phase Analysis
- Failure Analysis
- Product Comparison
- Contamination Analysis
- Surface Analysis
- Forensic Analysis
- Chemical Analysis
- Mechanical Testing
- R&D Support and Consulting
- 20 Years Of Experience

[www.EMSL.com](http://www.EMSL.com)  
800.220.3675



EMSL SERVICES: Air Quality, Environmental Microbiology,  
Industrial Hygiene, Lead, Materials, Forensic, Environmental Chemistry  
**CORPORATE LABORATORY**  
107 HADDON AVENUE  
WESTMONT, NJ



# MATERIALS RESOURCE CENTER: *Positions Available*



## Colorado School of Mines Metallurgical/Materials Engineering Assistant Professor – Lightweight Materials

Colorado School of Mines invites applications for a tenure-track Assistant Professor position in Lightweight Metals. The successful candidate will teach existing undergraduate and graduate level courses such as: foundry, welding metallurgy, advanced welding metallurgy, solidification, phase transformations, and transport in solids. Applicants must possess a Ph.D. or an equivalent degree in Metallurgical Engineering, Materials Science and Engineering, or related fields. The successful candidate will have the potential for teaching and developing a strong research program in the physical metallurgy of lightweight metals, with preferred emphasis in the welding, joining, and solidification of these alloys.

For a complete job announcement, more information about the position and the university, and instructions on how to apply, please visit: [http://www.mines.edu/Academic\\_Faculty](http://www.mines.edu/Academic_Faculty).

Mines is an EEO/AA employer.

Earth ♦ Energy ♦ Environment



## Colorado School of Mines Metallurgical/Materials Engineering Lecturer - Physicochemical Processing of Materials

Colorado School of Mines invites applications for an anticipated lecturer position in the area of physicochemical processing of materials. The successful candidate will have responsibility for teaching laboratory sections associated with required undergraduate courses in chemical processing of materials and senior design. Candidates must have a Masters of Science degree or higher in Metallurgical and Materials Engineering, Materials Science, or a related field, demonstrated teaching experience in laboratory-based application of the principles associated with physicochemical processing, and the ability to develop and present high quality lectures to undergraduate students in the department.

For a complete job announcement, more information about the position and the university, and instructions on how to apply, please visit: [http://www.mines.edu/Academic\\_Faculty](http://www.mines.edu/Academic_Faculty).

Mines is an EEO/AA employer.

Earth ♦ Energy ♦ Environment

### Tenure Track Faculty Position in Materials Engineering

The Chemical and Materials Engineering department at San Jose State University invites applicants for an assistant professor (tenure track position) in Materials Engineering. Preferred candidates for the position will have expertise in Materials Characterization and must hold a doctoral degree in Materials Science and Engineering or in a related discipline with appropriate experience. Successful candidates must have a demonstrated interest in developing characterization laboratory capabilities in either nanomaterials, biomaterials or structural materials, and in addressing the educational needs of undergraduates and graduate students through development of course materials, teaching strategies and research projects. Full details on the position can be found at <http://www.engr.sjsu.edu/about/emp>

For full consideration, send a letter of application, curriculum vitae, statement of teaching interests/philosophy and research plans, and at least three original letters of reference with contact information by February 15, 2009 to:

Dr. Stacy Gleixner, Chair, Search Committee,  
Department of Chemical and Materials Engineering  
San José State University  
One Washington Square  
San José, CA 95192-0082

Please include Job Opening ID #13558 on all correspondence.

San José State University is California's oldest institution of public higher learning. The campus is located on the southern end of San Francisco Bay in downtown San José (Pop. 945,000), hub of the world-famous Silicon Valley high-technology research and development center.

*SJSU is an Equal Opportunity/Affirmative Action Employer committed to nondiscrimination on the bases of race, color, religion, national origin, sex, sexual orientation, gender status, marital status, pregnancy, age, disability, or covered veteran status consistent with applicable federal and state laws. This policy applies to all SJSU students, faculty, and staff as well as University programs and activities. Reasonable accommodations are made for applicants with disabilities who self-disclose.*

If you have a key position to fill, **JOM Classified Advertising** can help you track down that special individual with the right qualifications and background to match your needs.

### I'VE SPECIALIZED FOR 29 YEARS

in the placement of Metallurgical, Materials, and Welding Engineers in the areas of R&D, Q.C. Production, Sales & Marketing, nationwide. My background as a Met. Eng. can help you! Salaries to \$150K. Fees paid by Co. Call/Send/E-mail Resume:

**Michael Heineman, Meta-Find, Inc.;**  
P.O. Box 610525, Bayside, NY, 11361;  
Phone (212) 867-8100;  
E-mail [mikeh@meta-findny.com](mailto:mikeh@meta-findny.com); Web: [www.meta-findny.com](http://www.meta-findny.com)

### Products and Services



ADVANCED X-RAY SOLUTIONS  
[www.bruker-axs.com](http://www.bruker-axs.com)



575 McCorkle Boulevard Westerville OH 43082  
Phone: (614) 891-2244 Fax: (614) 818-1600  
[info@lakeshore.com](mailto:info@lakeshore.com) [www.lakeshore.com](http://www.lakeshore.com)

# Beyond Flex Time: Retaining Female Scientists and Engineers

Lynne Robinson

**Editor's Note:** A more comprehensive version of this article can be found on the Materials@TMS web site.

Imagine the repercussions if a company routinely lost access to half of its most promising resources, even after investing a fortune in their development. According to "The Athena Factor: Reversing the Brain Drain in Science, Engineering, and Technology," a groundbreaking study published by the *Harvard Business Review* in June 2008, this is exactly the case with the retention of female scientists and engineers. The study found that, while women constitute 41 percent of all science, engineering, and technology professionals at the lower rungs of the career ladder, more than 50 percent of them eventually leave, with the peak of the exodus at around the ten-year career mark.

Providing input from the mining and metals industry on this issue was Pittsburgh-based Alcoa, one of the study's co-sponsors. "We really brought a different perspective," said Judi Nocito, assistant general counsel and co-leader of the Alcoa Women's Network. "We have unique challenges because we are in heavy industry. The result is that we struggle in attracting and retaining women, especially in operating roles within the company."

The Athena Factor study was conducted by the Center for Work-Life Policy (CWLP), an independent, non-profit research organization headquartered in New York. Alcoa's involvement with the project began when it joined with 35 other global corporations to form CWLP's Hidden Brain Drain Task Force. The task force, formed in 2004, has spearheaded a number of studies on sustaining female and minority talent. Alcoa was particularly interested in the Athena Factor, however, because of its

focus on women in science and engineering positions. "Prior to this work, we as a company had largely anecdotal information on the career challenges faced by women in operating roles in plants or in technical and engineering roles," said Nocito. "Data provide credibility to the issues."

As a co-sponsor, Alcoa opened its doors to CWLP researchers who conducted focus groups with women in engineering and technical fields at the Alcoa technical center in Pittsburgh, as well as its operations in Chicago, Russia, Australia, Western Europe, and Beijing. An electronic survey was also conducted of 2,300 male and female Alcoa employees with science or engineering degrees.

The study found that a number of factors contribute the departure of women from science and engineering positions, the study found. These include workplace cultures that are dismissive and even hostile toward female scientists and engineers, and hours and expectations that are not supportive of working mothers. The study called attention to the sense of isolation that many women experience when they are the only female at their level or on their team, as well as the frustration that many women feel because of unclear channels to information, opportunities, and career advancement.

The Athena Factor did muster some good news, however, by describing 14 programs that have started to demonstrate some success in not only retaining, but enabling women to advance in their careers. Highlighted among them was Alcoa's Women in Operations Virtual Extended Network (WOVEN), a pilot tested in the company's Global Primary Products Group (GPPG). Tar-

geted to women in operations roles with science, engineering, and technology backgrounds, WOVEN gives female professionals, who are not close geographically, the opportunity to meet and support one another virtually as they pursue their careers. Helping women make the transition to operations from other departments in the GPPG is another WOVEN goal.

A related effort being piloted in the GPPG is Alcoa's Manufacturing Manager Development Program. Although not limited to women, the program does address issues related to career advancement and isolation raised in the Athena Factor report by methodically preparing junior candidates for line management careers. This is accomplished by developing a well-planned and monitored program for each participant that offers exposure to different divisions and different types of management experience. The goal is that the candidate will be ready to take on a plant manager role within six to eight years after joining the company.

"When you look at the Athena Factor data as a whole, the women surveyed do not seem to perceive clear career paths," said Nocito. "They feel that they don't even have the chance to throw their hat into the ring because they are not aware of opportunities or don't have a mentor or network available to them. This goes hand-in-hand with the sense of isolation—that they are on their own.

"What this program offers women is a clear career plan so they can anticipate where they are going and can stay "in the loop" from a networking standpoint."

Lynne Robinson is the news writer for *Materials Technology@TMS*.

**Register before January 16  
to save as much as 100!  
(New Corporate Rate Available, Too)**

# TMS2009

**138th Annual Meeting & Exhibition**

February 15-19, 2009

Moscone West Convention Center  
San Francisco, California, USA

## *The Ultimate Networking Experience*

*"TMS provides a unique opportunity for professionals from academia, government and industry to interact. Participation at yearly TMS meetings also increases my awareness of recent advances in metallurgical and materials science and engineering."*

*– Amy Clarke,  
Engineer, Caterpillar Inc.*

**Record Number of Presentations to Choose From – 2,800**

**Scheduled Networking Events – 14**

**Short Courses and Workshops – 8**

**Special Lectures and Honorary Events**

**Global Exhibition and Employer Pavilion**

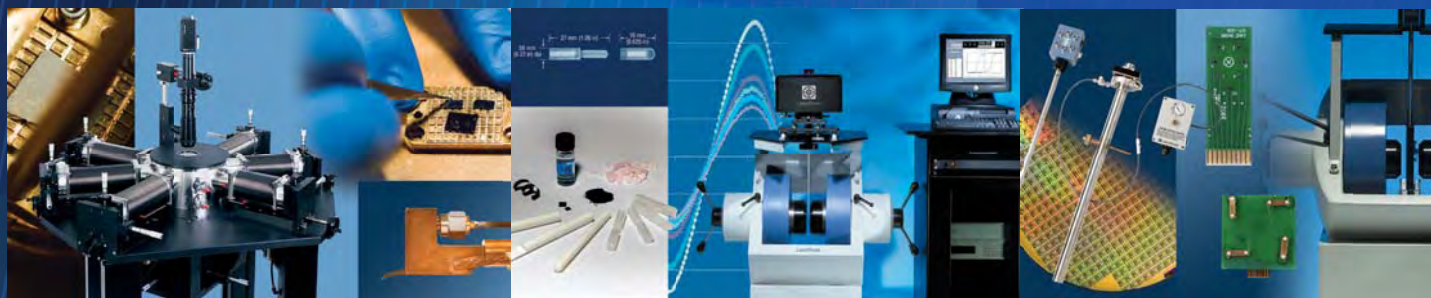
## *for Materials Professionals*



**Download the program and register online at  
[www.tms.org/annualmeeting.html](http://www.tms.org/annualmeeting.html)**

LEARN • NETWORK • ADVANCE

# L A K E S H O R E M A T E R I A L S C H A R A C T E R I Z A T I O N



## CRYOGENIC PROBE STATIONS

- Temperatures from 1.5 K – 475 K
- Measurements from DC to 67 GHz
- Probe up to 4-inch wafers
- Up to 6 micro-manipulated probe arms
- Vertical or horizontal field magnets
- High vacuum, load-lock, & cryogen-free

## HALL EFFECT MEASUREMENT SYSTEMS

- 10  $\mu\Omega$  to 200 G $\Omega$  resistances
- 2 K to 800 K temperatures
- Fields to 9 T
- Easy sample access
- Accommodate up to one 6-inch or four 1 cm<sup>2</sup> samples
- QMSA<sup>®</sup> resolves individual carriers in multi-carrier devices
- AC current for low resistance, high resolution measurement

## VIBRATING SAMPLE MAGNETOMETERS

- Low  $1 \times 10^{-7}$  emu noise floor
- High stability —  $\pm 0.05\%$  per day
- Excellent reproducibility
- Fields to  $>3$  T
- Widest available temperature range — 4.2 K to 1273 K
- Vector, magnetoresistance, and autorotation options

## OTHER LAKE SHORE PRODUCTS

- Cryogenic temperature sensors
- Cryogenic temperature instruments
- AC resistance bridge
- Superconducting magnet power supply
- Cryogenic accessories
- Magnetic sensors and instruments
- Electromagnets and power supplies

YOUR SINGLE SOURCE SOLUTION



# LakeShore<sup>®</sup>

575 McCorkle Boulevard  
Phone: (614) 891-2244  
info@lakeshore.com

Westerville OH 43082  
Fax: (614) 818-1600  
www.lakeshore.com